VNIVERSITAT DE VALÈNCIA

FACULTAD DE MEDICINA Y ODONTOLOGIA
DEPARTAMENTO DE PATOLOGIA

TESIS DOCTORAL:

Análisis de la microestructura del sistema de conducción cardíaco basado en histología y análisis de imagen. Descripción en el humano y otras especies animales.

Presentado por:
Fabián Alejandro Gómez Torres

Dirigida por:
Amparo Ruíz Sauri
Rafael Sebastian Aguilar

Programa de Doctorado de Medicina 3139
Junio 2021

VNIVERSITAT DE VALÈNCIA

Amparo Ruíz Sauri, Doctora en Medicina, Profesora Titular del Departamento de Patología de la Universitat de València;

Rafael Sebastian Aguilar, Doctor en Informática y Matemática Computacional, Profesor Titular del Departamento de Informática de la Universitat de València;

CERTIFICAN QUE:

Que la presente tesis doctoral elaborada mediante compendio de artículos, titulada “Análisis de la microestructura del sistema de conducción cardíaco basado en histología y análisis de imagen. Descripción en el humano y otras especies animales”, que presenta Don Fabián Alejandro Gómez Torres para optar al Grado de Doctor en Medicina por la Universidad de Valencia, ha sido realizada bajo su dirección en el Departamento de Patología de la Universitat de València, y que dicho trabajo reúne los requisitos necesarios para su presentación y defensa.

Y para que así conste, firman la presente en Valencia, a 20 de junio de 2021.

AMPARO|RUIZ|SAURI
Firmado digitalmente por AMPARO|RUIZ|SAURI
Fecha: 2021.06.21 08:51:51 +02'00'

Digitally signed by SEBASTIAN AGUILAR RAFAEL - 24351226E
Date: 2021.06.22 11:11:38 +02'00'

Amparo Ruíz Sauri
Profesora Titular
Universitat de València

Rafael Sebastian Aguilar
Profesor Titular
Universitat de València

A mi abuela, por la grandeza de su formación

A mi esposa, por su apoyo incondicional

AGRADECIMIENTOS

La presente tesis nace de un compendio de artículos publicados y realizados en equipo. Por ello quiero expresar mi agradecimiento, en primer lugar, al Departamento de Patología de la Facultad de Medicina y Odontología de la Universitat de València, que me ha acogido como si fuera un miembro más. A la Doctora Amparo Ruíz Sauri mi directora, que me dio la oportunidad de realizar esta tesis y con la que he forjado un gran camino en el área de la investigación. A mi codirector el Doctor Rafael Sebastian por sus inestimables consejos para realizar esta tesis. También quiero agradecer al Doctor Víctor García Bustos por su apoyo en el diseño estadístico, a la Doctora Pilar Molina por su entrenamiento en la toma de muestras, a Teresa Sagrado por su colaboración en la obtención de los tejidos histológicos mediante diferentes técnicas y a Rafael Navarro por su apoyo logístico para el desarrollo de esta tesis. En segundo lugar, al Grupo de Variaciones Anatómicas y Biomecánica Tendomuscular de la Universidad Industrial de Santander en Bucaramanga – Colombia, en cabeza del Doctor Luis Ernesto Ballesteros Acuña por su colaboración constante en la elaboración del trabajo de campo y a Hernando Yesid Estupiñán Velásquez por su apoyo en la construcción del material gráfico de las publicaciones. En tercer lugar, al Doctor Gerardo Valencia de la Universidad del Norte en Barranquilla – Colombia, por su apoyo logístico y la obtención de material fotográfico. Finalmente, a cada una de las instituciones que nos colaboraron en la consecución de las muestras anatómicas como el Instituto de Medicina Legal y Ciencias Forenses, la planta de beneficio de animales “Athena Foods” y a las clínicas veterinarias de pequeños animales de la ciudad de Bucaramanga – Colombia.

Gracias.

TABLA DE CONTENIDO

LISTA DE FIGURAS

LISTA DE TABLAS

A. ABREVIATURAS

ACD	*Arteria Coronaria Derecha*
ACI	*Arteria Coronaria Izquierda*
CP	*Células de Purkinje*
CT	*Células transicionales*
CTCC	*Contacto a Través de Cuerpos Celulares*
CTPC	*Contacto a Través de Prolongaciones Celulares*
CTCT	*Contacto a Través de Células Transicionales*
Cx	*Conexina*
DE	*Desviación Estándar*
EFC	*Esqueleto Fibroso Cardiaco*
FC	*Fallo Cardiaco*
FP	*Fibras de Purkinje*
FV	*Fibrilación Ventricular*
HH	*Haz de His*
NSA	*Nodo Sinoatrial*
NAV	*Nodo Atrioventricular*
PAS	*Ácido Peryódico de Schiff*
RCX	*Rama Circunfleja*
RNAV	*Rama del Nodo Atrioventricular*
RNS	*Rama del Nodo Sinoatrial*
SCC	*Sistema de Conducción Cardiaco*
TV	*Taquicardia Ventricular*
UPM	*Uniones Purkinje-miocardio*
VI	*Ventrículo izquierdo*

B. RESUMEN

El sistema de conducción cardíaca es una estructura ramificada que permite el inicio y la rápida propagación de impulsos eléctricos que desencadenan la despolarización eléctrica del tejido miocárdico. Los nodos cardíacos son la fuente del impulso eléctrico que se transmite al corazón y la función principal del sistema de conducción ventricular es la activación eléctrica rápida de los ventrículos. El objetivo de este trabajo fue estudiar las características histológicas y morfométricas de los diferentes componentes del sistema de conducción cardiaco en humanos, cerdos, caballos y perros, así como sus posibles variaciones. Se utilizó un grupo de diez corazones de humanos, diez de cerdo, diez de caballo y cinco de perro sin antecedentes clínicos de patologías cardíacas. La región de los nodos cardiacos se seccionó en serie y se extrajo el bloque de tejido para su estudio. Los ventrículos izquierdos se disecaron y se seccionaron en tres cortes de igual ancho (base, tercio medio y ápex). Se obtuvieron cortes histológicos de 5 µm de espesor y se tiñeron con hematoxilina-eosina y tricrómico de Masson y las células de Purkinje y sus uniones se identificaron mediante desmina y la tinción de PAS. Sobre estas muestras se realizó la adquisición de las imágenes con un microscopio óptico Leica DMD108 y se evaluaron mediante un análisis morfométrico con el software Image-ProPlus 7,1.

El nodo sinoatrial en humanos y cerdos es una estructura compacta, cuya forma es ovoide. La longitud del nodo sinoatrial en humanos está entre 1,7-7,4 mm y en cerdos se encuentra entre 1,3-3 mm. Las células P son grandes, pálidas y ubicadas en el centro o la periferia. El diámetro máximo de las células P en humanos (9,9 µm) es significativamente mayor que en cerdos (8,9 µm) (p=0,026). El nodo atrioventricular tiene una forma ovoide en humanos y cerdos. En caballos y perros la forma del nodo es triangular. La longitud del nodo atrioventricular en humanos se encuentra entre 1,7-2,5 mm, en cerdos entre 1,4-2,6 mm, en caballos entre 1,6-2,7 mm y en perros entre

1,1-3,1 mm. Observamos una disminución del tamaño del nodo, un aumento de las fibras de colágeno y una disminución del tamaño y el número de células P dentro del nodo atrioventricular en los cerdos, caballos y perros cuando presentaban cartílago en el esqueleto fibroso cardiaco. En cerdos las células P (25,3 µm) presentan un diámetro máximo significativamente mayor que en humanos (5,2 µm) (p=0,001). Se encontraron diferencias significativamente mayores en el diámetro máximo de las células P del nodo atrioventricular en los corazones que no presentaron cartílago en el esqueleto fibroso cardiaco (p=0,002).

Las fibras de Purkinje fueron difíciles de identificar en humanos, en su mayoría mostraban un color más oscuro o igual al de los cardiomiocitos y ocasionalmente se observaban con un tono más pálido. Las fibras de Purkinje en humanos se encontraron en el subendocardio y en los cerdos en el miocardio y subendocardio. Las fibras de Purkinje se ubicaron principalmente en la región septal en todas las especies estudiadas. Las uniones Purkinje-miocardio estuvieron presentes en el 10% de todas las micrografías analizadas en humanos y en el 24,2% en cerdos. El diámetro máximo de las células de Purkinje fue significativamente mayor en cerdos (22,85 µm) que en humanos (18,52 µm) (p=0.031).

El análisis morfométrico nos ha permitido cuantificar objetivamente cada uno de los componentes del sistema de conducción cardiaco y compararlos en las diferentes especies. La menor densidad celular en cualquiera de los nodos cardíacos, especialmente en las células P del nodo sinoatrial, puede disminuir la conducción eléctrica dentro de los nodos y en los tractos internodales. Además, la presencia de metaplasia cartilaginosa en el esqueleto fibroso cardíaco disminuye el tamaño del nodo atrioventricular y sus células y aumenta el porcentaje de fibras de colágeno dentro del nodo, lo que reflejaría la presencia de arritmias cardíacas derivadas de la mala conducción. El estudio de las fibras y células de Purkinje y sus uniones miocárdicas es vital para conocer su distribución normal en las especies analizadas.

C. INTRODUCCIÓN

El sistema de conducción cardíaco (SCC) se encarga de desencadenar y difundir a altas velocidades el impulso eléctrico responsable del latido cardíaco. Los principales componentes del SCC son: el nodo sinoatrial (NSA), el nodo atrioventricular (NAV), el haz de His (HH), las ramas derecha e izquierda del HH y finalmente, las fibras de Purkinje (FP). Durante la primera década del siglo XX, la anatomía macroscópica del SCC ha sido ampliamente estudiada[1,2], especialmente sus estructuras suprahisianas (por encima del HH) debido a sus implicaciones más claras en los trastornos del ritmo supraventricular y la complejidad del SCC en las secciones distales[3]. Las primeras descripciones del SCC se realizaron en corazones de humanos, ovejas, perros y bovinos; desde entonces, la histología de la vía de conducción ha sido descrita en numerosos estudios[1,2,4-10], pero hasta la fecha se han realizado pocas investigaciones sobre las características morfométricas de estas estructuras, que pueden ayudar a comprender mejor los trastornos relacionados con las arritmias ventriculares.

1. NODO SINOATRIAL

Cerca de la unión de la vena cava superior con el atrio derecho, debajo del *sulcus terminalis* se encuentra el NSA. La mayor parte del NSA se encuentra en la unión del seno intercavario (reconocido por la ausencia de un endocardio trabecular) con la pared lateral de la aurícula derecha en la cresta terminal[11-14]. El margen anterior del NSA está cerca de la unión del atrio con la vena cava superior marcada por una pequeña cresta epicárdica presente exactamente en ese punto.

Nodo Sinoatrial en humanos

El margen anterior del NSA humano rara vez cruza ese sitio de unión, pero casi siempre comienza de 1 a 2 mm por detrás de él. Desde su margen anterior, el NSA continúa posteriormente de 10 a 20 mm en un corazón humano adulto normal[12]. El NSA en humanos es una masa alargada de forma ovalada (en forma de huso) que mide entre 10-13 mm de largo y hasta 3-5 mm de ancho[15-18]. El NSA contiene dos tipos de células: células nodales (células P) y células transicionales (CT). Las células P son pequeñas, ovoides y pálidas que rodean la rama arterial nodal. Las CT son alargadas con características intermedias entre las células P y las células del miocardio auricular; están ubicadas en la periferia del nodo y hacen conexiones con las células P para propagar los impulsos eléctricos al resto del miocardio auricular. También es importante describir las células que se encuentran alrededor del NSA, que tienen características diferentes a las células nodales y juegan un papel vital en la transmisión del impulso eléctrico desde el nodo[6,12,18-20]. En humanos, se indica que el diámetro de las células P es de 3-10 μm[6,12]. En el corazón humano, la irrigación del NSA es proporcionada por una rama arterial conocida como rama del nodo sinoatrial (RNS), que proviene de la arteria coronaria derecha (ACD) en el 50-79% de los corazones[12,21-24], de la rama circunfleja (RCX), proveniente de la arteria

coronaria izquierda (ACI) en un 30-45%[12,24] y de ambas ramas arteriales en 3–23%[21,23-25]. Dentro del NSA, su rama arterial se encuentra con mayor frecuencia cerca del centro del nodo, proporcionando solo unas pocas ramas pequeñas que otorgan la nutrición y en cambio, parece pasar completamente a través del NSA con pocos cambios en su diámetro, una disposición que sugiere alguna función distinta a la simple provisión de nutrición y existe la posibilidad de que la pulsación de la RNS pueda estar relacionada con el proceso de generación y / o sincronización de impulsos[12]. El NSA humano está ricamente inervado por ramas tanto del sistema vago como del simpático. Hay numerosos ganglios en la vecindad del NSA, pero estos se encuentran principalmente en sus márgenes y es raro encontrar un ganglio dentro del NSA propiamente dicho, al menos en corazones humanos. Como se esperaría de la inervación cardíaca en el corazón humano en general, casi todos los ganglios son vagales[12].

Nodo Sinoatrial en cerdos

En los cerdos se identificó el NSA por los siguientes criterios: un elevado número de núcleos celulares cercanos entre sí, elevado número de fibras de colágeno y células. Entre el endocardio y el NSA se encuentra músculo auricular mientras que entre el epicardio y el NSA hay un haz muy grueso de tejido nervioso. El nodo tiene una longitud de 10-18 mm y una anchura de 3,5 mm[26]. Se indica que las células P tienen un diámetro de 4-8 μm y una longitud de 40 μm[26]. Otra investigación indica que su diámetro es aproximadamente el mismo que el de la célula del músculo auricular[27]. En los cerdos, la RNS se origina de la ACD en el 100% de los casos, pero no es tan prominente como en el corazón humano o canino[26,28,29]. Hay numerosas células ganglionares y fibras nerviosas en la periferia del NSA y ocasionalmente dentro del mismo[27].

Nodo Sinoatrial en caballos

Se ha descrito que el NSA en caballos es una estructura blanquecina mal definida, aunque su estructura y extensión no se puede determinar con precisión. Sin embargo, su ubicación es identificable por el abundante tejido

conectivo que se encuentra con el nodo en la cara lateral y posterior de la cresta terminal, justo debajo del epicardio del surco terminal. Histológicamente, la extensión completa del nodo se ve fácilmente en las tinciones tricrómicas debido a la estructura característica de las fibras del nodo y al abundante tejido conectivo rico en fibras de colágeno. El nodo tiene un cuerpo grande ubicado anterolateralmente, cerca de la cresta del atrio, debajo del epicardio del *sulcus terminalis*. Los pilares craneales y caudal ahusados rodean la mitad lateral de la unión de la precava con la aurícula derecha[30]. Su eje largo corre paralelo al surco y mide 3 cm de largo y entre 4,4-5 mm de ancho[16,30,31]. La RNS surge de la RCX de la ACI en el 100% de los casos[32]; es una rama grande presente de forma constante en el nodo que surge cerca del origen de la RCX. Cerca del tabique interauricular, se divide en varias ramas, una de las cuales continúa hacia el NSA en el margen anterior del orificio de la precava. En las secciones histológicas, se observa que esta rama se divide en ramas más pequeñas anterolateralmente en la cresta terminal y finalmente en arteriolas y capilares lateralmente sobre la cresta de la aurícula derecha. Sus ramas se ven en secciones transversales de la porción craneal del NSA[30,31]. Las fibras nerviosas son abundantes dentro del nodo y con frecuencia se pueden demostrar ganglios debajo del epicardio, pero no se ven dentro del tejido del nodo[30].

Nodo Sinoatrial en perros

Como en la mayoría de los vertebrados, el NSA en el perro se encuentra en la unión de la vena cava craneal y la pared libre del atrio derecho. Su margen anterior no llega del todo a la cresta de la unión de la aurícula con la vena cava craneal, por lo que se relaciona con este punto de referencia de manera similar al NSA humano[33]. Su forma es ovoide o como un huso, aunque a menudo es irregular. El área total del nodo es de aproximadamente 5 mm. Como en el hombre, el NSA del perro se encuentra a menos de 1 mm por debajo del epicardio, y está separado de esa superficie por una fina capa de grasa y tejido areolar laxo. En la sección transversal, tiene una forma menos consistente que la del hombre, que es aproximadamente triangular. Entre el

cuerpo del nodo y el endocardio suele haber algo de miocardio auricular derecho, pero el nodo a veces se extiende directamente al endocardio[33]. La RNS surge más comúnmente del tercio distal de la ACD (90%), siendo prácticamente una rama terminal de ese vaso. El cuerpo se dispone alrededor de una rama arterial central que lo nutre. Aunque la RNS del perro a veces termina en el NSA, más a menudo continúa a través del cuerpo del nodo para irrigar el miocardio auricular vecino[33]. Las fibras nerviosas dentro del NSA son más abundantes en el perro que en el hombre, pero las células ganglionares se encuentran sólo en la periferia del nodo y no dentro de su cuerpo, una observación también válida para el nodo humano[33].

2. TRACTOS INTERNODALES

Se ha podido demostrar histológicamente la presencia de haces continuos de miocardio con características similares a los componentes del SCC en tres regiones entre el NSA y el NAV. Los haces de miocardio corresponden a los tractos descritos por Bachmann (tracto internodal anterior), Wenckebach (tracto internodal medio), y Thorel (tracto internodal posterior). En general, las longitudes de los tractos internodal anterior y medio son casi iguales, y ambos eran más cortos que el tracto internodal posterior[34].

El tracto internodal anterior sale del NSA en dirección hacia adelante y se curva alrededor de la vena cava superior y la pared anterior de la aurícula derecha hacia el tracto internodal anterior, donde se divide en dos haces de fibras[34].

El tracto internodal medio, deja los márgenes dorsal y posterior del NSA y se curva detrás de la vena cava superior para atravesar el seno intercavario hacia la porción dorsal del tabique interauricular[34].

El tracto internodal posterior sale del margen posterior del NSA para entrar en la cresta terminal, siguiéndolo a lo largo de todo su recorrido hasta la región de la cresta de la válvula de la vena cava inferior (vena cava caudal en animales)[34]. Estos tractos se han descrito de manera similar en las 4 especies que nos ocupan.

3. NODO ATRIOVENTRICULAR

El NAV está solo unos pocos milímetros por delante del orificio del seno coronario. El nodo se encuentra debajo del endocardio del tabique auricular derecho y justo encima de la unión septal de la válvula tricúspide. Es importante tener en cuenta estos diversos puntos de referencia y su ubicación y relación entre sí para comprender las funciones normales y anormales del NAV[12,35,36]. A medida que el NAV humano maduro se asienta en su ubicación, también descansa sobre el cuerpo fibroso central que, a su vez, forma el ancla de la porción septal de la valva mural de la válvula mitral[12].

Nodo Atrioventricular en humanos

En humanos, el NAV es una estructura compacta ovoide que mide aproximadamente 5 mm de largo, 3 mm de ancho y 1 mm de grosor[5,35,36]. En humanos, los estudios de microscopía electrónica han descrito cuatro tipos de células en el NAV: células P, CT, cardiomiocitos y células de Purkinje (CP). Las CP a este nivel solo pueden ser reconocidas por microscopía electrónica, ya que utilizando microscopía óptica las CP pueden confundirse con cardiomiocitos ordinarios[34,36,37]. La mayoría de las células P en el NAV son individuales o en grupos muy pequeños y se ven distribuidas a través de la mayor parte del NAV. Este es un patrón relativamente uniforme excepto en el margen del NAV cerca del HH, donde tienden a agregarse más células P. Las CT están envueltas en vainas de colágeno, a diferencia de las células P que no poseen ningún tipo de envoltura[12]. En humanos, la rama del nodo atrioventricular (RNAV) se origina en la ACD en 85-92%[12,24,36,38-40], de la RCX de la ACI en un 10-15%[12,29,35,41,42] y con un origen dual en 2% (ACD o RCX)[24,39]. Hay numerosos nervios pequeños distribuidos a lo largo del nodo y algunos de ellos continúan hacia el HH. Aunque estos nervios son fáciles de identificar con micrografías electrónicas apropiadas, son difíciles de observar con microscopía óptica[12].

Nodo Atrioventricular en cerdos

El NAV en cerdos se encuentra en el lado derecho de la cresta del tabique ventricular, aunque más abajo en el tabique que en el humano. Hay un aumento marcado de fibras de colágeno y elásticas en comparación con el del miocardio ventricular[27]. En los cerdos, las células P, CT y los cardiomiocitos se han descrito mediante métodos convencionales, mostrando una disposición plexiforme[27]. En los cerdos, la RNAV se origina a partir de la ACD en el 100% de los casos[28,29,42]. En el cerdo las fibras nerviosas se encuentran en la periferia y en el propio NAV[27].

Nodo Atrioventricular en caballos

En el caballo, macroscópicamente este nodo no se diseca fácilmente, observándose como una masa plexiforme de fibras de color gris pálido, de forma irregular, aunque se han dado descripciones de su forma deltoidea, oval o fusiforme. Mide entre 0,6-0,8 cm de largo, 0,4-0,7 cm de ancho y 0,15 cm de espesor en el adulto[30,31]. Histológicamente, el NAV se encuentra en la porción dorsal del tabique fibroso adyacente a la aurícula derecha, justo por delante del orificio del seno coronario y aproximadamente 0,6 cm por encima de la inserción de la valva septal de la válvula tricúspide en el caballo adulto[30]. Está cubierto por el endocardio y 1,0-1,5 mm de fibras auriculares, muchas de las cuales se conectan dorsal y lateralmente con el NAV, mientras que otras pasan hasta la base de la válvula tricúspide. El NAV está incrustado en las fibras de colágeno del tabique fibroso que separan las fibras individuales del NAV en haces de interconexión discretos[30]. Está irrigado por una rama que se origina en la ACD en el 100% de los ejemplares[43]. Se ha descrito que está provisto de una arteria bien marcada[31], pero a su vez se ha indicado que ninguna arteria grande se asocia sistemáticamente con el NAV en los cortes histológicos. Varias arterias musculares medianas y pequeñas y arteriolas están presentes en el septum fibroso que son similares a las de otras partes del corazón[30]. Las fibras nerviosas son abundantes y los ganglios están presentes en el tabique fibroso adyacente, pero no dentro del nodo en sí[30].

Nodo Atrioventricular en perros

En los perros, el NAV se encuentra en la mitad derecha del tabique interauricular. Visto desde el lado de la aurícula derecha, el NAV es alargado y se asemeja a un pequeño bazo, que mide un poco menos de 2 mm de ancho y un poco más de 2 mm de largo. Su espesor máximo es de 0,5-1,0 mm. Entre las fibras del NAV hay fibras de colágeno sueltas y fibras elásticas dispersas[44]. La irrigación arterial del NAV de los perros es dual, con una porción significativa proveniente de la RCX cuando atraviesa la *crux cordis* del corazón, y el resto de las ramas terminales de la rama septal, que penetra hacia adentro desde la rama interventricular paraconal[44]. En la región entre el margen posterior del NAV y la pared anterior del seno coronario hay varios ganglios y nervios. Los nervios convergen hacia la superficie cóncava del NAV donde se entremezclan con las fibras del nodo. Dado que la influencia del nervio vago en la función del NAV es bien conocida, muchas de las fibras nerviosas que se ven dentro del nodo son fibras posganglionares-vagales[44].

3.1 VARIACIONES DEL SISTEMA DE CONDUCCIÓN EN LA ZONA ATRIOVENTRICULAR

La importancia del SCC en la zona atrioventricular radica en que el NAV se encarga de retrasar el paso del impulso eléctrico a los ventrículos para protegerlos de las despolarizaciones rápidas provenientes de las aurículas en condiciones normales o, incluso, cuando existen focos ectópicos auriculares debidos a arritmias supraventriculares. El conocimiento definitivo de la anatomía del sistema de conducción atrioventricular cardíaco es importante para comprender la base anatómica de una variedad de anomalías de la conducción[45].

En humanos se han descrito diferentes variaciones morfológicas a nivel atrioventricular debido a factores como el envejecimiento: bloqueo cardíaco por lesiones calcáreas en el HH[46] y lesiones similares que se refieren a ellas como “esclerosis del lado izquierdo del esqueleto cardíaco”.

Las lesiones consistían en fibrosis, con o sin calcificación, que afectaba a la zona superior del tabique interventricular, anillo mitral, parte membranosa y base de la aorta. Con el paso de la edad, los cambios suelen afectar a una parte del SCC[47,48].

En varias especies de mamíferos, una parte sustancial del esqueleto fibroso cardíaco (EFC) está compuesta de tejidos cartilaginosos. En los cerdos se ha encontrado cartílago principalmente de tipo hialino, pero en ocasiones también es posible observar cartílago fibroso en su EFC[49]. Tawara[4] describió la presencia de cartílago o tejido óseo en el área atrioventricular de corazones de ternera y oveja, pero que no había en el corazón humano.

Se ha encontrado un hueso muy característico en el cuerpo central fibroso cerca del NAV y del HH conocido como *os cordis* en corazones de diferentes mamíferos, especialmente en ungulados como ovejas y vacas. Pero es posible encontrar cartílago en corazones de caballos, búfalos de agua, perros y algunos gatos[12,50,51].

También se ha descrito que la metaplasia de cartílago en el esqueleto cardíaco con degeneración focal en el HH de perros Dóberman Pinscher de diferentes edades y con lesiones similares en todos ellos, conduce a muerte súbita[52]. Se encontró falta de comunicación entre las aurículas y el NAV, atrofia del NAV, interrupción en su continuidad con el HH y cambios degenerativos en todo el sistema de conducción en un perro Bóxer de 2 años con bloqueo cardíaco espontáneo[53].

Además, se ha descrito la presencia de metaplasia cartilaginosa u osificación y formación de hueso en el EFC de perros de razas grandes de diferentes edades. El principal cambio morfológico encontrado en el EFC fue la metaplasia condroidea. En todos los corazones examinados, se encontraron varios grados de metaplasia sin correlación con la edad o la raza. Esto varió desde unos pocos condroblastos y condrocitos hasta muchos condrocitos maduros y varios grados de mineralización (metaplasia condroide y osificación)[45].

El uso de animales como modelos de enfermedad cardiovascular se ha incrementado en los últimos años. El cerdo es un modelo muy utilizado para este propósito, debido a las amplias similitudes con el humano, en términos de fisiología e histología cardíaca[27,28,29,54-56], lo que hace relevante señalar sus diferencias. El conocimiento adecuado del NSA y NAV de caballos y perros, contribuye a la anatomía comparada, y facilita su uso para la realización de procedimientos quirúrgicos y diseño de modelos fisiológicos experimentales que involucren estas estructuras[57,58].

4. HAZ DE HIS

Descrito inicialmente por Wilhelm His en 1893, el HH es la continuación del NAV y de donde emergen las ramas derecha e izquierda de este haz, a nivel de la cresta del tabique interventricular; desde aquí, el impulso eléctrico se transmite desde las aurículas a los ventrículos[12,27,30,59-61]. El llamado HH es parte del sistema de conducción eléctrica especializado que, en el corazón normal, proporciona la conexión entre los compartimentos miocárdicos auricular y ventricular[4,7,62]. Solo hasta los hallazgos de Tawara[4,7], fue posible reconocer cuáles eran los límites del HH (conocido en ese momento como haz penetrante AV), que hacía la transición desde el NAV cuando el haz penetra en los tejidos aislantes del EFC y se extiende posteriormente a la cresta del tabique ventricular muscular donde se ramifica[4,7,12,62].

Pocos estudios han observado los parámetros morfométricos del HH y sus células, pero se ha descrito que esta estructura es de 0,25 a 0,75 mm de longitud en humanos[63]. Las células del HH en humanos son pequeñas, pálidas y con pocas miofibrillas y en mamíferos más grandes tienen las mismas características, pero son de mayor tamaño[2,27,30,64]. La mayor parte del suministro sanguíneo en el HH en humanos es el mismo que el del suministro principal del NAV. La RNAV siempre provee una pequeña rama que recorre el nodo y se dirige al HH donde usualmente termina[12,65]. Normalmente no hay ganglios autónomos en ninguna porción del HH humano o sus ramas. Sin embargo, existen fibras nerviosas que se originan de ganglios intra o extra cardiacos, que proporcionan una distribución nerviosa importante a través del NAV y el HH[12,66].

Las células del HH en cerdos y caballos se parecen mucho a las CP, pero son más pequeñas[5,27,30,31]. Se ha informado que las células del HH y sus ramas tienen una alta concentración de glucógeno en perros y caballos[30,67].

La longitud del HH en perros es de 1 a 1,5 mm de longitud, siendo más largo que en el hombre, posiblemente porque el EFC es más extenso en el perro[4,7,68].

Tanto la apariencia con microscopia óptica como electrónica del HH canino y humano son similares y no se han encontrado diferencias importantes entre las especies[37].

5. FIBRAS DE PURKINJE

El SCC genera el latido del corazón a través de una red de células miocárdicas especializadas mediante las cuales el impulso eléctrico se propaga de forma coordinada para obtener una contracción eficiente del músculo cardíaco[67] y así permitir una rápida activación eléctrica de los ventrículos[19,68]. En 1845, Johannes Evangelista Purkinje describió por primera vez las FP como una red de fibras grises, planas y gelatinosas ubicadas en el subendocardio ventricular de corazones de oveja[5,69]. A principios del siglo XX, se describió el papel de este sistema en la propagación eléctrica en corazones de humanos, perros, vacas y ovejas[2,4,7-10]. Desde entonces se ha estudiado ampliamente la anatomía e histología del SCC. La función principal del sistema de conducción ventricular es la activación eléctrica rápida de los ventrículos[19,68,70].

Las FP en humanos alcanzan solo la capa interior del miocardio, mientras que en ciertos animales se extienden a todo el miocardio[2]. En los ungulados se ha descrito una continuidad directa de las FP miocárdicas con las que se encuentran en posición subendocárdica, aunque esta conexión también se ha indicado en otras especies como los perros[71]. Las fibras de la parte distal del corazón se introducen en la superficie interna de los ventrículos para unirse a los cardiomiocitos activos. Aunque algunas fibras pueden ser visibles ocasionalmente a simple vista o con un microscopio óptico, estos métodos no permiten la visualización completa de la red[55], por lo que se necesitan tinciones o marcadores específicos para identificarlas y distinguirlas de otras células como los cardiomiocitos. La base anatómica de la conducción de señales eléctricas cardíacas y el funcionamiento fisiopatológico de la red de Purkinje no se comprenden completamente y la mayor parte de la evidencia que aborda este tema proviene generalmente de modelos basados en animales en lugar de sujetos humanos. La activación eléctrica cardíaca en los ventrículos depende de la geometría del complejo del sistema His-Purkinje y de sus propiedades eléctricas distintivas[10].

Se han desarrollado muchas técnicas para el análisis anatómico de las FP, tales como: reconstrucción de secciones seriadas, tinción mediante inyección de tinta china, microdisección, estereomicroscopía, microscopía electrónica de barrido, reconstrucción histoquímica de inmunoenzimas y expresión de eGFP transgénica[4,7,8,55,69,72,73]. En los últimos años se han visto técnicas de imagen no invasivas, como la resonancia magnética, la micro tomografía computarizada con contraste y la tomografía de coherencia óptica de dominio espectral de ultra alta resolución[74-77]. Desde el punto de vista histológico, las FP se han identificado a través de diferentes técnicas como la tinción de ácido peryódico de Schiff (PAS), la inmunofluorescencia[78] y la microscopía electrónica[69,79,80]. Sin embargo, la morfometría de las FP y las conexiones que permiten su identificación más precisa son áreas de estudio desatendidas[10]. Las FP son PAS positivas ya que contienen una cantidad considerable de glucógeno, que es típico de las células del sistema de conducción[81,82]. Una gran cantidad de glucógeno en las FP se metaboliza a través de enzimas anaeróbicas. Gracias a esta propiedad, estas células son más resistentes a la hipoxia que los cardiomiocitos ventriculares[83].

Las FP están formadas por las CP. Su morfología en mamíferos muestra grandes variaciones entre especies, por lo que la red de las FP se divide en tres grupos según el tamaño y ultraestructura de las CP: Grupo I, que se encuentra en ungulados (ovejas, cabras, vacas, caballos y cerdos) y cetáceos (ballenas y delfines), donde las células se caracterizan por ser grandes, bien diferenciadas y ubicadas en el subendocardio y el miocardio; grupo II, en humanos, monos, perros, gatos y focas, donde las células se describen como de tamaño intermedio a pequeño, con ciertas similitudes con los cardiomiocitos ventriculares y ubicadas en el subendocardio y grupo III, en roedores (ratones y ratas) y conejos, donde las células son aparentemente más pequeñas en tamaño que los cardiomiocitos ventriculares y están ubicadas en el subendocardio[60,67,69,84,85,]. Además, se ha descrito FP intramiocárdicas y a nivel perivascular en aves, ubicándolas en el grupo I[64, 86-88].

El sistema de Purkinje está presente en todos los animales superiores. En el hombre, la rama izquierda del HH se separa en fascículos que se desprenden del tronco principal en diferentes niveles. Estas pronto se convierten en FP, que se extienden por la superficie interna del miocardio ventricular. La rama derecha del HH ingresa al miocardio por debajo de la base tricúspide y corre dentro del miocardio hasta el músculo papilar. En la porción intramiocárdica las fibras de la rama son similares a las fibras miocárdicas ordinarias. A nivel del músculo papilar, la rama se vuelve subendocárdica y sus fibras cambian a CP que se extienden en hebras por debajo del endocardio[5]. A nivel subendocárdico en humanos, las CP son cilíndricas o fusiformes y están rodeadas por tejido conectivo individualmente en lugar de en haces[4,7,69,84,89]. Las CP humanas son aparentemente más grandes que los cardiomiocitos[61]. A nivel subendocárdico, las CP en humanos se han descrito como cilíndricas o fusiformes y su tamaño es de aproximadamente 10 a 46 µm[2,69,84]. Se ha reportado que las CP poseen un gran número de filamentos intermedios (FI) en su citoplasma. Las CP en el grupo II tales como corazones humanos, de mono y de perro exhibieron una reacción positiva más fuerte al FI desmina en comparación con las células del miocardio. Se encontró que las CP que mostraban una fuerte reacción positiva corrían en las trabéculas musculares del ventrículo izquierdo (VI) en corazones humanos y de ratón[84].

El sistema de Purkinje en ungulados hace que el haz principal del HH se bifurque en la parte más inferior del *septum membranaceum* y cada rama corre oblicuamente hacia abajo a través del miocardio hacia la superficie subendocárdica del corazón. La rama derecha se vuelve subendocárdica en la base de la banda moderadora; la izquierda, a gran distancia por encima de los músculos papilares. La ramificación secundaria se produce a ambos lados del tabique por debajo del punto donde las ramas se vuelven subendocárdicas, y a partir de esta ramificación se forma una red subendocárdica. El constituyente esencial del tronco principal, sus ramas y la red subendocárdica es la CP[5]. Las preparaciones histológicas con hematoxilina-eosina y tricrómico de Masson identifican la presencia de las FP

en ungulados (como cerdos y rumiantes) a nivel subendocárdico e intramiocárdico, que están rodeados por vainas de fibras reticulares[4,5,7,69,83,90]. En los ungulados, existe una vaina de tejido conectivo que rodea las FP que consisten en haces de 2-8 células ovaladas. Las CP en ungulados son considerablemente más grandes que los cardiomiocitos ventriculares[4,7,69,84,89]. Por otra parte, los estudios inmunohistoquímicos han demostrado que las CP del corazón bovino poseen un gran número de FI en todo el citoplasma[91,92]. En observaciones microscópicas ópticas de corazones de ovejas, se demostró una reacción positiva más fuerte de las CP para el anticuerpo anti-desmina en comparación con los cardiomiocitos[84].

El sistema de Purkinje en el perro se distribuye de forma muy similar al humano a nivel subendocardico[5]. Las CP en perros son solo un poco más grandes que los cardiomiocitos[69]. La citoarquitectura de las CP en perros es fundamentalmente similar a la de los humanos[69]. Las CP en el perro muestran una reacción positiva a la desmina más fuerte en comparación con los cardiomiocitos[84].

En los animales pertenecientes al grupo III las CP tienen un diámetro más pequeño que los cardiomiocitos[69]. Una observación sorprendente fue que un tipo celular más pequeño de CP de ratón (grupo III) también mostró una fuerte reacción positiva a la desmina. Así, los tres grupos de CP examinados mostraron una fuerte reacción positiva para el anticuerpo desmina. Los FI positivos para el anticuerpo anti-desmina parecían estar distribuidos por todo el citoplasma de las CP[84].

Desde las ramas derecha e izquierda del HH, las FP son las encargadas de recibir y transmitir el impulso eléctrico al miocardio ventricular para facilitar la contracción, pero también juegan un papel importante en la generación de arritmias ventriculares[13,68]. La taquicardia ventricular (TV) y la fibrilación ventricular (FV) son dos formas típicas de arritmia que ocurren tanto en humanos como en animales[93-96], llevando a investigadores a proponer el uso de corazones ungulados como modelo para estudiar estas patologías en humanos[55].

En los últimos años, los estudios de mapeo y ablación han demostrado que las FP tienen un papel central en la aparición de estas patologías cardíacas y pueden detectarse en pacientes con cardiopatía isquémica y también en corazones estructuralmente normales tanto en humanos como en animales[95-98]. En algunos casos las TV después de un infarto de miocardio tienen circuitos reentrantes mediados por FP: reentrada de rama, reentrada interfascicular, reentrada intrafascicular y TV de Purkinje focal[99-101]. Se ha descubierto que las FP pueden desempeñar un papel importante en el circuito de reentrada de la TV postinfarto caracterizada por complejos QRS estrechos[100,102]. Las CP juegan un papel crucial en la excitación ventricular, ya que garantizan un patrón de excitación correcto y, por tanto, una secuencia sincronizada de contracción cardíaca. Cada vez hay más pruebas que identifican a las CP como un desencadenante importante de arritmias[103,104].

El acoplamiento eléctrico cardíaco está regulado por uniones Purkinje-miocardio (UPM), que están formadas por canales transmembrana y cuyo componente principal son las conexinas[104,105]. Estas moléculas permiten la difusión de pequeñas moléculas e iones a través de sus gradientes electroquímicos. Las UPM actúan como sitios de baja resistencia para la propagación del impulso eléctrico[106-109]. Las UPM son las uniones entre las CP y cardiomiocitos ventriculares, en las que se han descrito tres variantes: contacto a través de cuerpos celulares (CTCC), contacto a través de prolongaciones celulares (CTPC) y contacto a través de células transicionales (CTCT)[10,107]. Hasta ahora se han identificado catorce conexinas de mamíferos, cuatro de las cuales, Cx43, Cx40, Cx45 y Cx37, se conocen por expresarse en el corazón[105,110]. Se cree que la expresión diferencial de estas conexinas confiere propiedades eléctricas pasivas distintivas a regiones específicas del corazón[105]. Cx43 se ha establecido ampliamente como la conexina principal de los miocitos ventriculares en una amplia gama de especies de mamíferos, y también es abundante en el miocardio auricular[105,111]. Cx40, por el contrario, se expresa típicamente en abundancia en los cardiomiocitos del sistema de conducción ventricular donde está implicado en la conducción rápida[105,106,109].

Algunos investigadores han estudiado los sitios de las UPM con registros de microelectrodos intracelulares, con mapas electro-anatómicos[112,113] y con mapas de superficie extracelular[114-116]. Este proceso parece involucrar a un grupo de células que parecen estar especializadas con respecto al curso temporal de su fase de aumento del potencial de acción. Estas células, que parecen estar interpuestas entre las CP y los cardiomiocitos en los sitios de las UPM, fueron denominadas CT[117]. Tal conexión entre una CP y una CT garantiza una alta resistencia de acoplamiento y una conducción rápida en el miocardio activo. Esta disposición está bien marcada en conejos y cerdos[118]. Por el contrario, no se detectaron CT en corazones humanos y de bovinos[2]. En perros, se demostró que existía una distribución espacial de los sitios de las UPM en los músculos papilares, localizadas preferentemente hacia la base del músculo[119,120].

D. HIPÓTESIS DE TRABAJO Y OBJETIVOS

Nuestra hipótesis general de trabajo es que en la actualidad poco se conoce acerca de la morfometría del sistema de conducción y de las uniones Purkinje-miocardio entre las células eléctricas y los cardiomiocitos de trabajo tanto en humanos como animales. Este conocimiento conllevaría a que los clínicos obtuvieran herramientas para poder determinar que parámetros normales existen en el sistema de conducción y así evaluar cómo prevenir las arritmias cardiacas. Esta relación se concreta con los siguientes objetivos:

1. Caracterizar la estructura histológica y morfométrica de los nodos sinoatrial, atrioventricular y sus componentes en humanos y cerdos, con el propósito de encontrar similitudes entre las dos especies que permitan utilizar el cerdo como modelo experimental cardíaco y lograr avances en la prevención de arritmias supraventriculares.
2. Evaluar los componentes del nodo atrioventricular desde el punto de vista histológico y morfométrico implicados en los trastornos de la conducción atrioventricular en humanos, cerdos, caballos y perros.
3. Describir las variaciones regionales de las células de Purkinje y sus uniones con el miocardio mediante estudio histológico y morfométrico comparativo en cerdos y humanos, que sirva para comprender la aparición de arritmias ventriculares.

E. METODOLOGÍA Y RESULTADOS DE LOS ARTÍCULOS PUBLICADOS

1. Morfometría e histología comparada de los nodos sinoatrial y atrioventricular en humanos y cerdos y su relevancia en la prevención de arritmias nodales

1.1 Objetivo

Evaluar y comparar las características histológicas y morfométricas de los nodos NSA y NAV en humanos y cerdos.

1.2 Resumen del método utilizado

Se analizaron 10 corazones de varones humanos adultos y 10 corazones de cerdo machos. En humanos y cerdos, la región del NSA se aisló de la zona de unión de la vena cava superior (vena cava craneal en animales) y el atrio derecho y posteriormente se seccionó longitudinalmente en rodajas de 5 mm de espesor. El NAV se aisló de la zona entre el orificio de salida del seno coronario y la unión del velo septal de la válvula tricúspide. También se seccionó en serie de la misma manera, y el bloque de tejido extraído para el estudio incorporó toda la unión de los tabiques interauricular e interventricular. Todas las muestras se fijaron en una solución de formaldehído al 5% y se incluyeron en parafina. Se realizaron cortes histológicos de 5 µm de espesor con un micrótomo y se tiñeron con hematoxilina-eosina (H-E) y tricrómico de Masson.

Las muestras se evaluaron con un microscopio óptico Leica DMD108 (Leica Microsystems, Wetzlar, Alemania). Se tomaron 380 micrografías de tejido del NSA y NAV para el análisis morfométrico a 1,6X, 4X, 10X y 20X. Medimos en los nodos: área, eje mayor, eje menor, densidad media, diámetro máximo, diámetro mínimo, perímetro, radio máximo, radio mínimo, redondez, longitud y ancho. Dentro de los nodos cuantificamos el número total de células y el área que ocupan, así como el área, diámetro máximo, diámetro mínimo, diámetro medio y redondez de las células P, CT y cardiomiocitos periféricos

en cada uno de los nodos (60 células para los tipos P, CT y cardiomiocitos). Se determinó el área, diámetro máximo y mínimo de la rama arterial nodal a 4X. Para visualizar los vasos sanguíneos en los nodos, utilizamos tinción inmunohistoquímica CD31 y se determinó el área, el diámetro máximo y mínimo y el número de vasos. Además, se realizó una tinción inmunohistoquímica con el clon D33-IR606 de anti-desmina humana (DAKO Corporation®) para visualizar los miofilamentos intermedios (desmina) presentes en las células de los nodos y compararlos con los cardiomiocitos circundantes. El estudio morfométrico computarizado fue realizado por el software Image-ProPlus 7.1 (Media Cybernetics, Silver Spring, MD, EE. UU.). Se calibró cada micrografía y se recogió el área total del tejido en μm^2 después de una selección manual basada en histogramas cromáticos.

Análisis estadístico

Las estadísticas descriptivas, representaciones gráficas y contraste de hipótesis se realizaron con el software SPSS 20 (SPSS, Chicago, IL, EE. UU.) y Microsoft Excel 2013. Las variables continuas se expresaron como media e intervalo de confianza del 95%. El nivel considerado como indicativo de significación estadística fue $p<0,05$. Se calcularon los estadísticos descriptivos para cada parámetro morfométrico y se realizó la prueba de normalidad de Kolmogorov Smirnov para cada muestra. En el caso de las variables cuantitativas se eligió la prueba U Mann-Whitney. Los datos se expresaron como desviación estándar media (DE) para todas las longitudes medidas.

1.3 Resultados

Determinamos el perfil morfométrico del NSA y NAV y sus componentes. Valoramos: área, eje mayor y menor, densidad media, diámetro máximo y mínimo, perímetro, máximo y radio mínimo, redondez, largo y ancho. En ellos se determinó los promedios y desviación estándar (Tablas 1 y 2).

Nodo Sinoatrial

El NSA en humanos es una estructura compacta, rodeada de gran cantidad de tejido adiposo. No está delimitado por una cápsula de tejido conectivo denso irregular, por lo que su identificación se realiza por las pocas células que se reconocen en algunas secciones del nodo. Las células del interior están unidas y rodeadas por cordones de tejido conectivo. El NSA tuvo una longitud entre 1,7 y 7,4 mm y un ancho entre 1 y 2,6 mm, lo que demuestra que su forma es ovoide (Figura 1a, 2a, 3a).

Tabla 1. Significancia estadística de los parámetros medidos en las células de los nodos sinoatrial y atrioventricular en humanos y cerdos.

Nodo	Parámetro	Humanos. µm (DE)	Cerdos. µm (DE)	Valor p
Nodo Sinoatrial	Diámetro máximo células P	9,9 (2,5)	8,9 (1,5)	0,026
	Área células T	825,7 (423)	508 (463,2)	0,001
	Diámetro medio células T	34,5 (8,2)	25,8 (10)	0,001
	Diámetro máximo células T	69,6 (22,4)	49,1 (21,8)	0,001
	Redondez células T	3,1 (1,2)	2,3 (0,6)	0,001
	Área Cardiomiocitos	77,4 (22,6)	101,6 (27)	0,023
	Diámetro medio cardiomiocitos	9,5 (1,4)	10,9 (1,4)	0,023
	Diámetro máximo cardiomiocitos	11,1 (1,7)	12,5 (1,7)	0,029
	Diámetro mínimo cardiomiocitos	8,1 (1,5)	9,5 (1,4)	0,027
Nodo Atrioventricular	Área cellular	20.348,2 (3.672)	933,5 (313,1)	0,008
	Número de células	1.408 (202,4)	252 (79,2)	0,008
	Área células P	17,8 (5,3)	377,4 (151,2)	0,001
	Diámetro medio células P	4,4 (0,7)	21 (4)	0,001
	Diámetro máximo células P	5,2 (0,9)	25,3 (7)	0,001
	Diámetro mínimo células P	3,7 (0,7)	17,6 (3)	0,001
	Redondez células P	1,03 (0,05)	1,16 (0,07)	0,001
	Área células T	573,2 (323,7)	715,2 (389,6)	0,029
	Diámetro medio células T	28,2 (7,1)	31,4 (7,2)	0,045
	Diámetro mínimo células T	10,9 (3,2)	13,1 (3,5)	0,004
	Área cardiomiocitos	70,8 (41,5)	100,5 (24,7)	0,047
	Diámetro medio cardiomiocitos	8,8 (2,7)	10,8 (1,4)	0,045

DE: desviación estándar. Las áreas se midieron en μm^2.

Según nuestro análisis morfométrico, podemos diferenciar dos tipos de células en el nodo que corresponden a las células P y CT, además de los cardiomiocitos circundantes (Figura 4).

Tabla 2. Valores medidos en los nodos sinoatrial, atrioventricular y sus células que muestran similitud en humanos y cerdos.

Nodo	Parámetro	Humanos. µm (DE)	Cerdos. µm (DE)	Valor p
Nodo Sinoatrial	Área	1.584.872,5 (996.466,4)	1.525.082,5 (756.809,5)	0,88
	Eje mayor	1.997,8 (552,4)	2.052,2 (661,7)	1,00
	Eje menor	1.005,1 (412)	949 (190,9)	0,57
	Densidad media	0,24 (0,06)	0,30 (0,12)	0,39
	Diámetro máximo	2.017,5 (517,6)	2.058,8 (586,5)	0,777
	Diámetro mínimo	915,6 (398,4)	827 (169,3)	0,48
	Perímetro	5.301,8 (1.416,9)	5.228,7 (1.398)	0,88
	Radio máximo	1.118,7 (289,7)	1.115,9 (355,3)	0,77
	Redondez	1,81 (0,94)	1,47 (0,13)	0,57
	Longitud	3.626,3 (552,8)	2.069,7 (742,1)	0,77
	Ancho	1.531,4 (390,8)	850,1 (240,7)	0,48
	Diámetro máximo arteria	765,1 (229,1)	840,3 (577,5)	0,86
	Diámetro mínimo arteria	465 (152,7)	414,2 (241,3)	0,73
	Área células P	57,9 (30,3)	49,7 (14,8)	0,089
	Diámetro medio células P	8,1 (1,9)	7,5 (1,1)	0,067
	Diámetro mínimo células P	6,3 (1,8)	6,4 (1,1)	0,382
	Redondez células P	1,14 (0,2)	1,07 (0,04)	0,295
	Diámetro mínimo células T	13,8 (5)	11,1 (4,9)	0,74
	Redondez cardiomiocitos	1,09 (0,03)	1,09 (0,02)	0,570
Nodo Atrioventricular	Área	1.617.321 (381.970,1)	1.541.833,3 (443.166,8)	0,57
	Eje menor	1.048,5 (287,2)	1.007,2 (178,3)	0,70
	Densidad media	0,23 (0,03)	0,24 (0,04)	0,70
	Diámetro máximo	2.227,5 (404,7)	2.080,3 (410,6)	0,34
	Diámetro mínimo	915,9 (272,4)	916,4 (173,9)	0,70
	Radio máximo	1.168,8 (511,7)	1.175,2 (197)	0,85
	Redondez	1,98 (0,61)	1,64 (0,29)	0,34
	Longitud	2.241 (349,3)	1.865,2 (408,8)	0,18
	Ancho	1.003,2 (169,5)	879,1 (194,2)	1,00
	Diámetro máximo células T	59,7 (26,7)	63,7 (24,8)	0,061
	Redondez células T	2,85 (1,19)	2,7 (1,21)	0,337
	Diámetro máximo cardiomiocitos	10,3 (3,5)	13,1 (2)	0,081
	Diámetro mínimo cardiomiocitos	7,4 (2,1)	9,1 (1,2)	0,116
	Redondez cardiomiocitos	1,08 (0,05)	1,11 (0,06)	0,896

DE: desviación estándar. Las áreas se midieron en μm^2.

En ellos se midieron diferentes parámetros como área, diámetro máximo, diámetro mínimo, diámetro medio y redondez (Tablas 1 y 2).

En el NSA humano, las células P analizadas fueron pequeñas (36,4 +/- 9,8 µm) (Figura 4a, e), su citoplasma fue más pálido que en los cardiomiocitos que rodean el nodo, su forma puede ser redondeada u ovalada, localizada hacia el centro y rodeando la RNS; las células nodales se agrupan en fascículos interconectados colocados sobre un fondo de matriz fibrosa. Son células con un solo núcleo redondeado y oscuro.

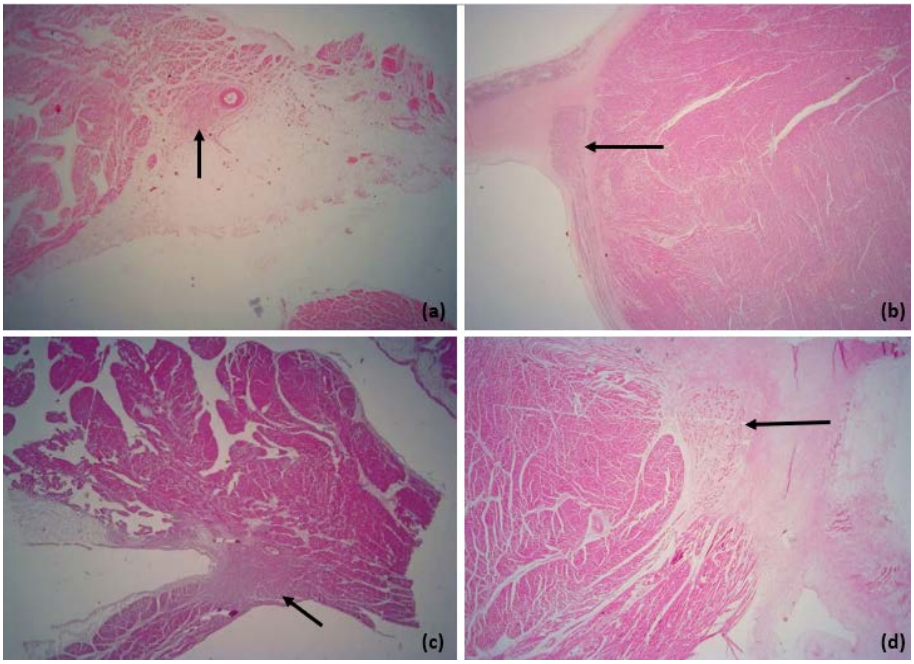

Figura 1. Localización de los nodos sinoatrial y atrioventricular de humanos y cerdos. Las flechas indican la posición histológica del nodo sinoatrial en humanos (a) y cerdos (c), así como la ubicación del NAV en humanos (b) y en cerdos (d). Tinción hematoxilina-eosina. Magnificación 1,6X.

En el ser humano, las CT presentaron un citoplasma pálido como el de las células P (Figura 4c, e), alargadas, muy pocas en comparación con las células P y ubicadas en la periferia. Presentaron un único núcleo oscuro y en determinadas zonas del nodo se organizaron formando estructuras fibrosas que se unen con las CT adyacentes.

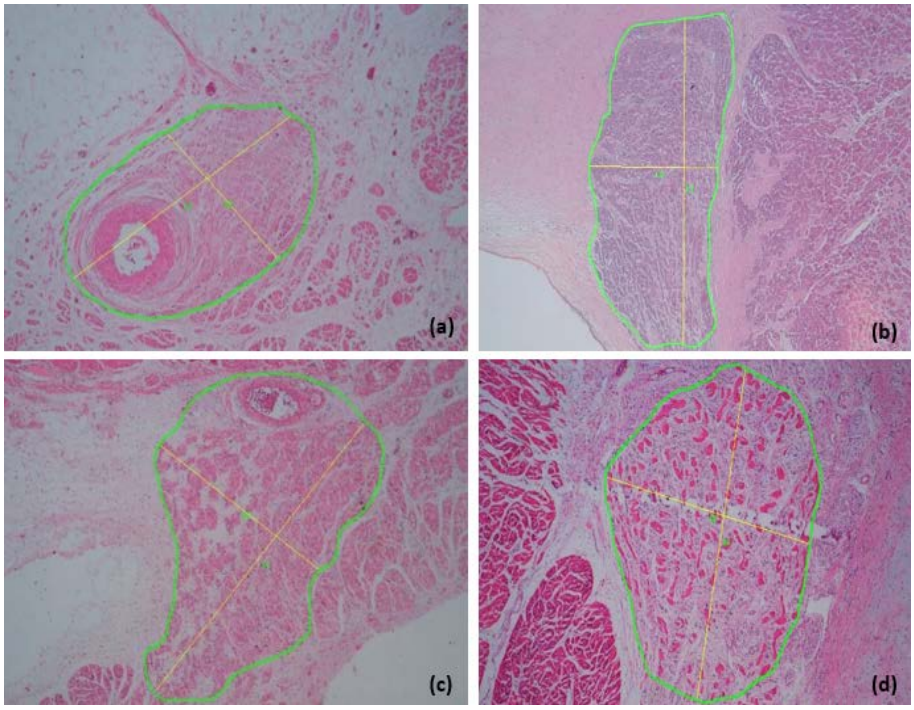

Figura 2. Morfometría de los nodos sinoatrial y atrioventricular de humanos y cerdos. El análisis morfométrico se realizó sobre muestras teñidas con hematoxilina-eosina en el nodo sinoatrial de humano (a) y cerdo (c) y en el nodo atrioventricular de humano (b) y cerdo (d). Magnificación 4X.

La RNS en humanos es una rama arterial que se encuentra a menudo cerca del centro del nodo y es responsable de proporcionar nutrientes, aunque a veces la rama arterial se desplaza hacia uno de sus polos. Para visualizar y medir correctamente los parámetros de los vasos sanguíneos de los nodos cardíacos en humanos, utilizamos tinción inmunohistoquímica con anti-CD31 (Tabla 3). En el NSA solo se observaron algunas fibras nerviosas.

La distribución del tejido conectivo, del tejido adiposo y de las células dentro del NSA en cerdos es similar al del humano. La longitud del NSA varía entre 1,3 y 3 mm y su ancho es de 0,6 a 1,1 mm, lo que indica que este nodo también tiene una forma ovoide (Figura 1c, 2c, 3c).

En los cerdos, las células P (Figura 4b, f) tienen las mismas características que en los humanos, excepto que las células pueden tener uno o dos núcleos.

En los cerdos, las CT (Figura 4d, f) presentan una distribución similar a la de los humanos.

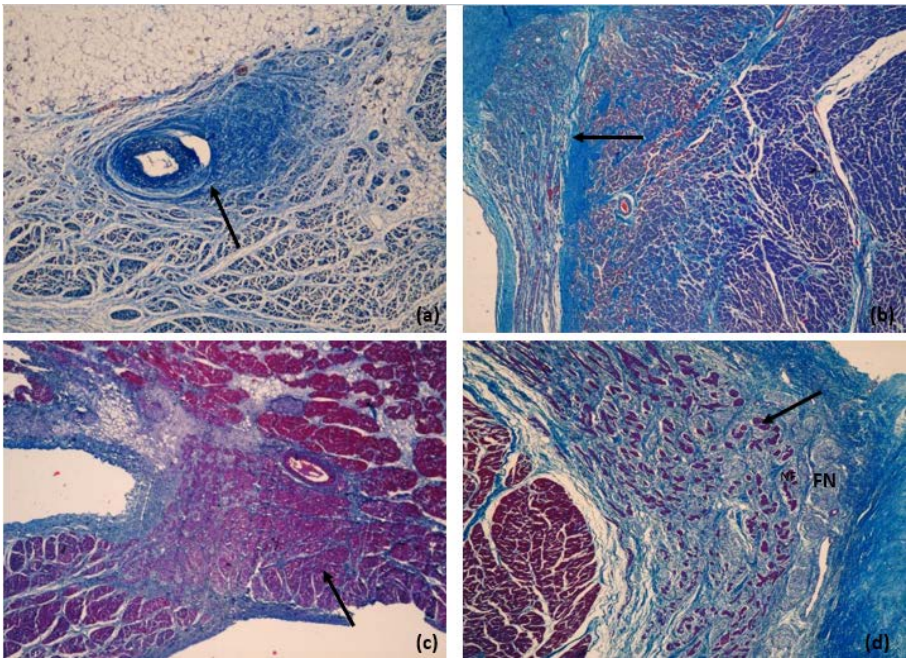

Figura 3. Detalle histológico del nodo sinoatrial humano (a) y de cerdo (c), así como del nodo atrioventricular de humano (b) y cerdo (d) teñido con tricrómico de Masson, indicando la posición de los nodos con flechas. FN: fascículo nervioso. Magnificación 4X.

En los cerdos la RNS es más común encontrarla desplazada hacia los polos y raramente en el centro del NSA. El nodo solo contiene fibras nerviosas en la periferia.

Encontramos que el diámetro máximo de las células P en el NSA en los humanos fue significativamente más grande que en los cerdos ($p=0,026$). En el análisis morfométrico pudimos determinar que las células P fueron redondeadas porque el parámetro de redondez es cercano a 1, siendo similar en ambas especies.

En las células T encontramos diferencias estadísticamente significativas en el diámetro máximo y medio ($p<0,001$ ambos valores) y en el área ($p=0,001$),

siendo mayor en humanos que en cerdos. Las CT se describen como alargadas, porque en el análisis morfométrico el parámetro se aleja de 1, siendo más planas en humanos que en cerdos (p=0,001).

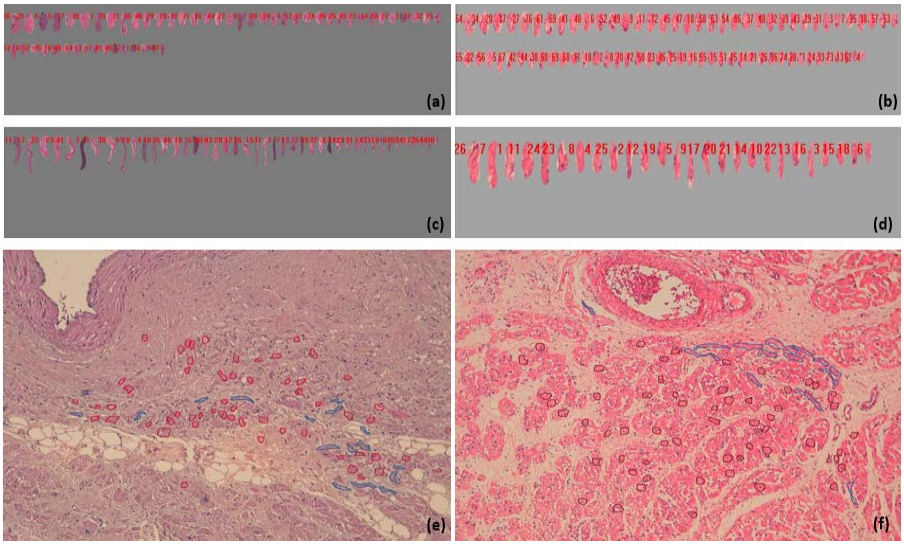

Figura 4. Células del nodo sinoatrial de humanos y cerdos teñidas con hematoxilina-eosina. Morfometría de células P (a) y células T (c) en humanos ordenadas de mayor a menor. Detalle histológico de las células P (rojo) y T (azul) en humanos (e). Morfometría de células P (b) y células T (d) en cerdos ordenadas de mayor a menor. Estructura histológica de las células P (rojo) y T (azul) en cerdos (f). Magnificación 10X.

Tabla 3. Resumen global de los parámetros morfométricos de los vasos sanguíneos de los nodos sinoatrial y atrioventricular en humanos. Inmunotinción con anti cuerpos frente a CD31.

Nodo	Área vasos mm^2 (DE)	Diámetro máximo mm (DE)	Diámetro mínimo mm (DE)	Número de vasos
Nodo Sinoatrial	0,00010 (0,00043)	0,010 (0,013)	0,006 (0,005)	517
Nodo Atrioventricular	0,00018 (0,00055)	0,015 (0,020)	0,008 (0,006)	359

DE: desviación estándar.

En los cardiomiocitos se observó que el área y los diámetros fueron significativamente mayores en los cerdos que en los humanos (p=0,023 para el área y el diámetro medio; p=0,029 para el diámetro máximo y p=0,027 para el diámetro mínimo).

En las ramas arteriales que irrigan los nodos en humanos y cerdos se midió el área, diámetro máximo, diámetro mínimo y el grosor del vaso nodal (Tablas 1 y 2). Se encontraron diferencias estadísticamente significativas en el área de la RNS (p=0,042), siendo mayor en humanos que en cerdos.

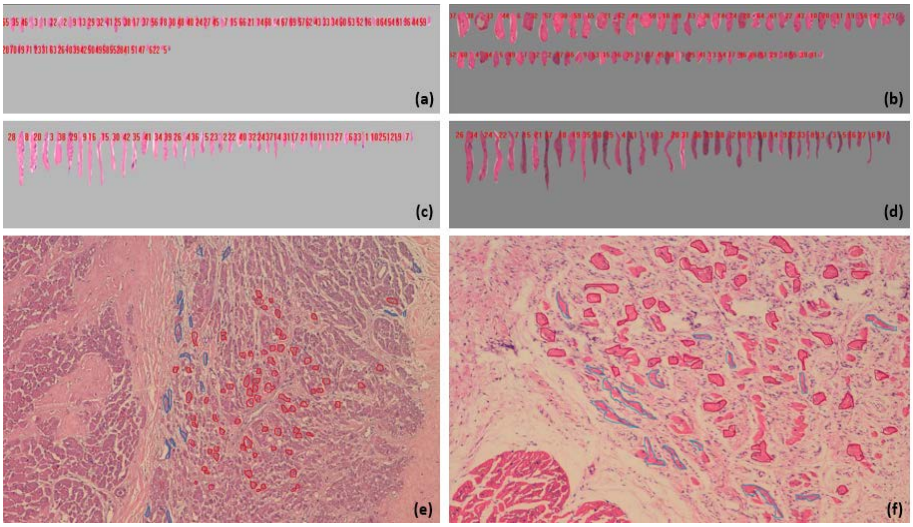

Figura 5. Células del nodo atrioventricular de humanos y cerdos teñidas con hematoxilina-eosina. Morfometría de células P (a) y células T (c) en humanos ordenadas de mayor a menor. Detalle histológico de las células P (rojo) y T (azul) en humanos (e). Morfometría de células P (b) y células T (d) en cerdos ordenadas de mayor a menor. Estructura histológica de las células P (rojo) y T (azul) en cerdos (f). Magnificación 10X.

Nodo Atrioventricular

En el NAV en humanos, hubo abundante tejido adiposo alrededor del nodo. Está delimitado por una fina cápsula de tejido conectivo denso irregular. El NAV tuvo una longitud de 1,9 a 2,6 mm y un ancho que varía entre 0,6 y 1,5 mm, característica que le proporciona una forma ovoide (Figura 1b, 2b, 3b).

En el NAV humano, las células P (18,20 +/- 10,80 µm) fueron más pequeñas que los cardiomiocitos (23,13 +/- 7.80 µm) (Figura 5a, e), oscuras, redondeadas u ovaladas, ubicadas en el centro y con un núcleo redondeado y oscuro, aunque en ocasiones se observaron células multinucleadas. Las CT fueron pálidas (Figura 5c, e), ubicadas periféricamente, alargadas y en ciertas áreas del margen del nodo están unidas, mostrando un aspecto lineal. Estas células tuvieron un núcleo oscuro y alargado. Los cardiomiocitos que se ubican en la periferia del nodo estaban orientados transversalmente. Mostraron un tamaño intermedio (23,13 +/- 7.80 µm), más grande que las células P, oscuras y con formas que varían de redondeadas a ovaladas. Se pueden encontrar en grupos individuales de células.

La RNAV en humanos no es claramente visible y cuando se observa, se localiza en la porción terminal del nodo. Para visualizar y medir correctamente los parámetros de los vasos sanguíneos en el NAV en humanos, utilizamos tinción inmunohistoquímica con anticuerpos frente a CD31 (Tabla 3) (Figura 6a, b). En el NAV no se observaron fibras nerviosas en la periferia ní dentro del nodo.

En los cerdos, no hay presencia de cápsula de tejido conectivo denso irregular alrededor del NAV. Las células están rodeadas de abundante tejido conectivo y pueden distinguirse fácilmente mediante observación histológica. La longitud del NAV varía entre 1,4 y 2,6 mm y su ancho entre 0,5 y 1 mm, lo que indica que este nodo también tiene una forma ovoide (Figura 1d, 2d, 3d). Lo cual se comprueba con los valores de redondez obtenidos en el nodo (1,98).

En los cerdos, a diferencia de lo que se observa en los humanos, las células P en el NAV fueron grandes (45,37 +/- 11,48 µm) (Figura 5b, f), con un citoplasma ligeramente más pálido que en los cardiomiocitos y con un solo núcleo. Las CT (Figura 5d, f) tuvieron las mismas características que se describieron para los humanos, a diferencia de que estas células tienen un tamaño mucho mayor (63,77 +/- 24,88 µm). En los cerdos, los cardiomiocitos son más pequeños (27,56 +/- 8,68 µm) que las células P.

La RNAV en cerdos se observa pocas veces y cuando está presente se localiza en la porción terminal del nodo. También tiene abundantes fibras nerviosas tanto en la periferia como dentro del nodo (Figura 3d).

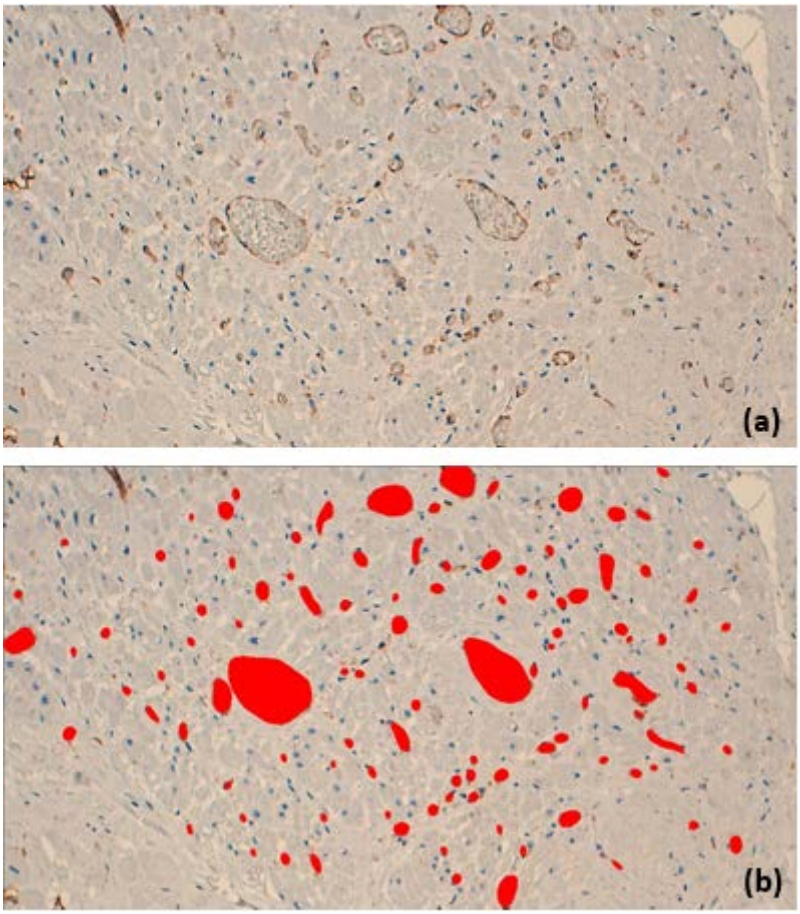

Figura 6. Inmunotinción con anticuerpos frente a CD31 del nodo atrioventricular en humanos. (a) Indica la visualización de los vasos con la inmunotinción; (b) Se observan los vasos sanguíneos dibujados con el programa de morfometría. Magnificación 20X.

En el NAV, el área celular y el número de células fueron significativamente mayores en humanos que en cerdos (p=0,008). La descripción del perfil morfométrico realizada en este estudio la resumimos en la tabla 4. Observamos que la redondez de los nodos en ambas especies se aleja de un valor cercano a 1, lo que indica que su forma es alargada u ovoide.

En el NAV, encontramos que las células P muestran diferencias estadísticamente significativas en el área y los diferentes diámetros (p=0,001 para todos los valores) siendo mayores en cerdos que en humanos.

Tabla 4. Perfil morfométrico de los nodos sinoatrial y atrioventricular en humanos y cerdos.

Parámetro	Humanos		Cerdos	
	Nodo sinoatrial. µm ($\bar{X}$)	Nodo atrioventricular. µm ($\bar{X}$)	Nodo sinoatrial. µm ($\bar{X}$)	Nodo atrioventricular. µm ($\bar{X}$)
Radio máximo	995-1.148 (1.071)	1.074-1.493 (1.283)	1.023-1.221 (1.122)	1.129-1.293 (1.211)
Radio mínimo	406-540 (473)	211- 304 (257)	313-444 (378)	358-457 (407)
Redondez	1,16-1,74 (1,45)	1,80-2,45 (2,12)	1,35-1,59 (1.47)	1,53-1,72 (1,62)

($\bar{X}$): media.

En el análisis morfométrico pudimos determinar que las células P fueron redondeadas porque su parámetro de redondez es cercano a 1, pero se encontró que eran más redondas en humanos que en cerdos (p=0,001). En las células T, observamos que el área (p=0,029), el diámetro mínimo (p=0,004) y el diámetro medio (p=0,045) fueron significativamente mayores en los cerdos que en los humanos. Se encontraron diferencias estadísticas significativas en el área y el diámetro medio de los cardiomiocitos (p=0,047 y p=0,045 respectivamente), siendo mayor en cerdos que en humanos.

Para identificar claramente las células del NSA y NAV, realizamos inmunotinción con anticuerpos frente a desmina en ambas especies, con el fin de visualizar los FI presentes en estas células. Aquí, pudimos ver que en el NSA humano las células se tiñeron levemente en comparación con algunos segmentos adyacentes del miocardio auricular, pero estas células nodales también mostraron mayor positividad que los cardiomiocitos en otros segmentos y a su vez estas células eran más pequeñas que los cardiomiocitos. (Figura 7a, b).

En los cerdos, a nivel del NSA se observó una gran positividad de las células nodales y los cardiomiocitos a los anticuerpos frente a desmina, pero las células nodales presentaron menos positividad que los cardiomiocitos, lo que indica una menor cantidad de FI en las células nodales (Figura 7c, d).

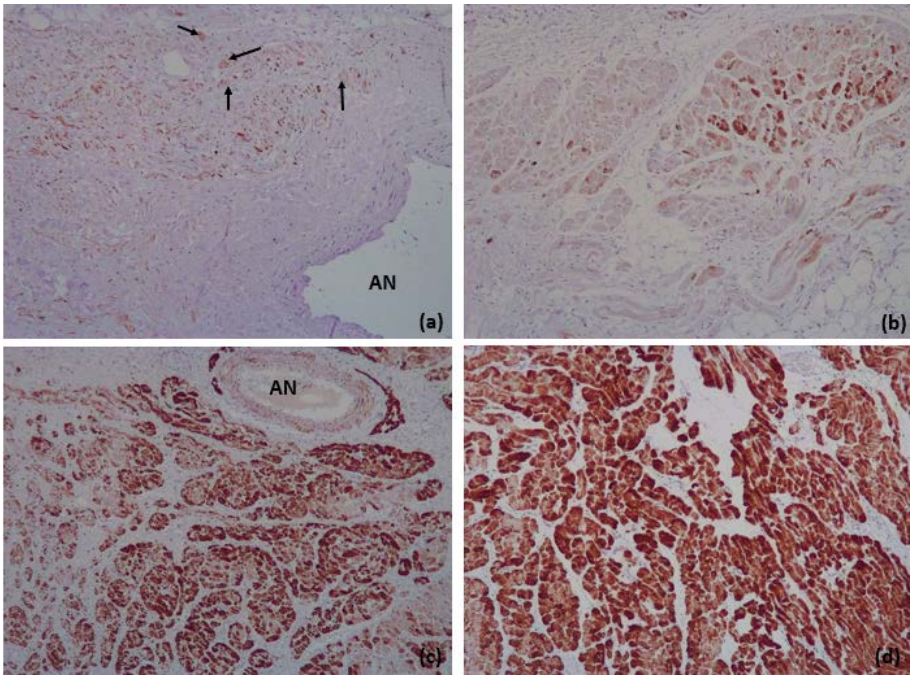

Figura 7. Células del nodo sinoatrial de humanos y cerdos con inmunotinción frente a desmina. (a) células del nodo sinoatrial humano; (b) cardiomiocitos periféricos del nodo sinoatrial humano; (c) células del nodo sinoatrial de los cerdos; (d) cardiomiocitos periféricos del nodo sinoatrial del cerdo. AN: arteria nodal. Las flechas indican las células P. Magnificación 10X.

Tabla 5. Perfil morfométrico de las células de los nodos sinoatrial y atrioventricular en humanos y cerdos, determinando el intervalo de mayor presentación y su media.

Especie	Parámetro	Nodo Sinoatrial (µm)			Nodo Atrioventricular (µm)		
		P	T	CM	P	T	CM
Humanos	D. máx.	9-11	57-75	10-12	4,7-5,4	45-69	8-12
	$\bar{X}$	(10)	(66)	(11)	(5)	(57)	(10)
	D. mín	5-7	11-14	7.5-9	3,5-4	9-11	6 – 9
	$\bar{X}$	(6)	(12)	(8)	(3,8)	(10)	(8)
	Redondez	1,05-1,12	2,35-3,13	1,07-1,11	1-1,04	2,11-3,10	1,05-1,10
	$\bar{X}$	(1,09)	(2,74)	(1,09)	(1,0.2)	(2,60)	(1,07)
Cerdos	D. máx	8,5-9,5	37-53	12-13	21-28	49-69	12-14
	$\bar{X}$	(9)	(45)	(12,5)	(25)	(59)	(13)
	D. mín	6-7	7-12	9-10	16-19	11-14	8,7-9,3
	$\bar{X}$	(6,5)	(10)	(9,5)	(18)	(12)	(9)
	Redondez	1,05-1,09	1,91-2,44	1,08-1,10	1,12-1,14	1,90-2,84	1,07-1,12
	$\bar{X}$	(1,07)	(2,17)	(1,09)	(1,13)	(2,37)	(1,10)

CM: cardiomiocito. $\bar{X}$: media

En humanos, las células del NAV mostraron mayor reacción a los anticuerpos frente a desmina que los cardiomiocitos, por lo que se observaron más oscuras y pequeñas que los cardiomiocitos auriculares, lo que confirma lo descrito en el perfil morfométrico realizado (Figura 8a, b). En el NAV de cerdos se constató que el gran tamaño (descrito en el estudio morfométrico) y las pocas células presentes en este nodo se observaban fácilmente con anticuerpos frente a desmina, al igual que con Hematoxilina-Eosina y Tricrómico de Masson (Figura 8c, d). El perfil morfométrico detallado de las células nodales y los cardiomiocitos periféricos se resumen en la tabla 5.

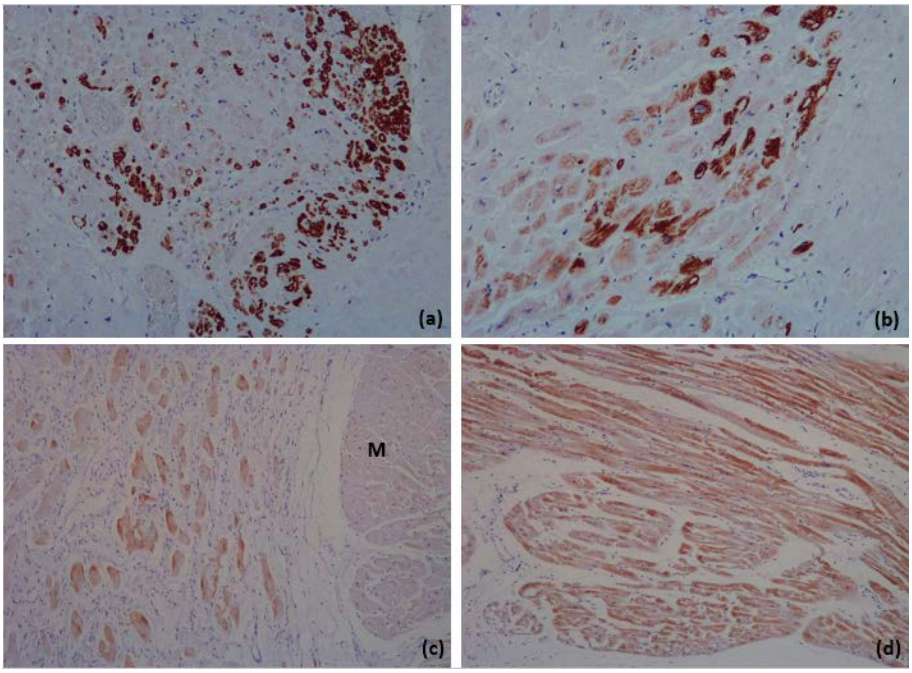

Figura 8. Células del nodo atrioventricular de humanos y cerdos. Inmunotinción con anticuerpos frente a desmina. (a) células del nodo atrioventricular de humanos; (b) cardiomiocitos periféricos del nodo atrioventricular humano. Magnificación 20X. (c) células del nodo atrioventricular de cerdos; (d) cardiomiocitos periféricos del nodo atrioventricular del cerdo. M: cardiomiocitos. Magnificación 10X.

2. Variaciones morfológicas del sistema de conducción en la zona atrioventricular y su relación clínica en diferentes especies

2.1 Objetivo

Evaluar las diferentes variaciones que puedan suceder en el sistema de conducción atrioventricular en diferentes especies.

2.2 Resumen del método utilizado

Se evaluaron diez corazones de varones humanos, ocho corazones de cerdo macho, nueve corazones de caballos machos y cinco corazones de perros machos. Las muestras de estudio no presentaban lesiones ni antecedentes clínicos de patologías cardíacas.

Las muestras obtenidas se fijaron en una solución de formaldehído al 5% y se incluyeron en parafina. En los ejemplares estudiados, en cada corazón, se cortaron cinco muestras longitudinalmente en rodajas de 5 mm de espesor del área atrioventricular. El NAV estaba en el segundo o tercer corte de la zona atrioventricular. Para realizar una reconstrucción tridimensional del NAV, el bloque de parafina que incluía el NAV se cortó íntegramente según el siguiente protocolo: se cortó el NAV completo en niveles histológicos seriados. Se realizó una sección de 5 µm y posteriormente se eliminó 40 µm de la muestra y se realizó otra sección de 5 µm con un micrótomo y se tiñeron con hematoxilina-eosina y tricrómico de Masson. Este protocolo se siguió hasta que se seccionó todo el NAV (Figura 9).

En total se analizaron 300 micrografías con un microscopio óptico Leica DMD108 (Leica Microsystems, Wetzlar, Alemania) tomadas a 1,6X, 4X, 10X, 20X, 40X y 63X. El estudio morfométrico computarizado se realizó mediante el software Image-ProPlus 7.1 (Media Cybernetics, Silver Spring, MD, EE. UU.). En cada micrografía calibrada, se midieron los siguientes parámetros de los diferentes componentes del sistema de conducción atrioventricular para el NAV: área, diámetro máximo, longitud, ancho. Para el tejido conectivo: porcentaje de fibras de colágeno y sustancia fundamental. Para las células P

se midieron área, diámetro máximo, diámetro mínimo, diámetro medio y redondez y para el cartílago se cuantificó área, diámetro máximo, longitud y ancho.

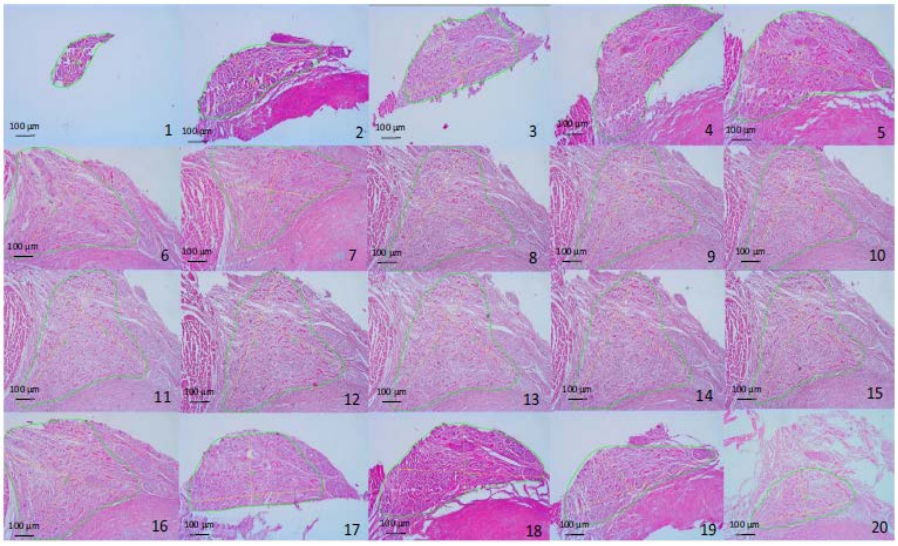

Figura 9. Cortes seriados en una muestra de corazón de cerdo en la zona atrioventricular, donde se indica el perfil del nodo realizado por morfometría. Magnificación 4X.

Análisis estadístico

Se estableció un nivel de corte de $p<0,05$ para significancia estadística. La estadística descriptiva se realizó mediante el software SPSS 20 (SPSS, Chicago, IL, EE. UU.) Y Microsoft Excel 2013. Las variables continuas se expresaron como el promedio de los hallazgos obtenidos. Para cada parámetro se realizó la prueba de normalidad de Kolmogorov-Smirnov y estadística descriptiva. Para las variables cuantitativas cuando se compararon dos grupos independientes y con una muestra mayor a 30 casos se utilizó la prueba T student; cuando la muestra era menor de 30, se eligió la prueba U Mann-Whitney. Para las variables cuantitativas con distribución normal dentro de cada grupo de especies se utilizó la prueba ANOVA, y cuando su distribución fue no paramétrica se eligió la prueba de Kruskal-

Wallis. Para todas las dimensiones medidas, los datos se expresaron como desviación estándar media (DE).

2.3 Resultados

Durante el análisis de la zona atrioventricular de las diferentes especies del estudio se encontró la presencia de cartílago en el EFC en cuatro corazones de cerdos (50%), siete corazones de caballos (77,8%) y tres corazones de perros (60%). Este fue cartílago de tipo hialino y en un caso en cerdos se encontró cartílago de tipo fibroso. En corazones humanos, no encontramos ningún tipo de cartílago en el EFC (Figuras 10, 11, 12, 13).

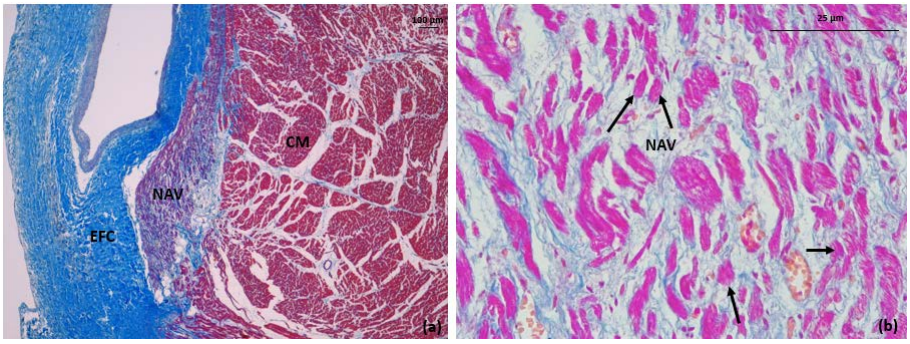

Figura 10. Área atrioventricular de humanos teñida con tricrómico de Masson. (a) Obsérvese la posición del nodo atrioventricular (NAV) en el esqueleto fibroso cardíaco (EFC) en el que no hay cartílago. Magnificación 4X. (b) Las células P están indicadas por flechas, que son oscuras, redondeadas u ovaladas. CM: cardiomiocitos. Magnificación 40X.

En nuestro estudio, usamos la porción compacta del NAV para hacer comparaciones entre casos con cartílago y casos sin cartílago. Después de unir cada una de las secciones realizadas a diferentes muestras para cada corazón a partir de los niveles histológicos seriados, encontramos que la forma del NAV en humanos y cerdos fue ovoide, en perros tiene forma de pirámide. En seis caballos fue una pirámide y en tres cilíndrica.

El tamaño del nodo en cada uno de los casos en las diferentes especies se puede ver en la tabla 6.

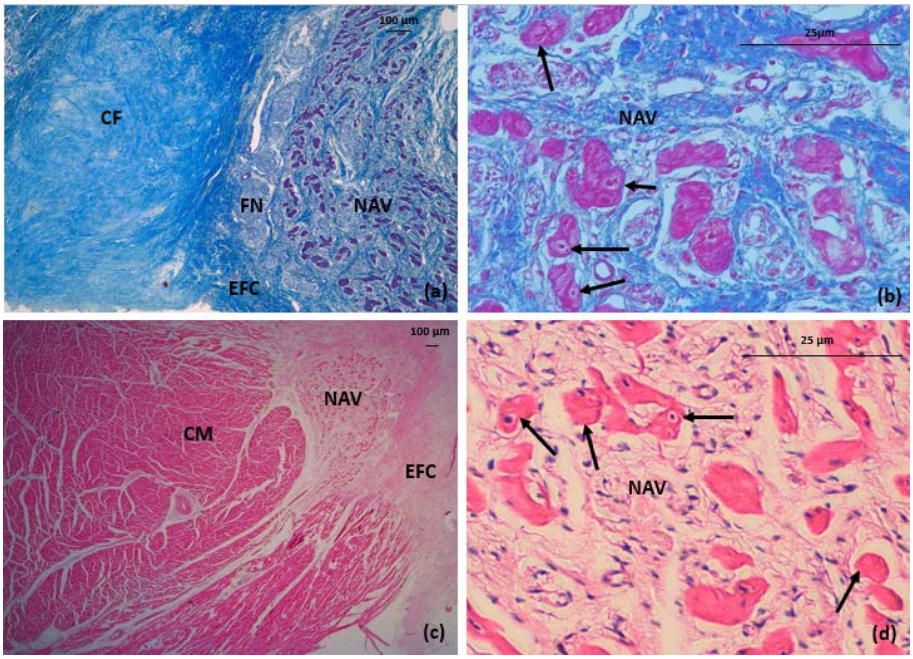

Figura 11. Área atrioventricular de cerdos teñida con hematoxilina-eosina y tricrómico de Masson, mostrando las diferencias entre los casos que presentaron cartílago (a, b) y los que no lo presentaron (c, d). (a) Obsérvese la metaplasia cartilaginosa en el esqueleto fibroso cardíaco (EFC) con cartílago fibroso (CF). Magnificación 4X. (b, d) Las células P están indicadas con flechas, estas células son muy grandes, con un citoplasma ligeramente más pálido que los cardiomiocitos (CM) observado en presencia de metaplasia cartilaginosa (b) y sin metaplasia cartilaginosa (d). NAV: nodo atrioventricular, FN: fibra nerviosa. Magnificación 40X.

Todos los componentes del NAV fueron de mayor tamaño en el grupo de animales sin presencia de cartílago en el EFC (Figura 14a). En los cerdos, el área, el diámetro máximo y el ancho del NAV fueron significativamente mayores (p=0,034 para todos los valores) en los casos que no mostraron cartílago en el EFC.

No se encontraron diferencias estadísticamente significativas entre los diferentes parámetros medidos en el NAV en perros y caballos (Tabla 6).

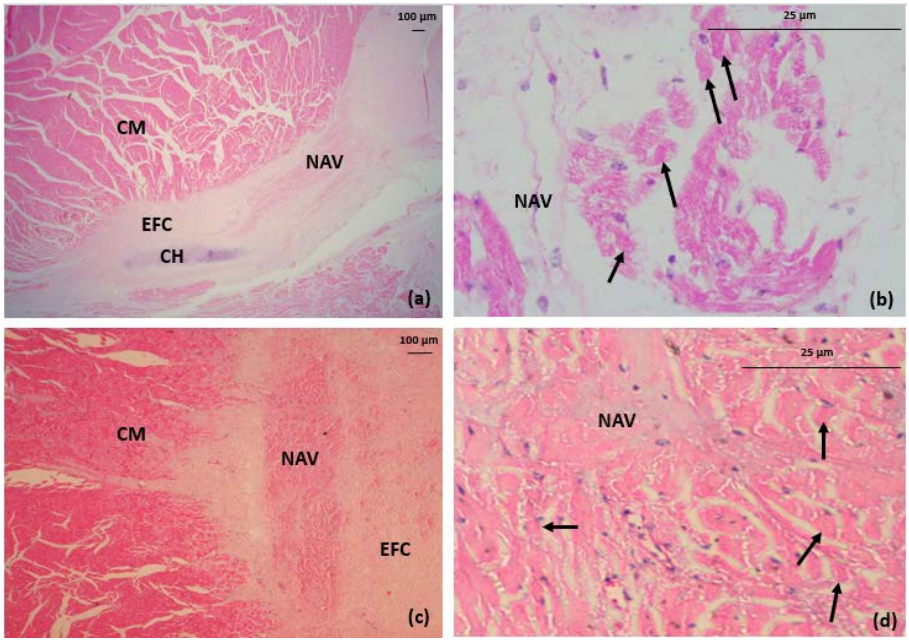

Figura 12. Área atrioventricular de caballos, teñida con hematoxilina-eosina, que muestra las diferencias entre los casos que presentaban cartílago (a, b) y los que no lo presentaban (c, d). (a) Obsérvese la metaplasia cartilaginosa en el esqueleto fibroso cardíaco (EFC) con cartílago hialino (CH). Magnificación 1.6X. Las células P están indicadas por flechas, estas células son pálidas, pequeñas y ovaladas en presencia de metaplasia cartilaginosa (b), magnificación 63X y sin metaplasia cartilaginosa (d). NAV: nodo atrioventricular, CM: cardiomiocitos. Magnificación 40X.

Además, hubo una disminución en el número y tamaño de las células (Figura 14b) y un aumento de las fibras de colágeno (Figura 15, 16) dentro del NAV en cerdos, caballos y perros en los casos que presentaban cartílago, lo que podría disminuir la transmisión del impulso eléctrico a través del NAV (Tabla 6).

Al comparar los parámetros en el NAV de humanos con los de otras especies animales sin presencia de cartílago en el EFC, el porcentaje de sustancia fundamental fue significativamente mayor en perros que en humanos ($p=0,007$) (Figura 15). Las mediciones del NAV humano también se compararon con los casos en los que había cartílago presente en especies animales, observándose que el porcentaje de fibras de colágeno en el NAV

de los cerdos fue significativamente mayor que en los humanos (p=0,023) (Tabla 6).

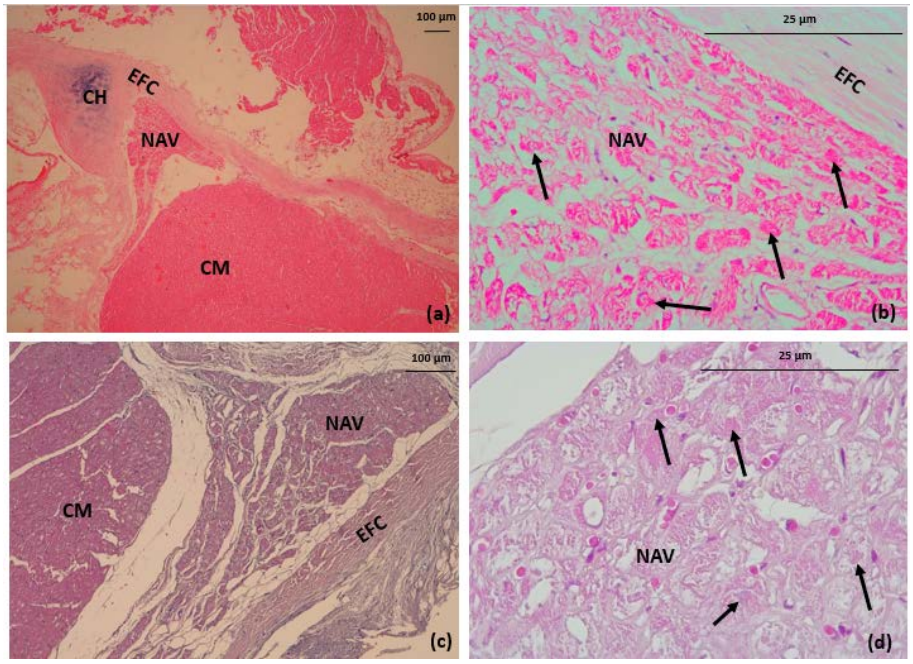

Figura 13. Área atrioventricular de perros teñida con hematoxilina-eosina, que muestra las diferencias entre los casos que tenían cartílago (a, b) y los que no (c, d). (a) Obsérvese la metaplasia cartilaginosa en el esqueleto fibroso cardíaco (EFC) con cartílago hialino (CH). Magnificación 4X. (b, d) Las células P están indicadas por flechas, estas células son grandes, redondeadas, de color similar a los cardiomiocitos (CM) observados en presencia de metaplasia del cartílago (b) y sin metaplasia cartilaginosa (d). NAV: nodo atrioventricular. Magnificación 63X.

Además, entre las especies animales sin cartílago en el EFC, el ancho del NAV fue mayor en cerdos (p=0,017) y en perros (p=0,009) que en caballos. El porcentaje de fibras de colágeno en cerdos (67,15%) dentro del NAV fue significativamente mayor que en perros (p=0,042) y el porcentaje de sustancia fundamental fue mayor en perros que en cerdos (p=0,007) y en caballos (p=0,013) (Tabla 6).

Tabla 6. Valores medios de los parámetros del nodo atrioventricular con o sin cartílago en perros, caballos, cerdos y humanos.

Especie	Área µm² (DE)	Diámetro máximo µm (DE)	Longitud µm (DE)	Ancho µm (DE)	Fibras de colágeno (%)	Sustancia fundament. (%)	Células (%)
Con cartílago							
Perros	413.552 (255.124,3)	1.164 (207,3)	1.419,9 (389,4)	718,3 (92)	27,05	44,49	28,46
Caballos	1.406.634,1 (990.743,5)	2.052,4 (670)	2.231,7 (649,5)	755,4 (319,7)	48,02	11,83	40,15
Cerdos	1.139.876,2 (253.654)	1.705,3 (233,1)	1.853 (663)	687,4 (97,2)	77.35	8,76	13,89
Sin cartílago							
Perros	925.746,3 (105.645,5)	1.304,6 (678,5)	1.895,1 (14,56)	1.176,2 (253)	9,75	63,98	26,27
Caballos	514.321,7 (176.236,4)	1.534,1 (613,7)	1.479,9 (406,6)	490,7 (88,2)	37,24	11,2	51,56
Cerdos	1.844.137,1 (262.267,5)	2.362,4 (242,1)	1.875,6 (199,1)	1.025 (65,1)	65,68	14,29	20,03
Humanos	1.615.290 (380.785,3)	2.223,1 (402,5)	2.150 (348,6)	884,8 (167,3)	38,91	15,47	45,62

DE: desviación estándar.

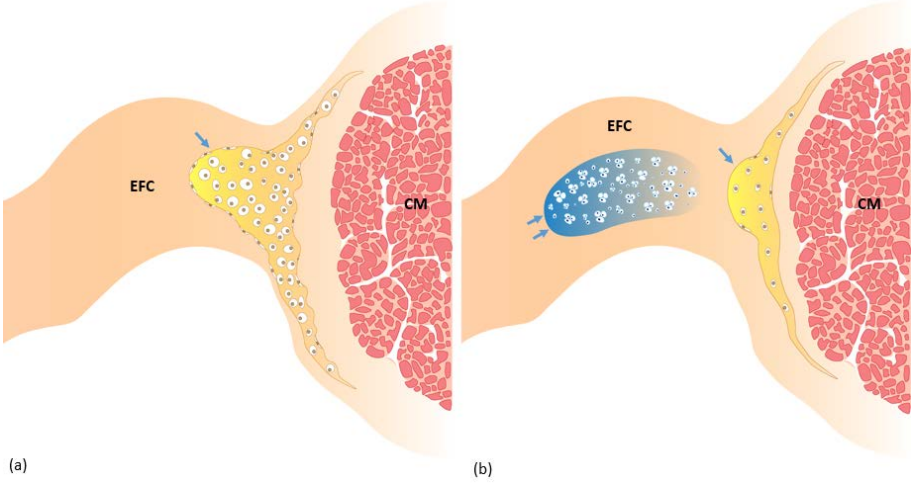

Figura 14. (a) Nodo atrioventricular (flecha simple) en el esqueleto fibroso cardíaco (EFC) con gran número de células. (b) Obsérvese el desplazamiento del nodo atrioventricular (flecha simple) hacia el músculo cardíaco ventricular (CM) y la disminución de su tamaño y del número de células cuando hay presencia de cartílago hialino (doble flecha) en el esqueleto fibroso cardíaco (EFC).

Finalmente, al comparar las tres especies animales con cartílago en la zona atrioventricular, el porcentaje de fibras de colágeno dentro del NAV fue significativamente mayor en cerdos (p=0,001) y caballos (p=0,042) que en perros, con una mayor cantidad en cerdos (74,69%) que en caballos (p=0,010). Así mismo, el porcentaje de sustancia fundamental en el nodo fue mayor en perros que en caballos (p=0,031) y en cerdos (p=0,050) (Tabla 6).

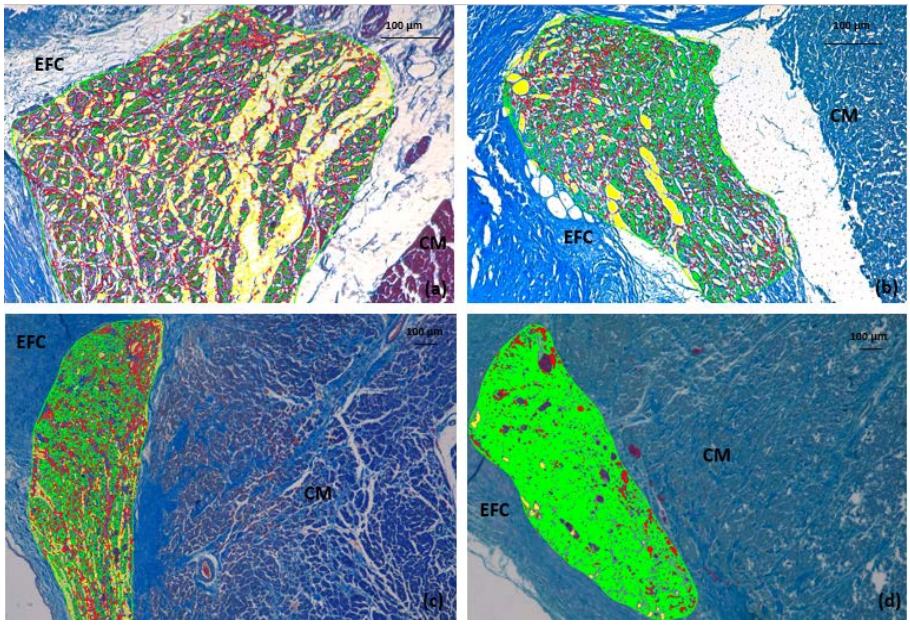

Figura 15. Análisis morfométrico del nodo atrioventricular con y sin metaplasia cartilaginosa en perros (a, b) y humanos (c, d). Tricrómico de Masson. El color rojo indica el porcentaje de fibras de colágeno. Nótese que es más abundante en los casos en que el cartílago está presente en el esqueleto fibroso cardíaco (EFC) (a) de perros a diferencia de los casos en los que no hay cartílago (b, c, d). Magnificación 10X. El color amarillo indica el porcentaje de sustancia fundamental y el verde el porcentaje de células dentro del nodo atrioventricular. En humanos no hay presencia de metaplasia cartilaginosa (c, d). CM: cardiomiocitos, EFC: esqueleto fibroso cardíaco. Magnificación 4X.

La longitud, el área y el diámetro máximo del cartílago en el EFC fueron significativamente mayores en los caballos que en los perros (p=0,011; p=0,039; p=0,023 respectivamente) (Tabla 7).

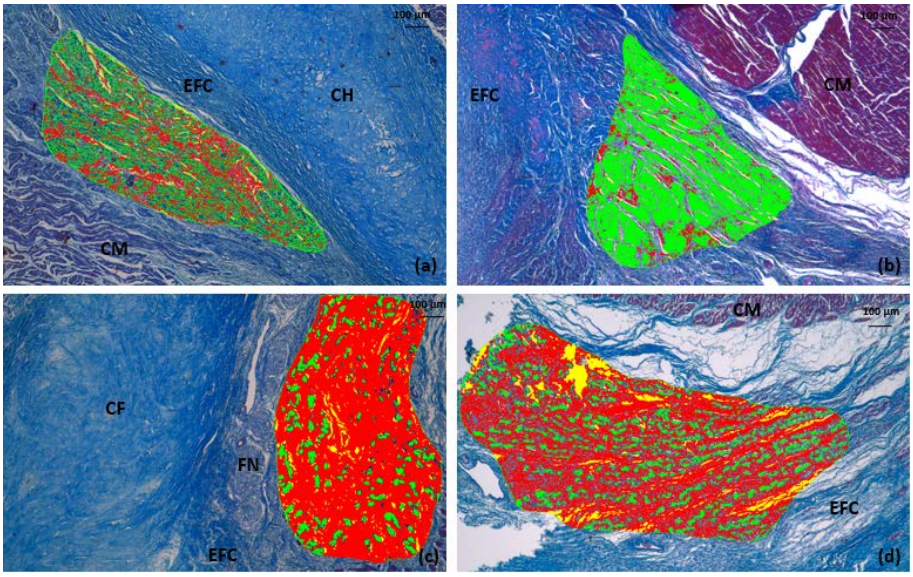

Figura 16. Análisis morfométrico del nodo atrioventricular con y sin metaplasia cartilaginosa en caballos (a, b) y cerdos (c, d). Tricrómico de Masson. El color rojo indica el porcentaje de fibras de colágeno. Nótese que es más abundante en los casos en que el cartílago está presente en el esqueleto fibroso cardíaco (EFC) (a, b) a diferencia de los casos en los que no hay cartílago (b, d); el color amarillo indica el porcentaje de sustancia fundamental y el verde el porcentaje de células dentro del NAV (especialmente en caballos). CH: Cartílago hialino, CF: cartílago fibroso, CM: cardiomiocitos, EFC: esqueleto fibroso cardíaco, FN: fibra nerviosa. Magnificación 4X.

Tabla 7. Parámetros del cartílago en el esqueleto fibroso cardíaco de perros, caballos y cerdos.

Especie	Longitud µm (DE)	Ancho µm (DE)	Área μm^2 (DE)	Diámetro µm (DE)
Perros	885,3	686	627.763,5	1.043,5
	(131,2)	(157,1)	(320.237,4)	(273,3)
Caballos	2.683,9	1.109,5	2.445.462,9	2.690,7
	(792,8)	(314,6)	(1.063.789,1)	(783)
Cerdos	2.293,3	735,2	1.590.459,2	2.224,7
	(431,4)	(206)	(311.567,3)	(577,4)

DE: desviación estándar.

En el ser humano, las células P fueron más pequeñas, oscuras, redondeadas u ovaladas que los cardiomiocitos. Están ubicadas en el centro del NAV y pueden tener múltiples núcleos o un solo núcleo (Figura 10b). En los cerdos,

estas células fueron muy grandes, con un citoplasma ligeramente más pálido que en los cardiomiocitos y con un solo núcleo (Figura 11b, d). Las células P en caballos fueron pálidas, grandes, ovaladas, ubicadas en el centro del nodo y con un solo núcleo (Figura 12b, d). En los perros, estas células fueron pequeñas, redondeadas, de color similar a los cardiomiocitos, ubicadas en el centro del nodo y con un solo núcleo (Figura 13b, d). Las células P en las especies se evaluaron según la presencia o ausencia de cartílago. Tanto en cerdos como en perros, el área y los diámetros de las células P fueron significativamente mayores en los casos sin cartílago ($p<0,001$ para todos los valores), también las células de estos mismos casos en perros fueron más redondas cuando tenían cartílago ($p<0,001$). En los caballos, se encontraron características histológicas similares de las células P como en cerdos y perros. Hubo diferencias significativamente mayores en área ($p=0,001$), diámetro máximo ($p=0,002$), diámetro mínimo ($p=0,004$) y diámetro medio ($p=0,002$) de las células P del NAV en los corazones que no presentaron cartílago en su EFC (Tabla 8).

En la comparación morfológica de las células P en el NAV, en el humano y las especies animales con cartílago ausente, encontramos que el área y diámetros celulares fueron más grandes en perros que en humanos, en cerdos que en perros, en caballos que en humanos y en cerdos que en caballos ($p=0,001$ para todos los casos). Asimismo, se encontró que el diámetro mínimo y medio era mayor en caballos que en perros ($p=0,023$ y $p=0,039$ respectivamente).

Cuando se realizó la comparación dentro de los casos con cartílago, el área y los diámetros de las células mostraron características similares a las de aquellos sin tejido cartilaginoso. Adicionalmente, el diámetro máximo ($p=0,014$), el diámetro mínimo ($p=0,015$) y el diámetro medio ($p=0,005$) fueron mayores en caballos que en perros. Además, las células P del NAV fueron más grandes en los cerdos y pequeñas en los humanos.

En perros y caballos, las células P mostraron un tamaño medio en comparación con las otras dos especies (Tabla 8).

Tabla 8. Valores medios de los parámetros de las células P del NAV con o sin cartílago en perros, caballos, cerdos y humanos.

Especie	Área μm^2 (DE)	Diámetro máximo µm (DE)	Diámetro mínimo µm (DE)	Diámetro medio µm (DE)	Redondez µm (DE)
Con cartílago					
Perros	168,32	15,23	10,79	12,96	1,11
	(53,74)	(2,37)	(2,30)	(2,24)	(0,03)
Caballos	248,36	17,58	14.52	15.87	1.14
	(68,54)	(2,77)	(2,38)	(2,47)	(0,04)
Cerdos	694,31	31,95	25,82	28,56	1,17
	(239,76)	(5,65)	(5,39)	(5,42)	(0,15)
Sin cartílago					
Perros	240,12	21,54	15,96	18,24	1,07
	(73,87)	(3,23)	(2,56)	(2,64)	(0,03)
Caballos	322,31	23,15	18,24	19,06	1,07
	(71,93)	(2,48)	(2,32)	(2,39)	(0,01)
Cerdos	992,04	42,98	31,48	35,82	1,15
	(373,43)	(9,12)	(5,63)	(6,94)	(0,04)
Humanos	18,65	6,74	4,08	5,23	1,04
	(5,29)	(0,86)	(0,83)	(0,84)	(0,05)

DE: desviación estándar.

3. Identificación de las células de Purkinje en humanos y cerdos según su distribución zonal, mediante estudio histológico, inmunohistoquímico y morfométrico

3.1 Objetivo

Describir las variaciones regionales de las CP y sus uniones con el miocardio en cerdos y humanos.

3.2 Resumen del método utilizado

Analizamos cinco corazones de varones humanos y cinco corazones de cerdos machos destinados al sacrificio. Para el análisis histológico, el VI se disecó y seccionó en tres rodajas: base, tercio medio y ápex. Cada rodaja se seccionó radialmente, obteniendo cinco muestras de la base, cinco del tercio medio y cuatro del ápex. Estas muestras fueron numeradas identificándose cada una de ellas en las regiones anterior, posterior, lateral y septal. Las muestras de corazón se fijaron con una solución de formaldehído al 5%, se etiquetaron para su identificación y se incluyeron en parafina. Para realizar una evaluación completa de las FP, se cortó el bloque de parafina que incluía las FP según el siguiente protocolo: Se realizó un corte de 5 µm para obtener la primera muestra de tejido, posteriormente se realizó un corte de 40 µm de la muestra que se desechó y posteriormente se realizó otro corte de 5 µm para obtener una nueva muestra y se continuó con el protocolo, hasta que se seccionaron todos las FP. Las secciones histológicas se tiñeron con hematoxilina-eosina y tricrómico de Masson.

Además, se utilizó un PAS (CYTEK®) para visualizar acumulaciones de glucógeno en las CP. También se realizó marcaje inmunohistoquímico con el clon D33-IR606 de Anti-Human Desmin (DAKO Corporation®), para visualizar los FI (desmina) presentes en las CP y compararlos con los cardiomiocitos circundantes. Se analizaron 2.000 imágenes histológicas para un estudio exhaustivo de las FP (600 en humanos a nivel subendocárdico y 1.400 en

cerdos a nivel subendocárdico e intramiocárdico), utilizando un microscopio óptico Leica DMD108 (Leica Microsystems, Wetzlar, Alemania).

El estudio morfométrico computarizado se realizó mediante el software Image-ProPlus 7.1 (Media Cybernetics, Silver Spring, MD, EE. UU.).

La densidad de las FP se calculó como el área ocupada por las fibras en comparación con el área total de tejido. Se calibró cada micrografía y se realizó la medición manual del área de las CP, así como la segmentación automática del área total del tejido en μm^2 a 20X. Además, la medición manual del grosor de los haces se realizó transversalmente a 10X. Posteriormente medimos el área, diámetro máximo, diámetro mínimo, diámetro medio y redondez con un aumento de 20X en las CP y cardiomiocitos.

Calculamos el porcentaje de las CP que muestran UPM y la distribución de cada unión con respecto a la rodaja (base, tercio medio y ápex), región (anterior, lateral, posterior y septal) y localización (subendocardio y miocardio).

Adicionalmente, se compararon los resultados obtenidos entre las diferentes especies estudiadas, para determinar diferencias significativas entre ellas con respecto a la densidad y grosor de la FP, el comportamiento de las UPM y los parámetros morfométricos de las CP y los cardiomiocitos ventriculares.

Análisis estadístico

Las variables continuas (área, grosor, diámetro) se expresaron como media e intervalo de confianza del 95%, mientras que las variables categóricas (tipo de unión, rodaja, región, localización) se expresaron como porcentaje. Se consideró que el nivel estadísticamente significativo era $p<0,05$. Se realizaron estadísticas descriptivas, representaciones gráficas y pruebas de hipótesis con el software SPSS 20 (SPSS, Chicago, IL, EE. UU.) y Microsoft Excel 2013.

Se calcularon estadísticas descriptivas para cada parámetro morfométrico y se realizó la prueba de normalidad de Kolmogorov-Smirnov para cada muestra. Se utilizó una prueba de Chi-cuadrado para comparar las variables dicotómicas cualitativas, como la presencia y el tipo de UPM. En el caso de las variables cuantitativas después de la distribución normal para grupos de regiones, se utilizó la prueba ANOVA y con distribución diferente se eligió la prueba no paramétrica de Kruskal-Wallis; Las pruebas T student se utilizaron en comparaciones de los diferentes parámetros entre humanos y cerdos. Los datos se expresaron como desviación estándar media (DE) para todas las longitudes medidas.

3.3 Resultados

Humanos

Las FP se localizaron exclusivamente en el subendocardio. Se utilizaron tinciones de hematoxilina-eosina, tricrómico de Masson (Figuras 17, 18) y anticuerpos frente a desmina (Figura 19d) para identificar las FP y las CP. Observamos que las FP fueron más gruesas en el tercio medio que en el ápex (p=0,046) (Tabla 9) (Figura 20a). Estas tinciones revelaron que las CP fueron ligeramente más pálidas que los cardiomiocitos debido al bajo número de miofibrillas, con una mayor cantidad de FI de desmina, por lo que la intensidad del marcado fue mayor. En ocasiones, las vainas de tejido conectivo rodearon las células, provenientes del cuerpo fibroso central y la porción membranosa del tabique interventricular (Figura 17e, f).

Además, para potenciar la identificación de las FP realizamos un PAS, con el cual observamos acumulación de glucógeno en todo el citoplasma de las CP, a diferencia de los cardiomiocitos cuya cantidad de glucógeno fue mucho menor (Figura 19a, b).

Los cardiomiocitos fueron de tamaño intermedio, ovalados y oscuros. En nuestro análisis morfométrico, pudimos determinar que las CP en humanos fueron más grandes (18.52 +/- 5.41 µm) que los cardiomiocitos (12.35 +/- 1.34 µm) cuando se evaluaron en sección transversal (Tabla 10).

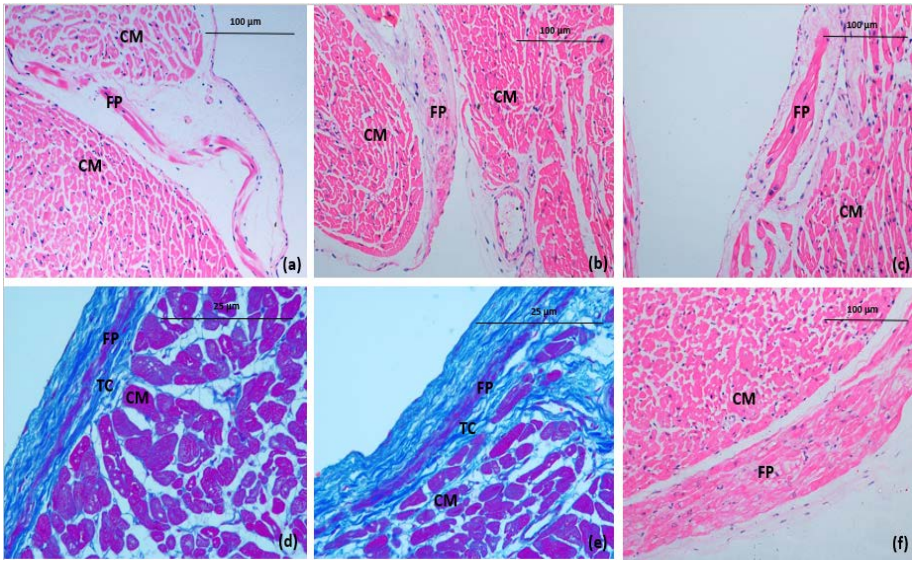

Figura 17. Fibras de Purkinje humanas en subendocardio, teñidas con hematoxilina-eosina (a-c, f), magnificación 20X y tricrómico de Masson (d, e). Magnificación 40X. Haces delgados de fibras de Purkinje, en la región lateral (a), la región posterior (b) y la región septal (c, d, e). Haces gruesos de fibras de Purkinje en la región septal (f). Las fibras se pueden ver en la base (b), en el tercio medio (a, d-f) y en el ápex (c). FP: fibras de Purkinje; CM: cardiomiocitos; TC: tejido conectivo. Magnificación 20X.

Adicionalmente, evaluamos la distribución general de las CP en el VI en cada región y rodaja (Tabla 11). El diámetro mínimo de las CP fue mayor en el ápex que en la base (p=0,015) o en el tercio medio (p=0,048). Además, las CP fueron más redondas en el tercio medio que en la base (p=0,017).

Las UPM se encontraron en el 10% de todas las micrografías analizadas; estas uniones se encontraron en mayor cantidad en el ápex que las otras dos rodajas (p<0.001) (Tabla 11, 12).

Las CTCC (7,2%) (Figura 21a) y CTPC (0,9%) (Figura 21b) se encontraron con mayor frecuencia en el ápex (p<0,001) que en las otras rodajas, y CTCT (1,9%) (Figura 21c) fueron localizados principalmente en la base (p<0,001) (Tabla 11, 13).

Además, al analizar los diferentes tipos de UPM en cada subdivisión de área descrita en nuestro estudio se encontraron CTCC en mayor cantidad que las otras dos uniones en todas las rodajas, regiones y localizaciones estudiadas (p<0,001) (Tabla 13).

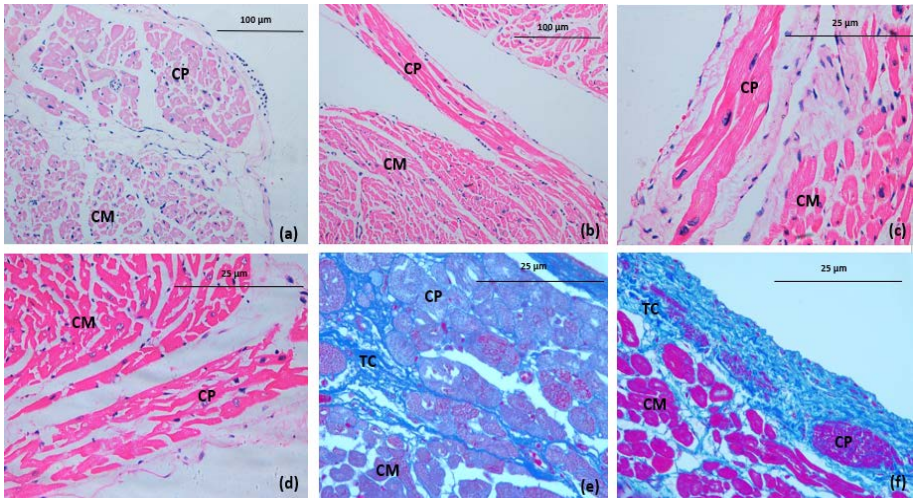

Figura 18. Morfología de las células de Purkinje en humanos en subendocardio, teñidas con hematoxilina-eosina (a-d) y tricrómico de Masson (e, f). En la región septal (a-c, e, f) y en la región lateral (d). Las células se pueden ver en el tercio medio (c-f), magnificación 40X y en el ápex (a, b). CP: células de Purkinje; CM: cardiomiocitos; TC: tejido conectivo. Magnificación 20X.

La morfología de las CP y la distribución de las FP y sus uniones por región se indican a continuación, considerando su ubicación en la rodaja (Figura 20a).

Base

Las FP se organizaron comúnmente en haces largos y delgados compuestos por aproximadamente 2 a 10 células, a veces rodeadas por tejido conectivo (Figura 17b). En cada una de las regiones que pertenecen a la base, las CP fueron ovaladas, con un solo núcleo que variaba entre claro y oscuro. El área, el diámetro máximo, el diámetro mínimo y el diámetro medio fueron mayores

en la región anterior que en la posterior (p<0,001 para cada parámetro); en la región lateral que en la región anterior (p<0,001 para cada parámetro) o en la región posterior (p<0,001 para cada parámetro) y en la región septal que en la región posterior (p<0,001 para cada parámetro).

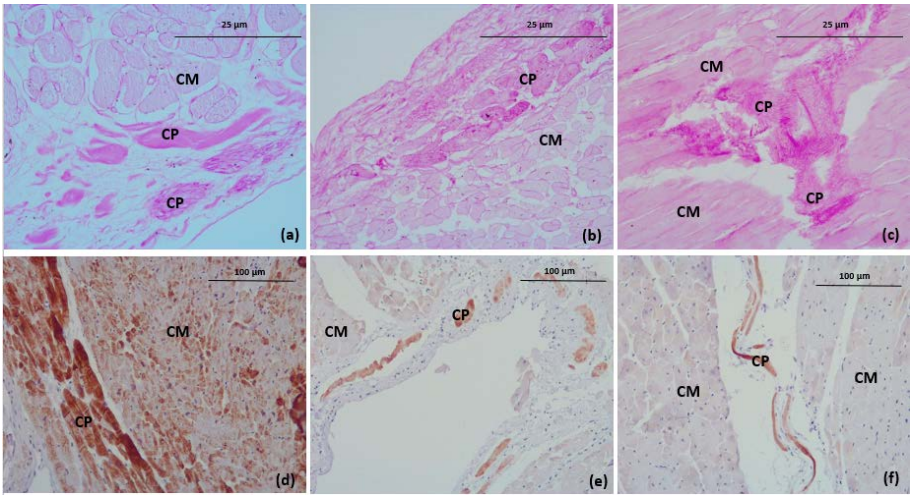

Figura 19. Identificación de las células de Purkinje por diferentes métodos en humanos y cerdos. Técnica de PAS para la detección de glucógeno intracitoplasmático en humanos en el subendocardio, en la región anterior (a) y en la región septal (b). Técnica de PAS en cerdos en miocardio, en la región anterior (c). Marcaje inmunohistoquímico con anticuerpos frente a desmina para la identificación de este filamento intermedio en humanos en subendocardio, en la región septal (d). Inmunomarcaje con anticuerpos frente a desmina en cerdos en subendocardio, en la región lateral (e) y miocardio, en la región lateral (f). Las células se pueden ver en la base (a-c), magnificación 40X y en el tercio medio (d-f). CP: células de Purkinje; CM: cardiomiocitos. Magnificación 20X.

El área (p=0,008), el diámetro mínimo (p=0,040) y el diámetro medio (p=0,012) de las CP fueron significativamente mayores en la región lateral que en la septal.

Tercio medio

Encontramos que las FP formaban haces largos y delgados, compuestos de 3 a 15 células sin estar rodeadas por tejido conectivo (Figura 17a). En cada

una de las regiones que pertenecen al tercio medio, las CP fueron ovaladas, y observamos un solo núcleo redondo, oscuro y centrado.

El área de las CP en la región septal fue mayor que en la región lateral (p=0,049). Además, el área (p=0,011), el diámetro máximo (p=0,010), el diámetro mínimo (p=0,039) y el diámetro medio (p=0,011) fueron significativamente mayores en la región septal que en la región posterior.

Tabla 9. Valores medios de densidad y grosor de las fibras de Purkinje según rodaja, región y localización en humanos y cerdos.

		Humano		Cerdo	
		Densidad fibras de Purkinje (%)	Grosor fascículo (µm)	Densidad fibras de Purkinje (%)	Grosor fascículo (µm)
Rodaja	Base	16,42	23,41	10,59	23,72
	Tercio medio	16,98	24,97	11,46	21,95
	Ápex	22,75	21,92	11,17	20,76
Región	Posterior	13,97	23,89	11,22	21,57
	Septal	22,59	23,15	11,27	22,36
	Anterior	19,90	23,85	11,07	22,55
	Lateral	13,09	24,29	10,46	22,56
Localización	Subendocardio	100	23,79	55,56	19,74
	Miocardio	-	-	42,89	25,51
	Epicardio	-	-	0,32	37,17
	Perivascular	-	-	1,23	21,91

En nuestro estudio observamos una mayor presencia de UPM en la región septal, en comparación con las otras regiones (p=0,017).

Ápex

Las FP formaban haces largos y delgados de 3 a 15 células, en corte longitudinal y no estaban rodeadas de tejido conectivo (Figura 17b). En la región septal hubo mayor densidad de las FP que en la región lateral (p=0,037). En cada una de las regiones que pertenecen al ápex, las CP fueron ovaladas con un núcleo redondo, grande y ligeramente pálido (Figura 18a, b).

Evaluamos la distribución de las CP, FP y UPM por región y rodaja en humanos (Tabla 12).

Cerdos

Las FP se localizaron principalmente en el subendocardio y miocardio, aunque en ocasiones fue posible observarlas en el epicardio y a nivel perivascular (Figura 22d).

Tabla 10. Resumen general de los parámetros morfométricos de las células de Purkinje y cardiomiocitos en humanos y cerdos.

Especie	Célula	Área. μm^2 (DE)	Diámetro máximo. µm (DE)	Diámetro mínimo. µm (DE)	Diámetro medio. µm (DE)	Redondez (DE)
	CP					
Humanos		480,8	18,52	9,79	14,15	1,12
		(281,7)	(5,41)	(5,42)	(5,73)	(0,05)
Cerdos		877,1	22,85	12,69	17,95	1,14
		(411,8)	(7,45)	(4,12)	(5,34)	(0,06)
	Cardiomiocito					
Humanos		165,5	12,35	9,37	10,86	1,20
		(48,5)	(1,34)	(2,15)	(2,04)	(0,13)
Cerdos		281,5	15,28	11,03	13,25	1,14
		(62,5)	(2,01)	(1,34)	(2,45)	(0,05)
	Esquema				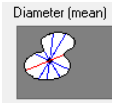	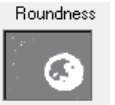

DE: desviación estándar. CP: células de Purkinje.

La densidad de las FP fue muy similar en cada rodaja evaluada (Tabla 9) y las diferencias no fueron estadísticamente significativas, a diferencia de la densidad de las fibras evaluadas por localización, donde encontramos mayor abundancia de FP en endocardio que en miocardio ($p<0,001$). Además, al evaluar la distribución a nivel de la rodaja y localización, determinamos que el grosor de las FP fue mayor en la base que en el ápex ($p=0,001$) y en el miocardio que en el endocardio ($p<0,001$) (Tabla 11) (Figura 20b). Al analizar la distribución de las FP a nivel miocárdico encontramos que las fibras fueron más gruesas en la base ($p=0,001$) y en el tercio medio ($p=0,044$) que en el ápex.

Para identificar las FP y las CP en nuestro estudio, se utilizaron diferentes tinciones como hematoxilina-eosina, tricrómico de Masson (Figuras 19, 20) y desmina (Figura 16e, f). La tinción reveló que las CP fueron más pálidas que los cardiomiocitos y, por tanto, más fáciles de detectar y que hubo una mayor intensidad de marcado debido al gran número de FI de desmina.

Además, pocas miofibrillas pudieron visualizarse en la periferia del citoplasma de las CP y a veces, estuvieron rodeadas de tejido conectivo que se originaba en el cuerpo fibroso central y la porción membranosa del tabique interventricular (Figura 23e, f).

Tabla 11. Distribución subendocárdica de las células de Purkinje, fibras de Purkinje y uniones Purkinje-miocardio por rodaja y región en humanos.

Rodaja	Región	Diámetro CP µm (DE)	Densidad FP (%)	Grosor FP µm (DE)	UPM (%)			
					Total	CTCC	CTPC	CTCT
Base	Anterior	17,59 (9,24)	20,93	25,96 (9,04)	3,4	-	-	3,4
	Lateral	22,80 (7,95)	14,32	23,51 (8,73)	13,8	10,4	-	3,4
	Posterior	10,17 (6,12)	6,04	19,78 (6,98)	15	5	5	5
	Septal	19,71 (8,47)	16.62	23,65 (8,34)	2,9	2,9	-	-
Tercio medio	Anterior	17,81 (9,27)	14,66	23,12 (10,80)	4,4	1,5	-	2,9
	Lateral	15,96 (7.,6)	13,73	27,10 (15,09)	3,4	3,4	-	-
	Posterior	14,01 (6,25)	19,44	27,97 (10,76)	3,3	3,3	-	-
	Septal	19,68 (9,87)	17,90	22,68 (7,28)	17,9	12,8	2,6	2,6
Ápex	Anterior	20,08 (9,16)	28,37	21,79 (5,85)	22,9	20	-	2,9
	Lateral	18,13 (8,73)	8,21	20,53 (12,04)	6,7	6,7	-	-
	Posterior	20,26 (9,93)	13,56	20,78 (7,68)	7,7	7,7	-	-
	Septal	16,07 (6,45)	27,15	23,19 (6,39)	31,2	25	3,1	3,1

CP: células de Purkinje. FP: fibras de Purkinje. UPM: uniones Purkinje-miocardio. CTCC: contacto a través de cuerpos celulares. CTPC: contacto a través de prolongaciones celulares. CTCT: contacto a través de células transicionales. DE: desviación estándar.

Como medio alternativo para identificar las FP, también utilizamos la técnica de PAS, observándose una notable acumulación de glucógeno en el citoplasma de estas células, a diferencia de los cardiomiocitos donde se detectó poca positividad (Figura 19c).

Tabla 12. Porcentaje de uniones Purkinje-miocardio por rodaja, región y localización en humanos y cerdos.

		Humanos (%)	Cerdos (%)
Rodaja	Base	7,1	28,5
	Tercio medio	6,6	24,8
	Ápex	21,1	18,2
Región	Posterior	7,9	20,1
	Septal	17,1	26
	Anterior	8,1	25,7
	Lateral	6,8	24,2
Localización	Subendocardio	10	6.4
	Miocardio	-	17.5
	Epicardio	-	0.1
	Perivascular	-	0.2

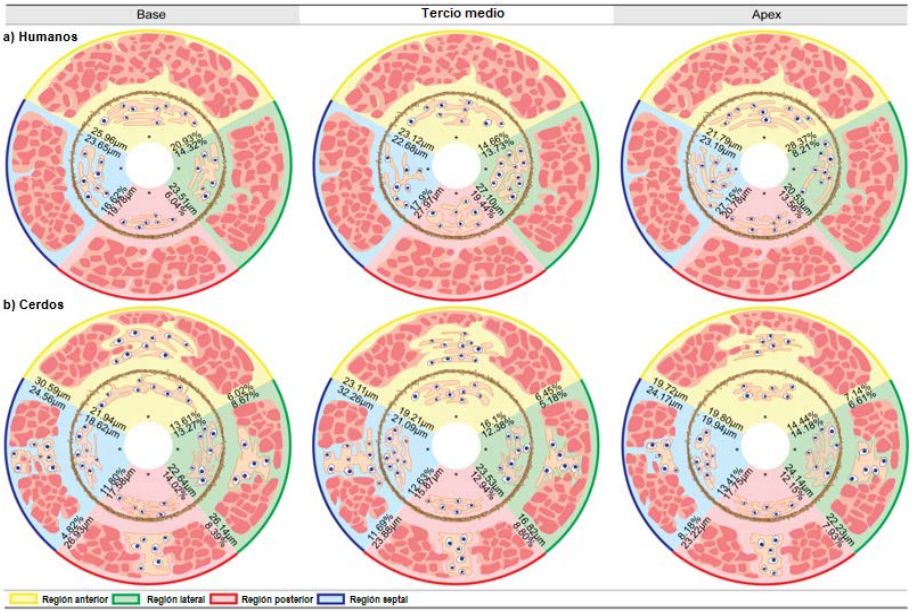

Figura 20. Distribución subendocárdica (*) de las fibras de Purkinje en humanos (a). Distribución subendocárdica (*) e intramiocárdica de las fibras de Purkinje en cerdos (b), indicando densidad (%) y grosor (µm) en cada uno de las rodajas y regiones del ventrículo izquierdo.

Los cardiomiocitos fueron oscuros, redondos u ovalados y pequeños cuando se observaban en sección transversal, y estuvieron organizados en haces de múltiples células. Las CP en cerdos fueron más grandes (21.32 +/- 6.45 µm) que los cardiomiocitos (15.28 +/- 2.01 µm) cuando se evaluaron en sección transversal, como se verificó mediante análisis morfométrico (Tabla 10).

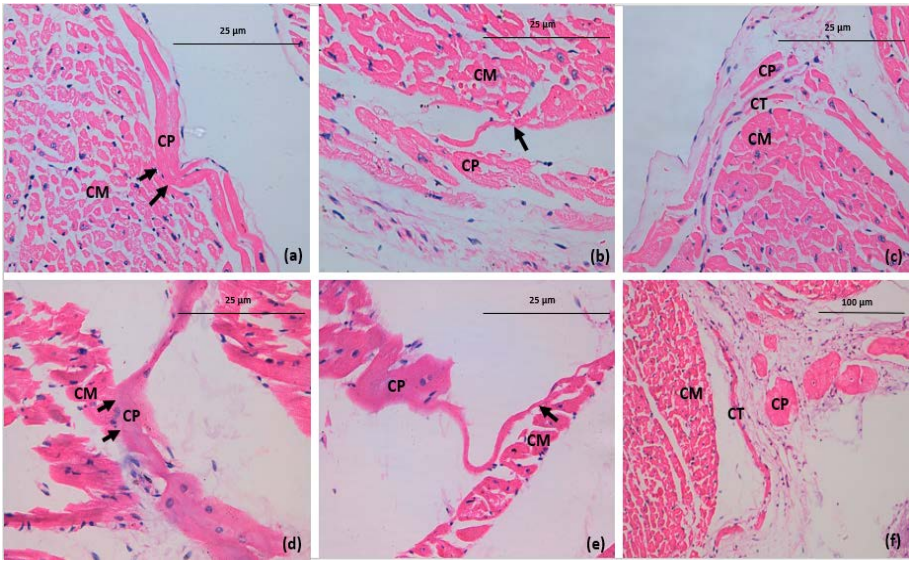

Figura 21. Diferentes tipos de uniones Purkinje-miocardio en humanos y porcinos, teñidas con hematoxilina-eosina. Magnificación 20X y 40X. Las flechas indican una unión de contacto a través de cuerpos celulares (CTCC) en subendocardio en humanos, en la región septal (a) y en miocardio en cerdos, en región septal (d). La flecha muestra el contacto a través de prolongaciones celulares (CTPC) en subendocardio en humanos, en región posterior (b) y en miocardio en cerdos, en región posterior (e). Observe el contacto a través de células transicionales (CTCT) en subendocardio en humanos, en la región posterior (c). Magnificación 40X. En subendocardio en cerdos se puede observar la unión CTCT, en la región posterior (f). Magnificación 20X. Las uniones se pueden ver en la base (b, c, e, f) y en el ápex (a, d). CP: células de Purkinje; CM: cardiomiocitos; CT: célula transicional. Magnificación 40X.

Además, también evaluamos la distribución general de las CP en el VI en cada una de las regiones, rodajas y localizaciones (Tabla 11). En el análisis de las CP en cerdos, encontramos que el área fue significativamente mayor

en el subendocardio que en el miocardio (p=0,003), al igual que el diámetro máximo (p=0,009), el diámetro mínimo (p=0,005) y el diámetro medio (p=0,002).

Al evaluar las células en ambas localizaciones, observamos que el área y el diámetro medio fueron mayores en la región lateral que en la región anterior (p=0,037 y p=0,042 respectivamente). Con respecto a la distribución de las CP en el miocardio estas células ocuparon un área más grande en la región lateral que en la anterior (p=0,049).

Tabla 13. Distribución de diferentes tipos de uniones según corte, región y ubicación en humanos y porcinos, con respecto al número de uniones en cada división.

		Humanos (%)			Cerdos (%)		
		CTCC	CTPC	CTCT	CTCC	CTPC	CTCT
Rodaja	Base	3,5	0,7	2,8	21,7	3,5	3,3
	Tercio medio	4,6	0,5	1,5	21,1	2,1	1,3
	Ápex	17,9	2,1	1,1	16,3	0,8	1,1
Región	Posterior	4,8	1,6	0,2	15,7	3,4	1,1
	Septal	13,3	1,9	0,5	20,4	2,8	2,8
	Anterior	5	0,6	0,9	21,5	1,9	2,4
	Lateral	5,8	-	0,2	21,2	1,2	1,7
Localización	Subendocardio	7,2	0,9	1,9	7,8	1	2,7
	Miocardio	-	-	-	35,9	3,8	1,3
	Epicardio	-	-	-	25	-	-
	Perivascular	-	-	-	6,7	6,7	-

CTCC: contacto a través de cuerpos celulares. CTPC: contacto a través de prolongaciones celulares. CTCT: contacto a través de células transicionales.

Al comparar los parámetros medidos de las CP en el subendocardio, encontramos que el área (p=0,001), el diámetro máximo (p=0,003), el diámetro mínimo (p=0,001) y el diámetro medio (p=0,001) fueron mayores en la base que en el tercio medio. Además, el área (p=0.039), el diámetro mínimo (p=0.035) y el diámetro medio (p=0.039) fueron significativamente mayores en la base que en el ápex. En el tercio medio las CP fueron más redondas que en la base (p=0.040). En el miocardio, el área (p=0.010), diámetro máximo (p=0.017), diámetro mínimo (p=0.010) y diámetro medio (p=0.005) de las CP fueron significativamente mayores en el ápex que en el tercio medio.

En los cerdos, las UPM estuvieron presentes en el 24,2% de todas las micrografías analizadas, encontrándose uniones con mayor frecuencia en la base que en las otras dos rodajas (p=0,002). Las uniones se distribuyeron de manera similar en todas las regiones (Tablas 12, 13). Además, encontramos una mayor presencia de uniones entre las CP y cardiomiocitos a nivel miocárdico que en otras localizaciones (p<0,001) (Tabla 13). Los CTCC (19,9%) (Figura 21d), CTPC (2,3%) (Figura 21e) y CTCT (2,1%) (Figura 21f) se encontraron con mayor frecuencia en la base que en las otras rodajas analizadas (p=0,003), lo cual es consistente con una mayor presencia general de uniones en la base descrita anteriormente.

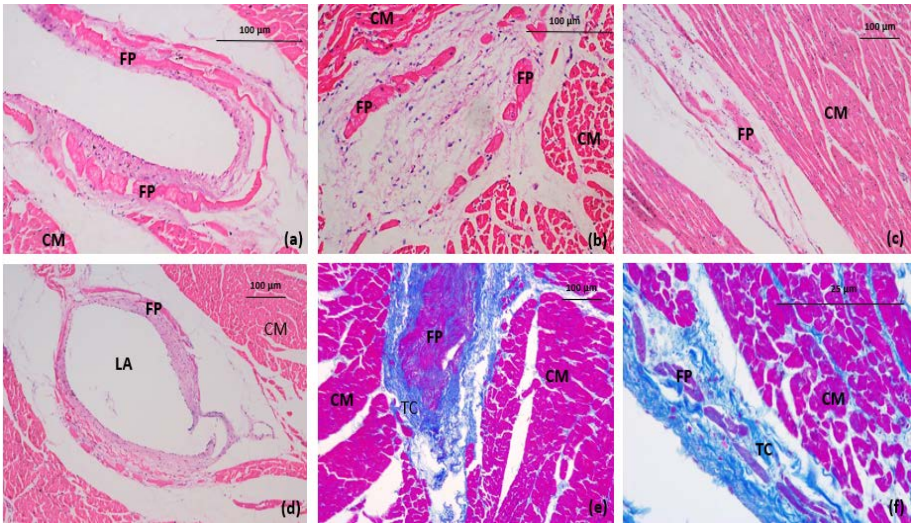

Figura 22. Fibras de Purkinje de cerdos en diferentes localizaciones, teñidas con hematoxilina-eosina (a-d) y tricrómico de Masson (e, f). Fibras de Purkinje a nivel subendocárdico, en la región lateral (a) y en la región anterior (f). Fibras de Purkinje a nivel perivascular, en la región posterior (b). Fibras de Purkinje a nivel intramiocárdico, en la región lateral (c) y en la región anterior (d, e). Las fibras se pueden ver en la base (c, d, e). Magnificación 10X. En el tercio medio (a, b). Magnificación 20X. En el ápex (f). FP: fibras de Purkinje; CM: cardiomiocitos; TC: tejido conectivo. LA: luz arterial. Magnificación 40X.

Tabla 14. Distribución de las células de Purkinje, fibras de Purkinje y uniones Purkinje-miocardio por rodaja, localización y región en cerdos.

Rodaja	Localización	Región	Diámetro CP µm (DE)	Densidad FP (%)	Grosor FP µm (DE)	UPM (%)			
						Total	CTCC	CTPC	CTCT
Base	Sub endocardio	Anterior	20.13 (6.45)	13.6	21.94 (7.92)	15.5	8.3	1	6.2
		Lateral	21.05 (7.34)	13.27	22.64 (10.34)	8.3	8.3	-	-
		Posterior	15.42 (5.14)	14.02	17.58 (3.78)	7	5.2	-	1.8
		Septal	17.53 (6.28)	11.80	18.62 (7.14)	18.4	8.2	4.1	6.1
	Miocardio	Anterior	23.91 (9.47)	6.02	30.59 (15.23)	54.9	46.5	4.2	4.2
		Lateral	25.20 (10.12)	8.67	26.14 (18.16)	42.2	37.5	3.1	1.6
		Posterior	26.55 (9.86)	8.39	26.93 (14.88)	37	24.1	11.1	1.8
		Septal	18.80 (7.37)	4.82	24.56 (18.30)	53.1	43.8	6.2	3.1
Tercio medio	Sub endocardio	Anterior	18.87 (7.62)	16.1	19.21 (8.37)	16.1	12.9	1.6	1.6
		Lateral	21.62 (8.90)	12.38	23.53 (6.26)	8.2	4.1	-	4.1
		Posterior	14.15 (6.92)	12.94	15.87 (8.19)	8.8	8.8	-	-
		Septal	18.24 (7.46)	12.63	21.09 (8.81)	18.1	12.5	2.8	2.8
	Miocardio	Anterior	16.49 (5.21)	6.45	23.11 (14.46)	38	35.2	2.8	-
		Lateral	16.03 (5.17)	5.18	16.82 (11.18)	37.5	37.5	-	-
		Posterior	22.75 (9.63)	8.80	23.88 (14.74)	41.7	36.1	5.6	-
		Septal	28.48 (12.43)	11.69	32.26 (13.98)	43.3	40	3.3	-
Ápex	Sub endocardio	Anterior	19.12 (9.57)	14.44	19.80 (7.58)	11.5	11.5	-	-
		Lateral	23.62 (11.21)	14.18	24.14 (10.90)	7.2	3.6	-	3.6
		Posterior	16.94 (7.83)	12.15	17.75 (6.54)	1.9	-	-	1.9
		Septal	18.89 (8.45)	13.41	19.94 (6.45)	8.6	5.8	1.4	1.4
	Miocardio	Anterior	19.07 (8.53)	7.14	19.72 (10.42)	20.4	18.5	1.9	-
		Lateral	21.76 (10.62)	6.61	22.23 (10.71)	42.9	40	2.9	-
		Posterior	22.47 (11.49)	7.93	23.22 (9.76)	33.3	33.3	-	-
		Septal	23.92 (12.14)	8.18	24.17 (12.01)	48.4	45.2	-	3.2

CP: células de Purkinje. FP: fibras de Purkinje. UPM: uniones Purkinje-miocardio. CTCC: contacto a través de cuerpos celulares. CTPC: contacto a través de prolongaciones celulares. CTCT: contacto a través de células transicionales. DE: desviación estándar.

Encontramos más CTCC que otros tipos de uniones en todas las rodajas, regiones y localizaciones descritas (p<0,001). En el miocardio hubo un mayor número de CTCC que los otros dos tipos de uniones en todas las rodajas (p=0,031). A continuación, se indica la morfología de las CP y la distribución de las FP y sus uniones, analizadas por región, considerando la rodaja y la localización (Tabla 14).

Base

En cada una de las regiones que pertenecen a la base en el subendocardio, las FP se organizaron típicamente en haces largos y delgados (Figura 19a, f) compuestos de aproximadamente 2 a 15 células rodeadas por tejido conectivo.

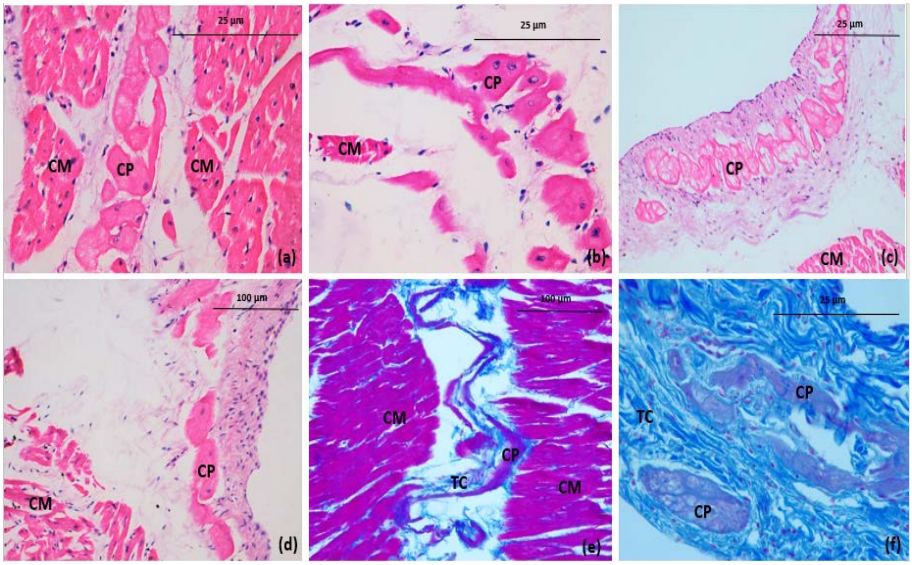

Figura 23. Morfología de las células de Purkinje en cerdos, teñidas con hematoxilina-eosina (a-d) y tricrómico de Masson (e-f). Células de Purkinje en el miocardio, en la región anterior (a, e) y en la región lateral (b). Células de Purkinje en el endocardio, en la región lateral (c), en la región posterior (d) y en la región anterior (f). Se pueden observar las células de Purkinje en la base (a, b, f). Magnificación 40X. En el tercio medio (c, d). Magnificación 20X. En el ápex (e). CP: células de Purkinje; CM: cardiomiocitos; TC: tejido conectivo. Magnificación 20X.

A veces, las fibras estaban formadas por células individuales creando una apariencia lineal. Las FP fueron más gruesas en la región anterior (p=0,004) y la región lateral (p=0,005) que en la región posterior. Las CP fueron ovaladas y con un solo núcleo ligeramente pálido, redondo y centrado (Figura 23c, f). Observamos que el diámetro mínimo y el diámetro medio de las CP fue significativamente mayor en la región lateral (p=0.030 y p=0.028 respectivamente) y en la región posterior (p=0.001 y p=0.011 respectivamente) que en la región septal.

En el miocardio, las FP se observaron generalmente en sección longitudinal, rodeados de tejido conectivo, fueron alargadas, delgadas y en agrupaciones de 3 a 15 células. Las CP fueron ovaladas, con núcleos redondeados, centrados y ligeramente pálidos.

Tercio medio

En cada una de las regiones que pertenecen al tercio medio del subendocardio, las FP formaron haces largos y delgados de 2-10 células, rodeadas por tejido conectivo. Las FP fueron significativamente más gruesas en la región septal que en la región posterior (p=0,001) o la región lateral (p=0,004).

Las CP fueron redondas y con un núcleo centrado, redondo, grande y oscuro. Las CP en la región anterior (p=0,006), la región lateral (p=0,047) y la región septal (p=0,001) fueron más redondas que en la región posterior. En el miocardio, las FP fueron alargadas y gruesas, compuestas de 3 a 10 células (Figura 22b) y rodeados por tejido conectivo. Encontramos que la densidad y el grosor de las FP fueron significativamente mayores en la región septal que en la región anterior (p=0.018 y p=0.026 respectivamente). Las CP fueron ovaladas con un único núcleo grande, redondo y ligeramente pálido centrado. El área (p=0.028), el diámetro máximo (p=0.007), el diámetro mínimo (p=0.025) y el diámetro medio (p=0.022) de las CP fueron significativamente mayores en la región septal que en la región posterior. Además, el diámetro máximo y el diámetro medio de estas células fueron mayores en la región

septal que en la región anterior (p=0.011 y p=0.020 respectivamente) y en la región lateral (p=0.010 y p=0.022 respectivamente).

Ápex

En cada una de las regiones que pertenecen al ápex del subendocardio, las FP se organizaron en haces largos, delgados y gruesos, formados por 3 a 15 células y rodeados de escaso tejido conectivo. Las FP fueron más gruesas en la región lateral que en la región posterior (p=0,002). Las CP fueron ovaladas con núcleos oscuros grandes, redondos y centrados. El diámetro mínimo de las CP fue significativamente mayor en la región posterior que en la región anterior (p=0.046). En el miocardio, observamos que las FP podían organizarse entre haces largos delgados y haces largos y gruesos, con grupos de 2 a 25 células, rodeados de tejido conectivo y generalmente en sección longitudinal. Las CP fueron ovaladas con núcleos grandes, redondos, ligeramente pálidos y centrados (Figura 23a, b). Observamos mayor cantidad de UPM en la región septal que en las otras regiones (p=0.036).

En cuanto a las FP en humanos y cerdos en nuestro estudio, encontramos una mayor densidad de fibras en humanos que en cerdos (p<0.001) pero observamos valores de grosor similares. La distribución de las FP y las CP se observó con mayor frecuencia en la región septal y en el subendocardio de las dos especies estudiadas (Figura 20a, b). Al comparar diferentes parámetros de las CP medidos entre las dos especies, encontramos que el área, los diámetros mínimo y medio fueron significativamente mayores en los cerdos que en los humanos (p<0,001 para todos los valores), al igual que el diámetro máximo (p=0,031). Además, el diámetro máximo de los cardiomiocitos fue mayor en los cerdos que en los humanos (p=0,001) (Tabla 10).

Al comparar el número de uniones presentes entre las especies, pudimos observar más uniones en cerdos que en humanos (p<0,001). Asimismo, el tipo de UPM más abundante fue CTCC en ambas especies, con mayor abundancia en cerdos que en humanos (p<0,001)

F. DISCUSIÓN

1. Morfometría e histología comparada de los nodos sinoatrial y atrioventricular en humanos y cerdos y su relevancia en la prevención de arritmias nodales

El estudio de las estructuras nodales en corazones humanos y porcinos con morfometría aporta objetividad a la visualización morfológica y nos ha permitido demostrar que existen similitudes entre ambas especies (humanos y cerdos), lo que podría permitir el uso de cerdos como modelo experimental alternativo al estudiar la fisiopatología del sistema de conducción cardíaca.

En humanos, se ha descrito comúnmente que el NSA tiene forma de huso y mide entre 10 y 13 mm de largo y entre 3 y 5 mm de ancho[12,15-18,121], aunque también se han encontrado longitudes más cortas entre 4 y 6 mm[122] y mayores entre 12 y 29 mm[123-125]. Al analizar 10 NSA en humanos, hemos identificado histológica y morfométricamente la forma del nodo, las características de sus células y el abundante tejido conectivo entre ellas. Observamos que tiene una forma ovoide, coincidiendo con estudios previos, aunque nuestras medidas fueron algo más bajas (1,7-7,4 mm), lo que podría explicarse por las diferentes técnicas utilizadas. Mediante morfometría solo en uno de los casos nuestro nodo fue de 7.4 mm, por lo que podemos decir que esta estructura es pequeña en humanos. La gran cantidad de tejido conectivo que se encuentra dentro del NSA en nuestro estudio coincide con lo descrito por otros autores[16,26,125-127], pero la presencia de pequeños tabiques fibrosos que separan el nodo de los cardiomiocitos en humanos en algunas áreas descritas por Waller[18], no se observó en nuestras preparaciones histológicas.

El colágeno especializado en el NSA puede proporcionar soporte estructural y también ayuda a brindar protección a las células P que son responsables de la función del marcapasos, evitando el estiramiento debido al aumento de la contracción del miocardio auricular que rodea el nodo[14,125,124]. Sin embargo,

en la insuficiencia cardíaca y los infartos de miocardio se ha demostrado un aumento del tejido conectivo (fibrosis) dentro del NSA[123-125,128], lo que interrumpe el acoplamiento normal entre las células especializadas del nodo y los cardiomiocitos circundantes, disminuyendo la capacidad vital del marcapasos provocando bradicardia, bloqueos de conducción o reentrada[128]. El mal funcionamiento del NSA en humanos puede predisponer a enfermedades cardíacas, como fibrilación auricular e insuficiencia cardiaca, que pueden causar síncope y muerte cardíaca súbita. Actualmente, la enfermedad del NSA en humanos y en especies animales como caninos se trata con medicamentos y marcapasos con tasas de éxito variables[125,129]. La prevalencia y gravedad de este fallo nodal hace necesario realizar estudios más detallados que identifiquen y describan aspectos estructurales y funcionales del NSA dirigidos a prevenir estas patologías cardíacas[125].

Conocer los parámetros de las ramas arteriales nodales es importante para determinar la cantidad aproximada de sangre necesaria para nutrir y oxigenar los nodos en condiciones normales. Se observa comúnmente una rama arterial grande en el centro o al lado del NSA en humanos[12,16,17,19,122,130]. En nuestro estudio encontramos fácilmente esta rama arterial en el centro del nodo, pero en ocasiones se desplazaba hacía la periferia como lo indica la bibliografía previa. En los seres humanos, hay fibras nerviosas en la periferia y dentro del NSA que están ricamente inervadas por ramas tanto del sistema vago como del simpático[1,12,16,19,66,130]. Solo pudimos observar la presencia de fibras nerviosas en la periferia del NSA. Esto es importante porque la cantidad de fibras nerviosas presentes puede influir en la actividad de marcapasos del NSA. Se ha descrito que algunas células nodales son más sensibles a la noradrenalina o acetilcolina, pudiendo cambiar el sitio de origen del marcapasos intranodal o que el sitio original simplemente dispara a un ritmo más rápido[38,131,132].

Histológicamente, se describe en humanos que las células P en el NSA son pequeñas (de 3 a 10 µm de diámetro), ovoides o redondas, pálidas y agrupadas en fascículos interconectados[6,12,18,19,127,130].

Se cree que estas células son las responsables de la formación de los impulsos en el NSA y se ubican en el centro del nodo. Las CT son alargadas con características intermedias entre las células P y los cardiomiocitos[18]. Se ubican en los márgenes del nodo y en otras áreas se proyectan, extendiéndose por distancias cortas en el miocardio auricular, también en la cresta terminal y otras partes de las vías internodales, mostrando una organización lineal con otras CT. Se piensa que son las encargadas de transmitir el impulso producido por las células P al miocardio[12,130]. Con respecto a las células P, nuestros hallazgos concuerdan con las descripciones realizadas por la bibliografía previa, incluido el tamaño de la célula. En cuanto a las CT, coincidimos con la ubicación y organización lineal que presentan, según lo descrito en la literatura.

De manera similar, en los cerdos el NSA tiene entre 10-18 mm de largo, 3,5 mm de ancho y una forma ovoide[26]. En nuestros hallazgos observamos la misma forma del nodo y el tamaño fue más pequeño de lo descrito, lo que podría explicarse por las diferentes técnicas utilizadas en la bibliografía previa. Al analizar 10 NSA en cerdos, se realizó una identificación del nodo observando sus células y una alta cantidad de tejido conectivo entre ellas, lo que coincide con lo descrito por otros autores[16,26,125-127]. Se observa de manera regular una rama arterial grande en el centro o al lado del NSA[16]. Nuestras observaciones fueron similares a lo descrito previamente, pero encontramos que esta rama arterial se ubica principalmente hacia los polos y en pocas ocasiones en el centro del nodo. En los cerdos, hay numerosas fibras nerviosas en la periferia y ocasionalmente dentro del nodo[27]. En nuestro estudio solo pudimos observar la presencia de fibras nerviosas en la periferia del NSA en cerdos.

En los cerdos, se ha observado la presencia de muchos núcleos próximos entre sí y una gran cantidad de fibras de colágeno y células pálidas (células P) con un diámetro entre 4-8 µm[26,127]. Encontramos que las características de las células P coinciden con la bibliografía previa, pero el diámetro de estas células en nuestra investigación fue ligeramente mayor. En otro estudio, se indica que el diámetro de estas células es igual al de los cardiomiocitos[27];

esto no es consistente con nuestros hallazgos, donde observamos que las células P eran más pequeñas que las células del miocardio.

Diferentes autores han encontrado que en humanos el NAV tiene forma ovalada o semi-ovalada, midiendo entre 5-7 mm de largo y entre 3-4 mm de ancho[5,36,130,133,134]. En nuestro estudio observamos que el nodo tiene forma ovoide y nuestras medidas son más pequeñas que las encontradas por otros autores. La RNAV que lo irriga en humanos se ubica entre dos prolongaciones del NAV compacto en dirección al HH[40,130], esto coincide con nuestras observaciones, aunque esta rama arterial rara vez es visible histológicamente. La inervación en el NAV de humanos es importante ya que puede influir en la actividad eléctrica hacia el HH y el sistema de Purkinje. En nuestra investigación, mediante microscopía óptica y tinción con Hematoxilina-Eosina, no encontramos fibras nerviosas en la periferia ni en el interior del nodo en humanos; lo cual concuerda con estudios previos donde describen la presencia de pequeñas fibras nerviosas en el interior y la periferia del NAV, pero que solo pueden identificarse mediante microscopía electrónica, ya que bajo microscopía óptica no es visible[5,12].

Investigaciones previas describen cuatro tipos de células en el NAV (células P, CT, cardiomiocitos y CP)[34,36,37], de las cuales, en nuestro estudio no se encontraron CP. Esto puede deberse al hecho de que estas células solo pueden visualizarse en este nivel mediante microscopía electrónica como lo describen estos autores. Estudios previos indican que las células P en el NAV en humanos son pequeñas, pálidas, ovoides o redondeadas, individuales o que forman grupos muy pequeños de células que se anastomosan. Tienen un diámetro máximo de 5 a 10 µm, siendo mucho más pequeñas que los cardiomiocitos[6,12,36]. Encontramos una descripción similar de las células P, aunque en nuestro estudio eran tan oscuras como los cardiomiocitos. La función de las células P en este nodo es principalmente retrasar el impulso eléctrico en su camino hacia los ventrículos. Se describe que en el NAV hay una gran cantidad de CT largas y delgadas dentro de cada nodo y en sus márgenes periféricos, que sirven para llevar la señal al cuerpo del nodo y también se transmiten a las vías de conducción ventricular[12]; estas

descripciones coinciden con lo encontrado en nuestra investigación, aunque observamos que las CT se ubicaron principalmente en la periferia.

En cerdos no se ha descrito la medición de los diferentes parámetros del NAV, pero pudimos observar en nuestro estudio que estos valores son similares a los encontrados en humanos. El reconocimiento histológico del nodo se realiza por su ubicación y las características particulares de sus células. Hemos encontrado que hay gran cantidad de tejido conectivo entre las pocas células presentes en el NAV mediante microscopía óptica. Pequeñas variaciones de estas condiciones podrían estar afectando dramáticamente su función normal de retrasar la transmisión del impulso eléctrico desde las aurículas a los ventrículos y de esta forma posibilitando la presencia de arritmias ventriculares o bloqueos de conducción de diferente grado. A pesar de que pocas veces fue posible observar la presencia de la RNAV en cerdos, esta se ubica en la parte distal del nodo cerca de la unión con el HH como ha sido descrito en humanos[40,130]. En los cerdos pudimos observar una gran cantidad de fibras nerviosas en el interior y en la periferia del nodo, lo que también ha sido descrito en un estudio previo[27]. Las células P del NAV en cerdos se describen como células pálidas en las que el diámetro es aproximadamente el mismo que el de los cardiomiocitos[27]. En nuestro estudio, las características físicas son las mismas que las descritas, pero el diámetro es mucho mayor que el de los cardiomiocitos, llegando incluso a valores que duplican su tamaño.

Se ha demostrado que la desmina es el principal FI presente en el músculo cardíaco y que suele acumularse en los discos intercalados y Z, logrando una conexión del aparato contráctil con los demás componentes celulares[135-137]. Además, se ha podido identificar la presencia de estos FI en las células del SCC en mayor cantidad que en los cardiomiocitos, esto es principalmente, porque la presencia de desmina se distribuye por todo el citoplasma de las células de conducción y no solo en puntos específicos como en las células del músculo cardíaco[84,138,139]. Por lo tanto, se pudo observar en nuestro estudio al utilizar el anticuerpo anti-desmina, que mostró una reacción mayor

a las células de conducción nodales que a los cardiomiocitos. Además, se ha descrito que las células del NSA muestran mayor positividad a desmina que las células del NAV[139], lo que hemos podido comprobar en nuestra investigación.

Se ha indicado que a partir de diferentes estudios del SCC en el caballo, vaca, oveja, cerdo, gato y mono, no se han encontrado diferencias notables en la anatomía del NSA y NAV en comparación con el corazón humano[12], lo que aporta valor a nuestros resultados, donde encontramos varias similitudes entre los parámetros medidos en ambos nodos de las dos especies estudiadas (Tabla 2) y aumenta la posibilidad de utilizar el cerdo como modelo animal[27] para experimentación clínica y hemodinámica en humanos con el fin de prevenir la presentación de arritmias supraventriculares.

2. Variaciones morfológicas del sistema de conducción en la zona atrioventricular y su relación clínica en diferentes especies

El estudio de las microestructuras ubicadas en la zona atrioventricular de humanos y otras especies animales es importante para la comprensión de las arritmias debido al papel protector que tienen las células P del NAV retrasando el paso del impulso eléctrico a los ventrículos.

Se han descrito diferentes variaciones morfológicas a nivel atrioventricular por envejecimiento en humanos: bloqueo cardíaco por lesiones calcáreas en el HH[46] y lesiones similares de "esclerosis del lado izquierdo del esqueleto cardíaco" con presencia de fibrosis, hialinización y calcificación[47,48,53,140,141]. En los seres humanos, estos cambios a menudo involucran el sistema de conducción atrioventricular adyacente, lo que conduce a una pérdida de fibras de conducción y un aumento de la fibrosis a este nivel[47], aunque la ausencia de cartílago y hueso en el EFC se encontró en un estudio en 250 corazones humanos[52,134]. Tanto el cartílago como el hueso se han observado raramente en corazones humanos, a veces en asociación con muerte súbita debido a arritmias cardíacas; estos hallazgos indicarían que esta alteración es causada por la presencia de cartílago en el EFC[142,143]. Esto coincide con nuestro estudio donde no encontramos metaplasia cartilaginosa en el EFC en el corazón humano y al compararlo con corazones de animales con cartílago, hubo un aumento de las fibras de colágeno y sustancia fundamental en el NAV en los corazones de cerdos y perros.

La presencia de cartílago con posterior formación de hueso (*os cordis*) se ha descrito como parte de la anatomía normal en corazones de ungulados como ovejas y vacas. De manera similar, esta estructura se ha descrito en corazones de caballos, búfalos de agua y algunos gatos[4,12,30]. Se ha propuesto que este hueso en el EFC de los ungulados puede proteger el NAV y el HH del estrés mecánico durante la sístole cardíaca en corazones de grandes mamíferos[12,144]. De manera similar, se ha informado la presencia de cartílago en el EFC en cerdos, principalmente del tipo hialino, y con menos

frecuencia de tipo fibroso[49]. Nuestros hallazgos en el EFC de las especies animales evaluadas son consistentes con esas descripciones.

Se ha afirmado que la metaplasia cartilaginosa en el EFC con degeneración focal en el HH de perros Dóberman Pinscher de diferentes edades conduce a muerte súbita[52]. Además, se ha descrito una falta de comunicación entre el atrio y el NAV, con atrofia de este último, con interrupción de la continuidad hacia el HH y cambios degenerativos en el SCC con bloqueo cardíaco espontáneo cuando hay presencia de metaplasia cartilaginosa[53]. En consecuencia, estos cambios en el EFC podrían alterar los componentes de este y provocar arritmias.

La presencia de cartílago en el EFC se considera como metaplasia cartilaginosa en el corazón de perro y otras especies animales, produciendo lesiones en el SCC y muerte súbita[45,52], aunque se ha observado cartílago en el EFC de perros con funcionamiento electrocardiográfico normal[44,50,51,145], así como en varias especies de mamíferos[49]. Al igual que estos estudios anteriores, en nuestra investigación encontramos presencia de cartílago en el EFC en cerdos, caballos y perros en porcentajes superiores al 50%. En nuestro estudio, también pensamos inicialmente en la posibilidad de que la presencia de cartílago estuviera relacionada con la edad del animal. Para descartar esta eventualidad, estudiamos caballos y perros entre 5 y 12 años, pero encontramos que había cartílago en el EFC de estas especies en los diferentes individuos evaluados, por lo que consideramos que la aparición de metaplasia cartilaginosa puede ser estructural para cada individuo y es independiente de la edad de presentación.

Estudios anteriores también han encontrado que el NAV de algunos corazones de perros de razas grandes sin enfermedad cardíaca aparente tenían un diámetro menor cuando había presencia de metaplasia cartilaginosa en el EFC y que algunos de los nodos evaluados se movían hacia el centro del tabique interauricular. en lugar de su posición subendocárdica habitual[45]. Además, los mismos autores encontraron que en perros, hubo un aumento en el estroma del tejido conectivo y pérdida de las

fibras conductoras en los NAV evaluados con metaplasia cartilaginosa[45]. En nuestro estudio, hubo una disminución significativa del tamaño del NAV en los cerdos cuando presentaron metaplasia cartilaginosa y un desplazamiento de su posición normal. Además, hubo un aumento en el porcentaje de fibras de colágeno y una disminución en el porcentaje de células dentro del nodo cuando había cartílago en el EFC. En caballos y perros, a pesar de no encontrar diferencias significativas, se observó que los NAV de estas dos especies tienen características similares a las de los cerdos. Esto significa que la detección precoz de este tejido cartilaginoso por métodos ecocardiográficos puede ayudar a determinar individuos de estas especies susceptibles de alteraciones en el ritmo cardíaco. Además, un estudio de perros de razas grandes con problemas cardíacos indicó que el principal cambio morfológico en el EFC fue la presencia de metaplasia cartilaginosa en el 98% de los casos evaluados sin correlacionarse con la edad o la raza[45]. Esto coincide con nuestros hallazgos, siendo uno de los principales cambios encontrados, pero en menor porcentaje en cada especie.

Sin embargo, no solo estos cambios se pueden observar en corazones normales; se ha descrito la presencia de metaplasia cartilaginosa en el EFC en corazones de gatos con cardiomiopatía idiopática[146]. Estos hallazgos apoyan la hipótesis de una función decreciente de las células del NAV cuando se encuentra cartílago en este tejido fibroso.

Asimismo, determinamos que el área y los diámetros de las células P en el NAV de cerdos, caballos y perros fueron significativamente mayores cuando no había presencia de metaplasia cartilaginosa en el EFC. A diferencia de lo descrito por Sandusky[45], donde indica que estos cambios en el EFC y el NAV eran variaciones normales en los corazones de los perros de razas grandes y no había relación con los cambios patológicos. Se desconocen las razones por las cuales ocurre la metaplasia cartilaginosa, pero encontramos que en todos los casos que la han tenido, hubo un aumento en la producción de tejido conectivo, lo cual no ocurre solo dentro del NAV con un aumento de las fibras de colágeno, sino también fuera de él, con la aparición de cartílago hialino o

fibroso, estos resultados son un hallazgo anatómico comprobable para el que no tenemos explicación. Esto se acompaña de una disminución en el número y tamaño de las células conductoras, lo que resulta en un retraso del impulso eléctrico a los ventrículos en animales de cualquier edad y sin cardiopatía previa.

3. Identificación de las células de Purkinje en humanos y cerdos según su distribución zonal, mediante estudio histológico, inmunohistoquímico y morfométrico

Las FP y las CP propagan un impulso eléctrico de una célula a otra y a los cardiomiocitos de manera coordinada por todo el VI, lo que permite la contracción del músculo cardíaco. Conocer las características específicas de estas células desde una perspectiva morfométrica en las diferentes regiones del VI es fundamental para comprender el comportamiento de estas células en el corazón normal, así como en diferentes patologías cardíacas como el infarto de miocardio y las arritmias cardíacas.

Histológicamente, la red de conducción cardíaca se describe como formada por fibras subendocárdicas eléctricamente aisladas que comprenden células especializadas con menos miofibrillas y mitocondrias que los cardiomiocitos, que muestran altos niveles de conexinas como sucede con la Cx40, canales de Na^+ y otras proteínas asociadas con la transmisión rápida de impulsos[95,147]. En nuestro estudio, determinamos que las FP eran más gruesas entre la base y el tercio medio en humanos. Esto es lógico porque estas fibras se originan a partir del HH en la parte superior de los ventrículos y es aquí también donde reciben el impulso eléctrico. Posteriormente se distribuyen en la gran musculatura presente en el tercio medio y se dirigen hacia la parte distal del corazón, ascendiendo finalmente hasta el borde libre de los ventrículos, y permitiendo la despolarización y contracción del músculo cardíaco.

Sin embargo, estas fibras también juegan un papel importante en la generación de arritmias ventriculares[13,68], otorgando así importancia al estudio de las características de las FP, para identificar las arritmias ventriculares que las afectan. La TV y la FV pueden estar presentes en humanos y animales con cardiopatía isquémica o en corazones completamente normales[93-96]. Se ha descrito que el sitio de reentrada en la

TV tras un infarto de miocardio se localizó principalmente en las regiones basal anteroseptal e inferolateral del VI en humanos[148].

Además, esta arritmia se genera en la red de Purkinje subendocárdica[94]. También se ha demostrado que los niveles de Cx40 y de Cx45 en el subendocardio septal en humanos están drásticamente disminuidos en la cardiomiopatía arritmogénica del ventrículo derecho[149]. Coincidiendo parcialmente con estos estudios, nuestros hallazgos indicaron que en humanos las FP se localizan y son más gruesas principalmente en la región anterior y septal en todas las rodajas analizadas (base, tercio medio y ápex). Analizando los datos obtenidos en nuestro estudio y de estudios previos relacionados con las patologías cardíacas, hemos observado que el principal punto de origen de las arritmias ventriculares es la región septal del corazón. Esto puede deberse a que esta región es donde se recibe el impulso del sistema de conducción atrioventricular y donde hay mayor cantidad de fibras, ya que está rodeada por el endocardio en su totalidad.

Las CP se han caracterizado previamente en humanos por tener una apariencia pálida con pocas miofibrillas y estar rodeadas individualmente por una vaina de tejido conectivo en lugar de en forma de haces como se encuentran en otras especies[4,7,69,84,89]. Esta descripción de las CP fue consistente con nuestro estudio, pero estas células rara vez se organizaron individualmente; por el contrario, se organizaron principalmente en pequeños haces delgados de 2-10 células, parcialmente rodeados de tejido conectivo y con un aspecto similar a los cardiomiocitos, lo que las hacía difíciles de reconocerlas. A nivel subendocárdico, las CP en humanos cuyo diámetro está entre 10-46 µm, se han descrito como cilíndricas o fusiformes y más grandes que los cardiomiocitos ventriculares (alrededor de 10 µm)[2,69,84], estos datos de las CP y cardiomiocitos fueron mayores que en nuestros hallazgos. Se ha descrito que en el grupo II, como en humanos, las CP tienen una gran positividad a la desmina en comparación con los cardiomiocitos[84,138]. En nuestro estudio, encontramos una alta positividad de las CP a la desmina en humanos y los cardiomiocitos reaccionaron positivamente, pero con menor intensidad.

Las UPM actúan como membranas de baja resistencia para que los impulsos eléctricos se propaguen, permitiendo que iones y moléculas pequeñas pasen a través de ellas[105,106,110]. Estas uniones son responsables del acoplamiento eléctrico en el corazón y lo realizan a través de canales transmembrana compuestos por conexinas[105,106]. En humanos, se ha descrito la distribución espacial de las UPM y se encontró que se ubicaban particularmente en la base[120]. En nuestro estudio, estas uniones se ubicaron principalmente en el ápex del corazón y a nivel de la región septal, lo que indica que la alta densidad de las fibras en esta región podría señalarse como el sitio principal de generación de arritmias ventriculares. Estudios previos indican la importancia de las CT en la transmisión de impulsos eléctricos a través de UPM en humanos[116,150,151]. La presencia de estas células entre las CP y los cardiomiocitos asegura un alto acoplamiento y una conducción rápida en el miocardio[2,118], aunque un estudio más reciente indicó que las CT no estaban presentes en las uniones de corazones de humanos y bovinos[2]. En nuestra investigación detectamos este tipo de unión (CTCT) localizada en humanos principalmente en la base cardíaca en pequeños porcentajes.

Las FP en cerdos se distribuyeron de manera similar entre regiones y rodajas a nivel subendocárdico, pero en el miocardio, generalmente se encontraron en la región septal especialmente en el tercio medio y el ápex. También observamos que las fibras fueron más gruesas en la región septal, en el miocardio. entre el tercio medio y el ápex. Esto indica, la alta transmisión del impulso cardíaco a través del endocardio para ser enviado al miocardio, logrando una rápida despolarización de las fibras cardíacas ventriculares. En los cerdos, se ha descrito que las FP están rodeadas por vainas de fibras de reticulina que forman haces compuestos entre 2-8 CP ovales[4,5,7,69,84]. En nuestro estudio las FP también presentaron vainas de tejido conectivo rodeando las fibras, pero parcialmente y formando haces con más células de las descritas. Las CP fueron identificadas por cuerpos celulares pálidos, con uno o dos núcleos y pocas miofibrillas ubicadas periféricamente[4,5,7,69,84]. Las características celulares coinciden con nuestro estudio, ya que las CP eran más grandes que los cardiomiocitos y fáciles de identificar.

Discusión

El aspecto pálido de las CP, principalmente en ungulados, pero observado también en otras especies, se ha atribuido a la baja presencia de miofibrillas y alta cantidad de glucógeno en su citoplasma, que es típico de las células de conducción[2,4,7,118,152]. La técnica de PAS para identificar las CP con grandes cantidades de glucógeno observado en su citoplasma se ha utilizado de manera eficiente en ungulados, aunque algunos estudios han encontrado que, en otras especies, incluidos los humanos estas células no se identifican claramente con este método[2,69]. Otro estudio sugiere que la cantidad de glucógeno presente en las CP en comparación con los cardiomiocitos no es del todo confiable como criterio diferencial seguro[152]. En nuestro estudio, la identificación de las CP con la técnica de PAS resultó ser una buena herramienta para este propósito en humanos y cerdos, a diferencia de resultados previos donde encontraron que el método tenía poco valor para identificar las CP en humanos. Se observó glucógeno en todo el citoplasma de las CP estudiado, lo que permite una buena diferenciación con los cardiomiocitos. En especies animales pertenecientes al grupo I, como los ungulados, una fuerte reacción positiva a la desmina por las CP también se ha observado[84,138]. También se ha indicado que los FI eran abundantes en las CP de aves y grandes mamíferos[85] y la diferenciación celular con cardiomiocitos es posible usando desmina como marcador[138,139]. En los cerdos, la desmina se distribuyó por todo el citoplasma de las CP tanto en el subendocardio como en el miocardio, mostrando una fuerte positividad en comparación con los cardiomiocitos, que reaccionaron ligeramente a la tinción.

En una serie de muestras evaluadas en algunas especies de ungulados (bovinos y ovinos), se encontró UPM en 15%[78]. En los cerdos, observamos la presencia de estas uniones en un mayor porcentaje y localizadas principalmente en la base y el miocardio a nivel septal, aunque estudios previos indican que las UPM solo ocurren en la parte distal del corazón[60]. En nuestro estudio, determinamos que estas uniones se distribuyeron a lo largo de la superficie ventricular. Como se indicó anteriormente, en los cerdos algunas FP se extendieron desde el endocardio al epicardio y sus UPM se

comportaron de la misma manera, lo que podría explicar por qué la activación transmural es casi instantánea en esta especie[60,153]. La presencia de CT en las UPM, que regulan la transmisión más rápida del impulso eléctrico, ha sido bien documentada en cerdos[2,118], esto se verificó en nuestro estudio donde encontramos este tipo de unión (CTCT) regulado por CT. Observamos que el mayor porcentaje de UPM en humanos y cerdos fue a través de las uniones CTCC en todas las regiones analizadas.

G. CONCLUSIONES

El sistema de conducción cardiaco tiene importancia en la transmisión de los impulsos eléctricos en los corazones de humanos y las especies animales y sus implicaciones en la prevención de arritmias cardiacas. Por lo tanto, podemos concluir que:

1.1 El estudio de la estructura y los componentes de los nodos sinoatrial y atrioventricular en humanos y cerdos mediante morfometría y descripción histológica, permitió profundizar el conocimiento de estas estructuras del sistema de conducción cardiaco.

1.2 La menor densidad celular en cualquiera de los nodos cardíacos, especialmente en las células P del nodo sinoatrial, puede disminuir la conducción eléctrica dentro de los nodos y en los tractos internodales, lo que reflejaría la presencia de arritmias cardíacas derivadas de la mala conducción, incluso en corazones morfológicamente normales.

1.3 A través de nuestro perfil morfométrico hemos observado que la estructura de los nodos sinoatrial y atrioventricular de humanos y cerdos presentan pocas diferencias, por lo que concluimos que esta especie animal puede ser utilizada como modelo para aplicaciones hemodinámicas y estudios experimentales que incluyan la conducción eléctrica auricular y de esta forma prevenir la presentación de arritmias en humanos.

2. La presencia de metaplasia cartilaginosa por edad o como característica estructural individual en el esqueleto fibroso cardiaco de cerdos, caballos y perros disminuye el tamaño del nodo atrioventricular y sus células y aumenta el porcentaje de fibras de colágeno dentro del nodo, lo que puede disminuir la transmisión del impulso eléctrico hacia los ventrículos y por lo tanto predisponen a arritmias ventriculares. En humanos no existe metaplasia cartilaginosa cardíaca.

3.1 Las fibras de Purkinje se encontraron principalmente en la región septal del corazón en humanos y cerdos. También fueron más gruesas

homogéneamente entre la base y el tercio medio, siendo el posible sitio de generación de arritmias ventriculares.

3.2 Las células de Purkinje son difíciles de identificar en humanos porque presentan un color similar a los cardiomiocitos, a diferencia de las de los cerdos donde son fácilmente identificables. Por lo tanto, recomendamos el uso de morfometría y de tinciones alternativas como tricrómico de Masson, desmina y la tinción de PAS para una identificación precisa de las células de Purkinje en humanos.

3.3 Se encontraron uniones Purkinje-miocardio en mayores cantidades en el ápex y la región septal en humanos, mientras que en cerdos fueron más abundantes en la base y la región septal.

3.4 Esta investigación contribuyó en gran medida a la generación de nuevos conocimientos sobre el sistema de conducción cardiaco en humanos, cerdos, caballos y perros

H. BIBLIOGRAFIA

1. Keith A, Flack M. The form and nature of the muscular connections between the primary division of the vertebrate heart. J Anat Physiol 1907; 41: 172-189.
2. Eliška O. Purkinje fibers of the heart conduction system-history and the present time. Cas Lek Cesk 2006; 145: 329-335.
3. Haissaguerre M, Cheniti G, Escande W, Zhao A, Hocini M, Bernus O. Idiopathic ventricular fibrillation with repetitive activity inducible within the distal Purkinje system. Heart Rhythm 2019; 16: 1268-1272.
4. Tawara S. Das Reizleitungssystem des Säugetierherzens; eine anatomisch-histologische Studie über das Atrioventrikularbündel und die Purkinjeschen Fäden. Jena, Marburg: Gustav Fischer; 1906.
5. Glomset DJ, Glomset ATA. A Morphologic study of the cardiac conduction system in ungulates, dog and man. Part II: The Purkinje system. Am Heart J 1940; 20: 677-701.
6. James TN, Sherf L, Fine G, Morales AR. Comparative ultrastructure of the sinus node in man and dog. Circulation 1966; 34: 139-163.
7. Tawara S. The conduction system of the mammalian heart. London: Imperial College Press; 2000.
8. Silverman M, Grove D, Upshaw CB Jr. Why does the heart beat? The discovery of the electrical system of the heart. Circulation 2006; 113: 2775–2781.

9. Pallante B, Giovannone S, Fang-Yu L, Zhang J, Lis N, Kang G, Dun W, Boyden PA, Fishman GI. Contactin-2 expression in the cardiac Purkinje fiber network. Circ Arrhythm Electrophysiol 2010; 3: 186-194.
10. Garcia-Bustos V, Sebastian R, Izquierdo M, Molina P, Chorro FJ, Ruiz-Sauri A. A quantitative structural and morphometric analysis of the Purkinje network and the Purkinje–myocardial junctions in pig hearts. J Anat 2017; 230: 664-678.
11. Davies F, Francis ETB. The conducting system of the vertebrate heart. Br Heart J 1942; 4: 66-76.
12. James TN. Structure and function of the sinus node, AV node and Hiss bundle of the human heart: Part I – Structure. Prog Cardiovasc Dis 2002; 45: 235-267.
13. Li N, Csepe TA, Hansen BJ, Dobrzynski H, Higgins RSD, Kilic A, Mohler PJ, Janssen PML, Rosen MR, Biesiadecki BJ, Fedorov VV. Molecular mapping of sinoatrial node HCN channel expression in the human heart. Circ Arrhythm Electrophysiol 2015; 8: 1219-1227.
14. Kennedy A, Finlay DD, Guldenring D, Bond R, Moran K, McLaughlin J. The cardiac conduction system. Generation and conduction of the cardiac impulse. Crit Care Nurs Clin North Am 2016; 28: 269-279.
15. Koch W. What significance does the sinus node have? Med Klin 1911; 328: 447.
16. Glomset DJ, Glomset ATA. Morphologic study of the cardiac conduction system in ungulates, dog and man. Part I: The sinoatrial node. Am Heart J 1940; 4: 389-398.

17. Chiu IS, Hung CR, How SW, Chen MR. Is the sinus node visible grossly? A histological study of normal hearts. Int J Cardiol 1989; 22: 83-87.
18. Waller B, Gering LE, Branyas NA, Slack JD. Anatomy, histology, and pathology of the cardiac conduction system: Part I. Clin Cardiol 1993; 16: 249-252.
19. Oosthoek PW, Virágh S, Lamers WH, Moorman AF. Immunohistochemical delineation of the conduction system I: the sinoatrial node. Circ Res 1993; 73: 473–481.
20. Dobrzynski H, Anderson RH, Atkinson A, Borbas Z, D'Souza A, Fraser JF, Inada S, Logantha SJRJ, Monfredi O, Morris GM, Moorman AFM, Nikolaidou T, Schneider H, Szuts V, Temple IP, Yanni J, Boyett MR. Structure, function and clinical relevance of the cardiac conduction system, including the atrioventricular ring and outflow tract tissues. Pharmacol Ther 2013; 139: 260–288.
21. Ortale JR, Paganoti CF, Marchiori GF. Anatomical variations in the human sinuatrial nodal artery. Clinics (Sao Paulo) 2006; 61: 551-558.
22. Zhang LJ, Wang YZ, Huang W, Chen P, Zhou CS, Lu GM. Anatomical investigation of the sinus node artery using dual source computed tomography. Circ J 2008; 72: 1615-1620.
23. Ramanathan L, Shetty P, Nayak SR, Krishnamurthy A, Chettiar GK, Chockalingam A. Origin of the sinoatrial and atrioventricular nodal arteries in South Indians: an angiographic study. Arq Bras Cardiol 2009; 92: 314-319.

24. Ballesteros LE, Ramírez LM, Quintero ID. Right coronary artery anatomy: anatomical and morphometric analysis. Rev Bras Cir Cardiovasc 2011; 26: 230-237.
25. Cademartiri F, La Grutta L, Malagò R, Alberghina F, Meijboom WB, Pugliese F, Maffei E, Palumbo AA, Aldrovandi A, Fusaro M, Brambilla, V, Coruzz P, Midiri M, Mollet NRA, Krestin GP. Prevalence of anatomical variants and coronary anomalies in 543 consecutive patients studied with 64-slice CT coronary angiography. Eur Radiol 2008; 18: 781-791.
26. Opthof T, de Jonge B, Jongsma HJ, Bouman LN. Functional morphology of the pig sinoatrial node. J Mol Cell Cardiol 1987; 19: 1221-1236.
27. Bharati S, Levine M, Huang SKS, Handler B, Parr GVS, Bauernfeind R, Lev M. The conduction system of the swine heart. Chest 1991; 100: 207-212.
28. Crick SJ, Sheppard MN, Ho SY, Gebstein L, Anderson RH. Anatomy of the pig heart: comparisons with normal human cardiac structure. J Anat 1998; 193: 105-119.
29. Gómez FA, Ballesteros LE. Anatomic study of the right coronary artery in pigs. Feature review in comparison with the human artery. Int J Morphol 2013; 31: 1289-1296.
30. Bishop SP, Cole CR. Morphology of the specialized conducting tissue in the atria of the equine heart. Anat Rec 1967; 158: 401-415.
31. Mettam RW. The atrioventricular system of the equine heart. Union Africa Department of Agriculture 13 and 14; 1928.

32. Gómez FA, Ballesteros LE, Estupiñan HY. Morphological characterization of the left coronary artery in horses. Comparative analysis with humans, pigs, and other animal species. Ital J Anat Embryol 2017; 122: 137-146.
33. James TN. Anatomy of the sinus node of the dog. Anat Rec 1964; 143: 251-265.
34. James TN. The connecting pathways between the sinus node and A-V node between the right and the left atrium in the human heart. Am Heart J 1963; 66: 498-508.
35. James TN. Morphology of the human atrioventricular node with remarks pertinent to its electrophysiology. Am Heart J 1961; 52: 756-771.
36. Waller B, Gering LE, Branyas NA, Slack JD. Anatomy, histology, and pathology of the cardiac conduction system: Part II. Clin Cardiol 1993; 16: 347-352.
37. James TN, Sherf L. Specialized tissue and preferential conduction in the atria of the heart. Am J Cardiol 1971; 28: 414-427.
38. Berdajs D, Kunzli A, Shurr U, Zünd G, Turina MI, Genonni M. Clinical anatomy of the atrioventricular node artery. J Heart Valve Dis 2006; 15: 225-229.
39. Saremi F, Abolhoda A, Ashikyan O, Milliken JC, Narula J, Gurudevan SV, Kaushal K, Raney A. Arterial supply to sinuatrial and atrioventricular nodes: imaging with multidetector CT. Radiology 2008; 246: 99-107.

40. Futami C, Tanuma K, Tanuma Y, Saito T. The arterial blood supply of the conducting system in normal human hearts. Surg Radiol Anat 2003; 25: 42-49.
41. Pejković B, Krajnc I, Anderhuber F, Kosutić D. Anatomical aspects of the arterial blood supply to the sinoatrial and atrioventricular nodes of the human heart. J Int Med Res 2008; 36: 691-698.
42. Sahni D, Kaur GD, Jit H, Jit I. Anatomy and distribution of coronary arteries in pig in comparison with man. Indian J Med Res 2008; 127: 564-570.
43. Gómez FA, Ballesteros LE, Estupiñan HY. Morphologic expression of the right coronary artery in horses. Comparative description with humans, pigs and other animal species. Austral J Vet Sci 2017; 49: 161-166.
44. James TN. Anatomy of the A-V node of the dog. Anat Rec 1964; 148: 15-27.
45. Sandusky Jr GE, Kerr KM, Capen CC. Morphologic variations and aging in the atrioventricular conduction system of large breed dogs. Anat Rec 1979; 193: 883-902.
46. Yater WM, Cornell VH. Heart block due to calcereous lesions of the bundle of His: review and report of a case with detailed histopathological study. Ann Intern Med 1935; 8: 777-789.
47. Lenegre J. Etiology and pathology of bilateral branch block in relation to complete heart block. Prog Cardiovasc Dis 1964; 6: 409-444.
48. Lev M. The pathology of complete atrioventricular block. Prog Cardiovasc Dis 1964; 6: 317-326.

49. Murata H, Yamada K. Glycosaminoglycans in the cartilage of the porcine heart as studied by light microscopic histochemical methods. Acta Histochem 1986; 79: 83-92
50. Buchanan JW. Chronic valvular disease (endocardiosis) in dogs. Adv Vet Sci Comp Med 1977; 21: 75-108.
51. Aupperle H, März I, Schoon HA. Detection and characterization of chondroid metaplasia in canine atrioventricular valves. J Comp Pathol 2008; 139: 113-120.
52. James TN, Drake EH. Sudden death in Doberman Pinschers. Ann Intern Med 1968; 68: 821-829.
53. Bharati S, Rosen KM, Milter RA, Lev M. Conduction system examination in a case of spontaneous heart block in a dog. Amer Heart J 1974; 88: 596-600.
54. Chorro FJ, Such-Belenguer L, López-Merino V. Animal models of cardiovascular disease. Rev Esp Cardiol 2009; 62: 69-84.
55. De Almeida MC, Lopes F, Fontes P, Barra F, Guimaraes R, Vilhena V. Ungulates heart model: a study of the Purkinje network using India ink injection, transparent specimens and computer tomography. Anat Sci Int 2015; 90: 240-250.
56. Row S, Swartz DD, Andreadis ST. Animal models of cardiovascular disease as test beds of bioengineered vascular grafts. Drug Discov Today: Disease Model 2017; 24: 37-45.
57. Cunningham SM, Rush JE. Transvenous pacemaker placement in a dog with atrioventricular block and persistent left cranial vena cava. J Vet Cardiol 2007; 9: 129-134.

58. Cervenec RM, Stauthammer CD, Fine DM, Kellihan HB, Scansen B. Survival time with pacemaker implantation for dogs diagnosed with persistent atrial standstill. J Vet Cardiol 2017; 19: 240-246.
59. Uhley HN, Rivkin L. Peripheral distribution of the canine AV conduction system; observations on gross morphology. Am J Cardiol 1960; 5: 688-691.
60. Vigmond EJ, Stuyvers BD. Modeling our understanding of the His-Purkinje system. Prog Biophys Mol Biol 2016; 120: 179-188.
61. Duan D, Yu S, Cui Y, Li C. Morphological study of the atrioventricular conduction system and Purkinje fibers in yak. J Morphol 2017; 278: 975-986.
62. Cabrera JA, Anderson RH, Macías Y, Nevado-Medina J, Porta-Sánchez A, Rubio JM, Sánchez-Quintana D. Variable arrangement of the atrioventricular conduction axis within the triangle of Koch: implications for permanent His bundle pacing. JACC Clin Electrophysiol 2020; 6: 362-377.
63. Ho SY, Kilpatrick L, Kanal T, Germroth PG, Thompson RP, Anderson RH. The architecture of the atrioventricular conduction axis in dog compared to man: Its significance to ablation of the atrioventricular nodal approaches. Cardiovasc Electrophysiol 1995; 6: 26-39.
64. Truex RC, Smythe MQ. Comparative morphology of the cardiac conduction tissue in animals. Ann N Y Acad Sci 1965; 127: 19-33.
65. James TN. Anatomy of the coronary arteries. Hagerstown, MD: Harper Bros; 1961.

66. James TN. Cardiac innervation: Anatomic and pharmacologic relations. Bull NY Acad Med 1967; 43: 1041-1086.
67. Sedmera D, Gourdie RG. Why do we have Purkinje fibers deep in our heart? Physiol Res 2014; 63: S9-S18.
68. Aouadi S, Mbarki W, Zemzemi N. Towards the modeling of the Purkinje/myocardium coupled problem: A well-posedness analysis. J Comput Appl Math 2019; 351: 136-152.
69. Ono N, Yamaguchi T, Ishikawa H, Arakawa M, Takahashi N, Saikawa T, Shimada T. Morphological varieties of the Purkinje fiber network in mammalian hearts, as revealed by light and electron microscopy. Arch Histol Cytol 2009; 72: 139-149.
70. Zimmermann A. Das Reizleitungssystem des Herzens bei Equiden. Anat Anz (Erg H) 1923; 57: 552-558.
71. Abramson DI, Margolin S. A Purkinje conduction network in the myocardium of the mammalian ventricles. J Anat 1936; 70: 250-260.
72. Atkinson A, Inada S, Li J, Tellez JO, Yanni J, Sleiman R, Allah EA, Anderson RH, Zhang H, Boyett MR, Dobrzynski H. Anatomical and molecular mapping of the left and right ventricular His-Purkinje conduction networks. J Mol Cell Cardiol 2011; 51: 689-701.
73. Romero D, Camara O, Sachse F, Sebastian R. Analysis of microstructure of the cardiac conduction system base on three-dimensional confocal microscopy. PLoS ONE 2016; 11: e0164093.
74. Benson A, Aslanidi O, Zhang H, Holden AV. The canine virtual ventricular wall: a platform for dissecting pharmacological effects on

propagation and arrhythmogenesis. Prog Biophys Mol Biol 2008; 96: 187-208.

75. Bordas R, Gillow K, Lou Q, Efimov IR, Gavaghan D, Kohl P, Grau V, Rodriguez B. Rabbit-specific ventricular model of cardiac electrophysiological function including specialized conduction system. Prog Biophys Mol Biol 2011; 107: 90-100.
76. Stephenson R, Boyett M, Hart G, Nikolaidou T, Cai X, Corno AF, Alphonso N, Jeffery N, Jarvis JC. Contrast enhanced micro-computed tomography resolves the 3-dimensional morphology of the cardiac conduction system in mammalian hearts. PLoS One 2012; 7: e35299.
77. Yao X, Gan Y, Marboe CC, Hendon CP. Myocardial imaging using ultrahigh-resolution spectral domain optical coherence tomography. J Biomed Opt 2016; 21: 61006.
78. Pieperhoff S, Borrmann C, Grund C, Barth M, Rizzo S, Franke WW. The area composita of adhering junctions connecting heart muscle cells of vertebrates. VII. The different types of lateral junctions between the special cardiomyocytes of the conduction system of ovine and bovine hearts. Eur J Cell Biol 2010; 89: 365–378.
79. Otsuka N, Hara T, Kataoka A. Experimentelle untersuchungen der PAS-reaktion zur darstellung des reizleitungs systems am hundeherzen. Acta Anat Nippon 1966; 41: 1-6.
80. Shimada T, Ushiki T, Fujita T. Purkinje fibers of the heart. Shinyaku to chiryou 1992; 42: 11-13.

81. Hondeghem L, Stroobandt R. Purkinje fibers of sheep papillary muscle: occurrence of discontinuous fibers. Am J Anat 1973; 141: 251-262.
82. Viragh S, Challice CE. The impulse generation and conduction system of the heart. In: Ultrastructure in biological systems. Ultrastructure of the mammalian heart. V 6. New york, London: Academic Press, 1973.
83. Friedman PL, Stewart JR, Fenoglio JJ Jr, Wit AL. Survival of subendocardial Purkinje fibers after extensive myocardial infarction in dogs. Circ Res 1973; 33: 597-611.
84. Yoshimura A, Yamaguchi T, Kawazato H, Takahashi N, Shimada T. Immuno-histochemistry and three-dimensional architecture of the intermediate filaments in Purkinje cells in mammalian hearts. Med Mol Morphol 2014; 47: 233-239.
85. Canale E, Campbell G, Smolich J. Cardiac Muscle: The conduction system. Berlin, Heidelberg, New York, Tokio: Springer-Verlag; 1986.
86. Gourdie RG, Green CR, Severs NJ, Anderson RH, Thompson RP. Evidence for a distinct gap-junctional phenotype in ventricular conduction tissues of the developing and mature avian heart. Circ Res 1993; 72: 278-289.
87. Harris BS, O'brien TX, Gourdie RG. Coronary arteriogenesis and differentiation of periarterial Purkinje fibers in the chick heart: is there a link? Tex Heart Inst J 2002; 29: 262-270.
88. Miquerol L, Meysen S, Mangoni M, Bois P, van Rijen H, Abran P, Jongsma H, Nargeot J, Gros D. Architectural and functional

asymmetry of the His-Purkinje system of the murine heart. Cardiovasc Res 2004; 63: 77-86.

89. Shimada T, Nakamura M, Kitahara Y, Sachi M. Surface morphology of chemically-digested Purkinje fibers of the goat heart. J Electron Microsc 1983; 32: 187-196.
90. Sebastian R, Zimmerman V, Romero D, Sanchez-Quintana D, Frangi AF. Characterization and modeling of the peripheral cardiac conduction system. IEEE Transactions on Medical Imaging 2013; 32: 45-55.
91. Eriksson A, Thornell LE. Intermediate (skeleton) filaments in heart Purkinje fibers. A correlative morphological and biochemical identification with evidence of a cytoskeletal function. J Cell Biol 1979; 80: 231–247.
92. Thornell LE, Eriksson A. Filament systems in the Purkinje fibers of the heart. Am J Physiol 1981; 241: 291–305.
93. Tabereaux PB, Dosdall DJ, Ideker RE. Mechanisms of VF maintenance: wandering wavelets, mother rotors, or foci. Heart Rhythm 2009; 6: 405-415.
94. Benito B, Josephson ME. Ventricular tachycardia in coronary artery disease. Rev Esp Cardiol 2012; 65: 939-955.
95. Krishnamoorthy J, Lakshmanan A, Mullasari A. Focal Purkinje ventricular tachycardia ablation in structurally normal heart. Asian Cardiovasc Thorac Ann 2015; 23: 855-857.

96. Gianni C, Burkhardt JD, Trivedi C, Mohanty S, Natale A. The role of the Purkinje network in premature ventricular complex-triggered ventricular fibrillation. J Intery Card Electrophysiol 2018; 52: 375-383.
97. Stevenson WG, Soejima K. Catheter ablation for ventricular tachycardia. Circulation 2007; 115: 2750–2760.
98. He BJ, Boyden P, Scheiman M. Ventricular arrhythmias involving the His-Purkinje system in the structurally abnormal heart. Pacing Clin Electrophysiol 2018; 41: 1051-1059.
99. Nogami A. Purkinje-related arrhythmias part I: monomorphic ventricular tachycardias. Pacing Clin Electrophysiol 2011; 34: 624-650.
100. Okubo Y, Uotani Y, Miyamoto S, Miyauchi S, Ikeuchi Y, Okamura S, Tokuyama T, Nakano Y. Use of a high-density mapping catheter for Purkinje-related ventricular tachycardia in a patient with a previous history of anterior myocardial infarction. Heart Rhythm Case Rep 2021; 7: 232-236.
101. García-Bustos V, Sabastian R, Izquierdo M, Rios-Navarro C, Bodí V, Chorro FJ, Ruiz-Sauri A. Changes in the spatial distribution of the Purkinje network after acute myocardial infarction in a swine model. PLoS ONE 2019; 14: e0212096.
102. Bogun F, Good E, Reich S, Elmouchi D, Igic P, Tschopp D, Dey S, Wimmer A, Jongnarangsin K, Oral H, Chugh H, Pelosi F, Morady F. Role of Purkinje fibers in post-infarction ventricular tachycardia. J Am Coll Cardiol 2006; 48: 2500-2507.

103. Haissaguerre M, Vigmond E, Stuyvers B, Hocini M, Bernus O. Ventricular arrythmias and the His-Purkinje system. Nat Rev Cardiol 2016; 13: 1-12.

104. Trovato C, Passini E, Nagy N, Varró A, Abi-Gerges N, Severi S, Rodriguez B. Human Purkinje in silico model enables mechanistic investigations into automaticity and pro-arrhythmic abnormalities. J Mol Cell Cardiol 2020; 142: 24-38.

105. Gros DB, Jongsma HJ. Connexins in mammalian heart function. BioEssays 1996; 18: 719-730.

106. Vozzi C, Dupont E, Coppen SR, Yeh HI, Severs NJ. Chamber-related differences in connexin expression in the human heart. J Mol Cell Cardiol 1999; 31: 991-1003.

107. Ter Borg H. The atrioventricular conduction system of the big domestic animals, and more especially on the terminal arborization of the Purkinje fibers and the so-called interventricular connections. Acta Neerl Morphol 1941; 4: 97-102.

108. Severs NJ, Coppen SR, Dupont E, Yeh HI, Ko YS, Matsushita T. Gap junction alterations in human cardiac disease. Cardiovasc Res 2004; 62: 368–377.

109. Severs NJ, Bruce AF, Dupont E, Rothery S. Remodelling of gap junctions and connexin expression in diseased myocardium. Cardiovasc Res 2008; 80: 9–19.

110. Bruzzone R, White TW, Paul DL. Connections with connexins: The molecular basis of direct intercellular signalling. Eur J Biochem 1996; 238: 1–27.

111. van Kempen MJA, ten Velde I, Wessels A, Oosthoek PW, Gros D, Jongsma HJ, Moorman AFM, Lamers WH. Differential connexin distribution accommodates cardiac function in different species. Microsc Res Tech 1995; 31: 420–436.

112. Barber F, Langfield P, Lozano M, Garcia-Fernandez I, Duchateau J, Meleze H, Haissaguerre M, Vigmond E, Sebastian R. Estimation of personalized minimal Purkinje system from human electro-anatomical maps. IEEE Transactions on Medical Imaging 2021; In Press.

113. Barber F, Lozano M, Garcia-Fernandez I, Sebastian R. Automatic estimation of Purkinje-myocardial junction hot-spots from noisy endocardical simples: A simulation study. Int J Numer Method Biomed Eng 2018; 34: e2988.

114. Veenstra RD, Joyner RW, Rawling DA. Purkinje and ventricular activation sequences of canine papillary muscle. Circ Res 1984; 54: 500-515.

115. Rawling DA, Joyner RW, Overholt ED. Variations in the functional electrical coupling between the subendocardial Purkinje and ventricular layers of the canine left ventricle. Circ Res 1985; 57: 252-261.

116. Rawling DA, Joyner RW. Characteristics of junctional regions between Purkinje and ventricular muscle cells of canine ventricular subendocardium. Circ Res 1987; 4: 580-585.

117. Alanis J, Benitez D. Transitional potentials and the propagation of impulses through different cardiac cells, in Sano T, Misuhira V,

Matsuda K (eds): Electrophysiology and Ultrastructure of the Heart. New York: Grune & Stratton; 1967.

118. Tranum-Jensen J, Wilde AA, Vermeulen JT, Janse MJ. Morphology of electrophysiologically identifed junctions between Purkinje fibers and ventricular muscle in rabbit and pig heart. Circ.Res 1991; 69: 429-437.
119. Myerburg RJ, Nilsson K, Gelband H. Physiology of canine interventricular conduction and endocardial excitation. Circ Res 1972; 30: 217-243.
120. Myerburg RJ, Nilsson K, Castellanos A, Lazarra R, Befeler B, Gelband H. The intraventricular conducting system and patterns of endocardial excitation. Adv Cardiol 1975; 14: 2-14.
121. Fedorov VV, Glukhov AV, Chang R, Kostecki G, Aferol H, Hucker WJ, Wuskell JP, Loew LM, Schuessler RB, Moazami N, Efimov IR. Optical mapping of the isolated coronary-perfused human sinus node. J Am Coll Cardiol 2010; 56: 1386–1394.
122. Anderson KR, Ho SY, Anderson RH. Location and vascular supply of sinus node in human heart. Br Heart J 1979; 41: 28–32.
123. Glukhov AV, Hage LT, Hansen BJ, Pedraza-Toscano A, Vargas-Pinto P, Hamlin RL, Weiss R, Carnes CA, Billman GE, Fedorov VV. Sinoatrial node reentry in a canine chronic left ventricular infarct model: role of intranodal fibrosis and heterogeneity of refractoriness. Circ Arrhythm Electrophysiol 2013; 6: 984–994.
124. Lou Q, Hansen BJ, Fedorenko O, Csepe TA, Kalyanasundaram A, Li N, Hage LT, Glukhov AV, Billman GE, Weiss R, Molher PJ, Gyorke S,

Biesiadecki BJ, Carnes CA, Fedorov VV. Upregulation of adenosine A1 receptors facilitates sinoatrial node dysfunction in chronic canine heart failure by exacerbating nodal conduction abnormalities revealed by novel dual-sided intramural optical mapping. Circulation 2014; 104: 915–923.

125. Kalyanasundaram A, Li N, Hansen BJ, Zhao J, Fedorov VV. Canine and human sinoatrial node: differences and similitaries in the structure, function, molecular profiles, and arrhythmia. J Vet Cardiol 2019; 22: 2–19.
126. De Maziere AMGL, van Ginneken ACG, Wilders R, Jongsma HJ, Bouman LN. Spatial and functional relationship between myocytes and fibroblasts in the rabbit sinoatrial node. J Moll Cell Cardiol 1992; 24: 567–578.
127. Boyett MR, Honjo H, Kodama I. The sinoatrial node, a heterogeneous pacemaker structure. Cardiovasc Res 2000; 47: 658–687.
128. Csepe TA, Kalyanasundaram A, Hansen BJ, Zhao J, Fedorov VV. Fibrosis: a structural modulator of sinoatrial node physiology and dysfunction. Front Physiol 2015; 6: 1-8.
129. Ward JL, DeFrancesco TC, Tou SP, Atkins CE, Griffith EH, Keene BW. Outcome and survival in canine sick sinus syndrome and sinus node dysfunction: 93 cases (2002-2014). J Vet Cardiol 2016; 18: 199–212.
130. Sánchez-Quintana D, Ho SY. Anatomy of cardiac nodes and atrioventricular specialized conduction system. Rev Esp Cardiol 2003; 56: 1085–1092.

131. Hoffman BF, Cranefield P. The physiologic basis of cardiac arrhythmias. Am J Med 1964; 37: 670–684.
132. Kawamura M. Experimental study of the pacemaker shift in the rabbit atrium by means of the microelectrode method. Jpn Circ J 1968; 32: 26–28.
133. Mani BC, Pavri BB. Dual atrioventricular nodal pathways physiology: a review of relevant anatomy, electrophysiology, and electrocardiographic manifestations Indian Pacing Electrophysiol J 2014; 14: 12–25.
134. Randhawa A, Gupta T, Aggarwal A, Sahni D, Singh RS. Histological topography of the atrioventricular node and its extensions in relation to the cardiothoracic surgical landmarks in normal human hearts. Cardiovasc Pathol 2017; 30: 38–44.
135. Fuchs E, Weber K. Intermediate filaments: structure, dynamics, function and disease. Annu Rev Biochem 1994; 63: 345–382.
136. Paulin D, Li Z. Desmin: a major intermediate filament protein essential for the structural integrity and function of muscle. Exp Cell Res 2004; 301: 1–7.
137. Lowery J, Kuczmarski ER, Hermann H, Goldman RD. Intermediate filaments play a pivotal role in regulating cell architecture and function. J Biol Chem 2015; 290: 17145–17153.
138. Eriksson A, Thornell LE, Torgny S. Skeletin immunoreactivity in heart Purkinje fibers from several species. J Histochem Cytochem 1979; 27: 1604–1609.

139. Forsgren S, Eriksson A, Kjorell U, Thornell LE. The conduction system in the human heart at midgestation – immunohistochemical demonstration of the intermediate filament protein skeleton. Histochemistry 1982; 75: 43–52.

140. van Nieuwenhoven FA, Munts C, Opt-Veld RC, González A, Díez J, Heymans S, Schoroen B, van Bilsen M. Cartilage intermediate layer protein 1 (CILP1): a novel mediator of cardiac extracelular matrix remodelling. Sci Rep 2017; 7: 1–8.

141. Zhang CL, Zhao Q, Liang H, Qiao X, Wang JY, Wu D, Wu LL, Li L. Cartilage intermediate layer protein-1 alleviates pressure overload-induced cardiac fibrosis via interfering TGF-β1 signaling. J Mol Cell Cardiol 2018; 116: 135–144.

142. Ferris JA, Aherne WA. Cartilage in relation to the conduction tissue of the heart in sudden death. Lancet 1971; 1: 64–66.

143. James TN, Marshal TK. Persistent fetal dispersion of the atrioventricular node and His bundle within central fibrous body. Circulation 1976; 53: 1026–1034.

144. James TN, Kawamura K, Meijler FL, Yamamoto S, Terasaki F, Hayashi T. Anatomy of the sinus node, AV node and His bundle of the heart of the sperm whale (*Physeter macrocephalus*), with a note on the absence of an os cordis. Anat Rec 1995; 242: 355–373.

145. Sokkar SM, Trautwein G. Endocardiosis of the atrioventricular valves of the dog I. Morphological and histochemical studies. Zbl Vet Med 1970; 17: 757–759.

146. Lui SK, Tilley LP, Tashjian RJ. Lesions of the conduction system in the cat with cardiomyopathy. Recent Adv Stud Cardiac Struct Metab 1975; 10: 681–693.

147. Moorman AFM, Christoffels VM. Cardiac chamber formation: development, genes, and evolution. Physiol Rev 2003; 83: 1223–1267.

148. Oh IY, Cha MJ, Lee TH, Seo JW, Oh S. Unsolved questions on the anatomy of the ventricular conduction system. Korean Circ J 2018; 48: 1081–1096.

149. Paul M, Wichter MD, Gerss J, Arps V, Schulze-Bahr E, Robenek H, Breithardt G, Weissen-Plenz G. Connexin expression patterns in arrhythmogenic right ventricular cardiomyopathy. Am J Cardiol 2013; 15: 1488–1495.

150. Alanis J, Benitez D. Rate of rise of Purkinje and transitional cells action potential and the propagation across the Purkinje myocardium junction. Jpn J Physiol 1970; 20: 217–232.

151. Mendez C, Mueller WJ, Urguiaga X. Propagation of impulses across the Purkinje fiber-muscle junctions in the dog heart. Circ Res 1970; 26: 135–150.

152. Sommer JR, Johnson EA. Cardiac muscle. a comparative study of Purkinje fibers and ventricular fibers. J Cell Biol 1968; 36: 497–526.

153. Meijborg VMF, Conrath CE, Opthof T, Belterman CNW, de Bakker JMT, Coronel R. Electrocardiographic T wave and its relation with ventricular repolarization along major anatomical axes. Circ Arrhythmia Electrophysiol 2014; 7: 524-553

I. ARTICULOS PUBLICADOS

Research in Veterinary Science 128 (2020) 275–285

Contents lists available at ScienceDirect

Research in Veterinary Science

journal homepage: www.elsevier.com/locate/rvsc

Morphometry and comparative histology of sinus and atrioventricular nodes in humans and pigs and their relevance in the prevention of nodal arrhythmias

F.A. Gómez-Torres[a,b], R. Sebastian[c], A. Ruíz-Sauri[a,d,*]

[a] Department of Pathology, Faculty of Medicine, Universitat de Valencia, Av. de Blasco Ibáñez, 15, 46010 Valencia, Spain
[b] Department of Basic Sciences, Medicine School, Universidad Industrial de Santander, Cra 32 # 29 31, 68002 Bucaramanga, Colombia
[c] Computational Multiscale Simulation Lab, Universitat de Valencia, Valencia 46100, Spain
[d] INCLIVA Biomedical Research Institute, Av. de Blasco Ibáñez, 17, 46010 Valencia, Spain

ARTICLE INFO

Keywords:
P cell
T cell
Conduction system
Area: diameter
Intermediate filaments

ABSTRACT

The cardiac conduction system is a network structure that allows the initiation and fast propagation of electrical impulses that trigger the electrical depolarization of the myocardial tissue. The purpose of this work is to study the histological and morphometric characteristics of the different components of the sinus and atrioventricular nodes in humans and pigs and their relationship with supraventricular arrhythmias.

In this study, we describe the morphometry of the sinus and atrioventricular nodes of 10 adult humans and 10 pig hearts. A computerized morphometric study has been carried out, where we determined the number of cells that compose the nodes as well as different parameters related to their shape and size.

The sinus node in human and pig is a compact structure, whose shape is oblong. Their cells (nodal and transitional cells) are pale and located in the center and the periphery, respectively. The atrioventricular node has also a shape oblong. P cells are pale in both species, but in humans, they are smaller than cardiomyocytes. The T cells are small and pale in both species, identified by hematoxylin-eosin and desmin stains. We have observed through a morphometric profile that the structure of sinus and atrioventricular nodes of pigs and humans show few differences. Pigs can be used as models for hemodynamic applications and experimental studies that include atrial electrical conduction and, in this way, prevent the presentation of arrhythmias that can generate sudden deaths in humans and pigs.

1. Introduction

The cardiac conduction system (CCS) is responsible for triggering and spreading at fast speeds the electrical impulse responsible for the heartbeat. The main CCS components are: the sinus node, the atrioventricular node, the penetrating bundle of His, the right and left branches of the bundle of His and finally, the Purkinje network. During the first decade of the 20th century the gross anatomy of the CCS has been widely studied (Keith and Flack, 1907; Eliška, 2006), specially its suprahisian (above the His bundle) structures owing to their clearer implications in supraventricular rhythm disorders and the complexity of the CCS at distal sections (Haissaguerre et al., 2019).

The SN in humans is an oval shaped elongated mass (spindle-shaped) measuring about 10–20 mm long and up to 3–5 mm width (Koch, 1911; Glomset and Glomset, 1940a; Chiu et al., 1989; Waller et al., 1993a). In pigs, it has a length of 10–18 mm and a width of 3.5 mm (Opthof et al., 1987). In both humans and pigs, the SN contains two types of cells: nodal cells and transitional cells. Nodal cells (P cells) are small, ovoid, pale cells surrounding the nodal artery. Transitional cells (T cells) are elongated cells with intermediate characteristics between P cells and atrial myocardial cells; they are located at the periphery of the node making connections with P cells to propagate electrical impulses to the rest of the atrial myocardium. It is also important to describe the cells that are around the SN, which have different characteristics to the nodal cells and play a vital role in the transmission of the electrical impulse from the node. (James et al., 1966; Oosthoek et al., 1993; Waller et al., 1993a; James, 2002; Dobrzynski et al., 2013). In humans, it is indicated that the diameter of P cells is 3–10 μm (James, 2002) and in pigs, the diameter of the P cells is approximately the same as that of the atrial muscle cell (Bharati et al., 1991); in another investigation it is indicated that its diameter is 4–8 μm and its length about 40 μm (Opthof et al., 1987).

* Corresponding author at: Department of Pathology, Faculty of Medicine, Universitat de Valencia, Av. de Blasco Ibáñez, 15., 46010 Valencia, Spain
E mail addresses: falegom@uis.edu.co (F.A. Gómez-Torres), rafael.sebastian@uv.es (R. Sebastian), Amparo.Ruiz-Sauri@uv.es (A. Ruíz-Saurí).

https://doi.org/10.1016/j.rvsc.2019.12.008
Received 7 October 2019; Received in revised form 3 December 2019; Accepted 4 December 2019
0034-5288/

In the human heart, SN irrigation is provided by an artery known as the sinus node branch, which comes from the right coronary artery (RCA) in 50–79% of the hearts (James, 2002; Ortale et al., 2006; Zhang et al., 2008; Ramanathan et al., 2009; Ballesteros et al., 2011), of the circumflex branch (CXB) of the left coronary artery (LCA) in 30–45% (James, 2002; Ballesteros et al., 2011) and from both arteries in 3–23% (Ortale et al., 2006; Cademartiri et al., 2008; Ramanathan et al., 2009; Ballesteros et al., 2011). In pigs the sinus node branch originates from the RCA in 100% of the cases (Crick et al., 1998; Gómez and Ballesteros, 2013).

In humans, AVN is an ovoid compact structure that measures approximately 5 mm in length, 3 mm in width and 1 mm in thickness. (Glomset and Glomset, 1940b; James, 1961; Waller et al., 1993b). In human, electron microscopy studies have described four types of cells in the AVN: P cells, T cells, myocardial cells and Purkinje cells (PC). PC at this level can only be recognized by electron microscopy, since using light microscopy PC can be confused with ordinary cardiomyocytes (James, 1963; James and Sherf, 1971; Waller et al., 1993b). In pigs, P, T cells and cardiomyocytes have been described by conventional methods (Bharati et al., 1991).

In humans the atrioventricular node branch originates from the RCA in 85–92% (Waller et al., 1993b; James, 2002; Berdajs et al., 2006; Saremi et al., 2008; Ballesteros et al., 2011), from the CXB of the LCA in 10–15% (Waller et al., 1993b; James, 2002; Futami et al., 2003; Pejković et al., 2008; Ballesteros et al., 2011) and with a dual origin in 2% (RCA or CXB) (Saremi et al., 2008; Ballesteros et al., 2011). In pigs, the atrioventricular node branch originated from the RCA in 100% of the cases (Crick et al., 1998; Sahni et al., 2008; Gómez and Ballesteros, 2013).

In the cardiac nodes it is important to know the cells that compose them, but they have been described by their morphological and some morphometric characteristics in most cases, except for some work done with electronic microscopy; so it is essential to obtain a complete morphometric profile of these cells, which we have performed by determining unmistakable parameters of each cell that allows its precise identification without being confused with other cells. The use of animals as models for cardiovascular disease has increased in recent years. The pig is a widely used model for this purpose, due to the broad similarities with the human, in terms of physiology and cardiac histology (Bharati et al., 1991; Crick et al., 1998; Chorro et al., 2009; Gómez and Ballesteros, 2013; De Almeida et al., 2015; Row et al., 2017), which makes it relevant to point out their differences.

Although the structure of these nodes has been described in the detail in both humans and pigs, there has not been a properly analysis from the morphometric point of view. There are discrepancies between different authors regarding their size, shape and content, therefore our study provides objectivity, since these data are relevant for the generation of the electrical impulse and therefore the aim of this work is to study the histological and morphometric characteristics of the different components of the sinus and atrioventricular nodes in humans and pigs, with the purpose of finding similarities between the two species that allow the pig to be used as an experimental model cardiac and progress in the prevention of supraventricular arrhythmias.

2. Material and methods

2.1. Tissue collection and processing of the samples

We analyzed 10 hearts of adult human males that were obtained from the autopsies of the Institute of Legal Medicine and Forensic Sciences of Bucaramanga, Colombia (adults between 20 and 60 years old and medium size between 60 and 80 Kg). At the same time, 10 pig male hearts (weighing 85–90 kg and average age of 5 months) destined for slaughter were used for the study. The procedures were in accordance with the Ethics Committee of the Universidad Cooperativa de Colombia (No. 014–2018) and will comply with resolution 008430 of 1993, decree 2164 of 1992 and Law 10 of 1990 of the local Ministry of Health and to the principles of the Declaration of Helsinki. Additionally, they comply with Law 84 of 1989 in the national context, which corresponds to the "National Statute for the Protection of Animals", in Chapter VI of the use of animals in experiments and research.

In humans and pigs, the SN region was sliced between the union of the superior vena cava (cranial vena cava in animals) and the right atrium, and were subsequently cut in slices 5 mm thick. The AVN was also sectioned serially in the same way, and the block of tissue removed for the study incorporated the entire junction of the interatrial and interventricular septa. A adjacent tissue from the septum (two centimeters) was included. Sections were cut perpendicular to the line of junction of the septa, obtaining approximately six samples per node. All samples were tagged for identification, fixed in 5% formaldehyde solution, and embedded in paraffin. Histological sections of 5 μm thickness were acquired with a microtome and stained with hematoxylin-eosin and Masson's trichrome.

2.2. Histopathological evaluation and image analysis

The samples were assessed using an optic microscope Leica DMD108 (Leica Microsystems, Wetzlar, Germany). 380 micrographs were taken from tissue of the sinusal and atrioventricular nodes for the morphometric analysis. The images were acquired at different magnifications: 4× to measure the parameters of the nodes, 10× to measure the parameters of the cells and 20× to measure the parameters of the nodal blood vessels. We measured in the nodes: area (length of shortest line joining two points of object's outline and passing through the centroid), major axis (length of major axis of ellipse with same moments of order 1 and 2 as the object), minor axis (length of minor axis of ellipse with same moments of order 1 and 2 as the object), mean density (average optical density (or intensity) of the object), maximum diameter (length of longest line joining two points of object's outline and passing through the centroid), minimum diameter (length of shortest line joining two points of object's outline and passing through the centroid), perimeter (length of the object's outline), maximum radius (maximum distance between object's centroid and outline), minimum radius (minimum distance between object's centroid and outline), roundness (surface of a round body), length (line or body dimension considering its extension on a straight line), width (smallest dimension of a flat figure) at 4×. As for the roundness, if the value obtained in the morphometric measurement is close to 1 μm, this indicates that the cell or node is rounder and if it moves away from 1 μm, the cell or node tends to be elongated or irregular in its outline.

Inside the nodes, we quantify the total number of cells and the area they occupy, as well as the area, maximum diameter, minimum diameter, mean diameter and roundness of the P cells, T cells and peripheral cardiomyocytes in each of the nodes (60 for each cell type). The area, maximum and minimum diameter of the nodal artery at 4× was determined. To visualize the blood vessels in the nodes, we used CD31 immuno-histochemistry staining and the area, maximum and minimum diameter and number of vessels was determined at 20×. In addition, immuno-histochemistry staining with Anti-Human Desmin Clone D33-IR606 (DAKO Corporation) was performed to visualize the intermediate myofilaments (desmin) present in the cells of the nodes and compare them with the surrounding cardiomyocytes. The computerized morphometric study was carried out by the software Image-Pro Plus 7.1 (Media Cybernetics, Silver Spring, MD, USA). Each micrograph was calibrated, and the total tissue area in μm^2 was collected after manual chromatic histogram-based selection.

2.3. Statistical analysis

The descriptive statistics, graph representations and hypotheses contrast were performed with the software SPSS 20 (SPSS, Chicago, IL, USA) and Microsoft Excel 2013. Once all data were obtained and

analyzed statistically with the SPSS program, to obtain a morphometric profile of the nodes and their cells, we obtained for each parameter the interval where 66% of the entire population was included and the mean of this interval, determining that the most conclusive parameters were: area; roundness; maximum, minimum and mean diameter.

Continuous variables were expressed as the mean and 95% confidence interval. The level considered to indicate statistical significance was $p < .05$. The descriptive statistics for each morphometric parameter were calculated and the Kolmogorov–Smirnov normality test was performed for each sample. In the case of quantitative variables, Mann-Whitney U test was chosen. The data were expressed as mean standard deviation (SD) for all measured lengths.

3. Results

We determine the morphometric prolife of SN and AVN and its components. We value: number, area, major and minor axis, mean density, maximum and minimum diameter, perimeter, maximum and minimum radius, roundness, length and width. In them, the mean and the standard deviation were determined (Tables 1 and 2).

3.1. Sinus node

The SN in humans is a compact structure, surrounded by large amount of adipose tissue and some nerve fibers. It is not delimited by a capsule of irregular dense connective tissue, so its identification is made by the few cells that are recognized in some sectors of the node. The cells inside are united and surrounded by cords of connective tissue. The SN has a length between 1.4 and 3 mm and a width between 0.4 and 1.6 mm, which shows that its shape is oblong (Fig. 1a, b, c).

The SN in pigs contains nerve fibers at the periphery of the node. Only the morphology of the cells makes it possible to identify it, since it is not surrounded by a capsule of irregular dense connective tissue. The cells form round or elongated cellular packets, surrounded by a large amount of connective tissue, mainly collagen and fibroblasts. The length of the SN varies between 1.3 and 3 mm and its width is 0.6–1.1 mm, indicating that this node has also an oblong shape (Fig. 1g, h, i).

The area of SN in humans was $1.58 \pm 0.99\,mm^2$ and the area occupied by all cells of the node was $0.008 \pm 0.006\,mm^2$. In pigs, the area of the node was $1.52 \pm 0.75\,mm^2$ and the area occupied by all cells of the node was $0.013 \pm 0.012\,mm^2$. When observing the SN with Masson's Trichromic it can be appreciated that the amount of connective tissue inside the node was abundant.

3.2. Atrioventricular node

In AVN in humans, no nerve fibers were observed in the periphery or inside the node, but there was abundant adipose tissue surrounding the node. It is delimited by a thin capsule of irregular dense connective tissue. The AVN has a length of 1.7–2.5 mm and a width that ranges between 0.6 and 1 mm, characteristic of an oblong shaped region (Fig. 1d, e, f).

In pigs, the AVN has abundant nerve fibers both in the periphery and within the node (Fig. 1l), but there is no presence of the capsule of irregular dense connective tissue. AVN cells are surrounded by abundant connective tissue, and can be easily distinguished by histological observation. The length of the AVN ranges between 1.4 and 2.6 mm and its width between 0.5 and 1 mm, indicating that this node has also an oblong shape (Fig. 1j, k, l).

The area of AVN in humans was $1.61 \pm 0.38\,mm^2$ and the area occupied by all cells of the node was $0.20 \pm 0.003\,mm^2$. In pigs, its area was $1.54 \pm 0.44\,mm^2$ and the area occupied by all cells of the node was $0.0009 \pm 0.0003\,mm^2$, which indicates that the amount of connective tissue visualized with Masson's Trichrome was greater in pigs than in humans. In AVN the cell area and the number of cells were significantly greater in humans than in pigs ($p = .008$).

The description of the morphometric profile made in this study we summarize in Table 3. We observed that the roundness of the nodes in both species moves away from a value close to 1 µm, which indicates that their shape is elongated or oblong.

3.3. Blood supply

The sinus node branch in humans is an artery that is often found near the center of the node and is responsible for providing nutrients, although sometimes the artery is displaced towards one of its poles. On the contrary, in pigs it is more common to find it displaced towards the poles and rarely in the center of SN. The arterial branch of the atrioventricular node in humans and pigs is not clearly visible, and when it is observed, it is located in the terminal portion of the node.

In the arterial branches that irrigate the nodes in humans and pigs, the area, maximum diameter, minimum diameter and the thickness of the nodal vessel were measured (Tables 1 and 2). Statistically

Table 1
Statistical significance of the parameters measured in cells the sinus and atrioventricular nodes in humans and pigs.

Node	Parameter	Humans. µm (SD)	Pigs. µm (SD)	p valor
Sinus node	P cells maximum diameter	9.9 (2.5)	8.9 (1.5)	0.026
	T cells area	825.7 (423)	508 (463.2)	0.001
	T cells mean diameter	34.5 (8.2)	25.8 (10)	0.001
	T cells maximum diameter	69.6 (22.4)	49.1 (21.8)	0.001
	T cells roundness	3.1 (1.2)	2.3 (0.6)	0.001
	Cardiomyocytes area	77.4 (22.6)	101.6 (27)	0.023
	Cardiomyocytes mean diameter	9.5 (1.4)	10.9 (1.4)	0.023
	Cardiomyocytes maximum diameter	11.1 (1.7)	12.5 (1.7)	0.029
	Cardiomyocytes minimum diameter	8.1 (1.5)	9.5 (1.4)	0.027
	Cell area	20,348.2 (3672)	933.5 (313.1)	0.008
	Cells number	1408 (202.4)	252 (79.2)	0.008
Atrioventricular node	P cells area	17.8 (5.3)	377.4 (151.2)	0.001
	P cells mean diameter	4.4 (0.7)	21 (4)	0.001
	P cells maximum diameter	5.2 (0.9)	25.3 (7)	0.001
	P cells minimum diameter	3.7 (0.7)	17.6 (3)	0.001
	P cells roundness	1.03 (0.05)	1.16 (0.07)	0.001
	T cells area	573.2 (323.7)	715.2 (389.6)	0.029
	T cells mean diameter	28.2 (7.1)	31.4 (7.2)	0.045
	T cells minimum diameter	10.9 (3.2)	13.1 (3.5)	0.004
	Cardiomyocytes area	70.8 (41.5)	100.5 (24.7)	0.047
	Cardiomyocytes mean diameter	8.8 (2.7)	10.8 (1.4)	0.045

The areas were measured in μm^2. SD: standard deviation.

Table 2
Values measured in the sinusal and atrioventricular nodes and their cells that show similarity in humans and pigs.

Node	Parameter	Humans. μm (SD)	Pigs. μm (SD)	p valor
	Area	1,584,872.5 (996,466.4)	1,525,082.5 (756,809.5)	0.88
	Axis major	1997.8 (552.4)	2052.2 (661.7)	1.00
	Axis minor	1005.1 (412)	949 (190.9)	0.57
	Density mean	0.24 (0.06)	0.30 (0.12)	0.39
	Diameter maximum	2017.5 (517.6)	2058.8 (586.5)	0.777
	Diameter minimum	915.6 (398.4)	827 (169.3)	0.48
	Perimeter	5301.8 (1416.9)	5228.7 (1398)	0.88
	Radius maximum	1118.7 (289.7)	1115.9 (355.3)	0.77
	Roundness	1.81 (0.94)	1.47 (0.13)	0.57
	Length	2026.3 (552.8)	2069.7 (742.1)	0.77
	Width	971.4 (390.8)	850.1 (240.7)	0.48
Sinus node	Artery máximum diameter	765.1 (229.1)	840.3 (577.5)	0.86
	Artery minimum diameter	465 (152.7)	414.2 (241.3)	0.73
	P cells area	57.9 (30.3)	49.7 (14.8)	0.089
	P cells mean diameter	8.1 (1.9)	7.5 (1.1)	0.067
	P cells minimum diameter	6.3 (1.8)	6.4 (1.1)	0.382
	P cells roundness	1.14 (0.2)	1.07 (0.04)	0.295
	T cells minimum diameter	13.8 (5)	11.1 (4.9)	0.74
	Cardiomyocytes roundness	1.09 (0.03)	1.09 (0.02)	0.570
	Area	1,617,321 (381,970.1)	1,541,833.3 (443,166,8)	0.57
	Axis minor	1048.5 (287.2)	1007.2 (178.3)	0.70
	Density mean	0.23 (0.03)	0.24 (0.04)	0.70
	Diameter máximum	2227.5 (404.7)	2080.3 (410.6)	0.34
	Diameter minimum	915.9 (272.4)	916.4 (173.9)	0.70
	Radius maximum	1168.8 (511.7)	1175.2 (197)	0.85
	Roundness	1.98 (0.61)	1.64 (0.29)	0.34
	Length	2151 (349.3)	1865.2 (408.8)	0.18
Atrioventricular node	Width	887.2 (169.5)	879.1 (194.2)	1.00
	T cells maximum diameter	59.7 (26.7)	63.7 (24.8)	0.061
	T cells roundness	2.85 (1.19)	2.7 (1.21)	0.337
	Cardiomyocytes maximum diameter	10.3 (3.5)	13.1 (2)	0.081
	Cardiomyocytes minimum diameter	7.4 (2.1)	9.1 (1.2)	0.116
	Cardiomyocytes roundness	1.08 (0.05)	1.11 (0.06)	0.896

The areas were measured in μm^2. SD: standard deviation.

significant differences were found in the area of the SN artery (p = .042), being higher in humans than in pigs.

To correctly visualize and measure the parameters of the blood vessels of cardiac nodes in humans, we used CD31 immunohistochemically staining (Fig. 2a, b). The area of the vessels was 0.00010 mm^2 in the SN, and 0.00018 mm^2 in the AVN. The number of blood vessels was > 350 in both nodes, which allowed us to observe that despite the large number of blood vessels present in the nodes, the area they occupy is minimal, and composed mostly of connective tissue (Table 4).

3.4. Nodal cells

According to our morphometric analysis, we can differentiate two types of cells in the nodes (Figs. 3 and 4) which correspond to P cells and T cells. It is also important to describe the cardiomyocytes that are found at the margins of the nodes due to their crucial role within of the transmission of the electric impulse. In them, different parameters were measured such as area, maximum diameter, minimum diameter, mean diameter and roundness (Tables 1 and 2).

In the human SN, P cells are small (Fig. 3a, e), their cytoplasm is paler than the cardiomyocytes that surround the node, its shape can be rounded or oval, located towards the center and surrounding the nodal artery; the nodal cells are grouped together in interconnecting fascicles placed in a background of fibrous matrix. They are cells with a single rounded and dark nucleus. In pigs, P cells (Fig. 3b, f) have the same characteristics as in humans, except that the cells may have one or two nuclei. In humans, T cells are small (Fig. 3c, e), with a pale cytoplasm like the one of the P cells, scarce, elongated and located in the periphery. They exhibit, a single dark nucleus and in certain areas of the node they are organized forming fiber-like structures joining with adjacent T cells. In pigs, T cells (Fig. 3d, f) have a similar distribution to humans. In the SN, the human and pig cardiomyocytes located in the periphery can be observed in cross-section. They are medium-sized, dark, round and can be seen individually or together forming strands or bundles of cells.

We have found that the maximum diameter of P cells in the SN in humans is significantly larger than in pigs (p = .026). In the morphometric analysis, we could determine that P cells are rounded because their value is close to 1 μm, being similar in both species. In T cells we found statistically significant differences in the maximum and mean diameter (p = .000 for both values) and in area (p = .001), being larger in humans than in pigs. The T cells are elongated, because in the morphometric analysis their value moves away from 1 μm, being flatter in humans than in pigs (p = .001). In cardiomyocytes it was observed that area and diameters were significantly higher in pigs than in humans (p = .023 for area and mean diameter; p = .029 for maximum diameter and p = .027 for minimum diameter).

In the human AVN, the P cells are smaller than cardiomyocytes (Fig. 4a, e), dark, rounded or oval, located in the center and with a rounded and dark nucleus, although sometimes multinucleated cells are observed. In pigs, unlike what is observed in humans, P cells are large (Fig. 4b, f), with a cytoplasm slightly paler than in cardiomyocytes and with a single nucleus. T cells in humans are pale (Fig. 4c, e), peripherally located, elongated that in certain areas of the node margin are joined, showing a linear appearance. These cells have a dark and elongated nucleus. T cells in pigs (Fig. 4d, f) have the same characteristics that were described for humans, unlike these cells have a much larger size. The cardiomyocytes that are located in the periphery of the node, are oriented transversely. They shown an intermediate size, larger than P cells in humans, dark and with shapes that vary from rounded to oval. They can be found in individual groups of cells. In pigs, cardiomyocytes are smaller than P cells.

In the AVN, we found that P cells show statistically significant

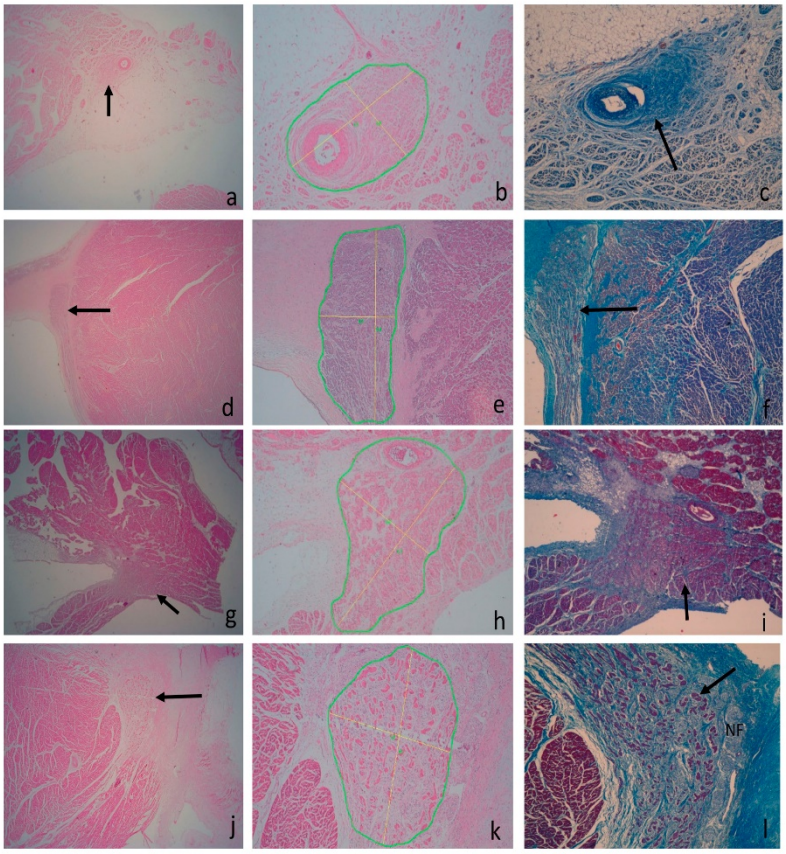

Fig. 1. Morphometry and location of sinus and atrioventricular nodes of humans and pigs. The arrows indicate the histological position of sinus node in humans (a) and pigs (g), as well as the location of atrioventricular node in humans (d) and in pigs (j) with Hematoxylin-eosin at 1.6×. The morphometric analysis was performed on samples stained with Hematoxylin-eosin at 4× in sinus node of human (b) and pig (h) and in atrioventricular node of human (e) and pig (k). Histological detail of human (C) and pig (i) sinus node, as well as atrioventricular node of human (f) and pig (l) stained with Masson's trichrome at 4×, indicating the position of the nodes with arrows. NF: nervous fascicle.

differences in area and different diameters ($p = .001$ for all values) being larger in pigs than in humans. In the morphometric analysis we could determine that P cells are rounded because their value is close to 1 μm, but they were found to be rounder in humans than in pigs ($p = .001$). In T cells, we observed that area ($p = .029$), minimum diameter ($p = .004$) and mean diameter ($p = .045$) were significantly

Table 3
Morphometric profile of the sinus and atrioventricular nodes in humans and pigs.

Parameter	Humans		Pigs	
	Sinus node. μm. (mean)	AV node. μm. (mean)	Sinus node. μm. (mean)	AV node. μm. (mean)
Maximum radius	995–1148 (1071)	1074–1493 (1283)	1023–1221 (1122)	1129–1293 (1211)
Minimum radius	406–540 (473)	211–304 (257)	313–444 (378)	358–457 (407)
Roundness	1.16–1.74 (1.45)	1.80–2.45 (2.12)	1.35–1.59 (1.47)	1.53–1.72 (1.62)

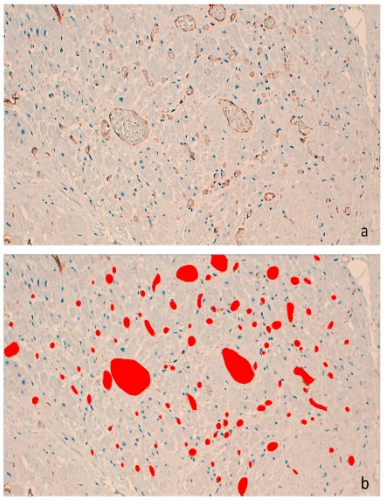

Fig. 2. Immunohistochemically staining with CD31 of the atrioventricular node in humans at 20×. (a) Indicates the visualization of the vessels with staining; (b) the blood vessels drawn with the morphometry program are observed.

larger in pigs than in humans. Significant statistical differences were found in area and mean diameter of cardiomyocytes ($p = .047$ and $p = .045$ respectively), being larger in pigs than in humans.

To clearly identify the SN and AVN cells, we performed an immunohistochemistry staining with Desmin in both species, in order to visualize the intermediate filaments present in these cells. Here, we could see that in the human SN the cells stained slightly compared to some adjacent segments of the atrial myocardium, but these nodal cells also showed larger positivity than cardiomyocytes in other segments, and in turn, these cells were smaller than heart muscle cells (Fig. 5a, b). In pigs, at the SN level a great positivity of the nodal cells and the cardiomyocytes was observed to immuno-histochemistry staining (desmin), but the nodal cells stained a little less than the cardiomyocytes, indicating a lower amount of intermediate filaments in node cells (Fig. 5c, d). In humans, AVN nodal cells showed a larger reaction to desmin than cardiomyocytes, therefore they were observed darker and smaller than atrial myocardiocytes, confirming what was described in the morphometric profile performed (Fig. 6a, b). In the AVN of pigs, it was confirmed that the large size (described in the morphometric study) and the few cells present in this node were easily observed with desmin, as was done with hematoxylin-eosin and Masson's trichrome. Nodal cells showed greater positivity to desmin compared to the myocardial tissue surrounding the AVN and in a few places; cardiomyocytes achieved the same positivity as node cells (Fig. 6c, d).

The detailed morphometric profile of nodal cells and peripheral cardiomyocytes is summarized in Table 5. By analyzing sample cross sections, we observed that the roundness of the P cells and the cardiomyocytes in both species is close to a value of 1 μm, which indicates that they have a rounded or oval shape. In contrast, the T cells show a value that is far from 1 μm, which indicates that their shape is elongated, as previously described by morphometric analysis.

4. Discussion

The study of nodal structures in human and pig hearts with morphometry provides objectivity to morphological visualization and has allowed us to demonstrate that there are similarities between both species (humans and pigs), which could allow the use of pigs as an alternative experimental model to study the pathophysiology of the cardiac conduction system.

In humans it is commonly reported that the SN has a spindle shape and is 10–20 mm long and 3–5 mm wide (Koch, 1911; Glomset and Glomset, 1940a; Chiu et al., 1989; Waller et al., 1993a; James, 2002; Fedorov et al., 2010), although shorter lengths between 4 and 6 mm (Anderson et al., 1979) and larger ones between 12 and 29 mm (Glukhov et al., 2013; Lou et al., 2014; Kalyanasundaram et al., 2019) have also been reported. Similarly, in pigs the SN 10–18 mm long and 3.5 mm wide (Opthof et al., 1987). By analyzing 10 SN in humans and 10 SN in pigs, we have identified the node in histological preparations by looking at the characteristics of their cells and the abundant connective tissue between them. We observed that it has an oblong shape in both species, coinciding with previous studies, although our measures were slightly lower in average (2 mm long in humans and pigs; wide: 0.9 mm in humans and 0.8 mm in pigs), which could be explained by the different techniques. The large amount of connective tissue found within the SN in both species coincides with that described by other authors (Glomset and Glomset, 1940a; Opthof et al., 1987; De Mazière et al., 1992; Boyett et al., 2000; Kalyanasundaram et al., 2019), but the presence of small fibrous septa separating the node from the cardiomyocytes in humans in some areas described by Waller et al., 1993a, was not observed in our histological preparations. The importance of knowing the area of the node lies in that it must be compared with its cellular component, which confirms through our morphometric analysis that there is a small number of cells with respect to the large amount of connective tissue within the node in both species. This fact has not only been corroborated in our histological but also in studies carried out by other authors (Boyett et al., 2000; Kalyanasundaram et al., 2019). The fatty infiltration found in the epicardial surface in our study in both species, coincides with that described in a previous report in humans (Chiu et al., 1989). It is known that dense collagen networks can provide structural support to cardiomyocytes, blood vessels, nerve fibers and other support cells to both preserve tissue architecture and help the pacemaker function of the SN. This enhanced collagen also helps to provide protection to the P cells that are responsible for the pacemaker function, avoiding stretching due to the increased contraction of the atrial myocardium surrounding the node. (Csepe et al., 2015; Kennedy et al., 2016; Kalyanasundaram et al., 2019). However, in Heart Failure (HF) and myocardial infarctions an increase in connective tissue (fibrosis) within the SN has been demonstrated (Glukhov et al., 2013; Lou et al., 2014; Csepe et al., 2015; Kalyanasundaram et al., 2019), which interrupts the normal coupling

Table 4
Global summary of the morphometric parameters of the blood vessels of the sinus and atrioventricular nodes in humans, stained with immunohistochemically test CD31.

Node	Vessels area mm^2 (SD)	Maximum diameter mm (SD)	Minimum diameter mm (SD)	Vessels number mm (SD)
Sinus node	0.00010 (0.00043)	0.010 (0.013)	0.006 (0.005)	517
Atrioventricular node	0.00018 (0.00055)	0.015 (0.020)	0.008 (0.006)	359

SD: standard deviation.

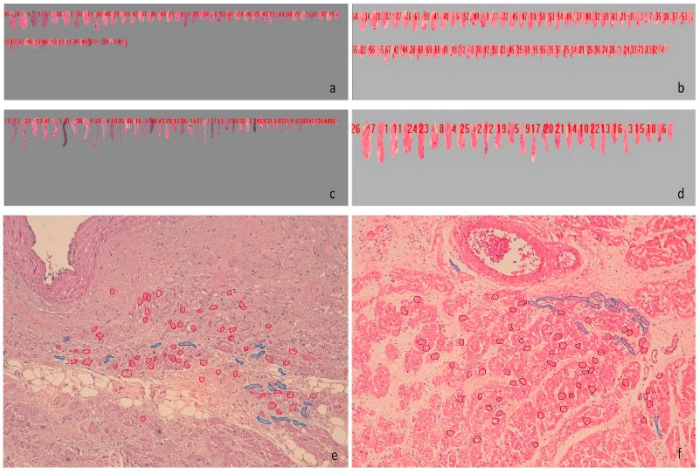

Fig. 3. Sinus node cells of humans and pigs stained with Hematoxylin-eosin at 10×. Morphometry of P cells (a) and T cells (c) in humans. Histological detail of P (red) and T (blue) cells in humans (e). Morphometry of P cells (b) and T cells (d) in pigs. Histological structure of P (red) and T (blue) cells in pigs (f). (For interpretation of the references to colour in this figure legend, the reader is referred to the web version of this article.)

between the specialized cells of the node and the surrounding cardiomyocytes, which decreases the vital capacity of the pacemaker leading bradycardia, conduction blocks or reentry. (Csepe et al., 2015). SN malfunction in humans can predispose to heart disease, such as atrial fibrillation and HF, which can cause syncope and sudden cardiac death. Currently, SN disease in humans and in animal species such as canines is treated with drugs and pacemakers with variable success rates (Ward et al., 2016; Kalyanasundaram et al., 2019). The prevalence and severity of this nodal failure causes the need for more detailed studies that identify and describe structural and functional aspects of the SN aimed at preventing these cardiac pathologies. (Kalyanasundaram et al., 2019).

In humans, there are nerve fibers in the periphery and within the SN that is richly innervated by branches of both the vagus and sympathetic

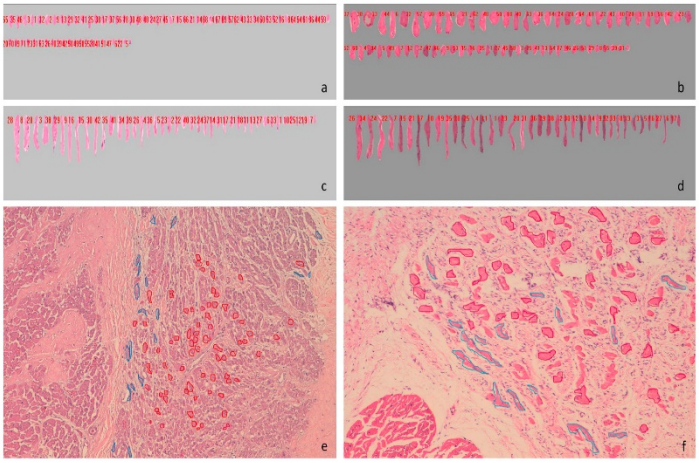

Fig. 4. Atrioventricular node cells of humans and pigs stained with Hematoxylin-eosin at 10×. Morphometry of P cells (a) and T cells (c) in humans. Histological detail of P (red) and T (blue) cells in humans (e). Morphometry of P cells (b) and T cells (d) in pigs. Histological structure of P (red) and T (blue) cells in pigs (f). (For interpretation of the references to colour in this figure legend, the reader is referred to the web version of this article.)

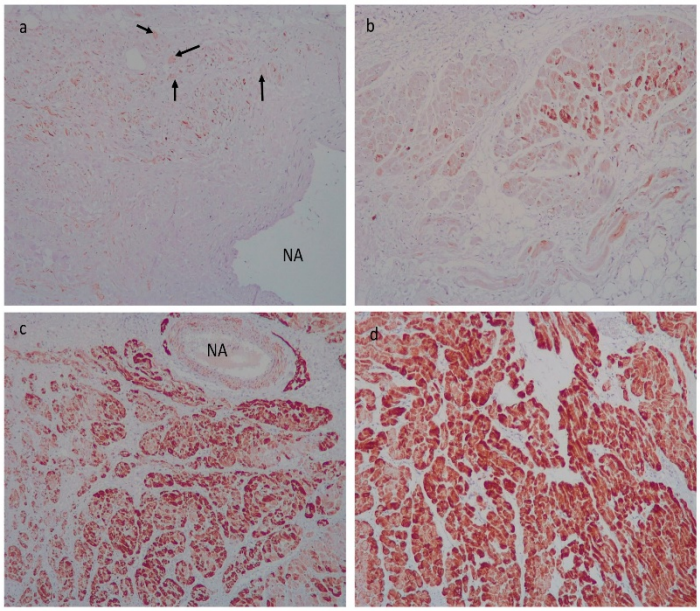

Fig. 5. Sinus node cells of humans and pigs stained with Desmin at 10×. (a) cells of the humans sinus node; (b) peripheral cardiomyocytes of the humans sinus node; (c) cells of pigs sinus node; (d) peripheral cardiomyocytes of the pigs sinus node. NA: nodal artery. Arrows indicate P cells.

systems (Keith and Flack, 1907; Glomset and Glomset, 1940b; James, 1967; Oosthoek et al., 1993; James, 2002; Sánchez-Quintana and Ho, 2003). In pigs, there are numerous nerve fibers on the periphery and occasionally within the node (Bharati et al., 1991). We could only observe the presence of nerve fibers in the periphery of the SN in humans and pigs. This is important because the amount of nerve fibers present can influence the pacemaking activity of the sinus node. It has been described that some nodal cells are more sensitive to norepinephrine or acetylcholine, being able to change the origin site of the intranodal pacemaker or that the original site simply firing at a faster rate (Hoffman and Cranefield, 1964; Kawamura, 1968; James and Sherf, 1971).

With respect to the AV node, we observed that our measurements are also smaller than those reported by different authors, which indicate that in humans it has an oval or semi-oval shape and is 5–7 mm long and 3–4 mm wide (Glomset and Glomset, 1940b; Waller et al., 1993b; Sánchez-Quintana and Ho, 2003; Mani and Pavrí, 2014; Randhawa et al., 2017). In pigs these parameters have not been described, but we could observe in our study that these values are similar (long: 2.1 mm; wide: 1.8 mm) to those found in humans.

The AVN area has not been reported in the literature for humans and pigs, but this parameter is important when compared to the number of cells present in this node. We have found that there is a large amount of connective tissue among the few cells present in the AVN, especially in pigs where it has been measured with light microscopy. This indicates that even if there is a small cellular damage in the AVN, the electrical conduction at the atrioventricular level could be affecting dramatically its normal function of delaying the transmission of the electrical impulse from the atria to the ventricles and in this way enabling the presence of ventricular arrhythmias or conduction blocks of different degrees. In addition, in pigs the histological recognition of the AVN is done by its location and the particular characteristics of its cells, which do not show a connective tissue capsule that surrounds them, differently to AVN in humans that shows a thin capsule that delimits it.

The innervation in the AVN of humans and pigs is important since it can influence the electrical activity downstream at the His bundle and the Purkinje system. In our investigation, by means of optical microscopy and staining with hematoxylin-eosin, we found no nerve fibers in the periphery or inside the nodule in humans; which is in agreement with previous studies where they describe the presence of small nerve fibers inside and the periphery of the AVN, but which can only be identified by electron microscopy, since under optical microscopy it is not visible (Glomset and Glomset, 1940b; James, 2002). In pigs, we were able to observe a large number of nerve fibers in the interior and in the periphery of the node, which has been also reported in a previous study (Bharati et al., 1991).

Knowing the parameters of the nodal arteries is important to determine the approximate amount of blood required to nourish and oxygenate the nodes under normal conditions. A large artery is commonly observed in the center or to the side of the SN (Glomset and Glomset, 1940a; Anderson et al., 1979; Chiu et al., 1989; Oosthoek et al., 1993; James, 2002; Sánchez-Quintana and Ho, 2003). The arterial branch of the atrioventricular node that irrigates it in humans is located between the two bifurcations of the AVN, namely the right and left branches of the His bundle (Futami et al., 2003; Sánchez-Quintana and Ho, 2003), which matches our observations in humans and pigs even though this arterial branch is rarely visible histologically. There are clinical conditions such as coronary obstructions by atheroma or myocardial bridges that affect differently depending on the species since the branches that nourish the nodes have different origins. It is

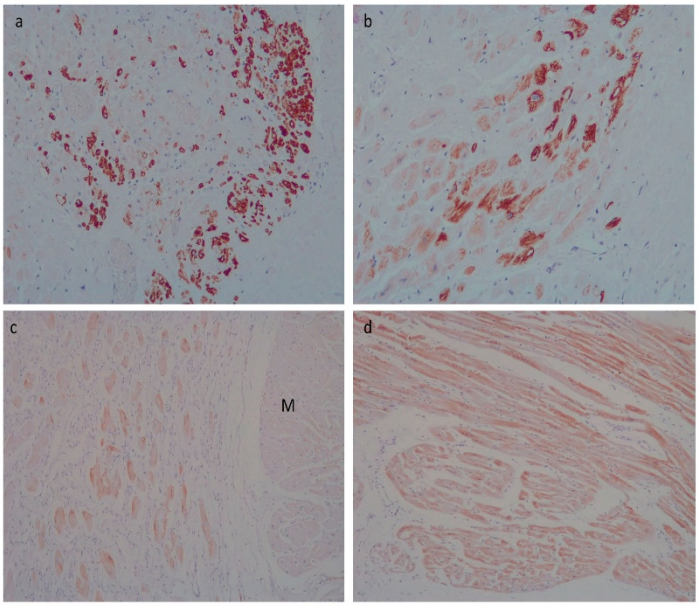

Fig. 6. Atrioventricular node cells of humans and pigs stained with Desmin. (a) atrioventricular node cells of humans at 20×; (b) peripheral cardiomyocytes of the human's atrioventricular node at 20×; (c) atrioventricular node cells of pigs at 10×; (d) peripheral cardiomyocytes of the pig's atrioventricular node at 10×. NA: nodal artery; M: cardiomyocytes.

Table 5
Morphometric profile of the cells of the sinus and atrioventricular nodes in humans and pigs, determining the interval of greatest presentation and its mean.

Species	Parameter	Sinus node (μm)			AV node (μm)		
		P	T	Cardiomy	P	T	Cardiomy
Humans	Maximum diameter	9–11 (10)	57–75 (66)	10–12 (11)	4.7–5.4 (5)	45–69 (57)	8–12 (10)
	Minimum diameter	5–7 (6)	11–14 (12)	7.5–9 (8)	3.5–4 (3.8)	9–11 (10)	6–9 (8)
	Roundness	1.05–1.12 (1.09)	2.35–3.13 (2.74)	1.07–1.11 (1.09)	1–1.04 (1.0.2)	2.11–3.10 (2.60)	1.05–1.10 (1.07)
Pigs	Maximum diameter	8.5–9.5 (9)	37–53 (45)	12–13 (12.5)	21–28 (25)	49–69 (59)	12–14 (13)
	Minimum diameter	6–7 (6.5)	7–12 (10)	9–10 (9.5)	16–19 (18)	11–14 (12)	8.7–9.3 (9)
	Roundness	1.05–1.09 (1.07)	1.91–2.44 (2.17)	1.08–1.10 (1.09)	1.12–1.14 (1.13)	1.90–2.84 (2.37)	1.07–1.12 (1.10)

more common that the two nodal arterial branches are derived from the RCA in both species, but sometimes there are also branches of the LCA (Waller et al., 1993b; Crick et al., 1998; Ramanathan et al., 2009; Ballesteros et al., 2011; Gómez and Ballesteros, 2013). Another important factor as indicated above is the presence of myocardial bridges that are more commonly located in the anterior interventricular branch in humans (left ventricular septum) (Ballesteros et al., 2009) and the subsinusal interventricular branch in pigs (right ventricular septum) (Gómez and Ballesteros, 2015), which allows to identify easily which side of the heart is the arterial obstruction. Likewise, in our morphometric analysis, by using CD31 immunohistochemically staining, we determined that the area of blood vessels in the cardiac nodes is smaller than that of the cells, even joining these two areas (cells and blood vessels areas). Therefore, we confirmed again that the surface of the nodes is composed mainly of connective tissue.

Histologically, it is described in humans that P cells in SN are small (3–10 μm in diameter), ovoid or round, pale and grouped together in interconnecting fascicles (James et al., 1966; Oosthoek et al., 1993; Waller et al., 1993a; Boyett et al., 2000; James, 2002; Sánchez-Quintana and Ho, 2003). It is believed that these cells are responsible for the formation of the impulses in the SN, which are located in the center of the node. T cells are elongated with intermediate characteristics between P cells and cardiomyocytes (Waller et al., 1993a). They are located at the margins of the node and in other areas are projected, extending for short distances in the atrial myocardium, also in the terminal crest and other parts of the internodal pathways show a longitudinal organization with other transition cells. It is thought that they are responsible for transmitting the impulse produced by P cells to the myocardium (James, 2002; Sánchez-Quintana and Ho, 2003). With respect to P cells, our findings agree with the descriptions made by previous reports, including cell size (9.9 μm). Regarding T cells, we agree with what has been described in the literature. In pigs, it has been reported the presence of many nuclei close to each other and a large amount of collagen fibers and pale cells (P cells) with a diameter of

4–8 μm. (Opthof et al., 1987; Boyett et al., 2000). We observed that the characteristics of the P cells coincide with previous reports, but the diameter of these cells in our investigation was slightly larger (8.9 μm). In another study, it is indicated that the diameter of these cells is equal to that of cardiomyocytes (Bharati et al., 1991); this is not consistent with our findings, where we observed that P cells were smaller than myocardial cells. In humans, pigs and other animal species it has been reported that atrial cardiomyocytes around the SN have a diameter of 15–20 μm (Oosthoek et al., 1993; Boyett et al., 2000); which does not match our findings in humans or pigs, being slightly lower than in previous reports (11.1 μm and 12.5 μm respectively). The importance of knowing the characteristics of the cardiomyocytes lies in their crucial role in the transmission of the electrical impulse to the atrial tissues and to the AVN.

Previous research describes four types of cells in the AVN (P cells, transitional cells, common myocardial cells, and Purkinje cells) (James, 1963; James and Sherf, 1971; Waller et al., 1993b), of which, in our study Purkinje cells were not found. This may be due to the fact that these cells can only be visualized at this level by electronic microscopy as described by these authors.

Previous reports indicate that P cells in the AVN in humans are small, pale, ovoid or rounded, individual or forming very small groups of cells that anastomose. They have a maximum diameter of 5–10 μm, being much smaller than the myocardial cells. (James et al., 1966; Waller et al., 1993b; James, 2002). We found a similar description of P cells, although in our study they were as dark as cardiomyocytes. The function of P cells in this node is mainly to delay the electrical impulse in its path towards the ventricles. It is described that in the AVN there is a large number of long and thin T cells within each node and in their peripheral margins, which serve to carry the signal to the body of the node and are also transmitted to the ventricular conduction pathways (James, 2002); these descriptions coincide with what was found in our research, although we observed that T cells were located mainly in the periphery. P cells of AVN in pigs are described as pale cells whose diameter is approximately the same as that of cardiomyocytes (Bharati et al., 1991). In our series, the physical characteristics are the same as those described, but the diameter is much larger than the cardiomyocytes, even reaching values that double their size (P cells: 25.3 μm; cardiomyocytes: 13 μm).

The differentiation of the nodal tissues in humans and pigs is difficult when trying to recognize their cells with the naked eye by light microscopy (it is done by location and characteristics of the surrounding connective tissue), for this reason the use of immuno-histochemistry stains such as the desmin becomes a vital tool for the proper recognition of these cells and thus being able to perform accurate morphometric analysis. It has been shown that desmin (also previously called "skeletin") is the main intermediate filament (IF) present in the heart muscle and that it usually accumulates in the intercalated and Z disks, achieving a connection of the contractile apparatus with the others cellular components (Fuchs and Weber, 1994; Paulin and Li, 2004; Lowery et al., 2015). In addition, it has been possible to identify the presence of this IF in the CCS cells in larger quantity than in the cardiomyocytes, This is mainly, because the presence of desmin is distributed throughout the entire cytoplasm of the conduction cells and not only at specific points as in cardiac muscle cells (Eriksson et al., 1979; Forsgren et al., 1982; Yoshimura et al., 2014). Therefore, they could be observed in our study when using the anti-desmin antibody, which showed a larger reaction to nodal conduction cells than to cardiomyocytes. In addition, it has been described that SN cells show greater positivity to desmin than AVN cells (Forsgren et al., 1982), which we have been able to verify in our research. This allowed us to confirm that the use of desmin as immuno-histochemistry staining for the recognition of CCS cells is adequate.

A morphometric profile of the cardiac node cells, is necessary to be able to determine the characteristics that allow them to be fully identified in normal conditions and in this way to detect the presence of any alteration that can be related to the existence of cardiac rhythm disturbances.

The use of animals as models for the study of various cardiovascular diseases has allowed a broad advance in the knowledge of their pathogenesis and the development of different diagnostic, therapeutic, pharmacological and surgical methods that include hemodynamic aspects, macroscopic cardiac structures or even the CCS (cardiac nodes and Purkinje system) (Opthof, 1988; Chorro et al., 2009; Row et al., 2017; Kalyanasundaram et al., 2019).

It has been indicated that from different studies of the CCS in the horse, cow, sheep, pig, cat and monkey, no notable differences have been found in the anatomy of the sinus and atrioventricular nodes compared with the human heart (James, 2002), which provides value to our results, where we find several similarities between the parameters measured in both nodes of the two species studied (Table 2) and increases the possibility of using the pig as an animal model (Bharati et al., 1991) for clinical and hemodynamic experimentation in humans in order to prevent the presentation of supraventricular arrhythmias.

The analysis and characterization of the cardiac nodes has been made by morphological evaluations, therefore the morphometric profile that we performed is of vital importance to know in detail the characteristics of them and obtain the precise measurements.

5. Conclusions

We have reported through a morphometric profile that the structure of sinus and atrioventricular nodes of humans and pigs show few differences, so we conclude that this type of animals can be used as models for hemodynamic applications and experimental studies that include atrial electrical conduction and in this way prevent the presentation of arrhythmias that can generate sudden deaths in both. In addition, desmin as a marker of conduction cells is useful for recognition and differentiation with cardiomyocytes.

Cardiac nodes are composed of multiple cells that are responsible for generating and transmitting the electrical impulse in different species. This allows the use of animal models to provide mechanisms similar to physiological processes in humans, which creates new possibilities for study.

Sources of funding

This work was supported by the "Instituto de Salud Carlos III" and co-funded by "FEDER (grant numbers PI14/00271, pie15/00013) and by the "Generalitat Valenciana" (grant number PROMETEO2013/007).

Declaration of Competing Interest

The authors declare that they have no conflicts of interest.

Acknowledgements

To the Institute of Legal Medicine and Forensic Sciences and to Vijagual Refrigerating Plan in the city of Bucaramanga, Colombia for the donation of specimens studied in this research.

References

Anderson, K.R., Ho, S.Y., Anderson, R.H., 1979. Location and vascular supply of sinus node in human heart. Br. Heart J. 41, 28–32.
Ballesteros, L.E., Ramírez, L.M., Saldarriaga, B., 2009. Morphological description and clinical implications of myocardial bridges: an anatomical study in Colombians. Arq. Bras. Cardiol. 92, 242–248.
Ballesteros, L.E., Ramírez, L.M., Quintero, I.D., 2011. Right coronary artery anatomy: anatomical and morphometric analysis. Rev. Bras. Cir. Cardiovasc. 26, 230–237.
Berdajs, D., Kunzli, A., Shurr, U., Zünd, G., Turina, M.I., Genonni, M., 2006. Clinical anatomy of the atrioventricular node artery. J. Heart. Valve. Dis. 15, 225–229.
Bharati, S., Levine, M., Huang, S.K.S., Handler, B., Parr, G.V.S., Bauemfeind, R., Lev, M., 1991. The conduction system of the swine heart. Chest. 100, 207–212.

Boyett, M.R., Honjo, H., Kodama, I., 2000. The sinoatrial node, a heterogeneous pacemaker structure. Cardiovasc. Res. 47, 658–687.
Cademartiri, F., La Grutta, L., Malagò, R., Alberghina, F., Meijboom, W.B., Pugliese, F., Maffei, E., Palumbo, A.A., Aldrovandi, A., Fusaro, M., Brambilla, V., Coruzz, P., Midiri, M., Mollet, N.R.A., Krestin, G.P., 2008. Prevalence of anatomical variants and coronary anomalies in 543 consecutive patients studied with 64-slice CT coronary angiography. Eur. Radiol. 18, 781–791.
Chiu, I.S., Hung, C.R., How, S.W., Chen, M.R., 1989. Is the sinus node visible grossly? A histological study of normal hearts. Int. J. Cardiol. 22, 83–87.
Chorro, F.J., Such-Belenguer, L., López-Merino, V., 2009. Animal models of cardiovascular disease. Rev. Esp. Cardiol. 62, 69–84.
Crick, S.J., Sheppard, M.N., Ho, S.Y., Gebstein, L., Anderson, R.H., 1998. Anatomy of the pig heart: comparisons with normal human cardiac structure. J. Anat. 193, 105–119.
Csepe, T.A., Kalyanasundaram, A., Hansen, B.J., Zhao, J., Fedorov, V.V., 2015. Fibrosis: a structural modulator of sinoatrial node physiology and dysfunction. Front. Physiol. 6, 37.
De Almeida, M.C., Lopes, F., Fontes, P., Barra, F., Guimaraes, R., Vilhena, V., 2015. Ungulates heart model: a study of the Purkinje network using India ink injection, transparent specimens and computer tomography. Anat. Sci. Int. 90, 240–250.
De Mazière, A.M.G.L., van Ginneken, A.C.G., Wilders, R., Jongsma, H.J., Bouman, L.N., 1992. Spatial and functional relationship between myocytes and fibroblasts in the rabbit sinoatrial node. J. Moll. Cell. Cardiol. 24, 567–578.
Dobrzynski, H., Anderson, R.H., Atkinson, A., Borbas, Z., D'Souza, A., Fraser, J.F., Inada, S., Logantha, S.J.R.J., Monfredi, O., Morris, G.M., Moorman, A.F.M., Nikolaidou, T., Schneider, H., Szuts, V., Temple, I.P., Yanni, J., Boyett, M.R., 2013. Structure, function and clinical relevance of the cardiac conduction system, including the atrioventricular ring and outflow tract tissues. Pharmacol. Ther. 139, 260–288.
Eliška, O., 2006. Purkinje fibers of the heart conduction system-history and the present time. Cas. Lek. Cesk. 145, 329–335.
Eriksson, A., Thornell, L.E., Torgny, S., 1979. Skeletin immunoreactivity in heart Purkinje fibers from several species. J. Histochem. Cytochem. 27, 1604–1609.
Fedorov, V.V., Glukhov, A.V., Chang, R., Kostecki, G., Aferol, H., Hucker, W.J., Wuskell, J.P., Loew, L.M., Schuessler, R.B., Moazzami, N., Efimov, I.R., 2010. Optical mapping of the isolated coronary-perfused human sinus node. J. Am. Coll. Cardiol. 56, 1386–1394.
Forsgren, S., Eriksson, A., Kjörell, U., Thornell, L.E., 1982. The conduction system in the human heart at midgestation – immunohistochemical demonstration of the intermediate filament protein skeleton. Histochemistry. 75, 43–52.
Fuchs, E., Weber, K., 1994. Intermediate filaments: structure, dynamics, function and disease. Annu. Rev. Biochem. 63, 345–382.
Futami, C., Tanuma, K., Tanuma, Y., Saito, T., 2003. The arterial blood supply of the conducting system in normal human hearts. Surg. Radiol. Anat. 25, 42–49.
Glomset, D.J., Glomset, A.T.A., 1940a. Morphologic study of the cardiac conduction system in ungulates, dog and man. Part I: The sinoatrial node. Am. Heart. J. 4, 389–398.
Glomset, D.J., Glomset, A.T.A., 1940b. Morphologic study of the cardiac conduction system in ungulates, dog and man. Part II: The Purkinje system. Am. Heart. J. 20, 677–701.
Glukhov, A.V., Hage, L.T., Hansen, B.J., Pedraza-Toscano, A., Vargas-Pinto, P., Hamlin, R.L., Weiss, R., Carnes, C.A., Billman, G.E., Fedorov, V.V., 2013. Sinoatrial node reentry in a canine chronic left ventricular infarct model: role of intranodal fibrosis and heterogeneity of refractoriness. Circ. Arrhythm. Electrophysiol. 6, 984–994.
Gómez, F.A., Ballesteros, L.E., 2013. Anatomic study of the right coronary artery in pigs. Feature review in comparison with the human artery. Int. J. Morphol. 31, 1289–1296.
Gómez, F.A., Ballesteros, L.E., 2015. Characterisation of myocardial bridges in pigs: a comparative anatomical analysis with the human heart. Folia Morphol. (Warsz) 74, 395–398.
Haissaguerre, M., Cheniti, G., Escande, W., Zhao, A., Hocini, M., Bernus, O., 2019. Idiopathic ventricular fibrillation with repetitive activity inducible within the distal Purkinje system. Heart Rhythm. 16, 1268–1272.
Hoffman, B.F., Cranefield, P., 1964. The physiologic basis of cardiac arrhythmias. Am. J. Med. 37, 670–684.
James, T.N., 1961. Morphology of the human atrioventricular node, with remarks pertinent to its electrophysiology. Am. Heart J. 62, 756–771.
James, T.N., 1963. The connecting pathways between the sinus node and the A-V node and between the right and left atrium in the human heart. Am. Heart J. 66, 498–508.
James, T.N., 1967. Cardiac innervation: anatomic and pharmacologic relations. Bull. N.Y. Acad. Med. 43, 1041–1086.
James, T.N., 2002. Structure and function of the sinus node, AV node and hiss bundle of the human heart: part I – structure. Prog. Cardiovasc. Dis. 45, 235–267.
James, T.N., Sherf, L., 1971. Specialized tissue and preferential conduction in the atria of the heart. Am. J. Cardiol. 28, 414–427.
James, T.N., Sherf, L., Fine, G., Morales, A.R., 1966. Comparative ultrastructure of the sinus node in man and dog. Circulation. 34, 139–163.
Kalyanasundaram, A., Li, N., Hansen, B.J., Zhao, J., Fedorov, V.V., 2019. Canine and human sinoatrial node: differences and similitaries in the structure, function, molecular profiles, and arrhythmia. J. Vet. Cardiol. 22, 2–19.
Kawamura, M., 1968. Experimental study of the pacemaker shift in the rabbit atrium by means of the microelectrode method. Jpn. Cic. J. 32, 26–28.
Keith, A., Flack, M., 1907. The form and nature of the muscular connections between the primary division of the vertebrate heart. J. Anat. Physiol. 41, 172–189.
Kennedy, A., Finlay, D.D., Guldenring, D., Bond, R., Moran, K., McLaughlin, J., 2016. The cardiac conduction system. Generation and conduction of the cardiac impulse. Crit. Care. Nurs. Clin. North. Am. 28, 269–279.
Koch, W., 1911. What significance does the sinus node have? Med. Klin. 328, 447.
Lou, Q., Hansen, B.J., Fedorenko, O., Csepe, T.A., Kalyanasundaram, A., Li, N., Hage, L.T., Glukhov, A.V., Billman, G.E., Weiss, R., Molher, P.J., Gyorke, S., Biesiadecki, B.J., Carnes, C.A., Fedorov, V.V., 2014. Upregulation of adenosine A1 receptors facilitates sinoatrial node dysfunction in chronic canine heart failure by exacerbating nodal conduction abnormalities revealed by novel dual-sided intramural optical mapping. Circulation. 104, 915–923.
Lowery, J., Kuczmarski, E.R., Hermann, H., Goldman, R.D., 2015. Intermediate filaments play a pivotal role in regulating cell architecture and function. J. Biol. Chem. 290, 17145–17153.
Mani, B.C., Pavri, B.B., 2014. Dual atrioventricular nodal pathways physiology: a review of relevant anatomy, electrophysiology, and electrocardiographic manifestations. Indian. Pacing. Electrophysiol. J. 14, 12–25.
Oosthoek, P.W., Viragh, S., Mayen, A.E.M., Van Kempen, M.J.A., Lamers, W.H., Moorman, A.F.M., 1993. Immunohistochemical delineation of the conduction system I: the sinoatrial node. Circ. Res. 73, 473–481.
Opthof, T., 1988. The mammalian sinoatrial node. Cardiovasc. Drugs Ther. 1, 573–597.
Opthof, T., de Jonge, B., Jongsma, H.J., Bouman, L.N., 1987. Functional morphology of the pig sinoatrial node. J. Mol. Cell. Cardiol. 19, 1221–1236.
Ortale, J.R., Paganoti, C.F., Marchiori, G.F., 2006. Anatomical variations in the human sinuatrial nodal artery. Clinics (Sao Paulo). 61, 551–558.
Paulin, D., Li, Z., 2004. Desmin: a major intermediate filament protein essential for the structural integrity and function of muscle. Exp. Cell Res. 301, 1–7.
Pejković, B., Krajnc, I., Anderhuber, F., Kosutić, D., 2008. Anatomical aspects of the arterial blood supply to the sinoatrial and atrioventricular nodes of the human heart. J. Int. Med. Res. 36, 691–698.
Ramanathan, L., Shetty, P., Nayak, S.R., Krishnamurthy, A., Chettiar, G.K., Chockalingam, A., 2009. Origin of the sinoatrial and atrioventricular nodal arteries in South Indians: an angiographic study. Arq. Bras. Cardiol. 92, 314–319.
Randhawa, A., Gupta, T., Aggarwal, A., Sahni, D., Singh, R.S., 2017. Histological topography of the atrioventricular node and its extensions in relation to the cardiothoracic surgical landmarks in normal human hearts. Cardiovasc. Pathol. 30, 38–44.
Row, S., Swartz, D.D., Andreadis, S.T., 2017. Animal models of cardiovascular disease as test beds of bioengineered vascular grafts. Drug. Discov. Today: Disease Model. 24, 37–45.
Sahni, D., Kaur, G.D., Jit, H., Jit, I., 2008. Anatomy and distribution of coronary arteries in pig in comparison with man. Indian J. Med. Res. 127, 564–570.
Sánchez-Quintana, D., Ho, S.Y., 2003. Anatomy of cardiac nodes and atrioventricular specialized conduction system. Rev. Esp. Cardiol. 56, 1085–1092.
Saremi, F., Abolhoda, A., Ashikyan, O., Milliken, J.C., Narula, J., Gurudevan, S.V., Kaushal, K., Raney, A., 2008. Arterial supply to sinuatrial and atrioventricular nodes: imaging with multidetector CT. Radiology. 246, 99–107.
Waller, B., Gering, L.E., Branyas, N.A., Slack, J.D., 1993a. Anatomy, histology, and pathology of the cardiac conduction system: part I. Clin. Cardiol. 16, 249–252.
Waller, B., Gering, L.E., Branyas, N.A., Slack, J.D., 1993b. Anatomy, histology, and pathology of the cardiac conduction system: part II. Clin. Cardiol. 16, 347–352.
Ward, J.L., DeFrancesco, T.C., Tou, S.P., Atkins, C.E., Griffith, E.H., Keene, B.W., 2016. Outcome and survival in canine sick sinus syndrome and sinus node dysfunction: 93 cases (2002-2014). J. Vet. Cardiol. 18, 199–212.
Yoshimura, A., Yamaguchi, T., Kawazato, H., Takahashi, N., Shimada, T., 2014. Immunohistochemistry and three-dimensional architecture of the intermediate filaments in Purkinje cells in mammalian hearts. Med. Mol. Morphol. 47, 233–239.
Zhang, L.J., Wang, Y.Z., Huang, W., Chen, P., Zhou, C.S., Lu, G.M., 2008. Anatomical investigation of the sinus node artery using dual source computed tomography. Circ. J. 72, 1615–1620.

Anatomical Science International (2021) 96:212–220
https://doi.org/10.1007/s12565-020-00575-7

ORIGINAL ARTICLE

Morphological variations of the conduction system in the atrioventricular zone and its clinical relationship in different species

Fabián Gómez-Torres[1,2] · Luis Ballesteros-Acuña[2] · Amparo Ruíz-Sauri[1,3]

Received: 18 February 2020 / Accepted: 12 September 2020 / Published online: 30 September 2020

Abstract
Atrioventricular node is responsible for delaying the passage of the electrical impulse to ventricles in order to protect them from fast depolarizations coming from the atria. The importance of this study is to identify the morphological variations of the components of atrioventricular zone that affect the conduction system and its clinical relationship in different species of mammals. We analyzed ten human hearts, nine from horses, eight from pigs, and five from dogs without a clinical history of cardiac pathologies. Histological section thickness of 5 µm were obtained with a microtome and stained with hematoxylin–eosin and Masson's trichrome. We observed both an increase in collagen fibers and a decrease in the size of P cells (nodal pacemaker cells) within the atrioventricular node in dogs, horses and pigs in cases that presented cartilage in fibrous body. The percentage of fundamental substance in atrioventricular node was significantly higher in dogs and the percentage of collagen fibers was higher in pigs, both than in humans. The presence of cartilaginous metaplasia in cardiac fibrous skeleton from different species decreases the size of atrioventricular node and its cells and increases the percentage of collagen fibers within the node, which can reduce the transmission of the electrical impulse to ventricles and therefore predispose to the presentation of ventricular arrhythmias. Morphometric analysis has allowed us to objectively quantify each of the components of AV node and compare them in the different species.

Keywords Arrhythmia · Atrioventricular node · Cartilage · Fibrous body · P cell

Abbreviations

CCS	Cardiac conduction system
AV	Atrioventricular
AVF	Atrioventricular fascicle
CFS	Cardiac fibrous skeleton

Introduction

The importance of cardiac conduction system (CCS) in atrioventricular zone is that atrioventricular (AV) node is responsible for delaying the passage of electrical impulse to ventricles to protect them from fast depolarizations coming from the atria under normal conditions or, even, when there are atrial ectopic foci due to supraventricular arrhythmias.

Different morphological variations at atrioventricular level due to factors such as aging have been reported in humans: cardiac block due to calcareous lesions in atrioventricular fascicle (AVF) (previously called His bundle) (Yater and Cornell 1935) and similar lesions referring to them as "sclerosis of the left side of cardiac skeleton" (Lenegre 1964; Lev 1964). It has also been indicated that cartilage metaplasia in the cardiac skeleton with focal degeneration in AVF from Doberman Pinscher dogs of different ages and with similar lesions in all of them, leads to sudden death (James and Drake 1968).

Moreover, the presence of cartilaginous metaplasia or ossification and bone formation in cardiac fibrous skeleton

✉ Amparo Ruíz-Sauri
Amparo.Ruiz-Sauri@uv.es

[1] Department of Pathology, Faculty of Medicine, 1st floor, Universitat de Valencia, Av. de Blasco Ibáñez, 15, 46010 Valencia, Spain

[2] Department of Basic Sciences, School of Medicine, Universidad Industrial de Santander, Cra 32 # 29–31, 68002 Bucaramanga, Colombia

[3] INCLIVA Biomedical Research Institute, Av. de Blasco Ibáñez, 17, 46010 Valencia, Spain

(CFS) of dogs of large breeds of different ages has been indicated (Sandusky et al. 1979). A very characteristic bone has been found in the fibrous central body near the AV node and AVF known as "os cordis" in hearts of different mammals, especially in ungulates such as sheep and cow. But it is possible to find cartilage in hearts of horses, water buffalo, dogs and some cats (Buchanan 1977; James 2002; Aupperle et al. 2008). In pigs it has been found cartilage mainly of the hyaline type, but sometimes it is also possible to observe fibrous cartilage in their cardiac skeleton (Murata and Yamada 1986). Tawara (1906) has described the presence of the cartilage or bone tissue in the atrioventricular area of calf and sheep hearts. He has also reported that there was no the cartilage in the human heart.

Due to the importance of electrical conduction in the middle zone of the heart, the aim of this is study is to evaluate the components of AV node involved in atrioventricular conduction disorders. To do so, we evaluated these structures using morphometry them with the components of nodes that display various morphological variations in humans, pigs, horses and dogs.

Materials and methods

Sample preparation and processing

We evaluated ten hearts from human males, which were collected from the autopsies from the Institute of Legal Medicine and Forensic Sciences of Bucaramanga, Colombia (adults between 20 and 60 years old and medium size between 60 and 80 kg). At the same time, eight male pig hearts (weighing 85–90 kg and an average age of 5 months old) and nine hearts of male horses (weighing 250–300 kg and 2.5–3.5 years old) were collected from slaughter plants. Also, five hearts of male dogs, who underwent autopsy in small animal clinics in the city of Bucaramanga, Colombia, were used (medium-sized adults with a weight of 8–19 kg and an age between 5 and 12 years old). The specimens of study did not display lesions or clinical history of cardiac pathologies. The procedures were in accordance with Ethics Committee of Universidad Cooperativa de Colombia (minute 014-2018) and complied with the Resolution 008430 of 1993, Decree 2164 of 1992 and Law 10 of 1990 of the Ministry of Health of Colombia and the principles of the Declaration of Helsinki and all subsequent revisions. In addition, this study complies with Law 84 of 1989 in the national context, which corresponds to the "National Statute for the Protection of Animals", in Chapter VI of the use of animals in experiments and research.

In the specimens studied, the atrioventricular zone was cut, and the block of tissue removed included the union of the interatrial and interventricular septum. Samples were fixed in 5% formaldehyde solution, marked for identification and included in paraffin. Histological section thickness of 5 µm were obtained with a microtome and stained with hematoxylin–eosin and Masson's trichrome. For each heart, five samples were cut in slices 5 mm thick of atrioventricular area. AV node was in the second or third cut of the atrioventricular zone. To do a three-dimensional reconstruction of the AV node, the paraffin block that included the AV node was cut entirely according to the following protocol: a whole AV node was cut in serial histological levels. A 5 µm section was performed and afterwards sample was devastated 40 µm and another 5 µm section was done. This protocol was followed until the whole AV node was sectioned (Fig. 1).

Morphometric evaluation and histological description

Twenty micrographs were taken for measurements and AV node shape at 4× in hematoxylin–eosin (20 micrographs). To measure the parameters of the P cells, 140 micrographs at 40× and 63× were taken in hematoxylin–eosin and Mason's trichrome (280 micrographs). In total 300 micrographs were analyzed for each heart with a Leica DMD108 optical microscope (Leica Microsystems, Wetzlar, Germany). All the samples were initially studied histologically. The computerized morphometric study was performed by Image-Pro Plus 7.1 software (Media Cybernetics, Silver Spring, MD, USA). In each calibrated micrograph, the following parameters of the different components of atrioventricular conduction system were measured for the AV node: area, maximum diameter, length, width at 4X; for the connective tissue: percentage of collagen fibers and fundamental substance; for the P cells: area, maximum diameter, minimum diameter, mean diameter and roundness and for the cartilage: area, maximum diameter, length and width at 4×, 10×, 20× magnification.

Statistical analysis

A cutoff level of 0.05 was set for statistical significance. Descriptive statistics were performed using SPSS 20 software (SPSS, Chicago, IL, USA) and Microsoft Excel 2013. Continuous variables were expressed as the average of the findings obtained. The Kolmogorov–Smirnov normality test and descriptive statistics were performed for each parameter. For the quantitative variables when two independent groups were compared and with a sample larger than 30 cases a Student´s t test was used; when the sample was less than 30, the Mann–Whitney *U* test was chosen. For the quantitative variables with a normal distribution within each species group, the ANOVA test was used, and when their distribution was non-parametric the Kruskal–Wallis test was chosen.

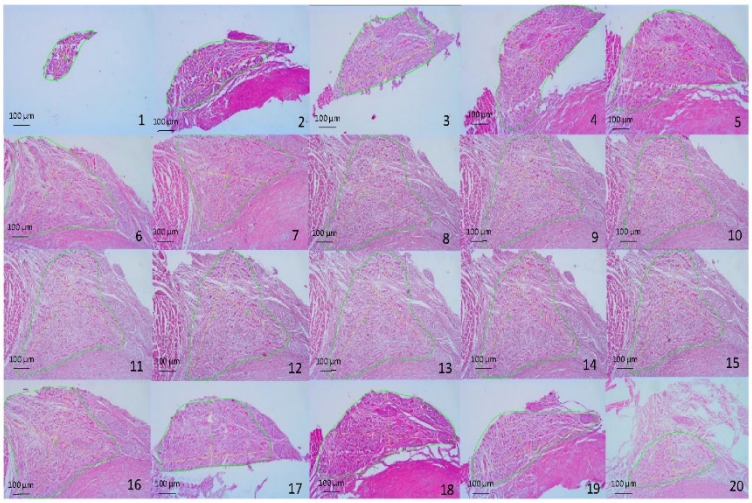

Fig. 1 Serial cuts in a pig heart sample in the atrioventricular area, where the morphometry of each one is indicated in order to measure the parameters throughout the thickness of the atrioventricular node at 4×

For all the measured dimensions, data were expressed as mean standard deviation (SD).

Results

During the analysis of the atrioventricular zone of the different species of the study the presence of cartilage was found in CFS in three hearts of dogs (60%), in seven hearts of horses (77.8%) and in four hearts of pigs (50%). This was hyaline type cartilage, and in one case in pigs, fibrous type cartilage was found. In human hearts, we did not find any cartilage type in CFS. (Figs. 2, 3, 4, 5).

In our study, we used the compact portion of AV node to make comparisons between cases with cartilage and cases without cartilage. After joining each of the sections made to different samples for each heart from the serial histological levels, we found that the shape of the AV node in six horses was a triangular pyramid, and in three it was cylindrical. In dogs, humans, and pigs, the shape of the AV node was a triangular pyramid. The size of the node in each of the cases in the different species can be seen in Table 1. When analyzing the measurements in the sections both in the cases with cartilage and in the case without the presence of cartilage, we observed that although the length and width of the AV node increased in the first 6–8 cuts, in the latter it decreased.

All components of the AV node were larger in the group of animals without presence of cartilage in the fibrous skeleton (Fig. 6a). No statistically significant differences were found between the different parameters measured in the AV node in dogs and horses. (Table 1). In pigs, the area, maximum diameter and width of AV node were significantly larger ($p = 0.034$ for all values) in the cases that did not show cartilage in the CFS. Furthermore, there was a decrease in the number and size of cells (Fig. 6b) and an increase in collagen fibers (Fig. 7) within the AV node in dogs, horses and pigs in cases that presented cartilage, which could decrease the transmission of the electrical impulse through the AV node (Table 1).

When comparing the parameters in AV node of humans with those of the other animal species with no presence of cartilage in CFS, the percentage of fundamental substance was significantly higher in dogs than in humans ($p = 0.007$) (Fig. 7). The measurements of the human AV node were also compared with cases where cartilage was present in animal species observing that the percentage of collagen fibers in AV node of pigs was significantly higher than in humans ($p = 0.023$) (Table 1).

Moreover, among the animal species with no cartilage in the CFS, the width of the AV node was larger in dogs ($p = 0.009$), and in pigs ($p = 0.017$) than in horses. The percentage of collagen fibers in pigs (67.15%) inside the AV

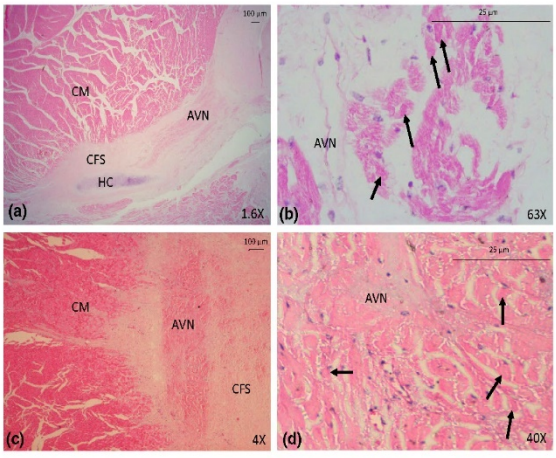

Fig. 2 Atrioventricular area of horses stained with hematoxylin eosin, showing the differences between the cases that presented cartilage (**a**, **b**) and those that did not present it (**c**, **d**). **a** Observe cartilage metaplasia in the cardiac fibrous skeleton (CFS) with hyaline cartilage (HC) at low magnifications. P cells are indicated by arrows, these cells are pale, small, and oval observed at high magnifications in the presence of cartilage metaplasia (**b**) and under normal conditions **d** at 40×. *AVN* atrioventricular node, *CM* cardiomyocytes

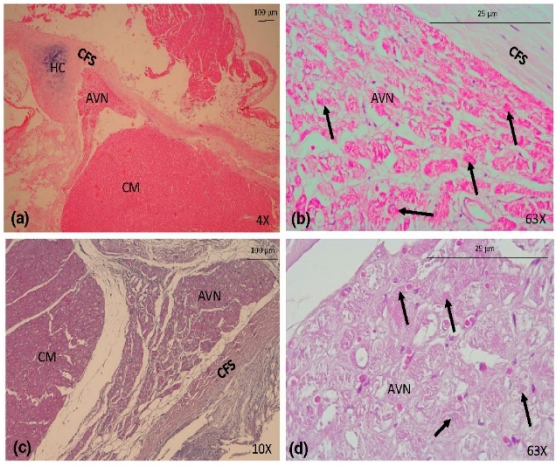

Fig. 3 Atrioventricular area of dogs stained with hematoxylin eosin, showing the differences between the cases that had cartilage (**a**, **b**) and those that did not (**c**, **d**). **a** Observe cartilage metaplasia in the cardiac fibrous skeleton (CFS) with hyaline cartilage (HC) at low magnifications. P cells are indicated by arrows, these cells are large, rounded, similar in color to cardiomyocytes (CM) observed at high magnifications in the presence of cartilage metaplasia (**b**) and under normal conditions **d** at 63×. *AVN* atrioventricular node

node was significantly higher than in dogs ($p=0.042$) and the percentage of fundamental substance was higher in dogs than in horses ($p=0.013$) and pigs ($p=0.007$). Finally, when comparing the three animal species with cartilage in the atrioventricular zone, the percentage of collagen fibers within the AV node was significantly higher in horses ($p=0.042$), and in pigs ($p=0.001$) than in dogs, with a larger amount in pigs (74.69%) than in horses ($p=0.010$). Likewise, the percentage of fundamental substance in the node was higher in dogs than in horses ($p=0.031$) and in pigs ($p=0.050$) (Table 1).

Length, area and maximum diameter of the cartilage in CFS were significantly larger in horses than in dogs ($p=0.011$; $p=0.039$; $p=0.023$ respectively) (Table 2). In

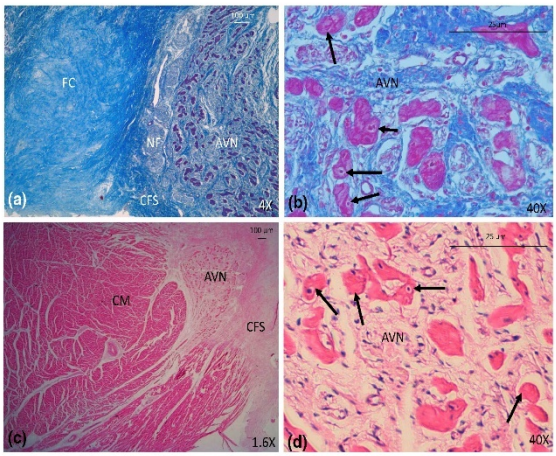

Fig. 4 Atrioventricular area of pigs stained with hematoxylin eosin and Manson's trichrome, showing the differences between the cases that presented cartilage (**a**, **b**) and those that did not present it (**c**, **d**). **a** Observe cartilage metaplasia in the cardiac fibrous skeleton (CFS) with fibrous cartilage (FC) at low magnification. P cells are indicated by arrows, these cells are very large, with a slightly paler cytoplasm than cardiomyocytes (CM) observed at high magnifications in the presence of cartilage metaplasia (**b**) and under normal conditions **d** at 40×. *AVN* atrioventricular node, *NF* nerve fiber

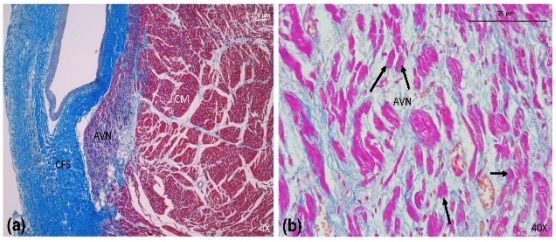

Fig. 5 Atrioventricular area of humans stained with Manson's Trichrome. **a** Note the position of the atrioventricular node (AVN) in the cardiac fibrous skeleton (CFS) in which there is no cartilage. **b** P cells are indicated by arrows, which are dark, rounded, or oval and smaller than cardiomyocytes (CM) observed at high magnifications (40×)

Table 1 Mean values of AV node parameters with or without cartilage in dogs, horses, pigs and humans

Species	Area (μm²/SD)	Maximum diameter (μm/SD)	Length (μm/SD)	Width (μm/SD)	Collagen fibers (%)	Fund. subst. (%)	Cells (%)
With cartilage							
Dogs	413,552 (255,124.3)	1164 (207.3)	1419.9 (389.4)	718.3 (92)	27.05	44.49	28.46
Horses	1,406,634.1 (990,743.5)	2052.4 (670)	2231.7 (649.5)	755.4 (319.7)	48.02	11.83	40.15
Pigs	1,139,876.2 (253,654)	1705.3 (233.1)	1853 (663)	687.4 (97.2)	77.35	8.76	13.89
Without cartilage							
Dogs	925,746.3 (105,645.5)	1304.6 (678.5)	1895.1 (14.56)	1176.2 (253)	9.75	63.98	26.27
Horses	514,321.7 (176,236.4)	1534.1 (613.7)	1479.9 (406.6)	490.7 (88.2)	37.24	11.2	51.56
Pigs	1,844,137.1 (262,267.5)	2362.4 (242.1)	1875.6 (199.1)	1,025 (65.1)	65.68	14.29	20.03
Humans	1,615,290 (380,785.3)	2223.1 (402.5)	2150 (348.6)	884.8 (167.3)	38.91	15.47	45.62

SD standard deviation

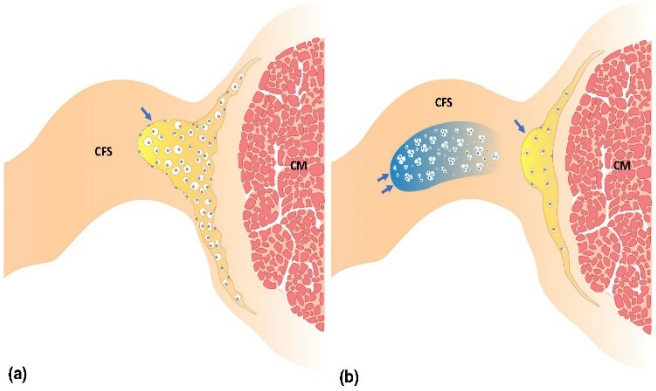

Fig. 6 **a** AV node (single arrow) in the cardiac fibrous skeleton (CFS) with a large number of cells. **b** Observe the displacement of the AV node (single arrow) towards the ventricular cardiac muscle (CM) and the decrease in its size and the number of cells when there is presence of hyaline cartilage (double arrow) in the cardiac fibrous skeleton (CFS)

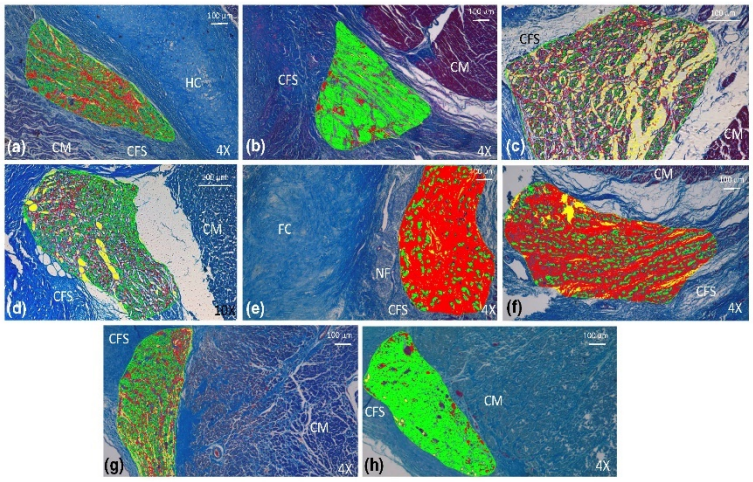

Fig. 7 Morphometric analysis of the AV node with and without cartilage metaplasia in horses (**a**, **b**), dogs (**c**, **d**), pigs (**e**, f) and humans (**g**, **h**). Note that the red color indicates the percentage of collagen fibers, which is more abundant in cases where cartilage is present in the cardiac fibrous skeleton (CFS) (**a**, **c**, **e**) unlike in cases where there is no cartilage (**b**, **d**, **f**, **g**, **h**); the yellow color indicates the percentage of fundamental substance (especially in dogs and humans) and green the percentage of cells within the AV node (especially in horses). *HC* hyaline cartilage, *FC* fibrous cartilage, *CM* cardiomyocytes, *CFS* cardiac fibrous skeleton

Table 2 Parameters of the cartilage in the cardiac fibrous body of dogs, horses and pigs

Species	Length (μm/SD)	Width (μm/SD)	Area (μm²/SD)	Max. diameter (μm/SD)
Dogs	885.3 (131.2)	686 (157.1)	627,763.5 (320,237.4)	1043.5 (273.3)
Horses	2683.9 (792.8)	1109.5 (314.6)	2,445,462.9 (1,063,789.1)	2690.7 (783)
Pigs	2293.3 (431.4)	735.2 (206)	1,590,459.2 (311,567.3)	2224.7 (577.4)

SD: standard deviation

all animal species the cartilage within the fibrous skeleton was hyaline type, while fibrous cartilage was found only in a pig sample.

P cells (nodal pacemaker cells) in horses were pale, large, oval, located in the center of the node and with a single nucleus (Fig. 2b, d). In dogs, these cells were small, rounded, similar in color to cardiomyocytes, located in the center of the node and with a single nucleus (Fig. 3b, d). In pigs, these cells were very large, with a cytoplasm slightly paler than in cardiomyocytes and with a single nucleus (Fig. 4b, d). In humans, P cells were smaller than cardiomyocytes, dark, rounded or oval, located in the center of AV node and with multinucleated cells or with a single nucleus (Fig. 5b). P cells in the species were evaluated according the presence or absence of cartilage. In both dogs and pigs, the area and the diameters of P cells were significantly larger in cases with no cartilage ($p < 0.001$ for all values), Also the cells of these same cases in dogs were rounder when they had cartilage ($p < 0.001$). In horses, similar histological characteristics of P cells were found both in dogs and pigs. There were significantly larger differences in area ($p = 0.001$), maximum diameter ($p = 0.002$), minimum diameter ($p = 0.004$) and mean diameter ($p = 0.002$) of P cells of AV node in the hearts without cartilage in their CFS (Table 3).

The morphological comparison of P cells in AV node, in human and animal species alike with absent cartilage, found larger cell area and diameters in dogs than in humans, in pigs than in dogs, in horses than in humans, and in pigs than in horses ($p = 0.001$ for all cases). Similarly, it was found that the minimum and mean diameter were larger in horses than in dogs ($p = 0.023$ and $p = 0.039$ respectively).

Also, the P cells were rounder in humans than in dogs, in dogs than in pigs, in humans than in horses, and in horses than in pigs ($p < 0.001$ for all cases). When the comparison was made within cases with cartilage, the area and cell diameters displayed similar features to those without cartilaginous tissue. Additionally, the maximum diameter ($p = 0.014$), the minimum diameter ($p = 0.015$) and the mean diameter ($p = 0.005$) were larger in horses than in dogs. In these cases, that the P cells were rounder in humans than in dogs and pigs ($p = 0.007$ and $p < 0.001$ respectively). Besides, P cells of the AV node were larger in pigs and small in humans. In dogs and horses, P cells showed a medium size (Table 3). Furthermore, it is important to indicate that the size of these cells was larger in animal species when they did not have cartilaginous tissue in CFS.

Discussion

The study of microstructures located in the atrioventricular zone of humans and other animal species is important for the understanding of arrhythmias due to the protective role P cells have delaying the passage of the electrical impulse to ventricles.

The presence of cartilage in CFS is considered as cartilaginous metaplasia in dog's hearts and other animal species, producing lesions in the CCS and sudden death (James and

Table 3 Mean values of AV node P cells parameters with or without cartilage in dogs, horses, pigs and humans

Species	Area (μm²/SD)	Maximum diameter (μm/SD)	Minimum diameter (μm/SD)	Mean diameter (μm/SD)	Roundness (μm/SD)
Cartilage					
Dogs	168.32 (53.74)	15.23 (2.37)	10.79 (2.30)	12.96 (2.24)	1.11 (0.03)
Horses	248.36 (68.54)	17.58 (2.77)	14.52 (2.38)	15.87 (2.47)	1.14 (0.04)
Pigs	694.31 (239.76)	31.95 (5.65)	25.82 (5.39)	28.56 (5.42)	1.17 (0.15)
Without cartilage					
Dogs	240.12 (73.87)	21.54 (3.23)	15.96 (2.56)	18.24 (2.64)	1.07 (0.03)
Horses	322.31 (71.93)	23.15 (2.48)	18.24 (2.32)	19.06 (2.39)	1.07 (0.01)
Pigs	992.04 (373.43)	42.98 (9.12)	31.48 (5.63)	35.82 (6.94)	1.15 (0.04)
Humans	18.65 (5.29)	6.74 (0.86)	4.08 (0.83)	5.23 (0.84)	1.04 (0.05)

SD standard deviation

Drake 1968; Sandusky et al. 1979), although cartilage in the cardiac skeleton of dogs with normal electrocardiographic functioning has been observed (James 1964; Sokkar and Trautwein 1970; Buchanan 1977; Aupperle et al. 2008) as well as in several species of mammals (Murata and Yamada 1986). Like these previous studies, in our research we found cartilage presence in CFS in dogs, horses and pigs in percentages greater than 50%. The presence of cartilage with subsequent bone formation (os cordis) has been described as part of the normal anatomy in ungulate hearts such as sheep and cow. Similarly, this structure has been described in hearts of horses, water buffalo and some cats (Tawara 1906; Bishop and Cole 1967; James 2002). It has been proposed that this bone in the central fibrous body of ungulates can protect the AV node and AVF from mechanical stress during cardiac systole in large mammalian hearts (James et al. 1995; James 2002). Similarly, the presence of cartilage in the cardiac skeleton has been reported in pigs, mainly from the hyaline type, and less frequently from fibrous type (Murata and Yamada 1986). Our findings in the CFS of the evaluated animal species are consistent with those descriptions.

It has been indicated that cartilage metaplasia in cardiac skeleton with focal degeneration in AVF of Doberman Pinscher dogs of different ages leads to sudden death (James and Drake 1968). Moreover, a lack of communication between the atria and the AV node, with atrophy of the latter with interruption of continuity towards AVF and degenerative changes in the CCS with spontaneous heart block have been described (Bharati et al. 1974). Consequently, these changes in the CFS could alter the components of the CCS and lead to arrhythmias. In our study, we also initially thought about the possibility that the presence of cartilage was related to the age of the animal. To rule out this eventuality, we studied dogs and horses between 5 and 12 years of age, so we consider that the appearance of cartilage metaplasia may be structural for each individual and is independent of the age of presentation.

Previous studies also have reported that the AV node of some hearts of large breed dogs without apparent heart disease had a smaller diameter when there was presence of cartilaginous metaplasia in CFS, and that some of the nodes evaluated moved towards the center of the interatrial septum, instead of his usual subendocardial position (Sandusky et al. 1979). Further, the same authors reported that in dogs, there was an increase in the connective tissue stroma and loss of the conductive fibers in the AV nodes evaluated with cartilaginous metaplasia (Sandusky et al. 1979). In our study, there was a significant decrease in the size of the AV node in pigs when it has cartilaginous metaplasia and a displacement from its normal position. Furthermore, there was an increase in percentage of collagen fibers and decrease in the percentage of cells inside the node when there was cartilage in CFS. In dogs and horses, despite not finding significant differences, it was observed that the AV nodes of these two species have similar features as in pigs. This means that early detection of this cartilaginous tissue by echocardiographic methods can help to determine individuals of these species susceptible to alterations in the heart rhythm. Additionally, a study of large breed dogs with heart problems indicated that the main morphological change in CFS was the presence of cartilaginous metaplasia in 98% of cases evaluated without being correlated with age or breed (Sandusky et al. 1979). This coincides with our findings, being one of the main changes found but in a smaller percentage in each species. Likewise, we determined that area and diameters of P cells in AV node of dogs, horses and pigs were significantly larger when there was no presence of cartilaginous metaplasia in CFS. Unlike what was described by Sandusky et al. (1979), that these changes in CFS and AV node were normal variations in dog's hearts of large breeds and there is no relation to pathological changes. The reasons why cartilage metaplasia occurs are unknown, but we found that in all cases that have had cartilage metaplasia, there was an increase in the production of connective tissue, which does not occur only inside the AV node with an increase in collagen fibers, but also outside it, with the appearance of hyaline or fibrous cartilage, these results are a verifiable anatomical finding for which we have no explanation. This is accompanied by a decrease in the number and size of the conducting cells, which results in a delay of the electrical impulse to the ventricles in animals of any age and without previous heart disease.

However, not only these changes can be observed in normal hearts; it has been reported cartilaginous metaplasia in CFS in hearts of cats with idiopathic cardiomyopathy (Lui et al. 1975). These findings support the hypothesis of a decrescent function of AV node cells when cartilage is found in this fibrous tissue.

Different morphological variations at atrioventricular level due to aging have been reported in humans: cardiac block due to calcareous lesions in AVF (Yater and Cornell 1935) and similar lesions of "sclerosis of the left side of the cardiac skeleton" with presence of fibrosis, hyalinization and calcification (Lenegre 1964; Lev 1964; Bharati et al. 1974; van Nieuwenhoven et al. 2017; Zhang et al. 2018). In humans, these changes often involve the adjacent AV conduction system, which leads to a loss of conduction fibers and an increase in fibrosis at this level (Lenegre 1964), although the absence of cartilage and bone in the CFS was reported in a study in 250 human hearts (James and Drake 1968; Randhawa et al. 2017). Both cartilage and bone have rarely been observed in human hearts, sometimes in association with sudden death due to cardiac arrhythmias; these findings would indicate that this alteration is caused by the presence of cartilage in CFS (Ferris and Aherne 1971; James and Marshal 1976). This coincides with our study where

we did not find cartilaginous metaplasia in the CFS in the human hearts, and when compared with the hearts of animals with cartilage, there was an increase in the collagen fibers and the fundamental substance in the AV node in the hearts of dogs and pigs.

Conclusions

To our knowledge, this is the largest quantitative evaluation of the cartilage in CFS of animal species and of morphological changes in the CCS to date, unlike earlier qualitative studies. The presence of cartilaginous metaplasia by age or as an individual structural feature in CFS of pigs, horses and dogs decreases the size of the AV node and its cells and increases the percentage of collagen fibers inside the node, which may decrease transmission of the electrical impulse towards the ventricles and therefore predispose to ventricular arrhythmias.

As in previous studies, no cartilaginous metaplasia in CFS was found in human hearts, which supports the hypothesis that in humans there is no cardiac cartilaginous metaplasia.

Morphometric analysis has allowed us to objectively quantify each of the components of AV node and compare them in the different species.

Acknowledgements The authors wish to thank the Colombian Institute of Legal Medicine and Forensic Sciences, the small animals veterinary clinics and the Vijagual Meat and Refrigerating Plant in the city of Bucaramanga, Colombia for the collection and donation of specimens for this research. We thank Dr. Hernando Yesid Estupiñan Velasquez for his collaboration in the iconographic design.

Author contributions All authors contributed to the study conception and design. Material preparation, data collection and analysis were performed by FG-T, LB-A and AR-S. The first draft of the manuscript was written by FG-T and all authors commented on previous versions of the manuscript. All authors read and approved the final manuscript.

Funding This work was supported by the "Instituto de Salud Carlos III" and co-funded by "FEDER (Grant Nos. PI14/00271, pie15/00013) and by the "Generalitat Valenciana" (Grant No. PROMETEO2013/007), Spain.

Compliance with ethical standards

Conflict of interest The authors declare that they have no conflicts of interest.

Ethical clearance The procedures were in accordance with Ethics Committee of Universidad Cooperativa de Colombia (minute 014-2018) and complied with the Resolution 008430 of 1993, Decree 2164 of 1992 and Law 10 of 1990 of the Ministry of Health of Colombia and the principles of the Declaration of Helsinki (1964) and all subsequent revisions. In addition, this study complies with Law 84 of 1989 in the national context, which corresponds to the "National Statute for the Protection of Animals", in Chapter VI of the use of animals in experiments and research.

References

Aupperle H, März I, Schoon HA (2008) Detection and characterization of chondroid metaplasia in canine atrioventricular valves. J Comp Pathol 139:113–120

Bharati S, Rosen KM, Milter RA, Lev M (1974) Conduction system examination in a case of spontaneous heart block in a dog. Am Heart J 88:596–600

Bishop SP, Cole CR (1967) Morphology of the specialized conducting tissue in the atria of the equine heart. Anat Rec 158:401–416

Buchanan JW (1977) Chronic valvular disease (endocardiosis) in dogs. Adv Vet Sci Comp Med 21:75–108

Ferris JA, Aherne WA (1971) Cartilage in relation to the conduction tissue of the heart in sudden death. Lancet 1:64–66

James TN (1964) Anatomy of the A–V node of the dog. Anat Rec 148:15–27

James TN (2002) Structure and function of the sinus node, AV node and Hiss bundle of the human heart: part I— structure. Prog Cardiovasc Dis 45:235–267

James TN, Drake EH (1968) Sudden death in Doberman Pinschers. Ann Intern Med 68:821–829

James TN, Marshal TK (1976) Persistent fetal dispersion of the atrioventricular node and His bundle within central fibrous body. Circulation 53:1026–1034

James TN, Kawamura K, Meijler FL, Yamamoto S, Terasaki F, Hayashi T (1995) Anatomy of the sinus node, AV node and His bundle of the heart of the sperm whale (*Physeter macrocephalus*), with a note on the absence of an os cordis. Anat Rec 242:355–373

Lenegre J (1964) Etiology and pathology of bilateral branch block in relation to complete heart block. Prog Cardiovasc Dis 6:409–444

Lev M (1964) The pathology of complete atrioventricular block. Prog Cardiovasc Dis 6:317–326

Lui SK, Tilley LP, Tashjian RJ (1975) Lesions of the conduction system in the cat with cardiomyopathy. Recent Adv Stud Cardiac Struct Metab 10:681–693

Murata H, Yamada K (1986) Glycosaminoglycans in the cartilage of the porcine heart as studied by light microscopic histochemical methods. Acta Histochem 79:83–92

Randhawa A, Gupta T, Aggarwal A, Sahni D, Singh RS (2017) Histological topography of the atrioventricular node and its extensions in relation to the cardiothoracic surgical landmarks in normal human hearts. Cardiovasc Pathol 30:38–44

Sandusky GE Jr, Kerr KM, Capen CC (1979) Morphologic variations and aging in the atrioventricular conduction system of large breed dogs. Anat Rec 193:883–902

Sokkar SM, Trautwein G (1970) Endocardiosis of the atrioventricular valves of the dog I. Morphological and histochemical studies. Zbl Vet Med 17:757–759

Tawara S (1906) Das Reizleitungssystem des Säugetierherzens; eine anatomisch-histologische Studie über das Atrioventrikularbündel und die Purkinjeschen Fäden. Gustatav Fischer, Jena, Marburg

van Nieuwenhoven FA, Munts C, Opt-Veld RC, González A, Díez J, Heymans S, Schoroen B, van Bilsen M (2017) Cartilage intermediate layer protein 1 (CILP1): a novel mediator of cardiac extracelular matrix remodelling. Sci Rep 7:1–8

Yater WM, Cornell VH (1935) Heart block due to calcareous lesions of the bundle of His: review and report of a case with detailed histopathological study. Ann Intern Med 8:777–789

Zhang CL, Zhao Q, Liang H, Qiao X, Wang JY, Wu D, Wu LL, Li L (2018) Cartilage intermediate layer protein-1 alleviates pressure overload-induced cardiac fibrosis via interfering TGF-β1 signaling. J Mol Cell Cardiol 116:135–144

Research in Veterinary Science 138 (2021) 137–147

Contents lists available at ScienceDirect

Research in Veterinary Science

journal homepage: www.elsevier.com/locate/rvsc

Identification to cardiac conduction cells in humans and pigs according to their zonal distribution, using histological, immunohistochemical and morphometric study.

Fabián Gómez-Torres [a,b], H. Yesid Estupiñán [b,c], Amparo Ruíz-Sauri [a,d,*]

[a] Department of Pathology, Faculty of Medicine, Universitat de Valencia, Av. de Blasco Ibáñez, 15, 46010 Valencia, Spain
[b] Department of Basic Sciences, Medicine School, Universidad Industrial de Santander, Cra 32 # 29-31, 68002 Bucaramanga, Colombia
[c] Department of Laboratory Medicine, Clinical Research Center, Karolinska Institute, Karolinska University Hospital Huddinge, SE-141 86 Huddinge, Sweden
[d] INCLIVA Biomedical Research Institute, Av. de Blasco Ibáñez, 17, 46010 Valencia, Spain

ARTICLE INFO

Keywords:
Cardiac conduction fibers
Myocardial junctions
Cardiac conduction cells
Desmin

ABSTRACT

Histologically, the cardiac conduction network is formed of electrically isolated subendocardial fibers that comprise specialized cells with fewer myofibrils and mitochondria than cardiomyocytes. Our aim is to uncover regional variations of cardiac conduction fibers through histological and morphometric study in a porcine and human model. We analyzed five male adult human hearts and five male pig hearts. The left ventricles were dissected and sectioned in the axial plane into three parts: basal, middle third and apex regions. Cardiac conduction fibers study was carried out using hematoxylin-eosin and Masson's trichrome staining, and cardiac conduction cells and their junctions were identified using desmin, and a PAS method. Cardiac conduction fibers were difficult to pinpoint in humans, mostly showing a darker color or equal to cardiomyocytes. Cardiac conduction fibers in humans were in the subendocardium and in pigs in the myocardium and subendocardium. Cardiac conduction fibers were located mainly in the septal region in both humans and pigs. In our morphometric analysis, we were able to determine that cardiac conduction cells in humans (18.52 +/− 5.41 μm) and pigs (21.32 +/− 6.45 μm) were large, compared to cardiomyocytes. Conduction fiber-myocardial junctions were present in 10% in humans and 24.2% in pigs. The performance of immunohistochemical methods made it possible to improve the identification of cardiac conduction cells in the species studied. Study of cardiac conduction fibers and cells and their myocardial junctions is vital to gain insight into their normal distribution in the species analyzed, and thus advance the use of pigs in experimental models of the cardiac conduction system in humans.

1. Introduction

The cardiac conduction system (CCS) generates the heartbeat through a network of specialized myocardial cells by which the electrical impulse is propagated in a coordinated way to obtain efficient cardiac muscle contraction (Sedmera and Gourdie, 2014) and thus allow rapid electrical activation of the ventricles (Oosthoek et al., 1993; Aouadi et al., 2019). Since the discovery of cardiac conduction fibers (CCF) in 1845, the anatomy of the CCS has been studied extensively. The fibers of the distal part of the heart are introduced into the inner surface of the ventricles to join the working cardiomyocytes. Although some fibers may occasionally be visible to the naked eye or using a light microscope, these methods do not allow complete visualization of the network (De Almeida et al., 2015), thus specific stains or markers are needed to identify these fibers specifically and distinguish them from other cells such as cardiomyocytes. The CCFs in the hearts of the animal species are formed mainly by groups of cardiac conduction cells (CCC) and small sheaths of connective tissue that surround them (Tawara, 1906; Canale et al., 1986; Tawara, 2000; Ono et al., 2009; Vigmond and Stuyvers, 2016).

Histological preparations with hematoxylin-eosin and Masson's trichrome identify the presence of CCF in ungulates (such as pigs and ruminants) at the subendocardium and intramyocardial level, which are surrounded by sheaths of reticular fibers (Tawara, 1906; Glomset and Glomset, 1940; Tawara, 2000; Ono et al., 2009; Yoshimura et al., 2014). At the subendocardial level, human CCC are cylindrical or fusiform and

* Correspondig author at: Department of Pathology, Faculty of Medicine, Universitat de Valencia, Av. de Blasco Ibáñez, 15, 46010 Valencia, Spain.
E-mail addresses: falegom@uis.edu.co (F. Gómez-Torres), hycstuve@uis.edu.co (H.Y. Estupiñán), Amparo.Ruiz-Sauri@uv.es (A. Ruíz-Sauri).

https://doi.org/10.1016/j.rvsc.2021.06.008
Received 21 January 2021; Received in revised form 23 May 2021; Accepted 7 June 2021
Available online 9 June 2021

are surrounded by connective tissue individually rather than in bundles (Tawara, 1906; Shimada et al., 1983; Tawara, 2000; Ono et al., 2009; Yoshimura et al., 2014).

The CCF network shows variability between species, because the morphology of the CCC presents great variations in mammals, for which it is divided into three groups based on their ultrastructure and size: Group I, found in ungulates (sheep, goats, cows, horses and pigs). and cetaceans (whales and dolphins). The cells are characterized by being large, well differentiated and located in the subendocardium and myocardium; group II, in humans, monkeys, dogs, cats and seals, where the cells are described as intermediate to small in size, with certain similarities to ventricular cardiomyocytes and located in the subendocardium and group III, in rodents (mice and rats) and rabbits, where the cells were apparently smaller in size than ventricular cardiomyocytes and are located in the subendocardium (Canale et al., 1986; Ono et al., 2009; Sedmera and Gourdie, 2014; Yoshimura et al., 2014; Vigmond and Stuyvers, 2016).

Cardiac electrical coupling is regulated by gap junctions, which are formed by transmembrane channels and whose main component are connexins (Gros and Jongsma, 1996; Vozzi et al., 1999). These molecules allow the diffusion of small molecules and ions through their electrochemical gradients. Gap junctions act as low resistance sites for the propagation of the electrical impulse (Vozzi et al., 1999; Severs et al., 2004; Severs et al., 2008). Conduction fiber-myocardial junctions (CFMJ) are the junctions between CCC and ventricular cardiomyocytes, in which three variants have been described: contact through cell bodies (CCB), contact through cell prolongations (CCP) and contact through transitional cardiomyocytes (CTC) (Rawling and Joyner, 1987).

CCF play an important role in development of ventricular arrhythmias (Li et al., 2015; Aouadi et al., 2019), of which the most studied is ventricular tachycardia (VT), a focal tachycardia of the CCF. (Krishnamoorthy et al., 2015). Ventricular fibrillation (VF) is one of the main causes of sudden death in the acute phase of an ischemic event and can be the first manifestation of the disease in more than half of all cases of patients with coronary artery disease (Benito and Josephson, 2012; Cherry et al., 2012; Haissaguerre et al., 2019).

In recent years, mapping and ablation studies have shown that CCF have a central role in the onset of these cardiac pathologies and can be detected in patients with ischemic heart disease and also in structurally normal hearts in both humans and animals (Stevenson and Soejima, 2007; Krishnamoorthy et al., 2015; Gianni et al., 2018; He et al., 2018). The use of ungulate hearts has also been proposed as a model to study these pathologies in humans (De Almeida et al., 2015).

Different techniques have been used for the analysis and description of CCFs, such as serial section reconstruction, India ink injection, identification by immunofluorescence or modified periodic acid Schiff (PAS) method, stereo-microscopy, scanning electron microscopy, transgenic eGFP expression, and ultra-high-resolution spectral domain optical coherence tomography (Otsuka et al., 1966; Silverman et al., 2006; Ono et al., 2009; Pieperhoff et al., 2010; Atkinson et al., 2011; Bordas et al., 2011; Stephenson et al., 2012; De Almeida et al., 2015; Yao et al., 2016), but obtaining the morphometry of the different parameters of CCFs and their junctions have been little investigated. Moreover, studies describing a morphometric profile of CCC, where the parameters of these cells are indicated in detail, represent an even more neglected area.

Our objective is to describe the regional variations of the CCC and their junctions with the cardiomyocytes through comparative histological and morphometric study in pigs and humans, which serves to understand the appearance of ventricular arrhythmias.

2. Materials and methods

2.1. Sampling, staining, and processing

We analyzed five male human hearts obtained from the autopsies of the Institute of Legal Medicine and Forensic Sciences of Bucaramanga, Colombia (adults between 20 and 60 years old and of medium weight, between 60 and 80 kg). Five hearts of male pigs (with average age of 5 months and a weight per animal of 85–90 kg) destined for slaughter were also used for the study. Procedures were in accordance with the Ethics Committee of the Universidad Cooperativa de Colombia (No. 014-2018) and comply with resolution 008430 of 1993, decree 2164 of 1992 and Law 10 of 1990 of the local Ministry of Health and the principles of the Declaration of Helsinki. Additionally, they comply with Law 84 of 1989 with a national scope, corresponding to Chapter VI of the "National Statute for the Protection of Animals", on use of animals in experiments and research.

For histological analysis, the LV of the hearts of both species were dissected and sectioned into three slices: base, middle third, and apex. Each slice was radially sectioned, yielding five samples from the base, five from the middle third and four from the apex and each slice was divided into four regions (anterior, posterior, lateral and septal). Heart samples were fixed with a 5% formaldehyde solution and were labeled for identification and embedded in paraffin. For each region, 5 samples were cut into 5 mm thick slices at the location of CCF. To perform a complete CCF evaluation, the paraffin block that included the fibers was cut according to the following protocol: A 5 μm section was made to obtain the first tissue sample, then the 40 μm sample was devastated and this tissue was removed and subsequently another 5 μm section was made to obtain a new sample and the protocol was continued, until all CCF were sectioned. Histological sections were stained with hematoxylin-eosin and Masson's trichrome.

In addition, a PAS method (periodic acid-Schiff) (CYTEK®) was performed for CCC verification to visualize glycogen accumulations. Immunohistochemical staining was also performed with clone D33-IR606 of Anti-Human Desmin (DAKO Corporation®) dilution 1/90, to visualize the intermediate myofilaments (desmin) present in CCC and compare them with the surrounding cardiomyocytes.

2.2. Image analysis and histological evaluation

Were analyzed 2000 images histological between both species for an exhaustive study of CCF (600 in humans at the subendocardial level and 1400 in pigs at the subendocardial and intramyocardial level), using a Leica DMD108 optical microscope (Leica Microsystems, Wetzlar, Germany). Computerized morphometric study was performed by Image-Pro Plus 7.1 software (Media Cybernetics, Silver Spring, MD, USA). Each sample was evaluated morphometrically and histologically in each of the analyzed fields, comparing all stains performed both conventionally and immunohistochemically.

CCF density was calculated as the area occupied by the fibers compared to the total area of tissue. Each micrograph was calibrated, and manual measurement of CCC area was performed, as well as automatic segmentation of the total tissue area in μm^2 at 20×. Additionally, manual measurement of the thickness of the bundles was performed transversely to 10×. Subsequently we measured area, maximum diameter, minimum diameter, mean diameter, and roundness at an increase of 20× in CCC and cardiomyocytes. To define roundness, a value obtained in the morphometric measurement close to 1 indicates that the cell is rounder and if it moves away from 1, the cell tends to be elongated or irregular in its contour.

We calculated the percentage of CCC showing CFMJ and the distribution of each junction with respect to slice (base, middle third, and apex), region (anterior, lateral, posterior, and septal) and location (subendocardium and myocardium). Presence or absence of CFMJ was also recorded in the micrographs by histological identification.

Additionally, the results obtained were compared among the different species studied, to determine any significant differences between them with respect to CCF density and thickness, CFMJ behavior and the morphometric parameters of CCC and ventricular cardiomyocytes.

2.3. Statistical analysis

Continuous variables (area, thickness, diameter) were expressed as mean and 95% confidence interval, while categorical variables (junction type, slice, region, location) were expressed as a percentage. Was considered to level statistically significant to be $p < 0.05$. Descriptive statistics, graphical representations and hypothesis testing were performed with SPSS 20 software (SPSS, Chicago, IL, USA) and Microsoft Excel 2013. Once the data were obtained, they were statistically analyzed with SPSS program.

Descriptive statistics were calculated for each morphometric parameter and the Kolmogorov-Smirnov normality test was performed for each sample. A chi-square test was used to compare qualitative dichotomy variables, such as presence and type of CFMJ. In case of quantitative variables after normal distribution for groups of regions, the ANOVA test was used, and with differing distribution, the non-parametric Kruskal-Wallis test was chosen; *t*-tests were used in comparisons of the different parameters between humans and pigs. Data were expressed as mean standard deviation (SD) for all measured lengths.

3. Results

3.1. Humans

CCF and CCC were located exclusively in the subendocardium and different stains were used to identify them (Figs. 1, 2, 3). These stains revealed that CCC were slightly paler than the cardiomyocytes due to the low number of myofibrils, with a larger amount of desmin intermediate filaments, so the intensity of the marking was greater. In addition, to enhance CCF identification we performed a PAS method, with which we observed accumulation of glycogen in the entire cytoplasm of CCC, unlike the cardiomyocytes which reacted negatively to staining (Fig. 3a, b). Few myofibrils were observed, and connective tissue sheaths sometimes surrounded the cells, coming came from the central fibrous body and the membranous portion of the interventricular septum (Fig. 1d, e). Cardiomyocytes were oval and dark. In our morphometric analysis, we were able to determine that CCC in humans were larger (18.52 +/− 5.41 μm) than cardiomyocytes (12.35 +/− 1.34 μm) when evaluated in cross section (Table 1). Minimum CCC diameter was larger in the apex than in the base ($p = 0.015$) or in the middle third ($p = 0.048$). In addition, CCC were rounder in the middle third than at the base ($p = 0.017$).

When we observed the mean of the CCF values according to slice, we found no significant differences between them in fiber density. We also observed that CCF were thicker in the middle third than in the apex ($p = 0.046$) (Table 2) (Fig. 4a).

The CFMJ were found in 10% of all micrographs analyzed; these junctions were found in larger quantity in apex than the other two slices ($p < 0.001$) (Table 3). The different types of junctions that we found in humans could be seen divided between the different locations. CCB (7.2%) (Fig. 5a) and CCP (0.9%) (Fig. 5b) were found more frequently in apex ($p < 0.001$) than in the other slices, and CTC (1.9%) (Fig. 5c) were located mainly in the base ($p < 0.001$) (Table 4). In addition, when analyzing the different types of CFMJ in each area subdivision described in our study, CCB were found in larger quantity than other two junctions in all slices, regions and locations studied ($p < 0.001$) (Tables 4, 5). Morphology and distribution of CCC, CCF and their junctions by region are indicated below, considering their location and the slice (Table 5).

3.1.1. Base

In each of the regions that belong to the base, the CCC were oval, with a single nucleus that varied between light and dark. Area, maximum diameter, minimum diameter, and mean diameter were larger in the anterior than posterior region ($p < 0.001$ for each parameter); in the lateral region than the anterior region ($p < 0.001$ for each parameter) or posterior region ($p < 0.001$ for each parameter); in septal region than in posterior region ($p < 0.001$ for each parameter). Area ($p = 0.008$), minimum diameter ($p = 0.040$) and mean diameter ($p = 0.012$) of the CCC were significantly larger in the lateral region than in the septal region. We noted that CCF were commonly organized in long thin bundles composed of approximately 2 to 10 cells sometimes surrounded by connective tissue (Fig. 1b).

No statistically significant differences were found in the percentage

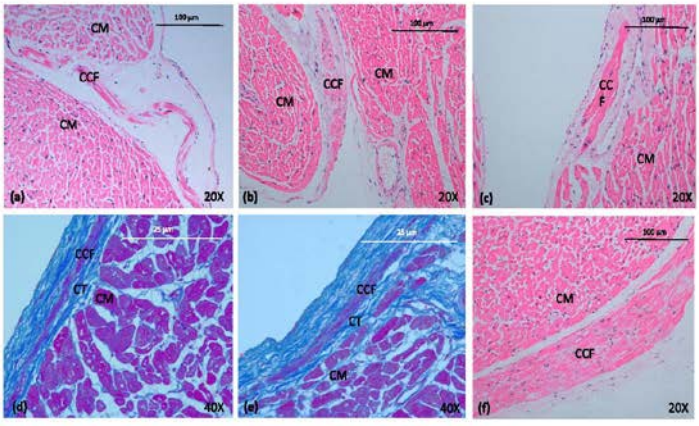

Fig. 1. Human cardiac conduction fibers in subendocardium, stained with hematoxylin-eosin (a–c, f) and Masson's trichrome (d, e). Thin bundles of cardiac conduction fibers, in the lateral region (a), the posterior region (b) and the septal region (c, d, e). Thick bundles of cardiac conduction fibers in the septal region (f). The fibers can be seen at the base (b), in the middle third (a, d–f) and at the apex (c). CCF: cardiac conduction fibers; CM: cardiomyocytes; CT: connective tissue.

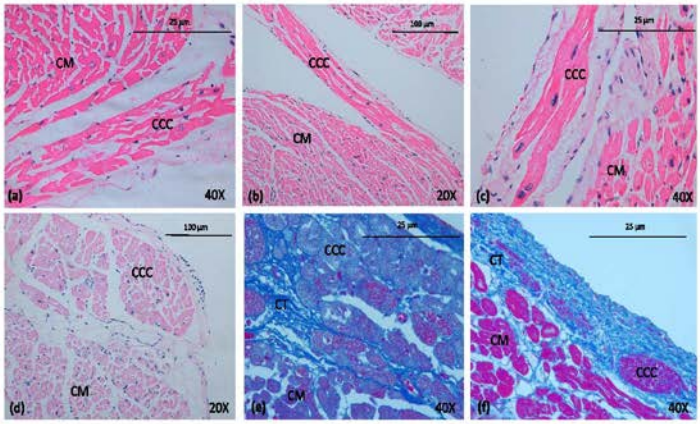

Fig. 2. Morphology of cardiac conduction cells in humans in subendocardium, stained with hematoxylin-eosin (a–d) and Masson's trichrome (e–f). In the lateral region (a) and in the septal region (b, c, d–f). The cells can be seen at the middle third (d–f) and at the apex (a–c). CCC: cardiac conduction cells; CM: cardiomyocytes; CT: connective tissue.

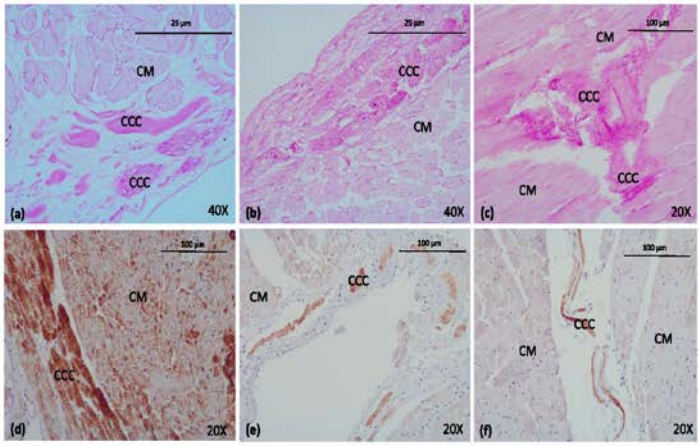

Fig. 3. Identification of cardiac conduction cells by different methods in humans and pigs. PAS method for detecting intracytoplasmic glycogen in humans in the subendocardium, in the anterior region (a) and in the septal region (b). PAS method in pigs in myocardium, in the anterior region (c). Immunohistochemical staining with desmin for identification this intermediate filament in humans in subendocardium, in the septal region (d). Desmin staining in pigs in subendocardium, in the lateral region (e) and myocardium, in lateral region (f). The cells can be seen at the base (a, c, d), and in the middle third (b, e, f). CCC: cardiac conduction cells; CM: cardiomyocytes.

of CFMJ between the different regions of the base.

3.1.2. *Middle third*

In each of the regions that belong to the middle third, the CCC were oval, and we observed a single round, dark centered nucleus. The CCC area in the septal region was larger than in lateral region ($p = 0.049$). Additionally, area ($p = 0.011$), maximum diameter ($p = 0.010$), minimum diameter ($p = 0.039$) and mean diameter ($p = 0.011$) were significantly larger in the septal region than in the posterior region. We found that the CCF formed long thin bundles, composed of 3 to 15 cells without being surrounded by connective tissue (Fig. 1a). In our study we observed a larger presence of CFMJ in the septal region, compared to the other regions ($p = 0.017$).

The thickness and density CCF parameters in the middle third

Table 1
Overall summary of morphometric parameters of cardiac conduction cells and cardiomyocytes in humans and pigs.

Species	Cell	Area (μm^2/SD)	Diameter maximum. (μm/SD)	Diameter minimum. (μm/ SD)	Diameter means. (μm/SD)	Roundness (SD)
Humans	Cardiac conduction cell	480.8 (281.7)	18.52 (5.41)	9.79 (5.42)	14.15 (5.73)	1.12 (0.05)
Pigs		877.1 (411.8)	22.85 (7.45)	12.69 (4.12)	17.95 (5.34)	1.14 (0.06)
Humans	Cardiomyocyte	165.5 (48.5)	12.35 (1.34)	9.37 (2.15)	10.86 (2.04)	1.20 (0.13)
Pigs		281.5 (62.5)	15.28 (2.01)	11.03 (1.34)	13.25 (2.45)	1.14 (0.05)
	Scheme	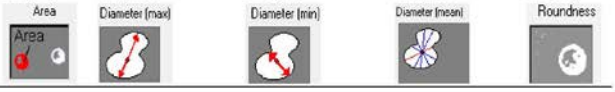				

SD: standard deviation.

Table 2
Mean values of cardiac conduction fiber density and thickness according to slice, region and location in humans and pigs.

		Human		Pig	
		Conduction fiber density (%)	Fascicle Thickness (μm)	Conduction fiber density (%)	Fascicle Thickness (μm)
Slice	Base	16.42	23.41	10.59	23.72
	Middle third	16.98	24.97	11.46	21.95
	Apex	22.75	21.92	11.17	20.76
Region	Posterior	13.97	23.69	11.22	21.57
	Septal	22.59	23.15	11.27	22.36
	Anterior	19.90	23.85	11.07	22.55
	Lateral	13.09	24.29	10.46	22.56
Location	Subendocardium	100	23,79	55.56	19.74
	Myocardium	–	–	42.89	25.51
	Epicardium	–	–	0.32	37.17
	Perivascular	–	–	1.23	21.91

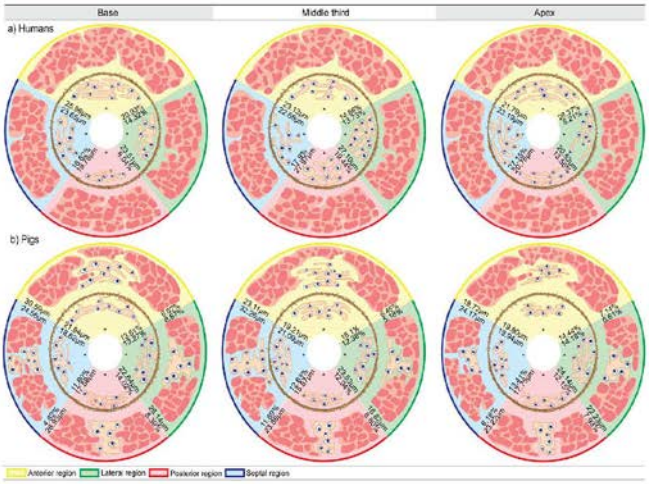

Fig. 4. Subendocardial distribution (*) of cardiac conduction fibers in humans (a). Subendocardial (*) and intramyocardial distribution of cardiac conduction fibers in pigs (b), indicating density (%) and thickness (μm) in each of the slices and regions of the left ventricle.

showed no statistically significant differences between the regions.

3.1.3. Apex

In each of the regions that belong to the apex, the CCC were oval with a round, large and slightly pale nucleus (Fig. 2a, b, c). The CCF formed long and thin bundles of 3 to 15 cells, in longitudinal section and that were not surrounded by connective tissue (Fig. 1b). In the septal region there was higher CCF density than in the lateral region ($p = 0.037$).

In the apex CCC parameters and CCF thickness and junctions showed no statistically significant differences between regions.

Table 3
Percentage of conduction fiber-myocardial junctions by slice, region and location in humans and pigs.

		Humans (%)	Pigs (%)
Slice	Base	7.1	28.5
	Middle third	6.6	24.8
	Apex	21.1	18.2
Region	Posterior	7.9	20.1
	Septal	17.1	26
	Anterior	8.1	25.7
	Lateral	6.8	24.2
Location	Subendocardium	10	6.4
	Myocardium	–	17.5
	Epicardium	–	0.1
	Perivascular level	–	0.2

3.2. Pigs

CCF were mainly identified in the subendocardium and myocardium, although it was occasionally possible to observe them in the epicardium and at the perivascular level, for which different stains were used (Figs. 3, 6, 7). Staining revealed that CCC were paler than cardiomyocytes and thus easier to spot, and that there was higher intensity of labeling due to the large number of intermediate desmin filaments. As an alternate means of identifying CCF, we also used a PAS method, observing a notable accumulation of glycogen in the cytoplasm of these cells, unlike cardiomyocytes where little or no positive staining was detected (Fig. 3c). Few myofibrils could be visualized on the periphery of the cytoplasm of CCC and were sometimes surrounded by connective tissue originating from the central fibrous body and the membranous portion of the interventricular septum (Fig. 7e, f). Cardiomyocytes were dark, round to oval and small when observed in cross-section, and organized into bundles of multiple cells. CCC in pigs were larger (21.32 +/− 6.45 μm) than cardiomyocytes (15.28 +/− 2.01 μm) when evaluated in cross section, as verified by morphometric analysis (Table 1). In analysis of porcine CCC, we found that the area was significantly larger in subendocardium than in myocardium ($p = 0.003$), as was maximum diameter ($p = 0.009$), minimum diameter ($p = 0.005$) and mean diameter ($p = 0.002$). Evaluating the cells in both locations, we observed that area and mean diameter were larger in lateral region than in the anterior region ($p = 0.037$ and $p = 0.042$ respectively). With respect to CCC distribution in subendocardium, we found no significant differences in any parameters analyzed, and in the myocardium these cells occupied a larger area in the lateral than anterior region ($p = 0.049$).

When comparing the measured parameters of CCC in the subendocardium, we found that area ($p = 0.001$), maximum diameter ($p = 0.003$), minimum diameter ($p = 0.001$) and mean diameter ($p = 0.001$) were larger at the base than in the middle third. In addition, the area ($p = 0.039$), minimum diameter ($p = 0.035$) and mean diameter ($p = 0.039$) were significantly larger at the base than at the apex. In the middle third CCC were rounder than at the base ($p = 0.040$). In the myocardium, the area ($p = 0.010$), maximum diameter ($p = 0.017$), minimum diameter ($p = 0.010$) and mean diameter ($p = 0.005$) were significantly larger in the apex than in the middle third.

CCF density was very similar in each slice evaluated (Table 2), and differences were not statistically significant, unlike fiber density evaluated by location, where we found greater abundance of CCF in subendocardium than in myocardium ($p < 0.001$). Furthermore, evaluating distribution at the slice level we determined that CCF thickness was larger at base than apex ($p = 0.001$). Analyzing CCF distribution in different locations, we observed that the fibers were thicker in the myocardium than in subendocardium ($p < 0.001$) (Table 2) (Fig. 4b). In addition, at intramyocardial level we found that the fibers were thicker

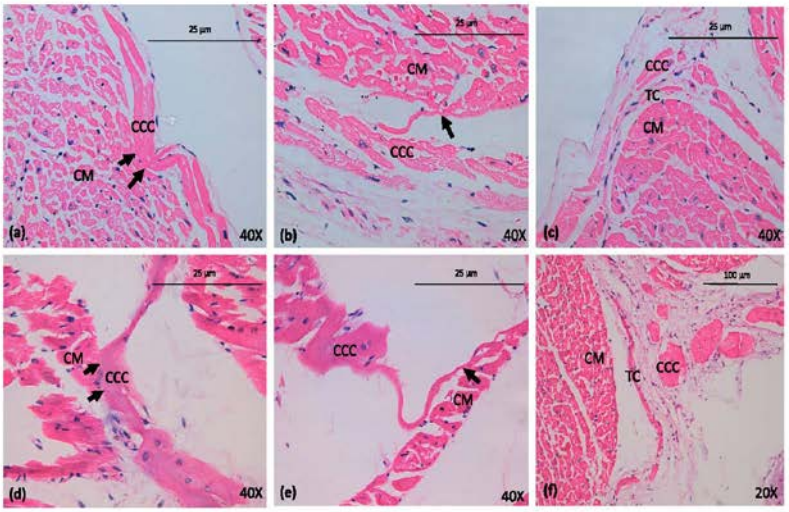

Fig. 5. Different types of conduction fiber-myocardial junctions in humans and pigs, stained with hematoxylin-eosin. The arrows indicate a contact junction through cell bodies (CCB) in subendocardium in humans, in the septal region (a) and in myocardium in pigs, in septal region (d). The arrow shows contact through cellular prolongations (CCP) in subendocardium in humans, in posterior region (b) and in myocardium in pigs, in the posterior region (e). Observe the contact through transitional cardiomyocytes (CTC) in subendocardium in humans, in the posterior region (c) and in subendocardium in pigs, in posterior region (f). The junctions can be seen at the base (b, c, e), and in the apex (a, d, f). CCC: cardiac conduction cells; CM: cardiomyocytes; TC: transitional cardiomyocytes.

Table 4
Distribution of different junction types according to slice, region and location in humans and pigs, with respect to the number of junctions in each division.

		Humans (%)			Pigs (%)		
		CCB	CCP	CTC	CCB	CCP	CTC
Slice	Base	3.5	0.7	2.8	21.7	3.5	3.3
	Middle third	4.6	0.5	1.5	21.1	2.1	1.3
	Apex	17.9	2.1	1.1	16.3	0.8	1.1
Region	Posterior	4.8	1.6	0.2	15.7	3.4	1.1
	Septal	13.3	1.9	0.5	20.4	2.8	2.8
	Anterior	5	0.6	0.9	21.5	1.9	2.4
	Lateral	5.8	–	0.2	21.2	1.2	1.7
Location	Subendocardium	7.2	0.9	1.9	7.8	1	2.7
	Myocardium	–	–	–	35.9	3.8	1.3
	Epicardium	–	–	–	25	–	–
	Perivascular level	–	–	–	6.7	6.7	–

CCB: contact through cell bodies. CCP: contact through cell prolongations. CTC: contact through transitional cardiomyocytes.

at the base ($p = 0.001$) and in the middle third ($p = 0.044$) than at the apex (Fig. 4b).

In pigs, CFMJ were present in 24.2% of all micrographs analyzed, with junctions found more frequently in the base than in the other two slices ($p = 0.002$). Junctions were distributed in a similar way in all the different regions (Tables 3, 4). In addition, we found a larger presence of junctions between CCC and cardiomyocytes at myocardial level than in other locations ($p < 0.001$) (Table 4). CCB (19.9%) (Fig. 5d), CCP (2.3%) (Fig. 5e) and CTC (2.1%) (Fig. 5f) were found more frequently in the base than in other slices analyzed ($p = 0.003$), which is consistent with a larger overall presence of junctions in the base described above. CCB and CCP type junctions were observed in larger quantity in myocardium than in other locations ($p < 0.001$) and CTC was greater in subendocardium ($p < 0.001$) (Table 4). We found more CCB than other types of junctions in all slices, regions and locations described ($p < 0.001$). CCB and CTC were sometimes detected in the same sample when histological and morphometric evaluation was performed. Morphology and distribution of CCC, CCF and their junctions by region are indicated below, considering their location and the slice (Table 6).

Table 5
Subendocardial distribution of cardiac conduction cells, cardiac conduction fibers, and conduction fiber-myocardial junctions by slice and region in humans.

Slice	Region	CCC diameter (μm/SD)	CCF density (%)	CCF thickness (μm/SD)	CFMJ			
					Total (%)	CCB (%)	CCP (%)	CTC (%)
Base	Anterior	17.59 (9.24)	20.93	25.96 (9.04)	3.4	–	–	3.4
	Lateral	22.80 (7.95)	14.32	23.51 (8.73)	13.8	10.4	–	3.4
	Posterior	10.17 (6.12)	6.04	19.78 (6.98)	15	5	5	5
	Septal	19.71 (8.47)	16.62	23.65 (8.34)	2.9	2.9	–	–
Middle third	Anterior	17.81 (9.27)	14.66	23.12 (10.80)	4.4	1.5	–	2.9
	Lateral	15.96 (7.36)	13.73	27.10 (15.09)	3.4	3.4	–	–
	Posterior	14.01 (6.25)	19.44	27.97 (10.76)	3.3	3.3	–	–
	Septal	19.68 (9.87)	17.90	22.68 (7.28)	17.9	12.8	2.6	2.6
Apex	Anterior	20.08 (9.16)	28.37	21.79 (5.65)	22.9	20	–	2.9
	Lateral	16.13 (8.73)	8.21	20.53 (12.04)	6.7	6.7	–	–
	Posterior	20.26 (9.93)	13.56	20.78 (7.68)	7.7	7.7	–	–
	Septal	16.07 (6.45)	27.15	23.19 (6.39)	31.2	25	3.1	3.1

CCC: cardiac conduction cells. CCF: cardiac conduction fibers. CFMJ: conduction fiber-myocardial junction. CCB: contact through cell bodies. CCP: contact through cell prolongations. CTC: contact through transitional cardiomyocytes. SD: standard deviation.

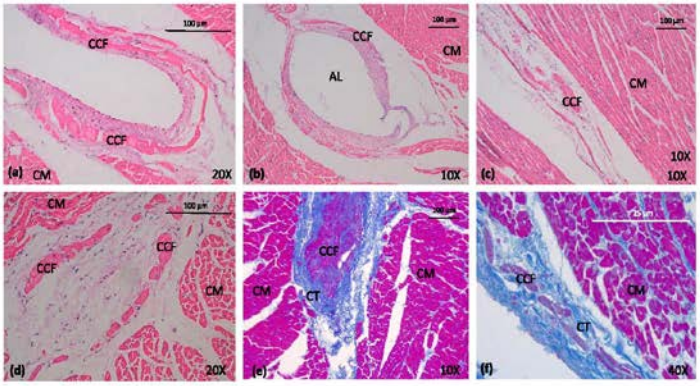

Fig. 6. Cardiac conduction fibers of pigs in different locations, stained with hematoxylin-eosin (a–d) and Masson's trichrome (e–f). Cardiac conduction fibers at the subendocardial level, in the lateral region (a) and in the anterior region (f). Cardiac conduction fibers at the perivascular level, in the posterior region (b). Cardiac conduction fibers at the intramyocardial level, in the lateral region (c) and in the anterior region (d, e). The fibers can be seen at the base (a, c, e, f), in the middle third (d) and at the apex (b). CCF: cardiac conduction fibers; CM: cardiomyocytes; CT: connective tissue. AL: artery light.

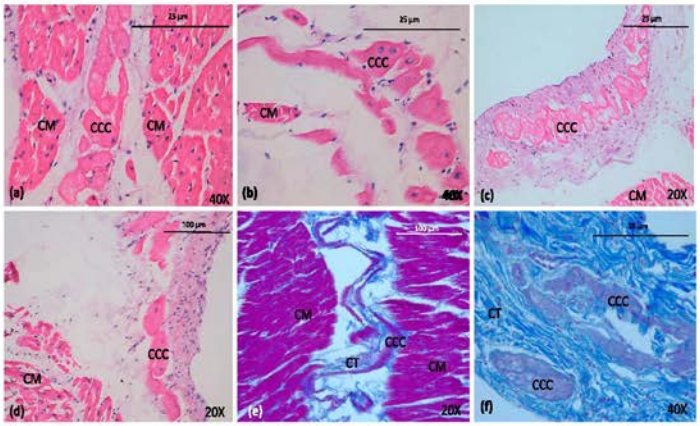

Fig. 7. Morphology of cardiac conduction cells in pigs, stained with hematoxylin-eosin (a–d) and Masson's trichrome (e–f). Cardiac conduction cells in myocardium, in the anterior region (a, e) and in the lateral region (b). Cardiac conduction cells in subendocardium, in the lateral region (c), in the posterior region (d) and in the anterior region (f). The cells can be seen at the base (c–f), and in the apex (a, b). CCC: cardiac conduction cells; CM: cardiomyocytes; CT: connective tissue.

3.2.1. Base

In each of the regions that belong to the base in the subendocardium, CCC were oval, and with a single slightly pale, round, and centered nucleus (Fig. 7c, f). We observed that the minimum diameter and mean diameter of the CCC was significantly larger in the lateral region ($p = 0.030$ and $p = 0.028$ respectively) and posterior region ($p = 0.001$ and $p = 0.011$ respectively) than in the septal region. CCF were typically organized in long and thin bundles (Fig. 6a, f) composed of approximately 2 to 15 cells surrounded by connective tissue. Sometimes the fibers were formed by individual cells creating a linear appearance. CCF were thicker in the anterior region ($p = 0.004$) and lateral region ($p = 0.005$) than in the posterior region. In the myocardium, CCC were oval, and with rounded, centered and slightly pale nuclei. CCF were elongated, thin and clusters of 3 to 15 cells were observed. CCF were generally observed in the longitudinal section, surrounded by connective tissue.

No statistically significant differences were found in CCF density, the general percentage of junctions or the specific type of junctions in the subendocardium and myocardium by region. In addition, there were no significant differences in CCF thickness in the myocardium by region.

Table 6
Distribution of cardiac conduction cells, cardiac conduction fibers, and conduction fiber-myocardial junctions by slice, location, and region in pigs.

Slice	Location	Region	CCC diameter (µm/SD)	CCF density (%)	CCF thickness (µm/SD)	CFMJ			
						Total (%)	CCB (%)	CCP (%)	CTC (%)
Base	Sub endocardium	Anterior	20.13 (6.45)	13.6	21.94 (7.92)	15.5	8.3	1	6.2
		Lateral	21.05 (7.34)	13.27	22.64 (10.34)	8.3	8.3	–	–
		Posterior	15.42 (5.14)	14.02	17.58 (3.78)	7	5.2	–	1.8
		Septal	17.53 (6.28)	11.80	18.62 (7.14)	18.4	8.2	4.1	6.1
	Myocardium	Anterior	23.91 (9.47)	6.02	30.59 (15.23)	54.9	46.5	4.2	4.2
		Lateral	25.20 (10.12)	8.67	26.14 (18.16)	42.2	37.5	3.1	1.6
		Posterior	26.55 (9.86)	8.39	26.93 (14.88)	37	24.1	11.1	1.8
		Septal	18.80 (7.37)	4.82	24.56 (18.30)	53.1	43.8	6.2	3.1
Middle third	Sub endocardium	Anterior	18.67 (7.62)	16.1	19.21 (8.37)	16.1	12.9	1.6	1.6
		Lateral	21.62 (8.90)	12.38	23.53 (6.26)	8.2	4.1	–	4.1
		Posterior	14.15 (6.92)	12.94	15.87 (8.19)	8.8	8.8	–	–
		Septal	18.24 (7.46)	12.63	21.09 (8.81)	18.1	12.5	2.8	2.8
	Myocardium	Anterior	16.49 (5.21)	6.45	23.11 (14.46)	38	35.2	2.8	–
		Lateral	16.03 (5.17)	5.18	16.82 (11.18)	37.5	37.5	–	–
		Posterior	22.75 (9.63)	8.80	23.88 (14.74)	41.7	36.1	5.6	–
		Septal	28.48 (12.43)	11.69	32.26 (13.98)	43.3	40	3.3	–
Apex	Sub endocardium	Anterior	19.12 (9.57)	14.44	19.80 (7.58)	11.5	11.5	–	–
		Lateral	23.62 (11.21)	14.18	24.14 (10.90)	7.2	3.6	–	3.6
		Posterior	16.94 (7.83)	12.15	17.75 (6.54)	1.9	–	–	1.9
		Septal	18.69 (8.45)	13.41	19.94 (6.45)	8.6	5.8	1.4	1.4
	Myocardium	Anterior	19.07 (8.53)	7.14	19.72 (10.42)	20.4	18.5	1.9	–
		Lateral	21.76 (10.62)	6.61	22.23 (10.71)	42.9	40	2.9	–
		Posterior	22.47 (11.49)	7.93	23.22 (9.76)	33.3	33.3	–	–
		Septal	23.92 (12.14)	8.18	24.17 (12.01)	48.4	45.2	–	3.2

CCC: cardiac conduction cells. CCF: cardiac conduction fibers. CFMJ: conduction fiber-myocardial junction. CCB: contact through cell bodies. CCP: contact through cell prolongations. CTC: contact through transitional cardiomyocytes.

3.2.2. Middle third

In each of the regions that belong to the middle third in the subendocardium, CCC were round, and with a centered, round, large and dark nucleus. CCC in the anterior region ($p = 0.006$), lateral region ($p = 0.047$) and septal region ($p = 0.001$) were rounder than in the posterior region. CCF formed long, thin bundles of 2–10 cells, surrounded by connective tissue. CCF was significantly thicker in the septal region than in the posterior region ($p = 0.001$) or the lateral region ($p = 0.004$). In the myocardium, CCC were oval with a single large, round, slightly pale centered nucleus. Area ($p = 0.028$), maximum diameter ($p = 0.007$), minimum diameter ($p = 0.025$) and mean diameter ($p = 0.022$) of CCC were significantly larger in the septal region than in the posterior region. Additionally, the maximum diameter and mean diameter of these cells were larger in the septal region than in the anterior region ($p = 0.011$ and $p = 0.020$ respectively) and in the lateral region ($p = 0.010$ and $p = 0.022$ respectively). CCF were elongated, and thick composed of 3 to 10 cells (Fig. 6d) and surrounded by connective tissue. We found that the density and thickness of the CCF were significantly higher in the septal region than in the anterior region ($p = 0.018$ and $p = 0.026$ respectively).

We found no significant differences in the percentage of CCF at the subendocardial level by region. Neither were differences found between the junctions and type of junctions in the subendocardium and myocardium by region.

3.2.3. Apex

In each of the regions that belong to the apex in the subendocardium, CCC were oval with large, round, centered dark nuclei. Minimum CCC diameter was significantly larger in the posterior region than in the anterior region ($p = 0.046$). CCF were organized into long thin and thick bundles, made up of 3 to 15 cells and surrounded by scarce connective tissue. CCF were thicker in the lateral region than in the posterior region ($p = 0.002$). In the myocardium, CCC were oval with large, round, slightly pale, centered nuclei (Fig. 7a, b). We noted that CCF could vary between long thin bundles and long thick bundles, with clusters of 2 to 25 cells, surrounded by connective tissue and generally in the longitudinal section. We observed greater abundance of CFMJ in the septal region than in the other regions ($p = 0.036$).

In the subendocardium no statistically significant differences between slices or regions were observed in CCF density, number of junctions or CFMJ. In the myocardium no statistical significance was found in the parameters measured in CCC, CCF thickness and CFMJ type between slices or regions.

Comparing different measured CCC parameters between the two species, we found that area, minimum and mean diameters were significantly larger in pigs than in humans ($p < 0.001$ for all values), as was maximum diameter ($p = 0.031$). In addition, the maximum diameter of cardiomyocytes was larger in pigs than in humans ($p = 0.001$) (Table 1). Turning to CCF in humans and pigs in our study, we found a higher density of fibers in humans than in pigs ($p < 0.001$) but observed similar thickness values. The distribution of CCF and CCC was observed more frequently in the septal region and in the subendocardium of the two species studied (Fig. 4a, b).

When comparing the number of junctions present between the species, we were able to observe more junctions in pigs than in humans ($p < 0.001$). Similarly, the most abundant CFMJ type was CCB in both species, with more abundance in pigs than in humans ($p < 0.001$).

4. Discussion

CCC propagate an electrical impulse from one cell to another and to working cardiomyocytes in a coordinated manner throughout the LV, enabling heart muscle contraction. Insight into the specific characteristics of these cells from a morphometric perspective in the different regions of the LV is essential to understand the behavior of these cells in the normal heart, as well as in different cardiac pathologies such as myocardial infarction and cardiac arrhythmias. By studying 2000 micrographs, we show the differential aspects of these cells in the different LV regions.

CCC have previously been characterized in humans as having a pale appearance with few myofibrils and as individually surrounded by a sheath of connective tissue rather than in the form of bundles found in other species (Tawara, 1906; Shimada et al., 1983; Tawara, 2000; Ono et al., 2009; Yoshimura et al., 2014). This description of CCC was consistent with our study, but these cells were rarely arranged individually; on the contrary, they were organized mainly into small thin bundles of 2–10 cells, partially surrounded by connective tissue and with a similar appearance to cardiomyocytes, which made them difficult to recognize. At the subendocardial level, CCC in humans have been described as cylindrical or fusiform and larger (20–40 μm) than ventricular cardiomyocytes (around 10 μm) (Ono et al., 2009; Yoshimura et al., 2014); these data were larger than our findings, and the cardiomyocytes were slightly larger.

The pale appearance of CCC, mainly in ungulates but observed also in other species, has been attributed to the low presence of myofibrils and high amount of glycogen in their cytoplasm, which is typical of conduction cells (Tawara, 1906; (Sommer and Johnson, 1968) Tranum-Jensen et al., 1991; Tawara, 2000; Eliška, 2006). The PAS method for identifying CCC with large amounts of glycogen observed in its cytoplasm has been used efficiently in ungulates, although some studies have reported that in other species, including humans, these cells are not clearly identified by this method (Eliška, 2006; Ono et al., 2009). Another study suggests that the amount of glycogen present in CCC compared to cardiomyocytes is not entirely reliable as a safe differential criterion (Sommer and Johnson, 1968). In our study CCC identification by PAS method was found to be a good tool for this purpose in humans and pigs, unlike previous reports that the method was of little value for identifying CCC. Glycogen was observed throughout the cytoplasm of the studied CCC and in the cardiomyocytes no positivity was seen, which emits good differentiation between the two cells. It has been reported that in group II, such as in humans, CCC have great positivity to desmin (originally also called skeletin) compared with cardiomyocytes, and in animal species belonging to group I, such as ungulates, a strong positive reaction to desmin by CCC has also been observed (Eriksson et al., 1979; Yoshimura et al., 2014). It has also been indicated that intermediate filaments were abundant in CCC of birds and large mammals (Canale et al., 1986) and cell differentiation with cardiomyocytes is possible using desmin as a marker (Eriksson et al., 1979) Forsgren et al., 1982). In our study, we found a high positivity of CCC to desmin in humans and cardiomyocytes reacted positively but with less intensity. In pigs, desmin was distributed throughout CCC cytoplasm in both subendocardium and myocardium, showing strong positivity compared to cardiomyocytes, which reacted only slightly to staining. In this way, our research is consistent with results of previous studies and shows that CCC have many intermediate filaments in humans and pigs.

In pigs, CCF have been described as surrounded by sheaths of reticular fibers that form bundles composed of 2–8 oval CCC; these cells were identified by pale cell bodies, with one or two nuclei and few peripherally located myofibrils (Tawara, 1906; Glomset and Glomset, 1940; Tawara, 2000; Ono et al., 2009; Yoshimura et al., 2014). In our study CCF also presented sheaths of connective tissue surrounding the fibers but partially and forming bundles with more cells than had been described. Likewise, the cellular characteristics are concurrent with our study, in that CCC were larger than the cardiomyocytes and very easy to identify.

Histologically, the cardiac conduction network is described as formed of electrically isolated subendocardial fibers that comprise specialized cells with fewer myofibrils and mitochondria than ventricular myocardiocytes, showing high levels of connexins (Cx40), Na + channels and other proteins associated with rapid impulse transmission (Moorman and Christoffels, 2003; Gianni et al., 2018). In our study, we determined that CCF were thicker between the base and the middle third

in humans and in the base and myocardium in pigs. This is logical because these fibers originate from the atrioventricular fascicle in the upper part of the ventricles, and this is also where they receive the electrical impulse. Subsequently they are distributed in the large musculature present in the middle third and are directed towards the distal part of the heart, finally ascending to the free edge of the ventricles, and enabling depolarization and contraction of the heart muscle. We also observed in pigs higher CCF density in the subendocardium and greater fiber thickness in the myocardium in all the slices and regions. This indicates, the high transmission of the cardiac impulse through the subendocardium to be sent to the myocardium, achieving rapid depolarization of the ventricular cardiac fibers. However, these fibers also play an important role in generating ventricular arrhythmias (Li et al., 2015; Aouadi et al., 2019), Thus bestowing importance on the study of CCF characteristics, to identify the ventricular arrhythmias that affect the CCF. VT and VF may be present in humans and animals with ischemic or completely normal heart disease (Tabereaux et al., 2009; Benito and Josephson, 2012; Krishnamoorthy et al., 2015; Gianni et al., 2018).

It has been indicated that the site of reentry in VT after myocardial infarction, was located mainly in the anteroseptal and inferolateral basal regions of the LV in humans (Oh et al., 2018). In addition, this arrhythmia is generated in the subendocardic cardiac conduction network (Benito and Josephson, 2012). It has also been shown that Cx40 and Cx45 levels in septal subendocardium in humans are drastically decreased in arrhythmogenic right ventricular cardiomyopathy (Paul et al., 2013). Partially coinciding with these reports, our observations indicated that in humans, CCF are mainly found in the septal and anterior region in all the slices analyzed (base, middle third, and apex). In pigs, these fibers were distributed similarly between regions and slices at the subendocardial level, but in the myocardium, they were generally found in the septal region, especially in the middle third and apex. CCF were thicker in the anterior and septal region in humans, while in pigs CCF were thicker in the septal region, both in the subendocardium and in the myocardium. Analyzing data obtained in our study and from previous studies related to heart conditions, we have discerned that the main point of origin of ventricular arrhythmias is the septal region of the heart. This may be because this region is where the impulse from the AV conduction system is received and where there is a larger quantity of fibers, as it is surrounded by the subendocardium. Some idiopathic VF have been associated with inducible repetitive activity in the cardiac conduction peripheral system, regardless of whether the ectopic focus is present or not (Haïssaguerre et al., 2019).

Gap junctions act as membranes of low resistance for electrical impulses to propagate, allowing ions and small molecules to pass through them (Bruzzone et al., 1996; Gros and Jongsma, 1996; Vozzi et al., 1999). These junctions are responsible for electrical coupling in the heart and perform it through transmembrane channels composed of connexins (Gros and Jongsma, 1996; Vozzi et al., 1999). These connexins are distributed throughout the heart and three types of these proteins have been identified in cardiac structure. In mammals Cx45 is frequently expressed in the sinoatrial and atrioventricular nodes, the atrioventricular fascicle and less frequently in CCF. Cx43 is the connexin found in the junctions between cardiomyocytes, at both atrial and ventricular levels. CCF junctions are formed by Cx40 expression (Gros and Jongsma, 1996; Vozzi et al., 1999; Severs et al., 2008).

In humans, the spatial distribution of CFMJ has been described and they were found to be located particularly at the base (Myerburg et al., 1975). In our study, these junctions were mainly located at the heart apex in humans and at the base in pigs, and when analyzing junctions by region according to slice and location, CFMJ were located mainly in the septal region. They presented the same distribution as CCF in both species, and high density of this region could therefore pinpoint it as the main site of ventricular arrhythmia generation. Previous reports indicate the importance of transitional cardiomyocytes (TC) in the transmission of electrical impulse through CFMJ in humans (Alanís and Benítez, 1970; Mendez et al., 1970; Rawling and Joyner, 1987). The presence of these cells between CCC and cardiomyocytes ensures high coupling and rapid conduction in the myocardium (Tranum-Jensen et al., 1991; Eliška, 2006), although a more recent study indicated that TC were not present in junctions of human and bovine hearts (Eliška, 2006). In our research we detected this type of junction in CTC located mainly in the cardiac base in small percentages.

In a series of samples evaluated in some ungulate species (cattle and sheep), CFMJ was found in 15% (Pieperhoff et al., 2010). In pigs, we observed the presence of these junctions in a higher percentage and located mainly in the base and myocardium, although previous studies indicate that CFMJ only occur in the distal part of the heart (Vigmond and Stuyvers, 2016). In our study, we determined that these junctions were distributed along the ventricular surface. As previously indicated, in pigs some CCF spread across from subendocardium to epicardium and their CFMJ behaved in the same way, which could explain why transmural activation is almost instantaneous in this species (Meijborg et al., 2014; Vigmond and Stuyvers, 2016). Presence in CFMJ of TC, which regulate faster transmission of the electrical impulse, has been well documented in pigs (Tranum-Jensen et al., 1991; Eliška, 2006), this was verified in our study where we found this type of junction (CTC) regulated by TC. We observed that the highest percentage of CFMJ in humans and pigs was through the CCB junctions in all regions analyzed.

5. Conclusions

By studying cardiac conduction fibers and cells and their myocardial junctions we can determine and document their normal distribution in each of the species analyzed.

CCF were distributed mainly in septal region in humans and pigs. These fibers were thicker between the base and the middle third in humans and in the base and myocardium in pigs In addition, CFMJ were found in larger quantities in the apex and septal region in humans and in the base and septal region in pigs.

The use of alternative stains such as desmin, and the PAS method, which enable precise CCC identification, are recommended in studies that include these cells.

This research greatly contributed to the generation of new knowledge of the cardiac conduction system in humans and pigs.

Sources of funding

This work was supported by a "Instituto de Salud Carlos III" grant and co-funded by "FEDER (grant numbers PI14/00271, pie15/00013) and by the "Generalitat Valenciana" (grant number PROMETEO2013/007).

Declaration of competing interest

The authors declare that they have no conflicts of interest.

Acknowledgements

We are indebted to the Institute of Legal Medicine and Forensic Sciences and to Vijagual Refrigerating Plant in the city of Bucaramanga, Colombia for the donation of specimens studied in this research. H.Y.E.V would like to acknowledge COLCIENCIAS, scholarship program 756 (2016).

References

Alanís, J., Benítez, D., 1970. Rate of rise of Purkinje and transitional cells action potential and the propagation across the Purkinje myocardium junction. Jpn. J. Physiol. 20, 217–232.

Aouadi, S., Mbarki, W., Zemzemi, N., 2019. Towards the modeling of the Purkinje/myocardium coupled problem: a well-posedness analysis. J. Comput. Appl. Math. 351, 136–152.

Atkinson, A., Inada, S., Li, J., Tellez, J.O., Yanni, J., Sleiman, R., Allah, E.A., Anderson, R. H., Zhang, H., Boyett, M.R., Dobrzynski, H., 2011. Anatomical and molecular mapping of the left and right ventricular His-Purkinje conduction networks. J. Mol. Cell. Cardiol. 51, 689–701.
Benito, B., Josephson, M.E., 2012. Ventricular tachycardia in coronary artery disease. Rev. Esp. Cardiol. 65, 939–955.
Bordas, R., Gillow, K., Lou, Q., Efimov, I.R., Gavaghan, D., Kohl, P., Grau, V., Rodriguez, B., 2011. Rabbit-specific ventricular model of cardiac electrophysiological function including specialized conduction system. Prog. Biophys. Mol. Biol. 107, 90–100.
Bruzzone, R., White, T.W., Paul, D.L., 1996. Connections with connexins: the molecular basis of direct inter cellular signalling. Eur. J. Biochem. 238, 1–27.
Canale, E., Campbell, G., Smolich, J., 1986. Cardiac Muscle: The Conduction System. Springer-Verlag, Berlin, Heidelberg, New York, Tokio.
Cherry, E.M., Fenton, F.H., Gilmour Jr., R.F., 2012. Mechanisms of ventricular arrhythmias: a dynamical systems-based perspective. Am. J. Physiol. Heart Circ. Physiol. 302, H2451–H2463.
De Almeida, M.C., Lopes, F., Fontes, F., Barra, F., Guimaraes, R., Vilhena, V., 2015. Ungulates heart model: a study of the Purkinje network using India ink injection, transparent specimens and computer tomography. Anat. Sci. Int. 90, 246–250.
Eliška, O., 2006. Purkinje fibers of the heart conduction system - history and the present time. Cas. Lek. Cesk. 145, 329–335.
Eriksson, A., Thornell, L.E., Stigbrand, T., 1979. Skeletin immunoreactivity in heart Purkinje fibers from several species. J. Histochem. Cytochem. 27, 1604–1609.
Forsgren, S., Eriksson, A., Kjörell, U., Thornell, L.E., 1982. The conduction system in the human heart at midgestation – immunohistochemical demonstration of the intermediate filament protein skeletin. Histochemistry. 74, 43–52.
Gianni, C., Burkhardt, J.D., Trivedi, C., Mohanty, S., Natale, A., 2018. The role of the Purkinje network in premature ventricular complex-triggered ventricular fibrillation. J. Interv. Card. Electrophysiol. 52, 375–383.
Gloomet J, D, Clomset T, A, 1940. A Morphologic study of the cardiac conduction system in ungulates, dog and man. Part II: the Purkinje system. Am. Heart. J. 20, 677–701. https://doi.org/10.1016/S0002-8703(40)90530-0. In this issue.
Gros, D.B., Jongsma, H.J., 1996. Connexins in mammalian heart function. BioEssays. 18, 719–730.
Haissaguerre, M., Cheniti, G., Escande, W., Zhao, A., Hocini, M., Bernus, O., 2019. Idiopathic ventricular fibrillation with repetitive activity inducible within the distal Purkinje system. Heart Rhythm. 16, 1268–1272.
He, B.J., Boyden, P., Scheinman, M., 2018. Ventricular arrhythmias involving the his-Purkinje system in the structurally abnormal heart. Pacing Clin. Electrophysiol. 41, 1031–1035.
Krishnamoorthy, J., Laishmanan, A., Mullasari, A., 2015. Focal Purkinje ventricular tachycardia ablation in structurally normal heart. Asian. Cardiovasc. Thorac. Ann. 23, 855–857.
Li, J., Logantha, S.J., Yanni, J., Cai, X., Dobrzynski, H., Hart, G., Boyett, M.R., 2015. From the Purkinje fibers to the ventricle: one dimensional computer simulation for the healthy and failing heart. Conf. Proc. IEEE. Eng. Med. Biol. Soc. 2015, 34–37.
Meijborg, V.M.F., Conrath, C.E., Opthof, T., Belterman, C.N.W., de Bakker, J.M.T., Coronel, R., 2014. Electrocardiographic T wave and its relation with ventricular repolarization along major anatomical axes. Circ. Arrhythm. Electrophysiol. 7, 524–531.
Mendez, C., Mueller, W.J., Urquiaga, X., 1970. Propagation of impulses across the Purkinje fiber-muscle junctions in the dog heart. Circ. Res. 26, 135–150.
Moorman, A.F.M., Christoffels, V.M., 2003. Cardiac chamber formation: development, genes, and evolution. Physiol. Rev. 83, 1223–1267.
Myerburg, R.J., Hilsson, K., Castellanos, A., 1975. The intraventricular conducting system and patterns of endocardial excitation. Adv. Cardiol. 14, 2–14.
Oh, I.Y., Cha, M.J., Lee, T.H., Seo, J.W., Oh, S., 2018. Unsolved questions on the anatomy of the ventricular conduction system. Korean. Circ. J. 48, 1081–1096.
Ono, N., Yamaguchi, T., Ishikawa, H., Arakawa, M., Takahashi, H., Saikawa, T., Shimada, T., 2009. Morphological varieties of the Purkinje fiber network in mammalian hearts, as revealed by light and electron microscopy. Arch. Histol. Cytol. 72, 139–149.
Oosthoek, P.W., Virágh, S., Lamers, W.H., Moorman, A.F., 1993. Immunohistochemical delineation of the conduction system II: the atrioventricular node and Purkinje fibers. Circ. Res. 73, 482–491.
Otsuka, N., Hara, T., Kacuoka, A., 1966. Experimentelle untersuchungen der PAS-reaktion zur darstellung des reizleitungs systems am hundehrzen. Acta. Acat. Nippon. 41, 1–6.
Peal, M., Wichter, M.D., Gerss, J., Arps, V., Schulze-Bahr, E., Robenek, H., Breithardt, G., Weissen-Plenz, G., 2013. Connexin expression patterns in arrhythmogenic right ventricular cardiomyopathy. Am. J. Cardiol. 15, 1488–1495.
Pieperhoff, S., Barmann, C., Grand, C., Barth, M., Rizzo, S., Franke, W.W., 2010. The area composita of adhering junctions connecting heart muscle cells of vertebrates VII. The different types of lateral junctions between the special cardiomyocytes of the conduction system of ovine and bovine hearts. Eur. J. Cell Biol. 89, 365–378.
Rawling, D.A., Joyner, R.W., 1987. Characteristics of junctional regions between Purkinje and ventricular muscle cells of canine ventricular subendocardium. Circ. Res. 4, 580–585.
Sedmera, D., Gourdie, R.G., 2014. Why do we have Purkinje fibers deep in our heart? Physiol. Res. 63 (Suppl. 1), S9–S18.
Severs, N.J., Coppen, S.R., Dupont, E., Yeh, H.I., Ko, Y.S., Matsushita, T., 2004. Gap junction alterations in human cardiac disease. Cardiovasc. Res. 62, 368–377.
Severs, N.J., Bruce, A.F., Dupont, E., Rothery, S., 2008. Remodelling of gap junctions and connexin expression in diseased myocardium. Cardiovasc. Res. 80, 9–19.
Shimada, T., Nakamura, M., Kitahara, Y., Sachi, M., 1983. Surface morphology of chemically-digested Purkinje fibers of the goat heart. J. Electron Microsc. 32, 187–196.
Silverman, M., Grove, D., Upshaw Jr., C.B., 2006. Why does the heart beat? The discovery of the electrical system of the heart. Circulation 113, 2775–2781.
Sommer, J.R., Johnson, E.R., 1968. Cardiac muscle. A Comparative Study of Purkinje Fibers and Ventricular Fibers. J. Cell. Biol. 36, 497–526.
Stephenson, R., Boyett, M., Hart, G., Nikolaidou, T., Cai, X., Corno, A.F., Alphonso, N., Jeffery, N., Jarvis, J.C., 2012. Contrast enhanced micro-computed tomography resolves the 3-dimensional morphology of the cardiac conduction system in mammalian hearts. PLoS One 7, e35299.
Stevenson, W.G., Soejima, K., 2007. Catheter ablation for ventricular tachycardia. Circulation 115, 2750–2760.
Tabereaux, P.B., Dosdall, D.J., Ideker, R.E., 2009. Mechanisms of VF maintenance: wandering wavelets, mother rotors, or foci. Heart Rhythm. 6, 405–415.
Tawara, S., 1906. Das Reizleitungssystem des Säugetierherzens: eine anatomisch-histologische Studie über das Atrioventrikularbündel und die Purkinjeschen Fäden. Gustavav Fischer, Jena, Marburg.
Tawara, S., 2000. The Conduction System of the Mammalian Heart. Imperial College Press, London.
Tranum-Jensen, J., Wilde, A.A.M., Vermeulen, J.T., Janse, M.J., 1991. Morphology of electrophysiologically identified junctions between Purkinje fibers and ventricular muscle in rabbit and pig hearts. Circ. Res. 69, 429–437.
Vigmond, E.J., Stuyvers, B.D., 2016. Modeling our understanding of the Ifi-Purkinje system. Prog. Biophys. Mol. Biol. 120, 179–188.
Vozzi, C., Dupont, E., Coppen, S.R., Yeh, H.I., Severs, N.J., 1999. Chamber-related differences in connexin expression in the human heart. J. Mol. Cell. Cardiol. 31, 991–1003.
Yao, X., Gan, Y., Marboe, C.C., Hendon, C.P., 2016. Myocardial imaging using ultrahigh-resolution spectral domain optical coherence tomography. J. Biomed. Opt. 21, 61006.
Yoshimura, A., Yamaguchi, T., Kawazato, H., Takahashi, H., Shimada, T., 2014. Immunohistochemistry and three-dimensional architecture of the intermediate filaments in Purkinje cells in mammalian hearts. Med. Mol. Morphol. 47, 233–239.

J. OTROS ARTICULOS Y COMUNICACIONES PUBLICADAS A PARTIR DEL PROCESO DE INVESTIGACIÓN

Research in Veterinary Science 126 (2019) 22–28

Contents lists available at ScienceDirect

Research in Veterinary Science

journal homepage: www.elsevier.com/locate/rvsc

Histological and morphometric study of the components of the sinus and atrioventricular nodes in horses and dogs

F.A. Gómez-Torres[a,b], L.E. Ballesteros-Acuña[b], A. Ruíz-Sauri[a,c,*]

[a] Department of Pathology, Faculty of Medicine, Universitat de Valencia, 1 floor, Av. de Blasco Ibáñez, 15, 46010 Valencia, Spain
[b] Department of Basic Sciences, Medicine School, Universidad Industrial de Santander, Cra 32 # 29-31, 680012 Bucaramanga, Colombia
[c] INCLIVA Biomedical Research Institute, Av. de Blasco Ibáñez, 17, 46010 Valencia, Spain

ARTICLE INFO

Keywords:
Atrioventricular node
Morphometry
P cells
Sinus node
T cells

ABSTRACT

The cardiac nodes are the source of the electrical impulse that is transmitted to the heart, the aim of this work is study the histological and morphometric characteristics of the different components of the sinus and atrioventricular nodes in horses and dogs that help to know the physiopathology of these nodes.

A group of ten horse hearts and five dog hearts were used. The region of the sinus and atrioventricular nodes was sectioned serially, and the block of tissue removed for study. The samples were assessed using a morphometric analysis with the Image-Pro Plus 7.1 software and the acquisition of the images using a Leica DMD108 optic microscope.

The shape of the horse's sinus node is oblong and its P cells are large. The shape of the dog's sinus is rounded or oblong. The P cells are large and pale. The area of P cells in horses was 976 (SD 223.7) μm^2 and in dogs the area for P cells was 106 (SD 30.4) μm^2, which indicates that the value for P cells in horses are significantly higher than in dogs ($p = .001$). The horse atrioventricular node presented an oblong shape and in dogs, presents a spindle shape. The lower cell density in any of the cardiac nodes, especially in P cells of sinus node, can decrease electrical conduction within the nodes and in the internodal tracts, which would reflect the presence of cardiac arrhythmias derived from poor conduction, even in morphologically normal hearts.

1. Introduction

The first descriptions of the cardiac conduction system were performed on the hearts of sheep, dogs and cattle; since then, the histology of the conduction pathway has been described in numerous studies (Keith and Flack, 1907; Glomset and Glomset, 1940; James et al., 1966), but little research has been done to date regarding the morphometric study of these structures, both in humans or animals.

Near the junction of the cranial vena cava with the right atrium, the sinus node (SN) lies directly beneath the sulcus terminalis. The greater part of the SN lies at the junction of the intercavarum sinus (recognized by the absence of a trabecular endocardium) with the lateral wall of the right atrium in the crista terminalis (Davies and Francis, 1942; Li et al., 2015; Kennedy et al., 2016). It is indicated that the SN in horses is an ill-defined, whitish structure. Its long axis runs parallel to the sulcus, and it is 3 cm long by 5 mm wide (Mettam, 1928; Glomset and Glomset, 1940); the shape of the SN in dogs is oblong or as a spindle, although it is often irregular. The total area of the node is approximately 5 mm. (James, 1964a).

There are three types of cells making up the SN. One of these is atrial myocardial cell and is found mainly at the margins of the node. The other one is the main cell of the sinus node, which is called the P cell, responsible for generating the electrical impulse. The third type are transitional cells that are not internally homogeneous, with one half resembling a P cell and the other half resembling a myocardial cell (T cells). These cells are found amidst the cells described above. (James et al., 1966; Oosthoek et al., 1993; Waller et al., 1993a). In horses, the sinus node branch arises from the left circumflex branch of left coronary artery in 100% of the cases (Gómez et al., 2017a); in dogs the sinus node artery arises most commonly from the distal third of the right coronary artery (90%), being virtually a terminal branch of that vessel (James, 1964a).

The atrioventricular node (AVN) is only a few millimeters anterior to the orifice of the coronary sinus. The node is located below the right atrial septal endocardium and just above the septal junction of the tricuspid valve (James, 1961; Waller et al., 1993b; James, 2002). In dogs, it is located in the right half of the interatrial septum. Viewed from the right atrial side, the AVN is elongated. It measures a little <

* Correspondig author at: Department of Pathology, Faculty of Medicine, Universitat de Valencia, 1 floor, Av. de Blasco Ibáñez, 15, 46010 Valencia, Spain.
E-mail addresses: falegom@uis.edu.co (F.A. Gómez-Torres), Amparo.Ruiz-Sauri@uv.es (A. Ruíz-Sauri).

https://doi.org/10.1016/j.rvsc.2019.08.001
Received 28 March 2019; Received in revised form 20 June 2019; Accepted 2 August 2019

2 mm wide and a little > 2 mm long. Its maximum thickness is 0.5–1.0 mm (James, 1964b). The AVN in horses is irrigated by a branch that originates from the right coronary artery in 100% of the specimens (Gómez et al., 2017b). The arterial supply of the AVN of dogs is dual, with a significant portion coming from the left circumflex artery when it crosses the crux cordis of the heart, and the rest from terminal branches of the septal branch, which penetrates inward from the paraconal interventricular branch (James, 1964b).

The adequate knowledge of the sinusal and atrioventricular nodes of dogs and horses, contributes to the comparative anatomy, and facilitates its use for the realization of surgical procedures and design of experimental physiological models that involve these structures (Cunningham and Rush, 2007; Cervenec et al., 2017).

The exhaustive knowledge of the cellular, stromal and vascular components from the morphometric point of view is fundamental to achieve this knowledge. Thus, the aim of this work is to study the histological and morphometric characteristics of the different components of the sinus and atrioventricular nodes in the dog and in the horse that help to know the physiopathology of these nodes and compare it in the two species.

2. Materials and methods

2.1. Tissue collection and processing of the samples

Ten hearts of male horses destined for slaughter (with a weight of 250–300 kg and 2.5–3.5 years old) and five hearts of male dogs were used from the necropsies performed in small animal clinics of the city of Bucaramanga-Colombia (adult medium-sized breed dogs with a weight of 8–19 kg and age between 5 and 12 years). The procedures were in agreement with the Ethics Committee of the "Universidad Cooperativa de Colombia, in the city of Bucaramanga, Colombia, with authorization 014-2018 of April 16, 2018; and they conform to the Law 84 of 1989 in the national context, which corresponds to "The National Statute for the Protection of Animals", in Chapter VI of the use of animals in experiments and research.

In horses and dogs, the region of the SN was removed in bloc, fixed in a 5% formaldehyde solution and then slices of 5 mm were cut. The AVN was sectioned serially, and the block of tissue removed for study incorporated the entire junction of the interatrial and interventricular septa from the posterior margin of the non-coronary sinus of the aorta to the anterior margin of the coronary sinus. Two adjacent centimeters of each septum were retained. Sections were cut perpendicular to the line of junction of the septa. All the samples were tagged for identification, fixed in a 5% formaldehyde solution, and embedded in paraffin. Histological sections of 5 μm thickness were acquired with a microtome and underwent staining with hematoxylin-eosin and Masson's trichrome.

2.2. Histopathological evaluation and image analysis

The samples were assessed using an optic microscope Leica DMD108 (Leica Microsystems, Wetzlar, Germany). For the morphometric analysis in the 10 hearts of horses we took 43 micrographs of the sinus node and 39 micrographs of the atrioventricular node; in the 5 hearts of dogs, we took 15 micrographs of the sinus node and 17 micrographs of the atrioventricular node. In each of these photos, we measured: area (length of shortest line joining two points of object's outline and passing through the centroid), major axis (length of major axis of ellipse with same moments of order 1 and 2 as object), minor axis (length of minor axis of ellipse with same moments of order 1 and 2 as object), mean density (average optical density (or intensity) of object), maximum diameter (length of longest line joining two points of object's outline and passing through the centroid), minimum diameter (length of shortest line joining two points of object's outline and passing through the centroid), perimeter (length of the object's outline), maximum radius (maximum distance between object's centroid and outline), minimum radius (minimum distance between object's centroid and outline), roundness (surface of a round body), length (line or body dimension considering its extension in line rect), width (smallest dimension of a flat figure) at 4×. The area, maximum and minimum diameter of the nodal artery were measured at 4×. We determine the number of cells as well as the total area they occupy these at 10×, as well as the area, maximum diameter, minimum diameter, mean diameter and roundness of the P cells, T cells and myocardiocytes in each of the nodes. The computerized morphometric study was carried out by the software Image-Pro Plus 7.1 (Media Cybernetics, Silver Spring, MD, USA). Each micrograph was calibrated, and the total tissue area in μm^2 was collected after manual chromatic histogram-based selection.

2.3. Statistical analysis

The descriptive statistics, the graphic representations and hypothesis contrast were made with SPSS 20 software (SPSS, Chicago, IL, USA) and Microsoft Excel 2013. The descriptive statistics for each morphometric parameter were calculated and the Kolmogorov-Smirnov normality test was performed, observing a normal population for each of the parameters. Because the sample was < 30, in the case of quantitative variables, nonparametric tests were used when comparing the two species and the Mann–Whitney U test was chosen to ensure greater statistical robustness and the level considered to indicate statistical significance was $p < .05$. To avoid the risk of Type I error, SPSS 20 performs the Bonferroni correction in the multiple comparisons for each experiment. The data were expressed as medians and ranges for all measured lengths and angles.

3. Results

According to our morphometric analysis we can classify the cells found (Figs. 1 and 2) within the sinus and atrioventricular nodes in two types: P cells and T cells. It is also important to describe the myocardiocytes that are found in the periphery of the nodes due to their crucial role in the transmission of electric impulses. In them, different parameters were measured such as area, maximum diameter, minimum diameter, mean diameter and roundness, which can be seen in Table 1. From these analyzes, we were able to determine that the parameters of the P and T cells in the SN in horses are significantly higher than in dogs (Table 2). Likewise, in the AVN, the parameters of the P and T cells in horses were greater than those found in dogs (Table 2).

As in most vertebrates, the SN in horses and dogs is located at the junction of the cranial vena cava and free wall of the right atrium. The substance of horses and dogs SN is arranged about a central artery, which nourishes it. This close relationship of the node to its artery is true for virtually every species in which it has been studied. In some cases, the nodal artery bifurcates in both species into the substance of the SN or moved towards one of its poles. The adventitia tunic of the SN artery in horses is large.

The shape of the horse's SN is oblong (Fig. 3a, b, c), with nerve fibers on the periphery of the node. The SN is not surrounded by a capsule of irregular dense connective tissue, due to this characteristic, only the morphology of the cells allows to identify the node. The cells have a syncytial disposition and in fascicles, surrounded by connective tissue. The P cells are large (Fig. 1a, e), their cytoplasm is paler than those of myocardiocytes, their shape is rounded, located in the center and around the nodal artery; with a single pale and round nuclei. The T cells are small (Fig. 1c, e), pale, elongated and located at the periphery of the node, with a single dark round nucleus. Myocardiocytes are dark, smaller than P cells of the node, which tend to unite with other cells to form fascicles. Its nuclei is central, dark and round.

The shape of the dogs SN varies from oblong to rounded (Fig. 3g, h, i), with nerve fibers within and at the periphery of node. Only the morphology of the cells makes it possible to identify the SN, which is

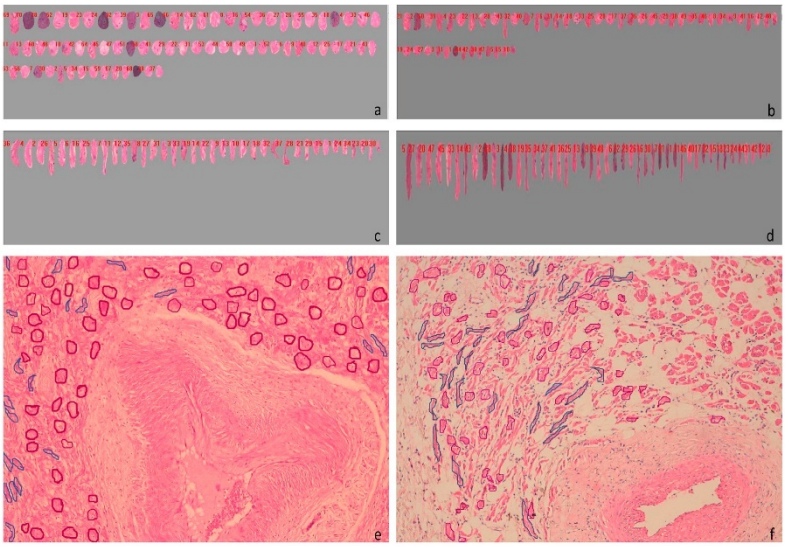

Fig. 1. Sinus node cells of horses and dogs colored with Hematoxylin-eosin at 10×. Morphometry of P cells (a) and T cells (c) in horses. Histological detail of P (red) and T (blue) cells in horses (e). Morphometry of P cells (b) and T cells (d) in dogs. Histological structure of P (red) and T (blue) cells in dogs (f). (For interpretation of the references to color in this figure legend, the reader is referred to the web version of this article.)

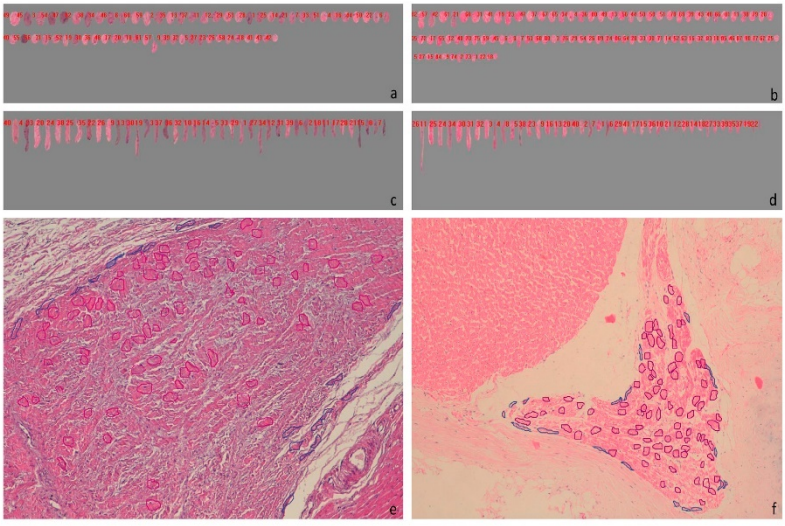

Fig. 2. Atrioventricular node cells of horses and dogs colored with Hematoxylin-eosin at 10×. Morphometry of P cells (a) and T cells (c) in horses. Histological detail of P (red) and T (blue) cells in horses (e). Morphometry of P cells (b) and T cells (d) in dogs. Histological structure of P (red) and T (blue) cells in dogs (f). (For interpretation of the references to color in this figure legend, the reader is referred to the web version of this article.)

Table 1
Global summary of medians of morphometric parameters of P cells, T cells and myocardiocytes of sinus and atrioventricular nodes of ten horses and five dogs.

Species	Cell	Node	Area. μm² (ranges)	Diameter maximum. μm (ranges)	Diameter minimum. μm (ranges)	Diameter mean. μm (ranges)	Roundness. μm (ranges)
Horses	P Cell	SN	1012 (611–1260)	42.2 (28.9–45.2)	31.3 (21.9–35.4)	33.2 (27.2–39.4)	1.11 (1.09–1.28)
		AVN	639.9 (470.9–681.2)	33.2 (27.1–34.3)	22.5 (20.6–26.3)	28.1 (24–29)	1.13 (1.09–1.17)
Dogs		SN	107.5 (57.7–157.2)	12 (8.8–15.2)	9.6 (7.1–12.1)	10.7 (8–13.5)	1.04 (1–1.08)
		AVN	378.2 (249.7–418.5)	24.7 (20.4–27.7)	18 (14.3–18.5)	21.2 (17.3–23.1)	1.1 (1.09–1.12)
Horses	T Cell	SN	1156.5 (806.7–1309.2)	69.5 (60.7–82.8)	20.4 (16.4–20.6)	37.9 (31.2–38)	1.96 (1.83–2.15)
		AVN	423.5 (400.7–549.6)	45.7 (42.6–55.7)	10.8 (8.4–12.7)	26.9 (26.1–29.4)	2.15 (1.91–2.82)
Dogs		SN	664.4 (398.8–930)	63.5 (46.7–80.4)	10.7 (6.5–14.9)	28.7 (24–33.4)	2.94 (1.75–4.14)
		AVN	176.3 (138–328.9)	25 (16.4–41.5)	9 (7.1–11.3)	15.3 (12.6–24.6)	1.62 (1.24–2.16)
Horses	Myocardiocyte	SN	452.3 (376.1–783.8)	28.3 (25.2–34.8)	19.7 (17.7–27.4)	24.2 (21.1–30.8)	1.13 (1.09–1.17)
		AVN	282.2 (155.8–471.7)	21.1 (15–26.5)	15.1 (12–21.9)	18.1 (13.6–24.1)	1.08 (1.02–1.18)
Dogs		SN	496.4 (274.4–718.4)	30.1 (19.4–40.7)	20.7 (16.7–24.6)	23.8 (18.1–29.6)	1.15 (1.04–1.27)
		AVN	291.5 (173.1–390.8)	20.6 (17.1–22.7)	16.9 (12–20.8)	18.6 (14.2–21.6)	1.08 (1.06–1.11)
Scheme			Area	Diameter (max)	Diameter (min)	Diameter (mean)	Roundness

not surrounded by a capsule of irregular dense connective tissue. Some cells are found surrounding the nodal artery, these cells are very close together forming cellular packets. Within the SN there is loose connective tissue surrounding the cells present in the node. The P cells are large (Fig. 1b, f), pale, their shape varies from round to oblong, located in the center of the node, with only a nucleus, which is dark and round. The T cells are small (Fig. 1d, f), the same color as the P cells, elongated, located at the periphery of the node, with a single elongated and pale nucleus. Myocardiocytes are small, dark, round and with a dark nucleus that is located in the center of the cell.

The horses and dogs AVN, lies just anterior to the ostium of the coronary sinus and just above the septal attachment of the tricuspid valve. It is in the right half of the interatrial septum, being located 1 mm or less beneath the endocardium.

Nervous fibers were found around the horses AVN, which presented an oblong shape (Fig. 3d, e, f). The AVN is not surrounded by a capsule of irregular dense connective tissue, due to this characteristic only the morphology of the cells allows to identify the node. The abundant AVN cells are joined together forming cellular cords and surrounded by scarse dense connective tissue. The P cells are large (Fig. 2a, e), pale, rounded and located in the center of the node, with a single nucleus, which is pale and round. The T cells are small (Fig. 2c, e), similar in color to the P cells, elongated, located in the periphery of the node, with a single nucleus, which is dark and elongated. Myocardiocytes are small, round, organized individually or forming cellular cords and with a central nucleus.

The AVN of dogs presents a spindle shape (Fig. 3j, k, l) and nerve fibers are observed within and on the node periphery. The AVN is surrounded by a thin capsule of irregular dense connective tissue that gives it its shape. The cells are abundant, unique and surrounded by scarse connective tissue. The P cells are large (Fig. 2b, f), similar in color to the myocardiocytes, rounded, and located in the center of the node, with a single nucleus, which are rounded and pale. The T cells are narrow (Fig. 2d, f), sparse, dark colored, elongated or basket-shaped,

Table 2
Statistical significance of the parameters measured in the sinus and atrioventricular nodes of ten horses and five dogs.

	Parameter	Horses. μm (ranges)	Dogs. μm (ranges)	*p* Value[b]
Sinus node				
P cells	Area[a]	1012 (611–1260)	107.5 (57.7–157.2)	0.001
	Maximum diameter	42.2 (28.9–45.2)	12 (8.8–15.2)	0.001
	Minimum diameter	31.3 (21.9–35.4)	9.6 (7.1–12.1)	0.001
	Mean diameter	33.2 (27.2–39.4)	10.7 (8–13.5)	0.001
	Roundness	1.11 (1.09–1.28)	1.04 (1–1.08)	0.001
T cells	Area[a]	1156.5 (806.7–1309.2)	664.4 (398.8–930)	0.039
	Minimum diameter	20.4 (16.4–20.6)	10.7 (6.5–14.9)	0.020
Node	Width	1465.6 (1380.5–2564.2)	715.5 (635.4–1064)	0.008
	Area[a]	2,086,936 (1,009,380–3,601,304)	836,760.2 (701,997.1–1,984,741)	0.038
	Minor axis	1377.1 (787.6–1856.4)	751.4 (654.8–1031.5)	0.023
	Minimum diameter	1363.3 (776.1–1759)	698.7 (612.2–728.2)	0.008
	Minimum radio	651.4 (346.1–851.7)	287 (224.1–325.4)	0.008
	Cell area[a]	11.5 (6.5–18.2)	16.5 (11.1–21.9)	0.059
Atrioventricular node				
P cells	Area[a]	639.9 (470.9–681.2)	378.2 (249.7–418.5)	0.004
	Maximum diameter	33.2 (27.1–34.3)	24.7 (20.4–27.7)	0.006
	Minimum diameter	22.5 (20.6–26.3)	18 (14.3–18.5)	0.004
	Mean diameter	28.1 (24–29)	21.2 (17.3–23.1)	0.004
T cells	Area[a]	423.5 (400.7–549.6)	176.3 (138–328.9)	0.021
	Maximum diameter	45.7 (42.6–55.7)	25 (16.4–41.5)	0.021
	Mean diameter	26.9 (26.1–29.4)	15.3 (12.6–24.6)	0.021

[a] The areas were measured in μm².
[b] The test used to find the *p*-value was Mann–Whitney U.

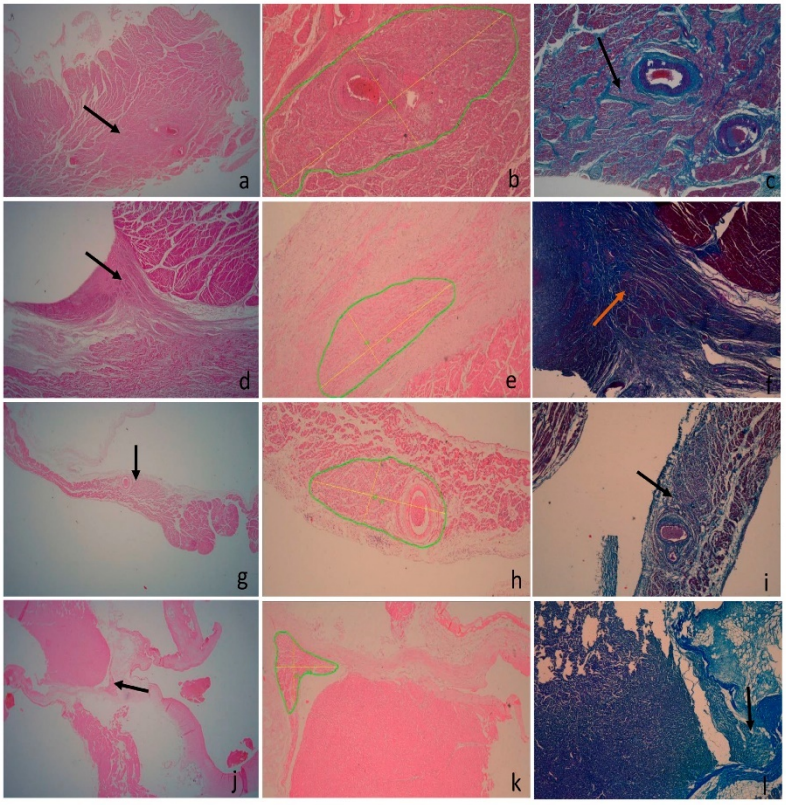

Fig. 3. Morphometry and location of sinus and atrioventricular nodes of horses and dogs. The arrows indicate the histological position of sinus node in horses (a) and dogs (g), as well as the location of atrioventricular node in horses (d) and in dogs (j) with Hematoxylin-eosin at 1.6×. The morphometric analysis was performed on samples stained with Hematoxylin-eosin at 4× in sinus node of horse (b) and dog (h) and in atrioventricular node of horse (e) and dog (k). Histological detail of horse (C) and dog (i) sinus node, as well as atrioventricular node of horse (f) and dog (l) stained with Masson's trichrome at 4×, indicating the position of the nodes with arrows.

and located in the periphery, with a single rounded and pale nucleus. Sometimes T cells appear in a linear organization with other transitional cells. Myocardiocytes are small, dark, round, with a dark nucleus that is located in the center of the cell and tend to join with each other forming cellular cords.

In the sinus and atrioventricular nodes, we measured: parameters such as area, major and minor axis, mean density, maximum and minimum diameter, perimeter, maximum and minimum radius, roundness, length, width, count and area of blood vessels, count and cell area. In them, the medians and ranges were determined, which can be observed in Table 3. It was observed that the size of the SN referring to width and the other parameters determined in this node are significantly higher in horses than in dogs (Table 2). This would be in agreement with the territory of influence of the SN in horses.

In nodes arteries of horses and dogs, the area, maximum diameter, minimum diameter and the thickness was measured (Table 3). In histological sections, it was difficult to find the AVN artery in both horses and dogs; only in one case was it possible to observe the presence of this artery in dogs. In this artery an area of 154.9 mm, a maximum diameter of 0.7 mm, a minimum diameter of 0.2 mm and a thickness of its wall of 0.06 mm was observed.

4. Discussion

The structure of SN and AVN has similarities in the hearts of horses and dogs, so the comparison of the results with previous studies are presented together.

Previous research indicates that the SN of dogs has a central artery that is responsible for nourishing it (Soderstrom, 1958; James, 1964a), which corresponds partially with our study because, in some cases, this artery is located at one of the poles of the node. Equally this condition was observed in horses.

Table 3
Global summary of morphometric parameters in regions of the sinus and atrioventricular nodes of ten horses and five dogs.

Parameter	Horses		Dogs	
	SN. mm (ranges)	AVN. mm (ranges)	SN. mm (ranges)	AVN. mm (ranges)
Area	2.08 (1–3.6)	0.95 (0.38–3.09)	0.83 (0.70–1.98)	0.34 (0.19–1.68)
Axis major	2 (1.6–2.4)	1.9 (1–2.8)	1.5 (1.2–2.7)	1.2 (0.8–1.8)
Axis minor	1.3 (0.7–1.8)	0.6 (0.4–1.3)	0.7 (0.6–1)	0.4 (0.3–1.2)
Density mean	2.1×10^{-4} (1.7×10^{-4}–3.6×10^{-6})	2.2×10^{-4} (1.0×10^{-4}–3.3×10^{-6})	1.7×10^{-6} (1.4×10^{-4}–2.1×10^{-6})	2.9×10^{-6} (2.2×10^{-4}–4.9×10^{-4})
Diameter maximum	2 (1.6–2.5)	1.9 (1.1–2.7)	1.5 (1.2–2.5)	1.3 (0.9–1.7)
Diameter minimum	1.3 (0.7–1.7)	0.5 (0.3–1.3)	0.6 (0.6–0.7)	0.2 (0.2–0.9)
Perimeter	5.4 (4.4–7)	4.2 (2.8–7)	3.7 (3.1–6.8)	3.6 (2.3–5.3)
Radius maximum	1.1 (0.8–1.3)	1 (0.6–1.5)	0.8 (0.6–1.4)	0.9 (0.6–0.9)
Radius minimum	0.6 (0.3–0.8)	0.2 (0.1–0.6)	0.2 (0.2–0.3)	0.1 (0.07–0.4)
Roundness	1.1×10^{-3} (1.0×10^{-3}–1.6×10^{-3})	1.8×10^{-3} (1.2×10^{-3}–2.2×10^{-3})	1.3×10^{-3} (1.1×10^{-3}–1.8×10^{-3})	2.2×10^{-3} (1.3×10^{-3}–3.3×10^{-3})
Length	2.1 (1.6–2.7)	1.9 (1.1–3.1)	1.5 (1.4–2.4)	1.8 (1.1–1.9)
Width	1.4 (1.3–2.5)	0.5 (0.4–1.3)	0.7 (0.6–1)	0.6 (0.6–1.3)
Cellular area	1.1×10^{-3} (6×10^{-7}–1.8×10^{-5})	1.2×10^{-3} (9×10^{-5}–2.8×10^{-5})	1.6×10^{-5} (1.1×10^{-5}–2.1×10^{-5})	2.3×10^{-5} (2.0×10^{-5}–4.7×10^{-5})
Cells number	719 (151–1428)	702 (429–1272)	1172 (503–2273)	793 (235–876)
Nodal artery area	0.34 (0.06–0.61)		0.08 (0.05–0.36)	0.15
Diameter maximum artery	0.7 (0.4–0.9)		0.6 (0.3–1)	0.7
Diameter minimum artery	0.4 (0.1–0.7)		0.3 (0.1–0.6)	0.2
Blood vessel thickness	0.16 (0.12–0.26)		0.06 (0.06–0.24)	0.06

The areas were measured in mm^2.

Some authors indicate that SN in horses is an ill-defined whitish structure (Mettam, 1928; Glomset and Glomset, 1940); this differs from our findings because we found that the node is oblong and very noticeable, despite not having connective tissue capsule. In dogs the shape of the node is oblong or as a spindle but it is often irregular (James, 1964a). This is partially in accordance with our results, where we observe that SN presents a variable form between oblong and rounded.

Previous studies in horses indicate that the SN is 3 cm long by 5 mm wide (Mettam, 1928; Glomset and Glomset, 1940), this differs from our findings because the measures found are less than those previously described. James, 1964a, observed that in dogs the total substance of the node is approximately 5 mm, being smaller than what was found in the present study.

Different authors indicate the presence of nerve fibers in the components of the SN. They have been observed within the substance of the node (Keith and Flack, 1907), in pigs there are numerous nerve fibers on the periphery (Bharati et al., 1991) and scarce fibers within the node (Opthof et al., 1987). In dogs abundant nerve fibers within the node have been described (James, 1964a). In our study, the presence of nerve fibers was found within and at the periphery of the sinus node of dogs. In horses, nerve fibers were found on the periphery. This is important because the amount of nerve fibers present can influence the pacemaking activity of the sinus node. It has been described that some nodal cells are more sensitive to norepinephrine or acetylcholine, being able to change the origin site of the intranodal pacemaker or that the original site simply firing at a faster rate (Hoffman and Cranefield, 1964; Kawamura, 1968; James and Sherf, 1971).

In dogs, it is described that P cells in the SN are pale, in contrast to myocardiocytes and many of its features resemble those to Purkinje cells. Most of the central portion of the SN is composed of clusters of P cells with syncytial disposition. The shape of cells is ovoid or round, with the dimensions of a single P cell averaging 5–10 μm in maximum diameter (James, 1964a; James et al., 1966), being similar to that found in our study with a maximum diameter of P cells of 12 μm. Glomset and Glomset (1940a) indicates that the nuclei are round or oval and occasionally multiple; which is partially in accordance with our investigation, because in our study we found cells with a single rounded nucleus. It is reported that T cells are located in the periphery of the SN (James, 1964a), which is in accordance with our findings. These cells are responsible for the transmission of electrical impulses from the interior of the node to the surrounding myocardiocytes and atrioventricular conduction pathways.

No previous reports of these descriptions were found in horses, but the characteristics of the P cells of this animal group are similar to those described in several investigations of other species, where nodal cells are thought to be the source of normal impulse formation in the sinus node, that is, the site of origin for the pacemaking function of this. (Bharati et al., 1991; Oosthoek et al., 1993; James, 2002). We have described in horses both the shape and the size of these cells, finding that they are large, pale, rounded and located around the nodal artery.

The shape of the AVN in dogs resembles a tiny spleen and is oblong (James, 1964b; Truex and Smythe, 1965), our results are in accordance with the previous literature because the node has a spindle shape. Previous research does not describe the shape of the node in horses, we found that the AVN of horses has an oblong shape. In horses, nerve fibers are abundantly present throughout the bundle and bundle branches. In dogs, some nerve fibers are present in the periphery of the AVN (James, 1964b; Bharati et al., 1991). In our study, nerve fibers were found in the periphery of the node in horses and both in the periphery and within the node in dogs. It has been described that the AVN of dogs measures a little < 2 mm high and a little > 2 mm long. Its maximum thickness is from 0.5 to 1.0 mm (James, 1964b), being similar than those found in the present study.

Sánchez-Quintana and Ho (2003), indicate that in dogs the AVN is not covered by transitional cells, this differs from our findings, because we found small basket-shaped transition cells around the dog's node, which are also described in the human AVN (James, 2002; Mani and Pavri, 2014; Randhawa et al., 2017). In humans, the presence of transitional cells is described in a linear organization with other T cells in the SN (James, 2002; Mani and Pavri, 2014; Randhawa et al., 2017), which we observed in our study in the AVN of dogs. The presence of this type of T cells would be involved in the transmission of extranodal electrical impulses from inside the nodes to the atrioventricular conduction pathways.

5. Conclusions

The size of the SN and AV in horses is greater than found in dogs, coinciding with the area that this specialized structure must cover in each of these animal species.

The P and T cells of nodes are larger in horses than in dogs, demonstrating the highest percentage of conduction required by the cardiac tissue of horses when the electrical impulse is generated and driven in these structures.

The lower cell density in any of the cardiac nodes, especially in P cells of sinus node, can decrease electrical conduction within the nodes and in the internodal tracts, which would reflect the presence of cardiac arrhythmias derived from poor conduction, even in morphologically normal hearts. The information obtained in our study is relevant for the use in humans in hemodynamic and experimental applications that allows knowing more thoroughly the functioning of the conduction system, because it has been reported that the differences found in the cardiac nodes of these two animal species are minimal compared to humans.

Sources of funding

This work was supported by the "Instituto de Salud Carlos III", Spain and co-funded by "FEDER" (grant numbers PI14/00271, pie15/00013) and by the "Generalitat Valenciana", Spain (grant number PROMETEO2013/007).

Declaration of competing interest

The authors declare that they have no conflicts of interest.

References

Bharati, S., Levine, M., Huang, S.K.S., Handler, B., Parr, G.V.S., Bauernfeind, R., Lev, M., 1991. The conduction system of the swine heart. Chest 100, 207–212.
Cervenec, R.M., Stauthammer, C.D., Fine, D.M., Kellihan, H.B., Scansen, B., 2017. Survival time with pacemaker implantation for dogs diagnosed with persistent atrial standstill. J. Vet. Cardiol. 19, 240–246.
Cunningham, S.M., Rush, J.E., 2007. Transvenous pacemaker placement in a dog with atrioventricular block and persistent left cranial vena cava. J. Vet. Cardiol. 9, 129–134.
Davies, F., Francis, E.T.B., 1942. The conducting system of the vertebrate heart. Br. Heart J. 4, 66–76.
Glomset, D.J., Glomset, A.T.A., 1940. Morphologic study of the cardiac conduction system in ungulates, dog and man. Part I: the sinoatrial node. Am. Heart J. 4, 389–398.
Gómez, F.A., Ballesteros, L.E., Estupiñan, H.Y., 2017a. Morphological characterization of the left coronary artery in horses. Comparative analysis with humans, pigs, and other animal species. Ital. J. Anat. Embryol. 122, 137–146.
Gómez, F.A., Ballesteros, L.E., Estupiñan, H.Y., 2017b. Morphologic expression of the right coronary artery in horses. Comparative description with humans, pigs and other animal species. Austral. J. Vet. Sci. 49, 161–166.
Hoffman, B.F., Cranefield, P., 1964. The physiologic basis of cardiac arrhythmias. Am. J. Med. 37, 670–684.
James, T.N., 1961. Morphology of the human atrioventricular node with remarks pertinent to its electrophysiology. Am. Heart J. 52, 756–771.
James, T.N., 1964a. Anatomy of the sinus node of the dog. Anat. Rec. 143, 251–265.
James, T.N., 1964b. Anatomy of the A-V node of the dog. Anat. Rec. 148, 15–27.
James, T.N., 2002. Structure and function of the sinus node, AV node and His bundle of the human heart: Part I – Structure. Prog. Cardiovasc. Dis. 45, 235–267.
James, T.N., Sherf, L., 1971. Specialized tissue and preferential conduction in the atria of the heart. Am. J. Cardiol. 28, 414–427.
James, T.N., Sherf, L., Fine, G., Morales, A.R., 1966. Comparative ultrastructure of the sinus node in man and dog. Circulation 34, 139–163.
Kawamura, M., 1968. Experimental study of the pacemaker shift in the rabbit atrium by means of the microelectrode method. Jpn. Circ. J. 32, 26–28.
Keith, A., Flack, M., 1907. The form and nature of the muscular connections between the primary division of the vertebrate heart. J. Anat. Physiol. 41, 172–189.
Kennedy, A., Finlay, D.D., Guldenring, D., Bond, R., Moran, K., McLaughlin, J., 2016. The cardiac conduction system: Generation and conduction of the cardiac impulse. Crit. Care Nurs. Clin. North Am. 28, 269–279.
Li, N., Csepe, T.A., Hansen, B.J., Dobrzynski, H., Higgins, R.S.D., Kilic, A., Mohler, P.J., Janssen, P.M.L., Rosen, M.R., Biesiadecki, B.J., et al., 2015. Molecular mapping of sinoatrial node HCN channel expression in the human heart. Circ. Arrhythm. Electrophysiol. 8, 1219–1227.
Mani, B.C., Pavri, B.B., 2014. Dual atrioventricular nodal pathways physiology: a review of relevant anatomy, electrophysiology, and electrocardiographic manifestations. Indian. Pacing. Electrophysiol. J. 14, 12–25.
Mettam, R.W., 1928. The atrioventricular system of the equine heart. In: Union Africa Department of Agriculture 13 and 14, pp. 745.
Oosthoek, P.W., Virogh, S., Mayen, A.E.M., Van Kempen, M.J.A., Lamers, W.H., Moorman, A.F.M., 1993. Immunohistochemical delineation of the conduction system. I: the sinoatrial node. Circ. Res. 73, 473–481.
Opthof, T., de Jonge, B., Jongsma, H.J., Bouman, L.N., 1987. Functional morphology of the pig sinoatrial node. J. Mol. Cell. Cardiol. 19, 1221–1236.
Randhawa, A., Gupta, T., Aggarwal, A., Sahni, D., Singh, R.S., 2017. Histological topography of the atrioventricular node and its extensions in relation to the cardiothoracic surgical landmarks in normal human hearts. Cardiovasc. Pathol. 30, 38–44.
Sánchez-Quintana, D., Ho, S.Y., 2003. Anatomy of cardiac nodes and atrioventricular specialized conduction system. Rev. Esp. Cardiol. 56, 1085–1092.
Soderstrom, N., 1958. Myocardial infarction and mural thrombosis in the atria of the heart. Acta. Med. Scand. Suppl. 217, 114.
Truex, R.C., Smythe, M.Q., 1965. Comparative morphology of the cardiac conduction tissue in animals. Ann. N. Y. Acad. Sci. 127, 19–33.
Waller, B., Gering, L.E., Branyas, N.A., Slack, J.D., 1993a. Anatomy, histology, and pathology of the cardiac conduction system: Part I. Clin. Cardiol. 16, 249–252.
Waller, B., Gering, L.E., Branyas, N.A., Slack, J.D., 1993b. Anatomy, histology, and pathology of the cardiac conduction system: Part II. Clin. Cardiol. 16, 347–352.

Research in Veterinary Science 135 (2021) 209–216

Contents lists available at ScienceDirect

Research in Veterinary Science

journal homepage: www.elsevier.com/locate/rvsc

Morphometric analysis of cardiac conduction fibers in horses and dogs, a comparative histological and immunohistochemical study with findings in human hearts

F.A. Gómez-Torres [a,b], H.Y. Estupiñán [b,c], A. Ruíz-Saurí [a,d,*]

[a] Department of Pathology, Faculty of Medicine, 1st floor, Universitat de Valencia, Av. de Blasco Ibáñez, 15, 46010 Valencia, Spain
[b] Department of Basic Sciences, School of Medicine, Universidad Industrial de Santander, Cra 32 # 29-31, 68002 Bucaramanga, Colombia
[c] Department of Laboratory Medicine, Clinical Research Center, Karolinska Institute, Karolinska University Hospital Huddinge, SE-141 86 Huddinge, Sweden
[d] INCLIVA Biomedical Research Institute, Av. de Blasco Ibáñez, 17, 46010 Valencia, Spain

ARTICLE INFO

Keywords:
Cardiac conduction fibers
Gap junctions
Desmin
Connexin
PAS method

ABSTRACT

The principal function of the ventricular conduction system is rapid electrical activation of the ventricles. The aim of this study is to conduct a morphometric study to pinpoint the morphological parameters that define cardiac conduction cells, allowing us to distinguish them from other cells.

Five male horse hearts and five male dog hearts were used in the study. The hearts were fixed in a 5% formaldehyde solution. Histological sections of 5 μm thickness were acquired and stained with hematoxylin-eosin and Masson's trichrome and cardiac conduction cells and their junctions were identified by desmin, connexin 40 and a PAS method.

We found statistically significant differences in cardiac conduction fibers density and thickness, which was much higher in horses than in dogs ($p = 0.000$ for both values). By comparing the measured parameters of the cells in both species, we determined that cardiac conduction cells area and diameters were greater in horses than in dogs ($p = 0.000$ for all values). In dogs there are more junctions (30.8%) than in horses (26.1%), a statistically significant difference ($p = 0.041$). Our findings regarding the cardiac conduction fibers distribution in the animal species studied becomes new knowledge that contributes to the morphological study of this component of the cardiac conduction system and also makes it possible to locate exactly the site with the highest density of cardiac conduction fibers as a contribution to the cardiological study of these structures that lead to the prevention of ventricular arrhythmias and the identification of their treatment site.

1. Introduction

Morphologically distinguishing the cardiac conduction system (CCS) from working cardiomyocytes is not an easy task. In 1845 Johannes Evangelista Purkinje first described the cardiac conduction fibers (CCF) as a network of gray, flat, gelatinous fibers located in the ventricular subendocardium of sheep hearts (Glomset and Glomset, 1940; Ono et al., 2009). In the early 20th century, the role of this system network in cardiac electrical conduction was subsequently described in human, dog, cow and sheep hearts (Tawara, 1906; Tawara, 2000; Eliška, 2006; Silverman et al., 2006; Pallante et al., 2010; Garcia-Bustos et al., 2017) and since then the anatomy and histology of the CCS has been widely studied. The principal function of the ventricular conduction system is rapid electrical activation of the ventricles (Zimmermann, 1923; Oosthoek et al., 1993; Aouadi et al., 2019). A direct continuity of the myocardial CCF with those lying subendocardially has been described in ungulates, although this connection has also been indicated in other species such as dogs (Abramson and Margolin, 1936). Research in this area is therefore pivotal to gain insight into the disorders related to ventricular arrhythmias.

Many techniques have been developed for anatomical analysis of CCF, such as: serial section reconstruction, India ink injection, micro-dissection, stereo-microscopy, scanning electron microscopy, immunoenzyme histochemistry reconstruction and transgenic eGFP expression (Tawara, 1906; Tawara, 2000; Silverman et al., 2006; Ono et al., 2009; Atkinson et al., 2011; De Almeida et al., 2015). Recent years have seen, non-invasive imaging techniques, such as magnetic resonance imaging, contrast-enhanced micro-computed tomography and

* Correspondig author at: Department of Pathology, Faculty of Medicine, 1st floor, Universitat de Valencia, Av. de Blasco Ibáñez, 15, 46010 Valencia, Spain.
E-mail addresses: falegom@uis.edu.co (F.A. Gómez-Torres), hyestuve@uis.edu.co (H.Y. Estupiñán), Amparo.Ruiz-Sauri@uv.es (A. Ruíz-Saurí).

https://doi.org/10.1016/j.rvsc.2021.02.013
Received 27 October 2020; Received in revised form 4 January 2021; Accepted 14 February 2021
Available online 16 February 2021

ultrahigh-resolution spectral domain optical coherence tomography (Benson et al., 2008; Bordas et al., 2011; Stephenson et al., 2012; Yao et al., 2016). From the histological point of view, CCF have been identified through different techniques such as modified periodic acid Schiff method (PAS), immunofluorescence (Pieperhoff et al., 2010) and electron microscopy (Otsuka et al., 1966; Shimada et al., 1992; Ono et al., 2009). However, the morphometry of CCF and the connections that allow their more precise identification are neglected areas of study (García-Bustos et al., 2017).

The morphology of cardiac conduction cells (CCC) in mammals shows great variations between species, so the CCF network is divided into three groups depending on CCC size and ultrastructure: Group I, found in ungulates (sheep, goats, cows, horses and pigs) and cetaceans (whales and dolphins); group II, in humans, monkeys, dogs, cats and seals and group III, in rodents (mice and rats) and rabbits (Canale et al., 1986; Ono et al., 2009; Sedmera and Gourdie, 2014; Yoshimura et al., 2014; Vigmond and Stuyvers, 2016). In addition, intramyocardial and perivascular CCF has been described in birds, placing them in group I (Truex and Smythe, 1965; Gourdie et al., 1993; Harris et al., 2002; Miquerol et al., 2004).

From the right and left branches of the atrioventricular trunk, CCF are responsible for receiving and transmitting the electrical impulse to the ventricular myocardium to facilitate contraction, but they also play an important role in generating ventricular arrhythmias (Li et al., 2015; Aouadi et al., 2019). Ventricular tachycardia (VT) and ventricular fibrillation (VF) are two typical forms of arrhythmia that occur both in humans and animals. (Tabereaux et al., 2009; Benito and Josephson, 2012; Krishnamoorthy et al., 2015; Gianni et al., 2018), leading researchers to propose the use of ungulate hearts as a model to study these pathologies in humans (De Almeida et al., 2015).

Gap junctions are clusters of transmembrane channels, which form direct intercellular communications. The junctions between the cells of the conduction system and cardiomyocytes mediate electrical coupling, forming cell-to-cell junctions that propagate the electrical excitation wave responsible for cardiac contraction (Ter Borg, 1941; Severs et al., 2004; Severs et al., 2008).

In this paper we make a comparative equine and canine study of the morphometric profile of CCC in different regions of the left ventricle using hundreds of micrographs and paying special attention to the connections between CCF structure and the working myocardial tissue, as a substrate for its better knowledge.

2. Materials and methods

2.1. Obtaining and processing samples

Five hearts of male horses destined for slaughter (with a weight of 250–300 kg and 2.5–3.5 years old) and five male dog hearts from necropsies performed in small animal clinics of the city of Bucaramanga, Colombia (adult medium-sized breed dogs with a weight of 8–19 kg and age between 5 and 12 years) were used. Procedures were in accordance with the Ethics Committee of the Universidad Cooperativa de Colombia (No. 014-2018) and conform to Law 84 of 1989 with a national scope, corresponding to Chapter VI of "The National Statute for the Protection of Animals", on use of animals in experiments and research.

The hearts were collected and fixed in a 5% formaldehyde solution. For histopathological analysis, left ventricles (LV) were dissected and sectioned into three slices of equal width. The hearts were divided into three parts: basal, middle third and apex regions. Each slice was radially sectioned, yielding in five samples from the base (coded 11–15), five from the middle third (coded 16–20) and four from the apex (coded 21–24) (Fig. 1). Additionally, in each of these sections serial samples were obtained (5–8) to cover the entire surface of CCF (these samples were coded the same as those of the slices but with lowercase letters for identification). All samples were labeled for identification and embedded in paraffin. For each region, 5 samples were cut into 5 mm thick slices at the location of CCF. To perform a three-dimensional reconstruction of CCF, the paraffin block that included the fibers was completely cut according to the following protocol: A 5 μm section was made and then the 40 μm sample was devastated and another section of 5 μm. This protocol was followed until all CCF were sectioned (Fig. 2). Histological sections were stained with hematoxylin-eosin and Masson's trichrome.

In addition, to check for CCC recognition, an immunohistochemical staining was performed with the D33-IR606 clone of the Anti-Human Desmin (DAKO Corporation) to visualize the intermediate myofilaments (desmin) present in CCC and compare them with the surrounding cardiomyocytes. Additionally, a PAS (Periodic acid–Schiff) method was performed to visualize the quantity of glycogen in these cells. We also used an immunohistochemical stain with Connexin 40 (Cx40) protein,

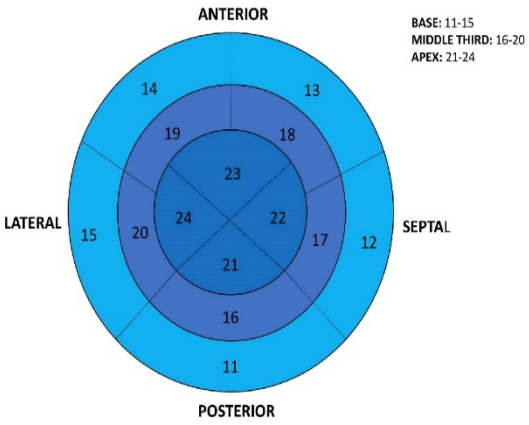

Fig. 1. Bull's eye plot representing the divisions made in the left ventricle into slices and regions.

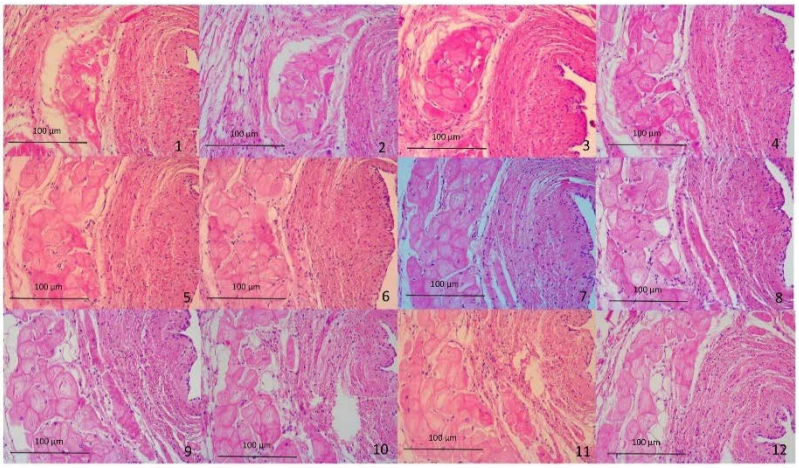

Fig. 2. Serial cuts in a horse heart sample at the endocardial level in the left ventricle, showing cardiac conduction fibers at 20×.

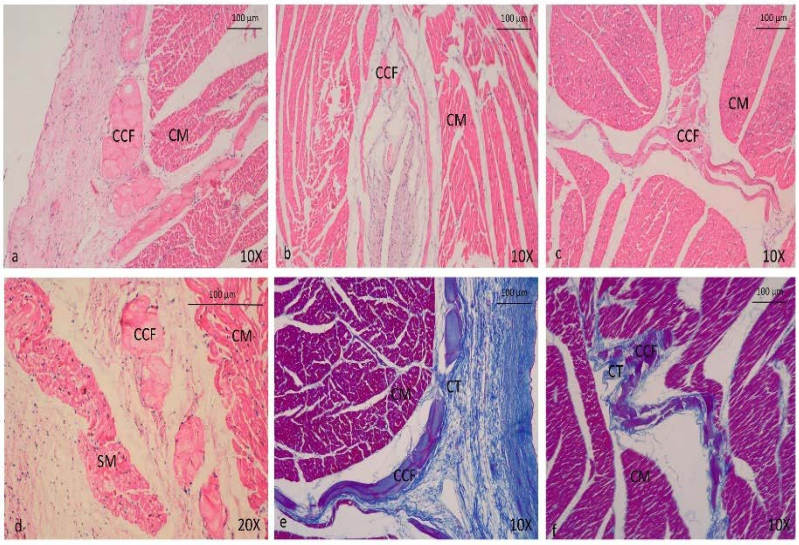

Fig. 3. Cardiac conduction fibers of horses in different locations and regions, stained with Hematoxylin-eosin (a-d) and Masson's trichrome (e, f). Cardiac conduction fibers at the endocardial level, in the anterior region (a, f). Cardiac conduction fibers at the perivascular level, in the anterior region (b). Cardiac conduction fibers at the intramyocardial level, in the septal region (d) and in the anterior region (e, c). CCF: cardiac conduction fibers; CM: cardiomyocytes; CT: connective tissue.

specific for marking CCCs at the level of GAP junctions. In horses, an ELISA kit (Horse Connexin 40 ELISA Kit) - MBS008134 My BioSource was used and in dogs a Connexin 40 (36–4900) Thermo Fisher Scientific polyconal antibody was used.

2.2. Morphometric and histological evaluation

Computerized morphometric study was performed by Image-Pro Plus 7.1 software (Media Cybernetics, Silver Spring, MD, USA). Each sample was assessed histologically and morphometrically in its entirety, and all stains performed both conventionally and immunohistochemically were compared. 2500 micrographs in both species were studied for exhaustive PF study, using a Leica DMD108 optical microscope (Leica Microsystems, Wetzlar, Germany).

Each micrograph was calibrated and total area of tissue and of the CCC in μm2 was obtained manually by segmentation at 10×. Next, CCF density was calculated as the area occupied by the fibers relative to the total tissue area. We also measured the maximum thickness of CCF bundles at 10× transversely and manually. In equine and canine CCC and ventricular cardiomyocytes, different parameters such as area, maximum diameter, minimum diameter, mean diameter and roundness were measured at a 20× magnification to observe their characteristics. Regarding roundness, values close to 1 μm obtained in morphometric measurement indicate that the cell is rounder and if they move away from 1 μm, the cell tends to have an elongated or irregular contour.

Three types of junctions between CCC and cardiomyocytes called conduction fiber-myocardial junctions (CFMJ), have been described: contact through cell bodies (CCB), contact through cell prolongations (CCP) and contact through transitional cardiomyocytes (CTC) (Rawling and Joyner, 1987; Garcia-Bustos et al., 2017). Presence or absence of CFMJ was also recorded on each micrograph. We calculated the percentage of CCCs showing CFMJ and the distribution of each of the joints with respect to slice (base, middle third and apex), region (anterior, lateral, posterior and septal) and location (endocardium and myocardium).

Subsequently, data obtained were compared to determine variability between species in terms of CCF density, thickness, CFMJ characteristics and the morphometric parameters of CCC and ventricular cardiomyocytes.

2.3. Statistical analysis

The descriptive statistics, graph representations and hypothesis contrast were made with the software SPSS 20 (SPSS, Chicago, IL, USA) and Microsoft Excel 2013. After all data were obtained and statistically analyzed with the SPSS program, we obtained from each parameter the interval where 66% of the total population was included and the mean of this interval to obtain a morphometric profile of the CCC and ventricular myocardiocytes, which the most conclusive parameters were area, roundness, maximum, minimum and mean diameter.

Continuous variables were expressed as mean and 95% confidence interval. Categorical variables were expressed as a percentage. The level considered to indicate statistical significance was $p < 0.05$. Descriptive statistics were calculated for each morphometric parameter and the Kolmogorov-Smirnov normality test was performed for each sample. In the comparison of qualitative dichotomy variables, such as the presence and type of CFMJ, a chi-square test was used. Where quantitative variables followed normal distribution for regions groups the ANOVA test was used, and where their distribution was not normal, the non-parametric Kruskal-Wallis test was chosen. *t*-tests were used to compare the different parameters between horses and dogs. The data were expressed as mean standard deviation (SD) for all measured lengths.

3. Results

3.1. Cardiac conduction fibers, morphometry, and distribution

The 2500-micrograph analysis allowed us a very thorough study of the left ventricular wall in the species examined. CCF in horses were easily recognizable by histological observation with hematoxylin-eosin and Masson's Trichrome in endocardium and myocardium (Fig. 3) and occasionally in epicardium and perivascular levels. CCF formed bundles composed mainly of 2–10 oval cells and were surrounded by a sheath of collagen fibers, although solitary CCC or large bundles formed by more than 20 cells were sometimes observed. CCF were mainly located in endocardium (55.4%) and myocardium (43.52%), with a larger density in subendocardium ($p < 0.001$). In addition, there was higher fiber density in the septal region (30.19%) than in the anterior (23.80%) ($p = 0.001$) or lateral regions (24.18%) ($p = 0.014$). CCF were distributed in comparable proportion in each slice type (base, middle third, and apex) (Table 1).

We observed statistically significant differences regarding thickness of CCF in the septal region (57.05 μm) compared to the anterior region ($p = 0.010$) and lateral region ($p = 0.031$). CCF were also found to be thicker at the base (56.69 μm) than in the middle third ($p = 0.012$) or the apex ($p = 0.003$) (Table 1). We studied changes in CCF thickness by location (Table 1) which were significantly thicker in endocardium (62.95 μm) than in myocardium ($p < 0.001$) or perivascular levels ($p = 0.003$). In the latter two locations, CCF mainly formed thin strands composed of multiple cells, only occasionally forming thick CCC bundles. The few CCF found in the epicardium were similar in thickness to those seen in the endocardium and always grouped into thick bundles.

CCF in dogs were located mainly in the endocardium and were sometimes observed in epicardium and perivascular levels. They are not easily identified by histological observation with hematoxylin eosin, because they are small and almost the same color as ventricular cardiomyocytes (Fig. 4a, b, c, d). However, CCF detection was enhanced using Masson's Trichrome stain due to a more intense tone than cardiomyocytes (Fig. 4e, f). In dogs, endocardium invaded the myocardium considerably increasing its size. CCF observed were formed mainly by individual oval cells and occasionally formed fiber bundles comprising thin strands of 2–3 cells; less commonly they were composed of 5–7 cells.

Regarding mean values by location (Table 1), CCF were significantly thicker in epicardium (34.11 μm) than in endocardium ($p = 0.028$). We observed statistically significant differences in CCF thickness in the septal region (21.3 μm) compared with the lateral region ($p = 0.004$). In turn in the anterior region (21.26 μm) CCF was thicker than in lateral region ($p = 0.002$). We found not significant differences in CCF thickness between the slices (base, middle third, and apex) (Table 1). Observing means in the regions evaluated (Table 1), CCF density in dogs was found to be higher in the septal region (23.98%) than in the posterior region ($p = 0.006$), lateral region ($p < 0.001$) or anterior region ($p = 0.002$). Observing means values according to slice (Table 1) CCF had higher density in the middle third (21.21%) than in the base ($p = 0.001$) or the apex ($p = 0.016$).

Comparing CCF bundles in the two species studied we could affirm statistically significant differences in density and thickness of the fibers, which were found to be greater in horses than in dogs ($p < 0.001$ for both values). The concentration of CCF and CCC was observed more frequently in the septal region and in the endocardium of the two species studied (Fig. 5).

3.2. Cardiac conduction cells morphometry

CCC in horses were very large, pale, oval and were easily isolated in all locations with hematoxylin-eosin and Masson's Trichrome (Fig. 6). The nucleus was rarely observed and when present was large, round, pale and located mainly on the periphery of the cell. We could easily

Table 1
Mean values of cardiac conduction fibers density and thickness according to slice, region and location in horses and dogs.

		Horse		Dog	
		Conduction fibers density (%)	Fascicle thickness (μm)	Conduction fibers density (%)	Fascicle thickness (μm)
Slice	Base	26.60	56.69	13.88	20.66
	Middle third	26.64	51.71	21.21	20.57
	Apex	23.38	51.02	15.18	18.60
Region	Posterior	25.19	54.24	15.65	19.23
	Septal	30.19	57.05	23.98	21.30
	Anterior	23.80	51.11	15.87	21.26
	Lateral	24.18	50.98	13.87	17.94
Location	Endocardium	55.40	62.95	99.2	20.06
	Myocardium	43.52	40.40		
	Epicardium	0.72	57.36	0.4	34.11
	Perivascular	0.36	25.42	0.4	25.31

observe the myofibrils in these cells, which were scarce and peripherally located. There was connective tissue around the fiber bundles and individual cells in all parts where they were identified, which was deriving from the central fibrous body and the membranous portion of the interventricular septum (Fig. 6e, f). Ventricular cardiomyocytes were small, dark, and round when observed through a cross-section. They could be seen individually or forming bundles of small and had dark centered nuclei.

Measuring different parameters by morphometric analysis, we determined that CCC in horses were larger in size (40–125 μm) than ventricular cardiomyocytes (10–30 μm) (Table 2). In our morphometric analysis, we examined equine CCC characteristics in the locations described, finding larger cell area and diameters in endocardium than in myocardium ($p < 0.001$ for all values). We evaluated CCC characteristics in all regions both in endocardium and in myocardium (Table 3). We found that area, mean diameter, maximum diameter and minimum diameter were larger in septal and lateral region than in anterior and posterior regions in both locations. These findings were statistically significant ($p < 0.001$).

In endocardium, area, minimum and mean diameters were larger lateral than the anterior region ($p = 0.005$, $p = 0.002$ and $p < 0.001$ respectively), and in the septal region than in the anterior ($p < 0.001$ for all parameters) or posterior ($p < 0.001$, $p = 0.001$ and $p < 0.001$ respectively). With respect to maximum diameter, we found this was larger in the lateral region than in the anterior ($p = 0.001$) or posterior ($p = 0.005$); in septal region than in anterior ($p < 0.001$) or posterior ($p < 0.001$). In myocardium, we observed that area, minimum and mean diameter were larger in the posterior region than in the anterior region ($p = 0.039$, $p = 0.044$ and $p = 0.035$ respectively), lateral region ($p = 0.025$ for all parameters) or septal region ($p < 0.001$ for all parameters). The maximum diameter was greater in the posterior region than in the septal region ($p = 0.004$). We found statistically significant differences when evaluating the cells in both locations and individually in each one, which indicated that CCC study by region, helps us to better pinpoint their location. Conduction speed through these cells would also be larger in septal and lateral regions due to an increased in CCC size.

Canine CCC were slightly larger than cardiomyocytes, round and difficult to differentiate from ventricular heart cells due to their similar color. It was only possible to perceive the difference at high magnification with Hematoxylin-Eosin (Fig. 7a, b, c, d), but visualization was improved using Masson's Trichrome (Fig. 7e, f). It was rarely possible to see the nucleus in the large number of individual cells observed in the tissues. When this nucleus was detected, it was mainly oval, dark, and located in the center of the cell, but could also have a rounded and pale appearance. We sometimes observed the few myofibrils that make up the CCC at high magnifications. There was connective tissue around the cells, which was derived from the membranous portion of the interventricular septum and the central fibrous body (Fig. 4f). Ventricular cardiomyocytes were dark, round, or oval and when viewed in a cross section, they could be visualized individually or forming small bundles.

We measured different parameters in CCC using morphometric analysis, finding that in dogs these cells were larger in size (18-40 μm) than ventricular cardiomyocytes (9-31 μm) (Table 2). We also evaluated CCC characteristics in each region (septal, lateral, anterior, posterior) (Table 3), finding no significant statistical differences in the parameters measured in these cells, which indicates that in dogs there was similar conduction speed in all regions because the CCC sizes were almost equal.

Comparing the measured cells parameters in both species revealed that CCC area and diameters of CCC were larger in horses than in dogs ($p < 0.001$ for all values). In addition, we observed that roundness values were higher in horses than in dogs ($p = 0.021$), but given the mean values obtained from roundness, we could conclude that in horses the cells are oval and round in dogs. CCC morphology, and distribution of CCF were analyzed by region in horses and dogs, taking into account the slice and location (Fig. 8).

CCC in horses and dogs contain a large amount of glycogen, so we used a PAS method to confirm identification. This method is important in dogs because these cells were difficult to identify via conventional stains. Using this method in horses, we observed a large amount of glycogen accumulated mainly in the periphery of CCC in endocardium (Fig. 9a) and at the level of myocardium (Fig. 9b) glycogen was seen throughout the cytoplasm of the cells, as was the case in dogs in their subendocardial location (Fig. 9c). In addition, CCC could be fully identified since the surrounding cardiomyocytes were PAS-negative. We performed immunohistochemical staining with desmin in both species to visualize the intermediate filaments present in these cells and thus clearly identify the CCC. In horses, we observed that CCC reacted positively to staining in both endocardium (Fig. 9d) and in myocardium (Fig. 9e) and were easily distinguished from desmin-negative or almost negative cardiomyocytes. In dogs, positivity was presented in both cells, but CCC stained intensely in endocardium (Fig. 9f) with the desmin compared to cardiomyocytes that presented a lower positivity. For this reason, desmin is useful as a marker for CCC recognition in both species. We constructed a morphometric profile of CCC, identifying the values of the most-repeated parameters to facilitate identification (Table 4).

3.3. *Conduction fiber-myocardial junctions*

In our research with connexin 40 immunostaining (Fig. 10), it was possible to observe three types of CFMJ (CCB, CCP, and CTC) in horses and dogs.

In horses, CFMJ was present in 26.1% of all micrographs studied, revealing that the number of junctions is higher in the apex than in other two slices ($p = 0.031$) (Table 5). Likewise, we found that the lateral region contained the largest number of junctions of the regions ($p = 0.009$). In myocardium we observed a great number of junctions than in endocardium ($p < 0.001$) (Table 5). Analyzing the characteristics of the different types of junctions according to the type of slice, we determined that CCB (24.7%) (Fig. 11a) and CCP (0.9%) (Fig. 11b) were in larger quantity in the apex ($p = 0.031$) than the other two slices and CTC

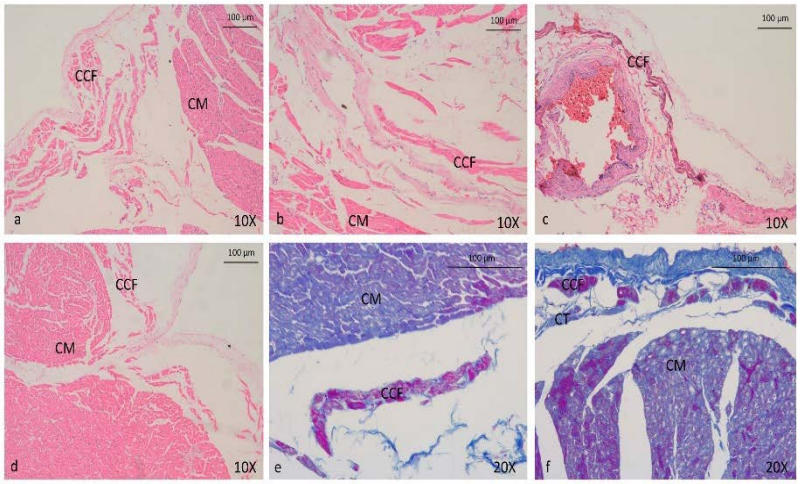

Fig. 4. Cardiac conduction fibers of dogs in different places, stained with hematoxylin-eosin (a-d) and Masson's trichrome (e, f). Cardiac conduction fibers at the endocardial level, in the anterior region (a, f), septal region (d) and posterior region (e). Cardiac conduction fibers at the perivascular level, in the posterior region (b). Cardiac conduction fibers at the epicardial level, in the anterior region (c). CCF: cardiac conduction fibers; CM: cardiomyocytes; CT: connective tissue.

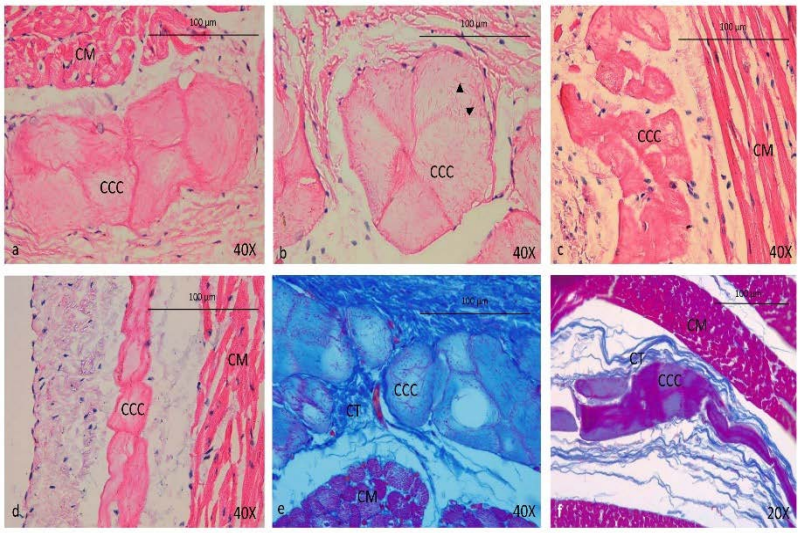

Fig. 6. Morphology of cardiac conduction cells in horses, stained with hematoxylin-eosin (a-d) and Masson's trichrome (e, f). Cardiac conduction cells in endocardium, in the lateral region (a), the septal region (b) and the anterior region (d, e). Cardiac conduction cells in myocardium, in anterior region (e, f). CCC: cardiac conduction cells; CM: cardiomyocytes; CT: connective tissue. The arrowheads indicate the myofibrils at the periphery of the cell.

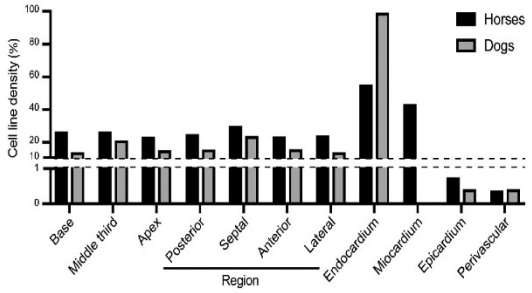

Fig. 5. Concentration of cell lines in the conduction fibers in the different cardiac segments in horses and dogs.

(0.5%) (Fig. 11c) were more visible in base ($p = 0.031$) than other slices (Table 5). Similarly, according to the type of region we were able to observe, that all three junction types were more abundant in the lateral region ($p = 0.048$) (Table 6). Comparing junction types by location, CCB and CCP were found more frequently in myocardium ($p < 0.001$) and CTC in endocardium ($p < 0.001$) (Table 6). We also analyzed the properties of the different CFMJ types, in each of the subdivisions of the areas proposed in this study. These CCP could be found simultaneously with CCB in the same histological section.

In dogs, we determined that CFMJ were present in 30.8% of all the analyzed micrographs, finding more junctions in the apex than in other two slices ($p = 0.009$), similar to that found in horses, since CCF were distributed more evenly at the distal portion of the heart (Table 5). We also observed more junctions in the lateral region than in other regions ($p < 0.001$). According to our morphometric analysis of slices we were able to determine that CCB (29.4%) (Fig. 11d) and CCP (1%) (Fig. 11e) were in larger quantities in apex ($p = 0.013$) and CTC (0.4%) (Fig. 11f) in middle third ($p = 0.013$) (Table 6), observing the strong transmission of the electrical impulse that is made towards the distal part of the heart. When analyzing the different regions, CCB were found most frequently in the lateral region, CCP in the posterior region and CTC in the septal region ($p < 0.001$ for all values) (Table 6).

We also analyzed the characteristics of different CFMJ types in horses and dogs in each of the subdivided areas proposed in this study. We observed that CCB were significantly higher than the other two junction types in all slices, regions, and locations ($p < 0.001$). At the endocardial level, we found thin piliform extensions of CCC in direct contact with the transitional cardiomyocytes or cardiomyocytes in horses and dogs. CTC were commonly found in sub-endocardium. The CCC, either through a piliform or thick prolongation, contacted the transition cell, which in turn contacted one or more cardiomyocytes. When comparing the number of junctions between the two species, there were more CFMJ in dogs (30.8%) than in horses (26.1%), which is statistically significant ($p = 0.041$).

4. Discussion

CCC size, shape, intercellular junctions, and distribution throughout the left ventricle show variations according to different species. In this work, we proposed a morphological, morphometric and immunohistochemical study of these cell characteristics in horses and dogs, to uncover the physiological implications and correlation with ventricular arrhythmias when these fibers undergo alterations. We analyzed 2500 micrographs to conduct a more detailed study of the entire left ventricular territory.

CCF show variations in cell cytoarchitecture in different species, which can be divided into three groups. In group I, cells were characterized by being large, well differentiated and located mainly in the endocardium and myocardium, a type found in cetaceans and ungulates (Truex and Smythe, 1965; Canale et al., 1986; Ono et al., 2009; Yoshimura et al., 2014; Vigmond and Stuyvers, 2016). This group includes horses, who as ungulates possess all the described characteristics of CCF in the animal species belonging to group I, enabling them to conduct and spread electrical impulses rapidly and stably through the ventricular myocardium. The intramyocardial location and the thick sheaths of collagen fibers surrounding the individual cells or bundles provide almost the same ventricular excitation time as humans (Abramson and Margolin, 1936; Oosthoek et al., 1993; Ono et al., 2009; De Almeida et al., 2015). For this reason, study of CCF in horses gives us valuable insight into the behavior of the CCS which can be extrapolated to human studies.

Dogs have been classified in group II, where cells are described as intermediate to small size, with certain similarities to ventricular cardiomyocytes and located mainly in the endocardium, which we also observed in our research (Truex and Smythe, 1965; Canale et al., 1986; Ono et al., 2009; Yoshimura et al., 2014; Vigmond and Stuyvers, 2016). The histologic differentiation of the CCF in dogs is less marked than other species (Abramson and Margolin, 1936), which was observed in our research where the color of CCF is similar to cardiomyocytes.

In ungulates CCF form bundles of 2–8 cells surrounded by collagen fiber sheaths (Tawara, 1906; Zimmermann, 1923; Ter Borg, 1937; Shimada et al., 1983; Canale et al., 1986; Tawara, 2000; Ono et al., 2009). Canine CCF are commonly organized into individual cells or forming fiber bundles of 4–8 cylindrical cells (Glomset and Glomset, 1940; Ono et al., 2009). The CCF of the system in dogs are found only in the subendocardium; they are always surrounded by a connective tissue sheath (Tawara, 1906; Tawara, 2000). In our research in horses CCF bundle formation was very similar to previous studies. In dogs we also observed that the CCF organization consisted mainly of individual cells, yet unlike the ones described in other studies these cells had an oval shape, and when the fiber bundles were visualized, they were formed by 2–3 cells.

In our analysis, canine and equine CCF were thicker and more abundant in the septal region than in other regions, because the septal region is surrounded by endocardium on its two surfaces. In addition, this is where the fibers emerge from the atrioventricular trunk branches and they need to be thicker in order to transmit the electrical impulses passing from the supraventricular region, from the interventricular septum to the cardiac distal region, then ascending through the edges free of ventricles. The CCF in horses, in addition to being more frequently concentrated in the septal region, which is the natural distribution path of these fibers, it was possible to observe that they are similarly distributed between the endocardium and the myocardium, allowing a greater transmission area of the electrical impulse than it translates into an adequate ventricular excitation time, as occurs in

Table 2
Overall summary of morphometric parameters of cardiac conduction cells and cardiomyocytes of horses and dogs.

Species	Cell	Area. (μm² /SD)	Diameter maximum (μm/SD)	Diameter minimum (μm/SD)	Diameter mean (μm/SD)	Roundness (μm/SD)
Horse	Cardiac conduction	3560.8 (1890)	77.40 (20.98)	53.74 (14.54)	63.98 (16.34)	1.20 (0.07)
Dog	cell	364.4 (148.4)	23.92 (5.39)	17.65 (4.07)	20.59 (4.38)	1.11 (0.06)
Horse	Cardiomyocyte	210.7 (98.4)	18.47 (4.11)	13.36 (2.91)	15.76 (3.16)	1.15 (0.06)
Dog		232.5 (174.8)	18.95 (6.31)	13.65 (4.31)	16.10 (4.97)	1.14 (0.05)
	Diagram				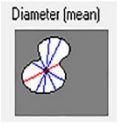	

SD: Standard deviation.

Table 3
Characteristics of the mean of the parameters measured in cardiac conduction cells in horses and dogs by region.

Location	Region	Area (μm²/SD)	Max. diameter (μm/SD)	Min. diameter (μm/SD)	Mean diameter (μm/SD)	Roundness (μm/SD)
Horse	Anterior	2870.3 (1407.7)	69.84 (19.14)	48.25 (12.40)	57.50 (13.91)	1.19 (0.09)
	Lateral	3871.1 (1647.1)	82.05 (18.28)	56.21 (12.79)	67.37 (14.33)	1.21 (0.07)
	Posterior	3279.3 (1716.7)	72.89 (17)	52.73 (13.41)	61.82 (14.52)	1.18 (0.04)
	Septal	4180.6 (2243.2)	84.64 (23.71)	57.69 (16.44)	69.14 (18.47)	1.20 (0.06)
Dog	Anterior	348.3 (162.4)	23.41 (6)	17.06 (4.51)	20.02 (4.82)	1.11 (0.08)
	Lateral	406.7 (129.2)	25.62 (4.77)	18.72 (2.99)	21.92 (3.57)	1.11 (0.04)
	Posterior	312.5 (144.4)	22.17 (4.74)	16.21 (4.27)	18.97 (4.36)	1.10 (0.05)
	Septal	384.4 (124.4)	24.35 (4.42)	18.56 (3.38)	21.33 (3.67)	1.10 (0.04)

SD: Standard deviation.

humans or canines that have these CCFs only in the endocardium, and the decrease in these fibers in these segments can cause electrical problems that can become arrhythmias. They also play an important role in the generation of ventricular arrhythmias (Li et al., 2015; Aouadi et al., 2019). For these reasons, pinpointing CCF location and thickness is vital to detect ventricular cardiac arrhythmias affecting the CCS. Clinical studies on VT after myocardial infarction indicated that the site of reentry was in the anteroseptal and inferolateral basal regions of the left ventricle (Oh et al., 2018) and that this arrhythmia begins in the CCF (Benito and Josephson, 2012). However, it has been shown that in human patients with arrhythmogenic right ventricular cardiomyopathy, the levels of Cx40 and Cx45 in septal subendocardium were drastically reduced (Paul et al., 2013). This coincides with the findings of our study, where canine and equine CCF were mainly located in septal region, as the region mostly covered by endocardium. They were also distributed homogeneously between the base and the middle third in both species. These findings therefore indicate that these places are where ventricular arrhythmias can be generated most frequently, as the source where CCF originate and where they are thickest. Study of these arrhythmias in animals such as dogs and horses serve to generate clinical models that can be applied to human medicine.

Various authors have described CCC in ungulates as with a pale appearance, few myofibrils distributed at the periphery of the cell, a large amount of glycogen in their cytoplasm, and larger than ventricular cardiomyocytes (Tawara, 1906; Zimmermann, 1923; Abramson and Margolin, 1936; Ter Borg, 1937; Truex and Smythe, 1965; Tawara, 2000; Ono et al., 2009; Yoshimura et al., 2014). This is concurrent with our findings, but we also found a larger number of intermediate filaments than ventricular cardiomyocytes in CCC visualized with desmin. We provide a morphometric profile with the most characteristic measurements of these cells (area: 3560.8 μm2. Maximum diameter: 77.40 μm). The above-mentioned authors also report CCCs with one, two and sometimes three nuclei, differing from our research in which we were rarely able to observe the presence of nuclei and when present, were only detected individually. This coincides with criteria indicated in another investigation where many equine CCC have no nuclei, with occasional detection of a diplonucleated cell (Glomset and Glomset, 1940). In addition, CCF were easily distinguished from cardiomyocytes (Bishop and Cole, 1967), as could be observed in our study with both Hematoxylin-eosin and Masson's trichrome. CCF of ungulates have abundant desmosomes and large gap junctions (Ter Borg, 1941; Canale et al., 1986; Shimada et al., 1986; Sugi and Hirakow, 1986). This, together with the large CCC size and the additional intramyocardial location in horses, allows them rapid and controlled transmission of electrical impulses through the entire ventricular surface, thus making depolarization and cardiac action more efficient.

Canine CCC had a pale appearance, and their identification was difficult when observed at the endocardial level (Truex and Smythe, 1965; Sommer and Johnson, 1968; Ono et al., 2009). In our research CCC were a similar color like myocardiocytes and difficult to identify. Using Masson's trichrome staining CCC showed a more intense color than cardiomyocytes. Different authors indicate that CCC in dogs were larger in diameter (20–40 μm) than ventricular cardiomyocytes (about 10 μm) and had a large amount of glycogen and few myofibrils (Glomset and Glomset, 1940; Nonidez, 1943; Ono et al., 2009). We observed these characteristics in our study but found slightly higher values in the two cell types analyzed and we rarely visualized myofibrils, especially in larger CCC. In another study, canine CCC had a value of 164 μm (Sheets et al., 1983), much higher than found in other studies or ours. It has also been indicated that these cells have high amounts of myofibrils in dogs (Sommer and Johnson, 1968), which disagrees with our research and previous reports.

It has been reported, primarily in ungulates but in other species too, that the pale appearance of CCC is due to the low presence of myofibrils and the high amount of glycogen in its cytoplasm, which is typical of conduction cells (Sommer and Johnson, 1968; Tranum-Jensen et al., 1991; Eliška, 2006; García-Bustos et al., 2017). The use of a PAS method for identifying CCCs with large amounts of glycogen in the cytoplasm was efficient in ungulates, although in other species these cells are not clearly identified by this method (Eliška, 2006; Ono et al., 2009). Another study indicates that quantity of glycogen in CCC compared to cardiomyocytes is not entirely reliable as a safe differential criterion

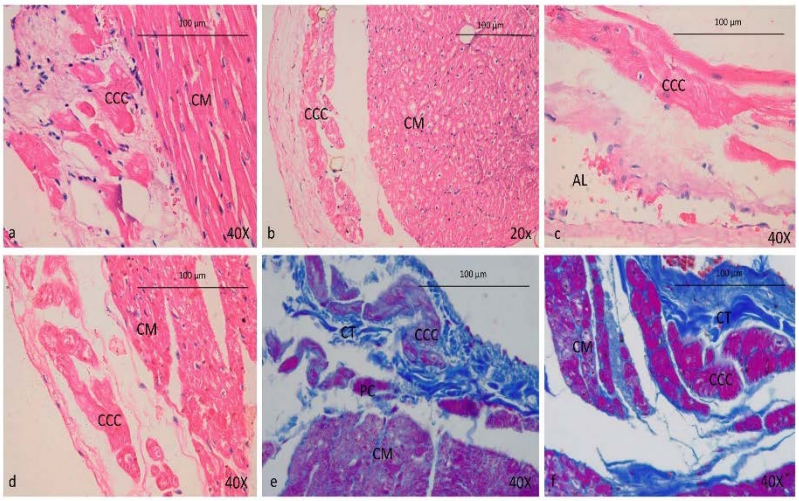

Fig. 7. Morphology of cardiac conduction cells in dogs, stained with hematoxylin-eosin (a-d) and Masson's trichrome (e, f). Cardiac conduction cells in endocardium, in the lateral region (a, e) and the anterior region (b, d, f). Cardiac conduction cells at the perivascular level, in the posterior region (c). CCC: cardiac conduction cells; CM: cardiomyocytes; AL: arterial light; CT: connective tissue.

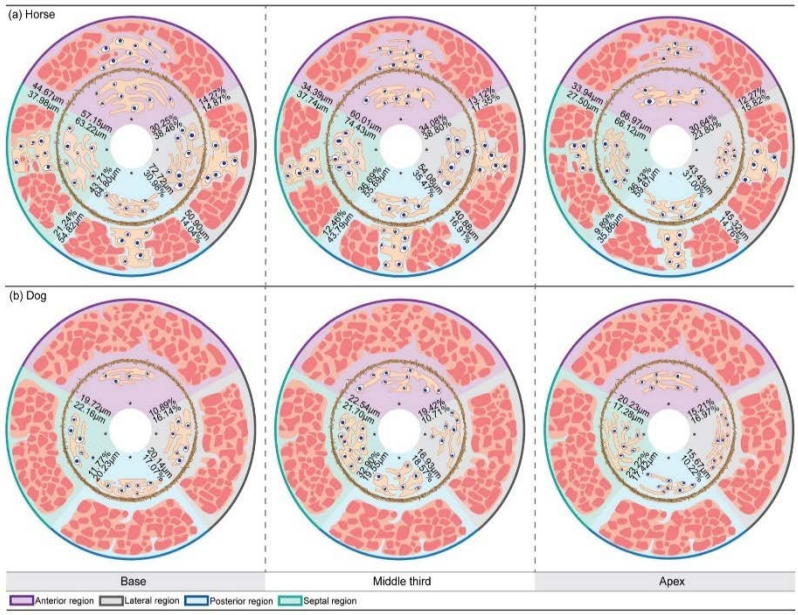

Fig. 8. Intramyocardial and subendocardial (*) distribution of Cardiac conduction fibers in horses (a) and dogs (b), indicating density (%) and thickness (µm) in each of the slices and regions of the left ventricle.

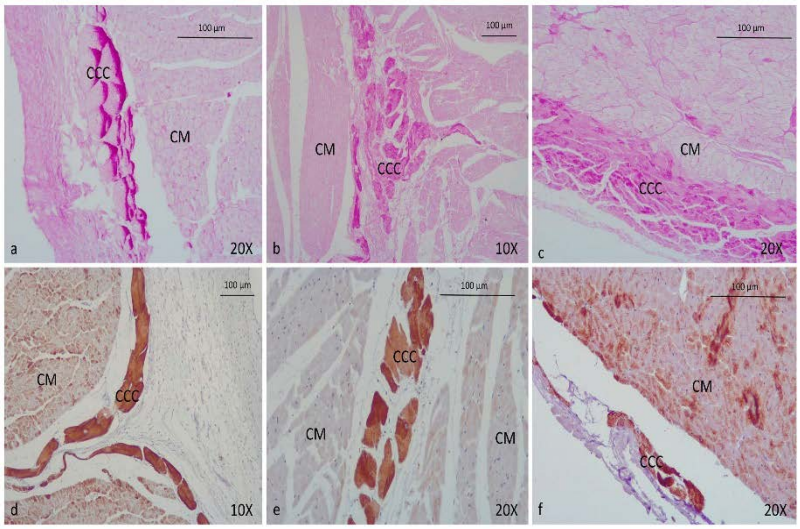

Fig. 9. Recognition of cardiac conduction cells detection by different methods in horses and dogs. PAS method for identification of intracytoplasmic glycogen in horses in endocardium, in the anterior region (a) and myocardium, in the anterior region (b). PAS method in dogs in endocardium, in the lateral region (c). Immunohistochemically staining with desmin for the identification of this intermediate filament in horses in endocardium, in the anterior region (d) and myocardium, in the anterior region (e). Desmin staining in dogs in endocardium, in the posterior region (f). CCC: cardiac conduction cells; CM: cardiomyocytes.

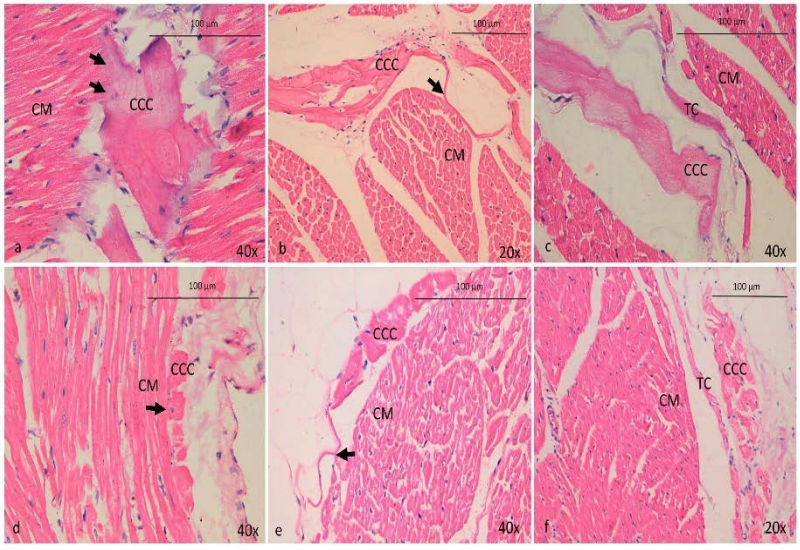

Fig. 11. Different types of conduction fiber-myocardial junctions in horses and dogs, stained with hematoxylin-eosin. The arrows indicate a contact junction through cell bodies (CCB) in myocardium in horses, in lateral region (a) and in endocardium in dogs, in anterior region (d). The arrow shows contact through cell prolongations (CCP) in myocardium in horses, in anterior region (b) and in endocardium in dogs, in the posterior region (e). Note the contact through transitional cardiomyocytes (CTC) in myocardium in horses, in the posterior region (c) and in endocardium in dogs, in the lateral region (f). CCC: cardiac conduction cells; CM: cardiomyocytes; TC: transitional cardiomyocytes.

Table 4
Morphometric profile of the cardiac conduction cells and cardiomyocytes in horses and dogs, determining the most frequent range and mean.

Species	Parameter	Cardiac conduction cells (μm)	Cardiomyocytes (μm)
Horse	Maximum diameter	66–84 (75)	16–18 (17)
	Minimum diameter	47–58 (52)	11–13 (12)
	Roundness	1.11–1.14 (1.13)	1.11–1.16 (1.13)
Dog	Maximum diameter	21–25 (23)	15–19 (17)
	Minimum diameter	15–19 (17)	11–13 (12)
	Roundness	1.08–1.11 (1.09)	1.11–1.16 (1.13)

(Sommer and Johnson, 1968). In our study, CCC identification was very reliable in horses and dogs using the PAS method. Glycogen was observed in large quantities, especially at the cell periphery in equine endocardium and distributed throughout the cytoplasm in equine myocardium and canine endocardium. In cardiomyocytes, no positivity was observed by this method, which allows them to be clearly differentiated from CCC. Therefore, other authors' findings partially agree with our study, since we concur that the PAS method is important for identifying CCC in ungulates, but we also elucidate its important role in other types of animals such as dogs, and whether it is a reliable CCC identification method.

It has been reported that CCC in group I species such as ungulates have a strong positive reaction to desmin (originally also termed "skeletin") and that CCC also exhibited a stronger positive reaction than cardiomyocytes in the case of dogs (group II) (Eriksson et al., 1979; Yoshimura et al., 2014). This is consistent with our results where we found a high desmin-positive cell distributed throughout the cytoplasm of equine CCC and very little positivity to staining by cardiomyocytes. In dogs, we observed that both CCC and cardiomyocytes showed positivity, but desmin was stained more strongly in CCC cytoplasm. This shows that CCC have many intermediate filaments in horses and dogs, showing as intensely desmin-positive. In a previous study these filaments were shown to be especially abundant in CCC of large birds and mammals (Canale et al., 1986) and CCC differentiation with cardiomyocytes was possible using desmin as a marker (Eriksson et al., 1979; Forsgren et al., 1982).

Gap junctions are responsible for electrical coupling in the heart and performed through transmembrane channels composed of connexins (Ter Borg, 1941; Gros and Jongsma, 1996; Vozzi et al., 1999). These junctions act as low resistance pathways for transmitting electrical impulses, allowing small molecules and ions to pass through them (Bruzzone et al., 1996; Gros and Jongsma, 1996; Vozzi et al., 1999). Three main types of connexins expressed in the heart have been identified, Cx43 is found in mammals primarily joining atrial and ventricular cardiomyocytes, Cx45 is most commonly expressed in the atrial conduction system, but is also found in low amounts in CCF, and finally, Cx40 has been found in higher values in the fibers of the ventricular conduction system (Gros and Jongsma, 1996; Vozzi et al., 1999; Severs et al., 2008). We used Cx40 immunohistochemical staining to identify the different types of CCC junctions with cardiomyocytes demonstrating that this staining allows full identification of the CFMJ in horses and dogs.

Table 5
Number of conduction fiber-myocardial junctions by slice, region and location in horses and dogs.

		Horses (%)	Dogs (%)
Slice	Base	22.8	28.5
	Middle third	25.5	26.4
	Apex	29.8	42
Region	Posterior	25.1	27.7
	Septal	21.2	21
	Anterior	26.1	27.2
	Lateral	32.4	50
Location	Endocardium	15.7	30.8
	Myocardium	39.4	

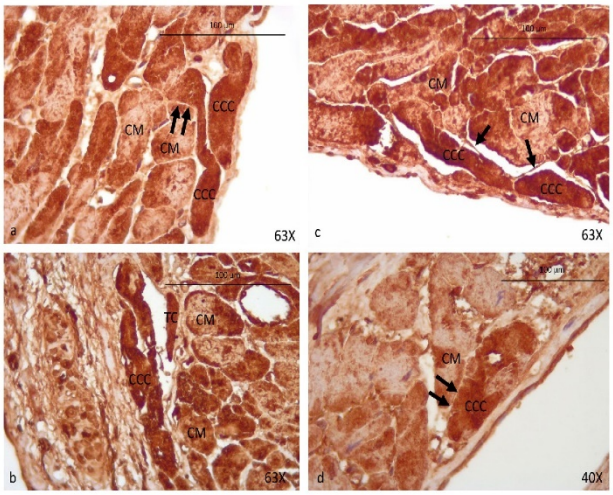

Fig. 10. Identification of conduction fiber-myocardial junctions with connexin 40 in subendocardium. The arrows indicate a contact junction through cell bodies (CCB) (a); contact through cell prolongations (CCP) (b) and contact through transitional cardiomyocyte (CTC) (c) in dogs. The arrow shows a contact junction through cell bodies (CCB) (d) in horses. CCC: cardiac conduction cells; CM: cardiomyocytes; CT: transitional cardiomyocytes.

Table 6
Characteristics of the different junction types according to slice, region and location in horses and dogs.

		Horses (%)			Dogs (%)		
		CCB	CCP	CTC	CCB	CCP	CTC
Slice	Base	21.2	0.6	1	27.3	1.2	0
	Middle third	24.7	0.5	0.3	25.5	0	0.9
	Apex	27.8	1.6	0.4	39.5	2.5	0
Region	Posterior	24.2	0.6	0.3	25.7	2	0
	Septal	20.1	0.6	0.6	19.4	0	1.6
	Anterior	25	0.6	0.5	26	1.2	0
	Lateral	29.4	2.1	0.9	49.1	0.9	0
Location	Endocardium	14.5	0.3	0.9	29.6	1	0.4
	Myocardium	37.6	1.7	0.1			

CCB: contact through cell bodies.
CCP: contact through cell prolongations.
CTC: contact through transitional cardiomyocytes.

In some species of ungulates (cattle and sheep), CFMJ have been found in approximately 15% of samples evaluated (Pieperhoff et al., 2010). In our research in horses, junctions were more frequent than is reported in other ungulates (26.1%), possibly because horses have a higher metabolism and more intense cardiac action owing to the strenuous daily activity to which these animals are subjected. Additionally, we found that equine CFMJ were distributed mainly at the apex, myocardium, and lateral region. This is expected since CCF are more commonly distributed in the distal part of the heart and the importance of these CFMJ in the rapid electrical conduction that occurs in horses through the myocardium has also been demonstrated.

Our analysis of CFMJ spatial distribution in dogs that they were located more widely towards the cardiac apex and the lateral region of the heart, in disagreement with other studies showing junctions distributed preferably towards the cardiac base (Myerburg et al., 1972; Myerburg et al., 1975). Finding more junctions towards the apex is quite expected since the fibers are more evenly distributed towards the distal part of the heart and there is a need for stronger transmission of electrical impulses.

Various authors have described the importance of electrical impulse transmission in CFMJ by means of transitional cardiomyocytes in humans and dogs (Alanis and Benitez, 1970; Mendez et al., 1970; Rawling and Joyner, 1987). This was confirmed in our research, but only the CTC were distributed in the septal region of the middle third of the LV and in small percentages. The highest percentage of equine and canine was through the CCB junctions in all regions analyzed. Cardiac injury results in junctions remodeling and loss, which in turn is associated with decreases in conduction velocity and increased susceptibility to arrhythmias (Severs et al., 2008; Wit and Peters, 2012; Hoagland et al., 2019). The greater or lesser number of junctions present in the ventricular conduction system may be related to a greater or lesser transmission of the electrical impulse, which could determine the presence or absence of ventricular arrhythmias.

We have found similarities with other authors between the few measured parameters of CCF and CCC in horses and dogs. In our research, we took into account different parameters that have not been analyzed in previous studies, such as the comparison of the thickness and density of the CCF, the area and diameters of CCC and the distribution of CFMJ in each of the locations, slices and regions described. This becomes new knowledge that contributes to the morphological study of this component of the CCS and also makes it possible to locate exactly the site with the highest density of CCF as a contribution to the cardiological study of these structures that lead to the prevention of ventricular arrhythmias and the identification of its treatment site. In addition, at present the economic and family importance of these two animal species demands a deeper knowledge of the cardiac components from the basic sciences that are aimed at understanding more adequately each of the diagnostic means used in the clinic of arrhythmias and its adequate resolution.

5. Conclusions

CCC are difficult to identify in dogs because they present a color similar to myocardiocytes, unlike in horses, where they are easily visible. We therefore recommend the use of morphometry and specific stains such as Masson's trichrome, PAS method and desmin for optimal CCC detection.

This research greatly contributed to the generation of new knowledge of the cardiac conduction system in horses and dogs, becoming a point of reference in humans.

CCF were found mainly in the septal region of the heart, being the possible site of generation of ventricular arrhythmias.

In horses and dogs, we observed that CFMJs were mostly distributed through the cardiac apex due to the great electrical impulse transmission occurring in this region.

Sources of funding

This work was supported by a "Instituto de Salud Carlos III" grant and co-funded by "FEDER" (grant numbers PI14/00271, pie15/00013) and by the "Generalitat Valenciana" (grant number PROMETEO2013/007).

Declaration of Competing Interest

The authors declare that they have no conflicts of interest.

Acknowledgements

The authors wish to thank the small animal veterinary clinics in the city of Bucaramanga, Colombia for the collection and donation of specimens for this research. H.Y.E.V would like to acknowledge COLCIENCIAS, scholarship program 756 (2016).

References

Abramson, D.I., Margolin, S., 1936. A Purkinje conduction network in the myocardium of the mammalian ventricles. J. Anat. 70, 250–260.
Alanis, J., Benitez, D., 1970. Rate of rise of Purkinje and transitional cells action potential and the propagation across the Purkinje myocardium junction. Jpn. J. Physiol. 20, 217–232.
Aouadi, S., Mbarki, W., Zemzemi, N., 2019. Towards the modeling of the Purkinje/myocardium coupled problem: a well-posedness analysis. J. Comput. Appl. Math. 351, 136–152.
Atkinson, A., Inada, S., Li, J., Tellez, J.O., Yanni, J., Sleiman, R., Allah, E.A., Anderson, R. H., Zhang, H., Boyett, M.R., Dobrzynski, H., 2011. Anatomical and molecular mapping of the left and right ventricular His-Purkinje conduction networks. J. Mol. Cell. Cardiol. 51, 689–701.
Benito, B., Josephson, M.E., 2012. Ventricular tachycardia in coronary artery disease. Rev. Esp. Cardiol. 65, 939–955.
Benson, A., Asfaridi, O., Zhang, H., Holden, A.V., 2008. The canine virtual ventricular wall: a platform for dissecting pharmacological effects on propagation and arrhythmogenesis. Prog. Biophys. Mol. Biol. 96, 187–208.
Bishop, S.P., Cole, C.R., 1967. Morphology of the specialized conducting tissue in the atria of the equine heart. Anat. Rec. 158, 401–416.
Bordas, R., Gillow, K., Lou, Q., Efimov, I.R., Gavaghan, D., Kohl, P., Grau, V., Rodriguez, B., 2011. Rabbit-specific ventricular model of cardiac electrophysiological function including specialized conduction system. Prog. Biophys. Mol. Biol. 107, 90–100.
Bruzzone, R., White, T.W., Paul, D.L., 1996. Connections with connexins: the molecular basis of direct inter cellular signalling. Eur. J. Biochem. 238, 1–27.
Canale, E., Campbell, G., Smolich, J., 1986. Cardiac Muscle: The Conduction System. Springer-Verlag, Berlin, Heidelberg, New York, Tokio.
De Almeida, M.C., Lopes, F., Fontes, P., Barra, F., Guimaraes, R., Vilhena, V., 2015. Ungulates heart model: a study of the Purkinje network using India ink injection, transparent specimens and computer tomography. Anat. Sci. Int. 90, 240–250.
Eliška, O., 2006. Purkinje fibers of the heart conduction system – history and the present time. Cas. Lek. Cesk. 145, 329–335.
Eriksson, A., Thornell, L.E., Stigbrand, T., 1979. Skeletin immunoreactivity in heart Purkinje fibers from several species. J. Histochem. Cytochem. 27, 1604–1609.

Forsgren, S., Eriksson, A., Kjörell, U., Thornell, L.E., 1982. The conduction system in the human heart at midgestation – immunohistochemical demonstration of the intermediate filament protein skeletin. Histochemistry 74, 43–52.
García-Bustos, V., Sebastian, R., Izquierdo, M., Molina, P., Chorro, F.J., Ruiz-Sauri, A., 2017. A quantitative structural and morphometric analysis of the Purkinje network and the Purkinje-myocardial junctions in pig hearts. J. Anat. 230, 664–678.
Gianni, C., Burkhardt, J.D., Trivedi, C., Mohanty, S., Natale, A., 2018. The role of the Purkinje network in premature ventricular complex-triggered ventricular fibrillation. J. Int. Card. Electrophysiol. 52, 375–383.
Glomset, D.J., Glomset, A.T.A., 1940. A morphologic study of the cardiac conduction system in ungulates, dog and man. Part II: the Purkinje system. Am. Heart. J. 20, 677–701.
Gourdie, R.G., Green, C.R., Severs, N.J., Anderson, R.H., Thompson, R.P., 1993. Evidence for a distinct gap-junctional phenotype in ventricular conduction tissues of the developing and mature avian heart. Circ. Res. 72, 278–289.
Gros, D.B., Jongsma, H.J., 1996. Connexins in mammalian heart function. BioEssays 18, 719–730.
Harris, B.S., O'brien, T.X., Gourdie, R.G., 2002. Coronary arteriogenesis and differentiation of periarterial Purkinje fibers in the chick heart: is there a link? Tex. Heart Inst. J. 29, 262–270.
Hoagland, D.T., Santos, W., Poelzing, S., Gourdie, R.G., 2019. The role of the gap junction perinexus in cardiac conduction: potential as a novel anti-arrhythmic drug target. Prog. Biophys. Mol. Biol. 144, 41–50.
Krishnamoorthy, J., Lakshmanan, A., Mullasari, A., 2015. Focal Purkinje ventricular tachycardia ablation in structurally normal heart. Asian. Cardiovasc. Thorac. Ann. 23, 855–857.
Li, J., Logantha, S.J., Yanni, J., Caj, X., Dobrzynski, H., Hart, G., Boyett, M.R., 2015. From the Purkinje fibers to the ventricle: one dimensional computer simulation for the healthy and failing heart. Conf. Proc. IEEE. Eng. Med. Biol. Soc. 2015, 34–37.
Mendez, C., Mueller, W.J., Urguiaga, X., 1970. Propagation of impulses across the Purkinje fiber-muscle junctions in the dog heart. Circ. Res. 26, 135–150.
Miquerol, L., Meysen, S., Mangoni, M., Bois, P., van Rijen, H., Abran, P., Jongsma, H., Nargeot, J., Gros, D., 2004. Architectural and functional asymmetry of the His-Purkinje system of the murine heart. Cardiovasc. Res. 63, 77–86.
Myerburg, R.J., Hilsson, K., Gelband, H., 1972. Physiology of canine interventricular conduction and endocardial excitation. Circ. Res. 30, 217–243.
Myerburg, R.J., Hilsson, K., Castellanos, A., 1975. The intraventricular conducting system and patterns of endocardial excitation. Adv. Cardiol. 14, 2–14.
Nonidez, J.F., 1943. The structure and innervation of the conductive system of the heart of the dog and rhesus monkey as seen with a silver impregnation technique. Am. Heart J. 26, 577–597.
Oh, I.Y., Cha, M.J., Lee, T.H., Seo, J.W., Oh, S., 2018. Unsolved questions on the anatomy of the ventricular conduction system. Korean Circ. J. 48, 1081–1096.
Ono, N., Yamaguchi, T., Ishikawa, H., Arakawa, M., Takahashi, N., Saikawa, T., Shimada, T., 2009. Morphological varieties of the Purkinje fiber network in mammalian hearts, as revealed by light and electron microscopy. Arch. Histol. Cytol. 72, 139–149.
Oosthoek, P.W., Virágh, S., Lamers, W.H., Moorman, A.F., 1993. Immunohistochemical delineation of the conduction system II: the atrioventricular node and Purkinje fibers. Circ. Res. 73, 482–491.
Otsuka, N., Hara, T., Kataoka, A., 1966. Experimentelle untersuchungen der PAS-reaktion zur darstellung des reizleitungs systems am hundeherzen. Acta. Anat. Nippon. 41, 1–6.
Pallante, B., Giovannone, S., Fang-Yu, L., Zhang, J., Liu, N., Kang, G., Dun, W., Boyden, P. A., Fishman, G.I., 2010. Contactin-2 expression in the cardiac Purkinje fiber network. Circ. Arrhythm. Electrophysiol. 3, 186–194.
Paul, M., Wichter, M.D., Gerss, J., Arps, V., Schulze-Bahr, E., Robenek, H., Breithardt, G., Weissen-Plenz, G., 2013. Connexin expression patterns in arrhythmogenic right ventricular cardiomyopathy. Am. J. Cardiol. 15, 1488–1495.
Pieperhoff, S., Borrmann, C., Grund, C., Barth, M., Rizzo, S., Franke, W.W., 2010. The area composita of adhering junctions connecting heart muscle cells of vertebrates. VII. The different types of lateral junctions between the special cardiomyocytes of the conduction system of ovine and bovine hearts. Eur. J. Cell. Biol. 89, 365–378.
Rawling, D.A., Joyner, R.W., 1987. Characteristics of junctional regions between Purkinje and ventricular muscle cells of canine ventricular subendocardium. Circ. Res. 4, 580–585.
Sedmera, D., Gourdie, R.G., 2014. Why do we have Purkinje fibers deep in our heart? Physiol. Res. 63, S9–S18.
Severs, N.J., Coppen, S.R., Dupont, E., Yeh, H.I., Ko, Y.S., Matsushita, T., 2004. Gap junction alterations in human cardiac disease. Cardiovasc. Res. 62, 368–377.
Severs, N.J., Bruce, A.F., Dupont, E., Rothery, S., 2008. Remodelling of gap junctions and connexin expression in diseased myocardium. Cardiovasc. Res. 80, 9–19.
Sheets, M.F., January, C.T., Fozzard, H.A., 1983. Isolation and characterization of single canine cardiac Purkinje cells. Circ. Res. 53, 544–548.
Shimada, T., Nakamura, M., Kitahara, Y., Sachi, M., 1983. Surface morphology of chemically-digested Purkinje fibers of the goat heart. J. Electron Microsc. 32, 187–196.
Shimada, T., Noguchi, T., Asami, I., Campbell, G.R., 1986. Functional morphology of the conduction system and the myocardium in the sheep heart as revealed by scanning and transmission electron microscopic analyses. Arch. Histol. Jpn. 49, 283–295.
Shimada, T., Ushiki, T., Fujita, T., 1992. Purkinje fibers of the heart. Shinyaku Chiryou 42, 11–13.
Silverman, M., Grove, D., Upshaw Jr., C.B., 2006. Why does the heart beat? The discovery of the electrical system of the heart. Circulation 113, 2775–2781.
Sommer, J.R., Johnson, E.A., 1968. Cardiac muscle. a comparative study of Purkinje fibers and ventricular fibers. J. Cell. Biol. 36, 497–526.
Stephenson, R., Boyett, M., Hart, G., Nikolaidou, T., Caj, X., Corno, A.F., Alphonso, N., Jeffery, N., Jarvis, J.C., 2012. Contrast enhanced micro-computed tomography resolves the 3-dimensional morphology of the cardiac conduction system in mammalian hearts. PLoS One 7, e35299.
Sugi, Y., Hirakow, R., 1986. Freeze-fracture studies of the sinoatrial and atrioventricular nodes of the caprine heart, with special reference to the nexus. Cell. Tissue Res. 245, 273–279.
Tabereaux, P.B., Dosdall, D.J., Ideker, R.E., 2009. Mechanisms of VF maintenance: wandering wavelets, mother rotors, or foci. Heart Rhythm. 6, 405–415.
Tawara, S., 1906. Das Reizleitungssystem des Säugetierherzens; eine anatomisch-histologische Studie über das Atrioventrikularbündel und die Purkinjeschen Fäden. Gustatav Fischer, Jena, Marburg.
Tawara, S., 2000. The Conduction System of the Mammalian Heart. Imperial College Press, London.
Ter Borg, H., 1937. Untersuchungen über das Vorkommen von Purkinje-Zellen in der Herzvorkammer unserer Haustiere unter besonderer Berücksichtigung des Pferdes. Acta. Neerl. Morphol. 1, 64–67.
Ter Borg, H., 1941. The atrioventricular conduction system of the big domestic animals, and more especially on the terminal arborization of the Purkinje fibers and the so-called interventricular connections. Acta. Neerl. Morphol. 4, 97.
Tranum-Jensen, J., Wilde, A.A.M., Vermeulen, J.T., Janse, M.J., 1991. Morphology of electrophysiologically identified junctions between Purkinje fibers and ventricular muscle in rabbit and pig hearts. Circ. Res. 69, 429–437.
Truex, R.C., Smythe, M.Q., 1965. Comparative morphology of the cardiac conduction tissue in animals. Ann. N. Y. Acad. Sci. 127, 19–33.
Vigmond, E.J., Stuyvers, B.D., 2016. Modeling our understanding of the His-Purkinje system. Prog. Biophys. Mol. Biol. 120, 179–188.
Vozzi, C., Dupont, E., Coppen, S.R., Yeh, H.I., Severs, N.J., 1999. Chamber-related differences in connexin expression in the human heart. J. Mol. Cell. Cardiol. 31, 991–1003.
Wit, A.L., Peters, N.S., 2012. The role of gap junctions of the arrythmias of ischemia and infarction. Hearth. Rhythm. 9, 308–311.
Yao, X., Gan, Y., Marboe, C.C., Hendon, C.P., 2016. Myocardial imaging using ultrahigh-resolution spectral domain optical coherence tomography. J. Biomed. Opt. 21, 61006.
Yoshimura, A., Yamaguchi, T., Kawazato, H., Takahashi, N., Shimada, T., 2014. Immunohistochemistry and three-dimensional architecture of the intermediate filaments in Purkinje cells in mammalian hearts. Med. Mol. Morphol. 47, 233–239.
Zimmermann, A., 1923. Das Reizleitungssystem der Herzens bei Equiden. Anat. Anz. (Erg. H) 57, 552–558.

El Comité Organizador del
XX CONGRESO DE LA SOCIEDAD ESPAÑOLA DE HISTOLOGÍA E INGENIERÍA TISULAR,
VIII INTERNATIONAL CONGRESS OF HISTOLOGY AND TISSUE ENGINEERING y
VI CONGRESO IBEROAMERICANO DE HISTOLOGÍA

Certifica que la Comunicación ORAL:

MORPHOMETRIC AND HISTOLOGICAL AND MORPHOMETRIC STRUCTURE OF THE SINUS AND ATRIOVENTRICULAR NODES IN HUMANS AND PIGS.

de la que son Autores:

Gómez-Torres FA, Sebastian- Aguilar R, Ruiz-Sauri A

Ha sido **presentada** en este Congreso, celebrado los días 4, 5 y 6 de Septiembre de 2019.

Y para que conste se expide y firma el presente certificado en

Murcia, a 6 de Septiembre de 2019,

Juan Francisco Madrid Cuevas
Presidente del Comité Organizador y Presidente de la SEHIT

Luis Miguel Pastor García
Presidente del Comité Organizador

El Comité Organizador del
XX CONGRESO DE LA SOCIEDAD ESPAÑOLA DE HISTOLOGÍA E INGENIERÍA TISULAR,
VIII INTERNATIONAL CONGRESS OF HISTOLOGY AND TISSUE ENGINEERING y
VI CONGRESO IBEROAMERICANO DE HISTOLOGÍA

Certifica que la Comunicación ORAL:

HISTOLOGICAL AND MORPHOMETRIC STUDY OF THE COMPONENTS OF THE SINUS AND ATRIOVENTRICULAR NODES IN HORSES AND DOGS.

de la que son Autores:

Gómez-Torres FA Ballesteros-Acuña LE, Ruiz-Sauri A

Ha sido **presentada** en este Congreso, celebrado los días 4, 5 y 6 de Septiembre de 2019.

Y para que conste se expide y firma el presente certificado en

Murcia, a 6 de Septiembre de 2019,

Juan Francisco Madrid Cuevas
Presidente del Comité Organizador y Presidente de la SEHIT

Luis Miguel Pastor García
Presidente del Comité Organizador

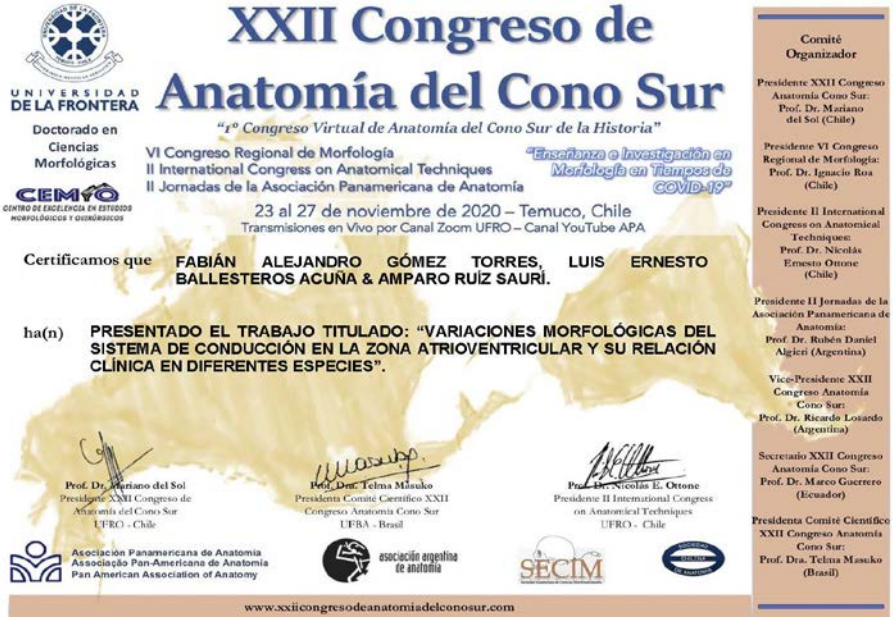

UNIVERSIDAD DE LA FRONTERA

Doctorado en Ciencias Morfológicas

CEMYQ
CENTRO DE EXCELENCIA EN ESTUDIOS MORFOLÓGICOS Y QUIRÚRGICOS

XXII Congreso de Anatomía del Cono Sur

"1º Congreso Virtual de Anatomía del Cono Sur de la Historia"

VI Congreso Regional de Morfología
II International Congress on Anatomical Techniques
II Jornadas de la Asociación Panamericana de Anatomía

"Enseñanza e Investigación en Morfología en Tiempos de COVID-19"

23 al 27 de noviembre de 2020 – Temuco, Chile
Transmisiones en Vivo por Canal Zoom UFRO – Canal YouTube APA

Certificamos que **FABIÁN ALEJANDRO GÓMEZ TORRES, LUIS ERNESTO BALLESTEROS ACUÑA & AMPARO RUÍZ SAURÍ.**

ha(n) **PRESENTADO EL TRABAJO TITULADO: "VARIACIONES MORFOLÓGICAS DEL SISTEMA DE CONDUCCIÓN EN LA ZONA ATRIOVENTRICULAR Y SU RELACIÓN CLÍNICA EN DIFERENTES ESPECIES".**

Prof. Dr. Mariano del Sol
Presidente XXII Congreso de Anatomía del Cono Sur
UFRO - Chile

Prof. Dra. Telma Maszko
Presidenta Comité Científico XXII Congreso Anatomía Cono Sur
UFBA - Brasil

Prof. Dr. Nicolás E. Ottone
Presidente II International Congress on Anatomical Techniques
UFRO - Chile

Asociación Panamericana de Anatomía
Associação Pan-Americana de Anatomia
Pan American Association of Anatomy

asociación argentina de anatomía

SECIM

www.xxiicongresodeanatomiadelconosur.com

Comité Organizador

Presidente XXII Congreso Anatomía Cono Sur: Prof. Dr. Mariano del Sol (Chile)

Presidente VI Congreso Regional de Morfología: Prof. Dr. Ignacio Roa (Chile)

Presidente II International Congress on Anatomical Techniques: Prof. Dr. Nicolás Ernesto Ottone (Chile)

Presidente II Jornadas de la Asociación Panamericana de Anatomía: Prof. Dr. Rubén Daniel Algieri (Argentina)

Vice-Presidente XXII Congreso Anatomía Cono Sur: Prof. Dr. Ricardo Losardo (Argentina)

Secretario XXII Congreso Anatomía Cono Sur: Prof. Dr. Marco Guerrero (Ecuador)

Presidenta Comité Científico XXII Congreso Anatomía Cono Sur: Prof. Dra. Telma Maszko (Brasil)

La Sociedad Española de Cardiología certifica que

el Póster titulado

Distribución de las células de Purkinje mediante el estudio histológico y morfométrico en humanos y cerdos: un enfoque para la prevención de las arritmias ventriculares

firmado por los siguientes autores

Fabián A. Gómez Torres(1), H Yesid Estupiñan(1), César Ríos Navarro(2), María Ortega(1), Fco. Javier Chorro Gascó(3), Vicente Bodí Peris(3) y Amparo Ruiz Sauri(1) de (1)Universitat de València, Valencia, (2)Fundación de Investigación del Hospital Clínico de Valencia - INCLIVA, Valencia y (3)Hospital Clínico Universitario. Universitat de València. INCLIVA. CIBERCV, Valencia

ha sido presentado en el eCongreso SEC 2020 de la Salud Cardiovascular (28/31 octubre 2020)

Madrid, a 28 de octubre de 2020

Ángel R. Cequier Fillat,
Presidente de la SEC